Surface Analysis of Adsorbed Proteins: A Multi-Technique Approach to Characterize Surface Structure

Elaine Hillenmeyer Tronic

A dissertation
submitted in partial fulfillment of the
requirements for the degree of

Doctor of Philosophy

University of Washington
2012

Reading Committee:
David G. Castner, Chair
Wendy E. Thomas
Thomas A Horbett

Program Authorized to Offer Degree:

Bioengineering

Elaine Hillenmeyer Tronic

University of Washington

Abstract

Surface Analysis of Adsorbed Proteins: A Multi-Technique Approach to Characterize Surface Structure

Elaine Hillenmeyer Tronic

Chair of the Supervisory Committee:

Professor David G. Castner

Depts. of Bioengineering and Chemical Engineering

Adsorbed proteins on surfaces are important in many applications, including medical implants, sensors, marine materials, and *in vitro* substrates for cell culture and other uses. Understanding the protein structure on the surface would allow better control of the interaction of the material with the surrounding environment and a more reproducible system response. Protein adsorption is a complex process, and characterization requires the combination of multiple analysis techniques. In this thesis, adsorbed protein amounts were measured using x-ray photoelectron spectroscopy (XPS) and radiolabeled proteins. Protein conformation and orientation were measured using time-of-flight secondary ion mass spectrometry (ToF-SIMS), near edge x-ray absorption fine structure (NEXAFS), sum frequency generation (SFG), and enzyme-linked immunosorbent assays (ELISA). Surface type influenced the adsorbed surface concentration of albumin and fibronectin on surfaces of

glass, polystyrene, titanium, and sulfonated polystyrene as measured by XPS and radiolabeled protein adsorption. More albumin adsorbed onto polystyrene than glass. More albumin and fibronectin adsorbed onto sulfonated polystyrene than titanium. ToF-SIMS also showed differences in structure of the proteins adsorbed onto the different surfaces. The A1 domain of von Willebrand Factor adsorbed in similar amounts onto glass, tissue culture polystyrene, and polystyrene surfaces, as measured by XPS. However, ToF-SIMS showed differences in solution exposure of A1 domain amino acids when adsorbed onto the three surfaces and NEXAFS showed the most ordered β-sheet structure when A1 was adsorbed onto polystyrene. ELISA showed lowest binding of antibodies recognizing a nonlinear epitopes within A1 when A1 was adsorbed onto polystyrene. Functional studies using a parallel plate flow chamber measured platelet binding to A1 adsorbed onto the three surfaces. At high shear (20dyne/cm^2), platelets showed most detachment from A1 adsorbed onto glass. At low shear (0.2dyne/cm^2), platelets showed most detachment from A1 adsorbed onto polystyrene. Surface analysis was also useful in characterizing collagen substrates created under different experimental conditions, including material source and pH. Collagen obtained from different sources exhibited altered adsorption behavior, both in amount adsorbed as measured by XPS and interaction with the A1 domain of von Willebrand Factor as measured by ToF-SIMS. SFG was used to identify differences in ordering of collagen adsorbed from solutions at different pH values. Collagen adsorbed at pH 8.0 showed higher SFG amide signal than collagen adsorbed at pH 6.5, suggesting greater ordering of the peptide backbone at pH 8.0. The differences in SFG signal were not due to the amount adsorbed protein, as XPS showed more collagen adsorbed onto tissue culture polystyrene at pH 6.5 than pH 8.0. These studies demonstrated that the surface type can have a large impact

on adsorbed proteins, both in amount adsorbed and surface structure. These studies also showed that surface analysis is very useful in creating defined *in vitro* protein substrates. In all cases, it was crucial to use multiple analysis techniques to understand these systems.

TABLE OF CONTENTS

LIST OF FIGURES

Figure number *Page*

LIST OF TABLES

Table number *Page*

ACKNOWLEDGEMENTS

The author would like to thank her advisor, Professor David Castner, and the supervisory committee members, Dr. Wendy Thomas, Dr. Thomas Horbett, and Dr. Dan Ratner, for their guidance and valuable discussions.

The author thanks members of the Castner lab including Dr. Joe Baio and Dr. Gilad Zorn for many valuable discussions while sharing an office, Dr. Dan Graham for training on ToF-SIMS, Gerry Hammer for training on XPS, Rami Foster for help with radiolabeled protein adsorption studies, and Winston Ciridon for help troubleshooting experiments. The author also thanks members of the Thomas lab including Dr. Olga Yakovenko and Dr. Becky Penkala for collecting flow chamber data, Dr. Gianluca Interlandi for discussions on protein simulations, and Dr. An-yue Tu for assistance in wet lab techniques. Helpful discussions with colleagues Dr. Jen Osborn and Matt Manganiello are also appreciated.

Finally I would like to thank my husband Tristan and my family. I could not have done this without their love and support.

Chapter 1 Introduction

1.1 Protein adsorption

When a solid material comes in contact with a solution containing protein, the surface is almost immediately and irreversibly coated with adsorbed proteins. This adsorbed protein layer then modulates the interaction of the material with the surrounding environment [1]. Protein adsorption is therefore an important consideration for many applications including passivating coatings for sensors [2,3], fouling of marine materials [4], and implanted devices [5,6].

Protein adsorption is controlled by forces including hydrophobic interactions, electrostatic interactions, and hydrogen bonding [7-9]. Proteins adsorb onto a surface within seconds to minutes, but the layer can undergo changes in conformation over time [10,11] and proteins can exchange on the surface over time if adsorbed from a complex mixture [12].

Although protein adsorption has been extensively studied, prediction of how a protein will interact with a surface is still not possible [13-16,5]. Characteristics of an adsorbed protein layer include amount of protein adsorbed to a surface, spatial organization of adsorbed proteins (monolayer versus aggregates), conformation (secondary and tertiary structure), orientation (direction of protein with respect to the surface), and biological activity (interaction with small molecules, proteins, or cells). These characteristics of the adsorbed protein layer then control the interaction with the surrounding proteins and cells.

For implanted devices, protein adsorption can be important in controlling biocompatibility through effects on inflammation [6,5], cell adhesion, [17-20], cell differentiation [18], and clotting [21,5,22,23].

1.1.1 Driving forces for protein adsorption

In solution, proteins can self-assemble into a highly ordered secondary and tertiary structure [24]. The protein favors the folded state over the unfolded coil due to a number of thermodynamic factors. During protein folding, the loss of conformational entropy is outweighed by a decrease in free energy due to the enthalpy and entropy changes from electrostatic interactions, van der Waals interactions, hydrogen bonding, and hydration

[25,24,26-28]. Entropic and enthalpic factors can influence the adsorption, but protein adsorption is an entropically driven process. The free energy change is thought to be dominated by a gain of entropy achieved from release of water molecules from the adsorbent surface when a protein denatures on a surface. This has never been directly shown, but is supported by previously published models comparing the enthalpic to entropic contributions to adsorption [29-31].

As the protein adsorbs to a surface, its structure can change from the solution conformation to achieve a new structure when in contact with the surface. The surface structure of the protein will depend on properties of both the protein and surface. Protein parameters influencing adsorption include structure, size, and structural stability [32]. Important surface properties include hydrophobicity and surface chemistry [33-38]. While it is not possible to predict how a given protein will interact with a given surface, surface properties are important because surfaces with different chemistries will have different free energy landscapes for the adsorption process, therefore influencing how the protein adsorbs onto a given surface.

1.1.2 Conformational changes

Conformational changes that occur during protein adsorption can affect biological activity [39,5]. Conformation changes on the surface are driven by the entropy gain derived from rearranging the protein structure [31] and the hydrophobic effect, minimizing the interfacial free energy between the protein, surface, and solution [40]. These time-dependent changes are influenced by the protein and the surface.

Although proteins quickly come in contact with a surface, the conformation of a protein on a surface can change over time. Several experimental techniques have been used to observe this time-dependent conformational change, including FTIR. FTIR measurements of fibronectin adsorbed to polystyrene showed a fast loss of unhydrated β-sheets (within five minutes). The conformation was then stable [41]. Using FTIR to measure albumin adsorption, increasing adsorption time onto polyHEMA resulted in a decrease in α-helical content up to 2 hours, after which conformation was stable [42]. Another study measured the adsorption of albumin and lysozyme onto poly tris(trimethylsiloxy)silylstyrene. FTIR showed a decrease in α-helix content and increase in random content, stabilizing after about

five hours [43]. When lysozyme was adsorbed to PTFE, an initial fast change was observed using FTIR which corresponded to loss of α-helices within the first minute of adsorption. Then a slow step α-helix to β-sheet transition occurred over several hours [44]. A recent study used FTIR to track conformation changes over time in insulin adsorbed onto hydrophobic phenyldimethylmethoxysilane [45]

Ellipsometry measurements have also given insight into protein conformation changes on surfaces over time [46]. When albumin was adsorbed to a TiO_2 surface, after a fast initial adsorption step within the first minute, the total amount of protein on the surface remained constant [46]. However, the thickness of the layer increased as the protein conformation changed over a period of one hour. Past one hour, the protein layer did not change further. Spreading of albumin and fibrinogen on CH_3 SAMs has also been tracked using total internal reflectance fluorescence (TIRF) [47]. On CH_3 SAMS, the footprint of both albumin and fibronectin increased approximately 3-fold over a period of 20 minutes, suggesting conformational changes occurred on the surface. AFM has also been used to probe time-dependent changes of albumin and fibronectin in contact with low density polyethylene [48]. Greater surface-protein adhesion forces were measured at longer contact times, again suggesting conformational changes in the proteins. Circular dichroism can also be used to measure changes in adsorbed protein conformation, which has been used to track protein adsorption onto silica [49]. When alcohol dehydrogenase and aldose reductase were adsorbed onto silica, both proteins exhibited an increase in β-sheet structure and decrease in α-helix structure compared to the respective native protein secondary structures.

1.1.3 Protein exchange on surface

Protein adsorption on a surface is generally considered to be irreversible. However, exchange of proteins can occur on the surface, the so-called Vroman Effect [50,12,51]. When a solution containing multiple proteins comes in contact with a surface, the surface can initially be coated with highly concentrated proteins that interact weakly with the surface. Over time, the proteins on the surface can be displaced by larger proteins that have higher surface affinity. Proteins can also undergo some surface exchange from a single component solution [52-54]. Brash, et al. demonstrated protein exchange on a surface by adsorbing fibrinogen labeled with ^{125}I onto surfaces. Then the surfaces were exposed to unlabeled

fibrinogen, and the amount of radioactivity on the surface was tracked as a function of time. After 180 minutes of exchange time, the surface retained 60-80% of its radioactivity on the surfaces tested.

The composition of the adsorbed protein layer is important for regulating the interaction of the surface with the surrounding environment. One previous study showed that human neuron-derived cells showed poor spreading and no neurite formation when grown on substrates of fibronectin adsorbed onto self-assembled monolayer surfaces terminated with CH_3 groups. However, when the self-assembled monolayer surfaces were adsorbed with a mixture of fibronectin and albumin, the cells formed neurites [55]. Another study showed that coadsorption of fibronectin with albumin onto polytetrafluoroethylene increased binding of an anti-fibronectin antibody compared to adsorbed fibronectin alone [56]. Antibody binding was correlated with attachment of endothelial cells, demonstrating the surface composition of proteins influenced the cell response.

1.1.4 Effects of adsorption on protein function

The changes that occur within a protein upon adsorption to a solid surface can affect the biological activity of the protein. Previous studies have shown that adsorption can affect the function of albumin. Although albumin is generally considered to be nonadhesive, platelets can adhere to albumin adsorbed onto COOH, NH_2, CF_3, and CH_3 SAMs [57]. Platelets were able to adhere to adsorbed albumin when it had lost 30% or more of its α-helix content, as measured by circular dichroism. Addition of soluble RGD peptides inhibited platelet binding, indicating platelets were binding through integrin receptors to the adsorbed albumin.

The surface function of the extracellular matrix protein fibronectin has been extensively studied. Previous reports have shown that the surface to which fibronectin is adsorbed affects many aspects of cell function. Differences in cell adhesion [18,19,17,20], spreading [20], proliferation [58,59], differentiation [60], and mineralization [18] have been reported when cells are cultured on fibronectin adsorbed onto different surfaces. These differences have been hypothesized to be due to differential exposure of RGD integrin-binding sites when fibrinogen is adsorbed onto different surfaces.

The presence of multiple proteins on a surface can also affect biological activity. A previous study showed fibroblasts exhibited poor spreading when cultured on fibronectin adsorbed onto hydrophobic CH_3 SAMs [55]. However, when fibronectin and albumin were coadsorbed onto the surface, fibroblast spreading was observed. Improved spreading was not due to a higher concentration of fibronectin, since some surface sites were occupied by adsorbed albumin. Instead, the spreading was likely due to a difference in fibronectin conformation caused by the presence of albumin, termed 'albumin rescuing'. Another study of endothelial cell adhesion to fibronectin and albumin co-adsorbed onto polytetrafluoroethylene observed a similar effect [56].

1.2 Tools for characterizing protein adsorption

As outlined above, the adsorbed protein layer on a surface controls the interaction of the surface with the surrounding environment. For any given protein-surface interaction, the amount of protein adsorbed onto a surface, the conformation/orientation of the protein on the surface, and biological activity are important considerations. Many techniques have been developed or adapted for studying characteristics of adsorbed proteins. Highlighted here are the techniques used in the proposed studies and their advantages for protein characterization.

1.2.1 XPS

X-ray photoelectron spectroscopy (XPS) is a valuable technique to gain quantitative information about the chemical surface composition of a sample [61,62]. In XPS, a sample is placed under vacuum then irradiated with x-rays. The incoming x-rays can interact with a core-level or a valence electron leading to total transfer of the photon energy to the electron. This causes emission of the electron from the atom if the photon energy is greater than the electron binding energy.

Some of these emitted photoelectrons travel into the vacuum chamber, where they can be separated based on kinetic energy. Based on conservation of energy, the kinetic energy (*KE*) of the emitted photoelectrons is the difference between the incoming x-ray energy, which is known, and the binding energy (*BE*) of the electron in the atom. This relationship is described in Eq. 1.1, where $h\nu$ is the known incoming x-ray energy.

$$KE = \mathrm{h}\nu - BE \qquad \text{(Eq. 1.1)}$$

The binding energy of each emitted photoelectron depends on the atomic and molecular environment in which it was located. If an electron is located close to an atom's nucleus, it will have a higher binding energy than an electron located further away. Other atoms bound to the emitting atom will also influence the binding energy of the photoelectron since bound atoms change the electron distribution of the molecule. Binding energies are not strongly influenced by changes in isotopes or weak atomic interactions such as crystallization or hydrogen bonding. Therefore shifts in binding energy give information about molecular environment of the atom, including oxidation state and covalently bound atoms.

The number of photoelectrons emitted from the sample at each binding energy depends on the concentration of atoms in that chemical and molecular state present in the sample. Therefore, we can calculate the relative amount of each element in the sample using the peak areas in the XPS spectrum, instrument parameters, and the photoionization cross-section, which is the probability that the incident x-ray will create a photoelectron in the atom. Calculated photoionization cross-sections are available for each electron from each element [63]. With this information, XPS allows quantitative determination of atomic composition for all elements except H and He within an error of less than 10%.

The sampling depth of XPS is governed by the emitted photoelectrons. As an electron travels through matter, it loses energy due to inelastic collisions. X-rays can travel deep into a sample. However, electrons travel much smaller distances. Since only the photoelectrons emitted into the vacuum chamber are detected, photoelectrons from deep within the sample are not measured, limiting the sampling depth.

The distance traveled by the electron is described by its inelastic mean free path, which is defined as thickness of matter through which 63% of traversing electrons will lose energy [61]. Sampling depth is then controlled by the inelastic mean free path of the electrons. The sampling depth is generally defined as 3 times the inelastic mean free path, which is the region of the sample from which 95% of the detected electrons originate.

For transmission of electrons through a sample, Beers law of molecular absorption (Eq. 1.2) describes how the number of detected electrons maintaining the same energy will decrease when passing through a sample of thickness *t*

$$I_k = I_o e^{(-t/\lambda\cos\theta)} \qquad \text{(Eq. 1.2)}$$

Where I_k is the exiting intensity, I_o is the incident intensity, t is the thickness of the sample, λ is the inelastic mean free path of the electron, and θ is the angle between the surface normal and the detector, or takeoff angle.

The flux of electrons from a surface can be decreased by the presence of an overlayer, such as in the case of a protein adsorbed onto a polymer. As protein adsorbs onto a surface, the substrate signal is attenuated by the protein. The extent of the decrease is determined by the thickness and fractional coverage of the overlayer as described by equations 1.3 and 1.4 [61]:

Overlayer:

$$I_{k_O} = I_{o_o}\gamma\left[1 - e^{(-t/\lambda\cos\theta)}\right] \qquad \text{(Eq. 1.3)}$$

Substrate:

$$I_{k_s} = I_{o_s}\left[(1-\gamma) + \gamma e^{(-t/\lambda\cos\theta)}\right] \qquad \text{(Eq. 1.4)}$$

Where I_k is the measured intensity, I_o is the intensity of a pure sample of the substance, γ is the fraction of surface covered, and t is the protein overlayer thickness, λ is the inelastic mean free path of the photoelectron, and θ is the photoelectron takeoff angle. Therefore XPS can give us information about the thickness of an overlayer based on the attenuation of the substrate signal and intensity of the overlayer signal.

XPS can also be used to create adsorption isotherms for proteins adsorbed onto surfaces. If the substrate does not contain nitrogen, any nitrogen detected in XPS can be assumed to originate from adsorbed protein. Then adsorption isotherms can be created by measuring the amount of nitrogen on the surface at varying solution protein concentrations. By combining XPS with another technique that measures the total amount of adsorbed protein, protein layer thickness and fractional coverage can be calculated (chapter 2.3.5).

1.2.2 Radiolabeled protein adsorption

In addition to XPS, another way to measure the amount of protein adsorbed to a surface is to label the protein with a radioactive atom, ^{125}I for the studies in this document [64]. Radioiodination has been used since at least the 1950s [65,66] to track proteins in

biological assays. Radioiodination is sensitive and allowing quantitative measurement through detection of the radioisotope covalently bound to the protein of interest.

^{125}I is a gamma emitter, allowing direct detection of the radioactivity, in contrast to b-emitting radionuclides such as ^{3}H and ^{14}C, which require additional sample preparation. The count rate of ^{125}I per gram is also orders of magnitude higher than ^{3}H and ^{14}C per gram, respectively, allowing more sensitive detection [67]. The half-life of ^{125}I is 60 days, giving sufficient time to perform to perform in vitro experiments.

Proteins are covalently labeled by oxidizing the ^{125}I- into the reactive $^{125}I_2$ or ^{125}I+. These reactive species covalently react with the tyrosine residues in the protein, and can also react at much lower efficiency with histidine, cysteine, and tryptophan [67]. After labeling, the protein is purified using gel filtration to remove free radioactive ^{125}I.

The labeled protein can then be adsorbed onto a surface of interest, and the retained radioactivity can be measured. The amount of protein on the surface can then be calculated from retained radioactivity (corrected for background), specific activity of the protein solution in counts per mass of protein, and surface area of the sample as described in equation 1.5.

$$\frac{mass\ protein}{surface\ area} = \frac{counts - background}{specific\ activity \times sample\ surface\ area} \qquad \text{(Eq. 1.5)}$$

By combining radiolabeling with XPS, protein layer thickness and fractional coverage can be calculated (chapter 2.6).

1.2.3 ToF-SIMS

Time-of-flight secondary ion mass spectrometry (ToF-SIMS) can be used to obtain information about the conformation of a protein on a surface. Previous studies have shown that ToF-SIMS can distinguish between proteins in different orientations [68,69] and conformations on different surfaces [70-72,35,73,74].

ToF-SIMS is a surface analysis tool that probes to the outermost 2-3nm of a surface [75]. In this technique, a sample surface is bombarded with high energy primary ions (typically in the keV range). The energy of the primary ion is transferred to the surface, which causes a collision cascade between the atoms in the material. This results in ejection

of atoms and molecular fragments from the surface. A small fraction of the ejected species are ionized during the emission process.

The secondary ion current of species m is determined by the following equation:

$$I_s^m = I_p y_m \alpha^{\pm} \theta_m \eta \qquad \text{(Eq. 1.6)}$$

Where I_s^m is the secondary ion current, I_p is the primary ion flux, y_m is the sputter yield, $\alpha^{\pm}$ is the ionization probability for either positive and negative ions, θ_m is the fractional concentration of species *m* in the surface, and η is the transmission function for the instrument. The sputter yield increases as the energy of the primary ion increases, up to a maximum value of 5-50keV [76].

Ionization of atoms is a complex process and can occur by several mechanisms: acid-base reactions within polar molecules to form (M+H)+ or (M-H)+/- ions; cationization or anionization of neutral molecules; or ejection of an electron from a molecule. A very small fraction of particles ejected from the surface become ionized (<1%) and ionization of these particles likely occurs within the materials or in the region just above the surface. Ionization can be affected by the electron structure of other atoms in close proximity to the ejected atom. This generally prevents a quantitative determination of the amount of each species present in the sample, and is termed the 'matrix effect'.

Sputtering is inherently a destructive process. However, analysis of the outermost atoms can be achieved by using a low primary ion flux so there is a low probability of a spot on the surface being hit with a primary ion more than once. Since each impact occurs on an area of the surface that has not previously been damaged, the same chemistry is sampled by each collision. This is termed static SIMS, as opposed to dynamic SIMS which involves sputtering through a material to measure elemental composition as a function of depth. A primary ion generally disrupts an area on the surface of 10nm^2. Therefore 10^{13} primary ions per square centimeter would disrupt the entire surface, and is termed the static limit. To avoid multiple collisions on a single spot on the sample, generally a maximum primary ion dose of 1 x 10^{12} primary ions/cm^2 is used.

There are several types of mass analyzers used to detect the secondary ions created in SIMS, including quadrupole RF mass filter, magnetic sector, and time-of-flight analyzers.

This discussion focuses on time-of-flight (ToF) analysis because that type of mass analyzer was used exclusively to collect the data contained in this document.

In ToF analysis, charged species are accelerated to a set potential. Then the ions travel through a flight tube where flight time is measured. Flight time is determined by mass, i.e. the smaller species move faster than the larger species. Using the flight path length *L* and accelerating potential *V*, the relationship between the flight times and the mass-to-charge ratio *m/z* is shown in Eq. 1.7:

$$t = L\left(\frac{m}{2zV}\right)^{\frac{1}{2}} \qquad \text{(Eq. 1.7)}$$

The flight time of the ejected ions are measured, and a mass spectrum can be generated from the flight time data. Transmission in a ToF-SIMS system is typically 10-50% and has a high mass range (>1000 amu).

ToF-SIMS has been used to analyze complex biological systems, including proteins adsorbed onto surfaces. By collecting ToF-SIMS data from poly(homo-amino acids), reference spectra for the amino acids have been produced [77,78] and characteristic ToF-SIMS fragmentation patterns have been identified for each amino acid. These characteristic peaks can then be used to determine the relative concentration of amino acids present in the surface layer.

Because the sampling depth of ToF-SIMS is generally smaller than the thickness of an adsorbed protein layer, these relative amino acid concentrations can be used to determine protein orientation [68,69], conformations on different surfaces [70-72,35,73,74] and to distinguish a mixture of proteins on a surface [79-82].

ToF-SIMS analysis produces large complex datasets containing up to hundreds of peaks that can be challenging to analyze. One can compare the peak intensities of a few individual peaks selected due to their presumed importance in the system, but that approach excludes portions of the data that could also contain important information. Principal component analysis (PCA), an established multivariate analysis technique [78,83-85], can be used to gather further information from spectra by using all the peaks in the spectrum, not just comparing the intensities of a few selected peaks.

PCA transforms the ToF-SIMS data to a new set of orthogonal axes, termed principal components, such that the greatest variance in the projection of the data lies on the first principal component, the second greatest variance lies on the second principal component, etc. For further information, Wold provides an excellent description of the mathematics of PCA [84]. Briefly, PCA decomposes a large dataset into two cross-product matrices: scores and loadings. The scores plot displays the value of each data point on the new axes, or principal components. The scores plot gives information about the relationship of the samples to each other and how alike or different they are. The loadings plot indicates which peaks from the original spectra contribute to the principal components.

PCA is a mathematical tool to help understand a given dataset, and has limitations. The PCA results in themselves do not necessarily have physical meaning related to the experiment. Once PCA is performed, it is important to go back to the original dataset to examine if the original data also supports the conclusions suggested by PCA. For PCA to be a useful tool, an experiment must be well designed initially, with carefully controlled variables. PCA can identify differences between samples, but it cannot fix a poorly designed experiment. Care must be taken when using PCA to understand the inputs for the analysis. The output can be affected by scaling and normalization, so it is important to understand the purpose of any data pretreatment and if it applies to a given analysis.

1.2.5 ELISA

Enzyme-linked immunosorbent assays (ELISAs) can also give valuable information about the conformation of a protein on a surface [86]. ELISA measures the binding of an antibody to an antigen within a protein immobilized on a surface. The antibody is coupled with an enzyme to allow detection [87].

In a typical ELISA protocol, the antigen protein is adsorbed onto a surface. A primary monoclonal or polyclonal antibody is allowed to interact with the immobilized antigen. The surface is then probed with a secondary polyclonal antibody with an enzyme, typically horse-radish peroxidase (HRP), conjugated to it. A reagent is added to the solution, which reacts with the HRP to produce a color change in the solution. A spectrophotometer can be used to measure the transmission of a specific wavelength of light through the solution. The enzyme amplifies the signal in fixed proportionality to the amount of enzyme

present, allowing the color change to be related back to the level of binding of the primary antibody.

Antibodies used in ELISA can be polyclonal or monoclonal. Polyclonal antibodies recognize multiple sites on an antigen. Polyclonal antibodies are typically produced by collecting the serum from an animal that has been inoculated with an antigen of interest. The serum will contain multiple antibodies produced by different immune cells that bind to multiple epitopes on the antigen. Polyclonal antibodies can be useful in ELISA for detecting the amount of antigen present, for example in diagnosing disease.

Monoclonal antibodies, in contrast, bind to only one site on a given antigen. Monoclonal antibodies are typically produced by immunizing a mouse with an antigen. Then spleen cells are collected from the mouse and fused with myeloma cells. Because each cell line is produced from a single immune cell, the resulting cells will produce antibodies that recognize a single epitope on the antigen.

Monoclonal antibodies can recognize continuous linear sequences in the antigen amino acid primary sequence, termed a linear epitope [88]. These epitopes typically consist of 6-9 amino acids [88], but can contain as few as 5 amino acids [89] Antibody recognition of linear epitopes can be favored during antibody production if the antigen is denatured, by heat treatment for example, before being introduced into the animal.

Monoclonal antibodies can also recognize nonlinear epitopes that are discontinuous in the primary amino acid sequence, typically 9-22 total residues, but are close together in 3D space [88,90]. It is estimated that approximately 90% of epitopes are formed from nonlinear amino acid segments [91,92]. If the amino acids which make up the nonlinear epitope are not in the proper position to allow recognition by the antibody, the antibody will not bind.

Methods for mapping the locations of epitopes include x-ray crystallography [91], testing for binding of antibodies to short peptide sequences [93], mutagenesis studies [94], and computational methods [95].

We can potentially observe differences in protein surface conformation using ELISA by using a monoclonal antibody which binds to a nonlinear epitope in the antigen [96]. When a protein is immobilized on a surface at a given surface coverage, a lack of binding by a primary antibody suggests that the epitope is no longer accessible for binding. One reason for a lack of accessibility could be orientation of the protein on the surface, whether the

epitope is linear or nonlinear. If the epitope is oriented toward a surface, it would not be accessible for antibody binding. If the antibody binds to a nonlinear epitope, decreased binding could also be due to a disruption of the 3D structure of the epitope. Therefore, different levels of binding of an antibody with a nonlinear epitope suggest that proteins are in different orientations or conformations, or a combination of the two, changing the ability of the antibody to recognize the epitope.

1.2.6 Flow chamber

The bioactivity of adhesive proteins can be measured using a parallel plate flow chamber to flow cell suspensions over a preadsorbed surface [97-99]. A parallel plate flow chamber simulates the fluid shear stress experienced by platelets or other cells in vivo. Platelet diffusivity is very low so they do not cross stream lines unless red blood cells are present to cause it. The parallel plate flow chamber can produce well-defined shear stresses from 0.01-30 dyne/cm^2, which encompasses the range of physiological shear stress in the circulatory system [100,101].

In a parallel plate flow chamber, a plate is coated with an adhesive ligand of interest. Then a microfluidic channel is created over the surface using a cover and gasket, with the cover sealed onto the plate surface by the gasket. There are inlet and outlet ports to allow fluid to pass through the channel. The movement of fluid through the channel is controlled by a syringe pump. In this way, platelets or other particles can be introduced to the surface.

Within the flow chamber, the wall shear stress (τ) is a function of flow rate (Q), fluid viscosity (μ), and chamber height (h) and chamber width (w) according to the following equation [97]:

$$\tau=6Q\mu/(wh^2) \qquad \text{(Eq. 1.8)}$$

Platelet binding to surfaces of von Willebrand Factor (VWF) is characterized by rolling behavior [102,98,103-106]. This rolling behavior is possible due to the rapid on rate of the platelet receptor GP1bα with VWF [98] Platelet rolling velocity on a surface is affected by the bond lifetime, which changes with force for the von Willebrand Factor (VWF) interaction with ligand GP1bα [102,107]. Leukocytes are another cell type that

exhibits rolling behavior, and leukocyte rolling on endothelial cells has been shown to be strongly influenced by dissociation rate [108], and dissociation rate of the VWF-GP1bα interaction is also varies with force [105]. Rolling can also be influenced by deforming the platelet surface, increasing the contact area [109,110]. Bond lifetime decreases with increasing membrane stiffness in leukocyte-endothelial cell interactions [111], and rigid beads also had faster dissociation rates than more flexible leukocytes during rolling [112]. Platelet adhesion is also influenced by the amount of adhesive protein on the surface [104,103] or platelet receptor density [103,104].

To measure the platelet-surface interaction, we can measure the number of platelets in contact with the adhesive surface. Platelets in contact with a surface are measured using an optical light microscope and camera to record the platelets moving across the surface. Image analysis software can then track the particles moving across the surface, distinguishing between stationary and rolling platelets.

Platelets interacting with a surface in a parallel plate flow chamber does not give information about individual ligand-receptor bonds since there are likely multiple bonds present at any given time. Instead, the assay gives a macroscopic measurement of many simultaneous ligand-receptor interactions, allowing comparison of overall ligand biological activity.

1.2.7 Sum Frequency Generation

Sum Frequency Generation (SFG) is a nonlinear optical technique that is sensitive to ordered bonds at an interface [113]. In this technique, a visible and infrared laser are overlapped in time and space on a surface. Photons are emitted which have the frequency of the sum of the two incoming photons. Vibrational spectroscopy can be performed by varying the wavelength of the infrared light.

The intensity of the SFG signal is described by the following equation

$$I(\omega) \propto \left|\chi^{(2)}\right|^2 I_1(\omega_1) I_2(\omega_2) \qquad \text{(Eq. 1.9)}$$

Where I_1 and ω_1 are the intensity and frequency, respectively, of one incoming light beam and I_2 and ω_2 are the intensity and frequency, respectively, of the other incoming light

beam [113]. χ^2 is the second order susceptibility of the system. This susceptibility is zero in centrosymmetric matter, and is zero in disordered matter. Therefore, an SFG signal is only generated at an interface where the inversion symmetry is broken. Signal is also only be generated from ordered structures.

SFG can detect submonolayer levels of material [113] and has been used to study protein structure on surfaces. Protein secondary structure on surfaces, including alpha-helix [114,69,115-117] and beta sheet [69,118,116], have been identified using SFG. SFG has also been used to examine protein orientation on surfaces [69,36,119]. This can be achieved by varying the polarization of the visible, IR, and SFG light.

1.2.8 Near-edge x-ray absorption fine structure

Near-edge x-ray absorption fine structure (NEXAFS) is an electron spectroscopy which gives information about the electronic structure of the atoms and bonds within a surface [120]. The technique is performed by irradiating a sample with x-rays, causing emission of photoelectrons. The probability of photoemission depends on the atom's chemical and physical state. The resulting Auger electrons or fluorescent photons are then measured.

NEXAFS studies are typically performed using polarized synchrotron x-rays. When using polarized x-rays, the probability of photoemission depends on the orientation of the incoming x-rays with respect to the dipole moment of the measured orbital [120]. By varying the incident angle of x-rays, information about the orientation of orbitals on the surface can be obtained. NEXAFS has previously been used to characterize orientation of proteins on surfaces by examining the angle-dependent NEXAFS signal of the π^* feature of the nitrogen k-edge, corresponding to the amide backbone of the protein [69,36,114].

1.3 Proteins in the proposed studies

1.3.1 Albumin

Albumin is a small serum protein that is the most prevalent protein in the blood with concentrations of approximately 40mg/ml [121]. Albumin is considered non-adhesive [122-

124] and its main function is to maintain osmotic pressure in the blood [121]. Albumin can also bind a range of hydrophobic ligands including fatty acids, warfarin, steroids, and anesthetics, transporting them in the blood [121].

Because of its smaller size and high concentration, albumin is likely among the first proteins that arrive at a biomaterial surface after implantation [47]. Therefore characterizing its adsorption behavior is important for understanding the interaction of a material with a biological fluid.

Previous studies have shown that the surface to which albumin is adsorbed influences its adsorption behavior. Fluorescence and ^{125}I-bovine serum albumin (BSA) studies have shown that more BSA adsorbs onto hydrophobic polystyrene [125] or CH_3 SAMs [126,47,127] than comparative hydrophilic surfaces of silica [125], OH SAMs [126,47], or COOH SAMs [127]. Previous studies have also shown that BSA diffuses [128] and spreads [47] more quickly on hydrophilic surfaces than hydrophobic surfaces.

Albumin conformation and orientation can also be affected by the adsorption surface. ToF-SIMS studies have identified different conformations of albumin when adsorbed onto various surfaces (different polyethylene glycol contents [35], titanium, gold, and PTFE [72]). Michel, et al. demonstrated that albumin denaturation decreased as polyethylene glycol content of the surface increased, as demonstrated by decreasing exposure of nonpolar amino acids [35]. Tidwell, et al. showed that the amino acid intensities of glycine, alanine, proline, lysine, and leucine/isoleucine were different when albumin was adsorbed onto gold, titanium, polytetrafluoroethylene and tetrafluoroethylene surfaces [72]. Amino acid intensity was highest intensity on titanium and polytetrafluoroethylene surfaces, and lower on gold and tetrafluoroethylene surfaces. These differences in amino acid exposure suggest differences in albumin surface structure. Another ToF-SIMS study showed hydrophobic amino acid residues were oriented preferentially toward a hydrophobic polystyrene surface, exposing the hydrophilic amino acids at the protein-solution interface [129]. Native albumin secondary structure consists of less than 10% b-sheet and over 60% a-helix as measured by circular dichroism [57]. Studies using circular dichroism have shown that albumin exhibits different α-helix and β-sheet content when adsorbed to different SAMs (ranging from 15-45% α-helix and 15-30% β-sheet) [57,8], quartz surfaces (50% α-helix, 20% β-sheet) [128], silica (60% α-helix, 20% β-sheet) [52], polystyrene (50% α-helix, 25% β-sheet) [52], polypropylene

(10% α-helix, β-sheet not reported) [130], and polyHEMA (15% α-helix, β-sheet not reported) [130]. FTIR measurements have shown albumin contains different α-helix content when adsorbed to germanium versus polystyrene [131]. These studies clearly show that the adsorption surface can impact albumin adsorption characteristics.

1.3.2 Fibronectin

Fibronectin is a large (450kDa) multidomain glycoprotein, present in the blood and in interstitial space [132,133]. Fibronectin is an adhesive protein and plays an important role in the extracellular matrix. Fibronectin allows cell attachment and signaling through integrin surface receptors on cells [5,6]. Integrin signaling then controls many important cell functions, including proliferation [134], differentiation [135], and survival [136].

Fibronectin has been widely studied in relation to biomaterials because of its important role in influencing cell behavior around biomedical implants [5,6]. Several studies show that adsorption of fibronectin is influenced by material surface characteristics. Using FTIR, a loss of β-sheet structure has been observed when fibronectin is adsorbed onto hydrophobic surfaces and at lower surface densities [41,137,138,55]. Ability to elute fibronectin from the surface was also different on polystyrene versus tissue culture polystyrene, indicating fibronectin was in different conformations on the two surfaces [139]. More fibronectin was eluted from the tissue culture polystyrene surface during a 15 minute incubation with SDS than from the polystyrene surface.

It is hypothesized that conformational changes of fibronectin on surfaces affect the presentation of integrin binding sites. Indeed, anti-RGD antibodies showed lower binding when fibronectin was adsorbed onto more hydrophobic surfaces [140-142], supporting this hypothesis. Changes in integrin binding can then affect cell function.

In vitro studies have observed that the function of cells cultured on adsorbed fibronectin is influenced by the surface to which fibronectin is adsorbed. Osteoblasts showed more adhesion and mineralization when cultured on surfaces of fibronectin adsorbed onto tissue culture polystyrene than polystyrene [18]. As compared to polystyrene and tissue culture polystyrene, even lower adhesion was observed when osteoblast-like cells were cultured on fibronectin adsorbed onto polyHEMA [20]. Osteoblast-like cells also showed different adhesion when cultured on fibronectin adsorbed onto CH_3, OH, COOH, and NH_2

SAMs [19], with the most cells adhering to fibronectin on OH SAMS and the fewest cells adhering to the CH_3 SAMs. The surface to which fibronectin was adsorbed also affected the function of other cell types, including macrophages [143], myoblasts [58,60], fibroblasts [144,141,55,145], and endothelial cells [146,59,147].

Since surface characteristics can affect fibronectin adsorption, which can then influence cell behavior, fibronectin adsorption is important to consider for biomaterial applications.

1.3.3 von Willebrand Factor

Von Willebrand Factor (VWF) is a soluble blood protein that is responsible for primary tethering of platelets in regions of high shear [148]. VWF is a large, multi-domain protein consisting of the following domain structure: D1-D2-D'-D3-A1-A2-A3-D4-B1-B2-B3-C1-C2-CK. The VWF monomers are disulfide bonded at the N and C terminus to other VWF monomers, existing in the blood as large multimers of many different degrees of multimerization up to 40-mers [149]. The A1 domain contains the binding site for the GP1bα receptor on platelets [150]. In normal circulating blood, VWF does not interact with platelets [151]. However, when attached to a surface in regions of high shear, or in the presence of a small molecule activator such as ristocetin, VWF becomes competent to bind platelets [148,152-154].

The exact mechanism of VWF activation is not understood. However, it is generally believed that a conformational change within VWF exposes a cryptic binding site to allow GP1bα binding. There is evidence that the D'D3 region (N-terminal of A1) inhibits GP1bα binding to VWF [151]. There is also evidence that the A2 domain plays an inhibitory role in VWF- GP1bα binding [149,155]. Removing either the N-terminal or C-terminal portion of VWF from the A1 domain results in increased GP1bα binding activity. However, the removal of the D'D3 domain is not enough to constitutively activate VWF to bind GP1bα under static conditions [151]; the presence of a small-molecule activator such as ristocetin is still required to activate VWF. This suggests that although the domains flanking A1 play a regulatory role, a conformational change within the A1 domain itself is also required to allow GP1bα binding.

The activation of VWF is a surface event, occurring when VWF is immobilized. *In vivo* during an injury event, VWF is bound to a collagen surface. *In vitro*, VWF is typically immobilized on a synthetic material for testing. Previous studies measuring VWF function have used a variety of surfaces, including glass [156,103], collagen [156,157], polyethylene [158], and polystyrene [159]. VWF adsorption onto synthetic surfaces could also be of interest for blood-contacting biomaterials.

The question of surface-induced changes in VWF structure has not been well addressed in the literature. One previous study used atomic force microscopy to examine VWF topography when adsorbed to hydrophilic and hydrophobic surfaces [160]. VWF was adsorbed under static conditions and was not sheared before analysis. When VWF was adsorbed onto hydrophilic mica, the protein showed an extended conformation. On hydrophobic octadecyltrichlorosilane (OTS) modified glass, VWF appeared as compact structures, suggesting that VWF adsorption can be affected by the substrate to which it is absorbed. However, previous studies have not examined to what extent potential differences in surface behavior affect VWF function. An understanding of surface-induced conformational changes in VWF will give valuable information about the mechanism of VWF activation.

1.3.4 Collagen

Collagen is an extremely important ECM protein in the body, making up 25-35% of the body's total protein [161]. There have been 28 types of collagen identified, but 90% of the collagen in the body is type I [162].

In vivo, collagen forms a hierarchical fibril structure [163]. The smallest unit is the peptide chain, containing a high concentration of glycine, proline, and hydroxyproline amino acids. Three peptide chains come together to form a left-handed helix approximately 300nm long and 1.5nm wide, making it more elongated than an α-helix. The presence of the rigid proline residues in the helix prevent the formation of α-helices [161]. Then three of these helices join together in a right-handed helix to form a microfibril. These microfibrils can then form larger fibrillar bundles.

In addition to its structural and mechanical properties, collagen also interacts with other ECM molecules, clotting proteins, cell adhesion proteins, and growth factors [162].

Both VWF [164,165] and fibronectin [166,162] bind to collagen. The binding sites on collagen have been elucidated for some of these proteins [162,167]. Collagen is also important for tissue engineering applications, where it can provide structural stability, support cell attachment and signaling, and promote angiogenesis [168-170].

Since collagen plays such an important biological role, it is commonly used as a substrate for in vitro assays [171]. Previous studies have shown that differences in preparation of the collagen substrate can affect cell function [172,173,169]. Therefore gaining a deeper understanding of collagen substrates would allow better defined in vitro systems that could more easily be related to in vivo function.

1.4 Overview of this document

Following this introductory chapter, this document is organized into 7 total chapters. The chapters are organized as follows:

Chapter 2 describes in more detail the experimental methods used in these studies.

Chapter 3 describes work completed to determine differences in adsorption behavior of albumin onto polystyrene and glass surfaces.

Chapter 4 describes work completed to determine differences in adsorption behavior of albumin and fibronectin on titanium and sulfonated polystyrene surfaces.

Chapter 5 describes work completed to determine function and adsorption behavior of von Willebrand Factor A1 domain and full-length von Willebrand Factor onto materials commonly used for in vitro testing.

Chapter 6 describes work completed to characterize the adsorption behavior of collagen onto surfaces.

Chapter 7 gives an overall conclusion to this work and future directions.

Chapter 2 Experimental Methods

2.1 Proteins used in these studies

Bovine serum albumin was obtained from Sigma. The A1 domain of von Willebrand Factor was produced in *E. coli* containing residues 1238-1472 of mature VWF with 12 residues at the N terminus from the expression vector (MRGSHHHHHHGS) [174]. The protein was generously provided by Miguel Cruz. Full-length plasma von Willebrand Factor was obtained from Haematologic Technologies Inc. (Essex Junction, VT). Human placenta type III collagen was obtained from Sigma and Abcam (Cambridge, MA). Human plasma fibronectin was obtained from Sigma. All proteins were used without further purification.

2.2 Substrates used in these studies

Preparation of each substrate for protein adsorption can be different, so care should be taken to establish proper cleaning steps. Glass coverslips (8mm, ProSciTech, Thuringowa, Australia) were cleaned by sequential sonication in dichloromethane, acetone, methanol, 2 times each for 5 minutes in each solvent. Glass coverslips were analyzed by XPS to confirm that any surface contaminants had been removed.

For some experiments, polystyrene substrates were created using spin-casting. Polystyrene powder (MW2500, Sigma) was dissolved in toluene (3wt%) and spin-cast onto glass coverslips cleaned using the method described above.

Polystyrene and TCPS cell culture plates (Corning) were also used for some protein adsorption experiments. To create substrates for protein adsorption, cell culture plates were wrapped in aluminum foil with the non-shiny side facing the plate. Cell culture plates were then cut into pieces of approximately $1cm^2$ using a shear. After samples were cut, they were sonicated in water 2 times for 5 minutes each before use to remove any contamination that might have been introduced during cutting. For TCPS substrates, the back of each sample was marked using marker or a scratch since only one side is treated. PS and TCPS substrates were analyzed by XPS to confirm that any surface contaminants had been removed and only expected elements were present.

Titanium samples (Ti) were prepared by electron beam evaporation of thin Ti layers (~50nm) onto 1cm^2 silicon wafers. Deposition was performed at the University of Washington Microfabrication Facility. Following deposition, Ti substrates were cleaned by subsequent sonication in dichloromethane, acetone, and methanol, 2 times each for 5 minutes in each solvent.

Sulfonated substrates were made by sulfonating polystyrene surfaces. Polystyrene petri dishes (Corning) were diced into 1cm^2 pieces as described above. Following sonication in water 2 times for 5 minutes each, polystyrene samples were thoroughly dried using a stream of nitrogen. Any glassware used for sulfonation reactions were heated before use to minimize the presence of water. Polystyrene pieces were then allowed to react with concentrated sulfuric acid for 1-24h at room temperature. Samples were removed from the sulfuric acid and quickly rinsed with water from a squirt bottle. Then samples were sonicated in water for 1h to remove any sulfuric acid non-covalently associated with the surface. Following sonication, samples were dried using a stream of nitrogen and stored in an inert nitrogen atmosphere until use.

The number of sulfonate groups on the sulfonated polystyrene surface was quantified according to the method of Helary, et al. [175]. Samples were immersed in an aqueous solution of toluidine blue ($5x10^{-4}$ M) for 6h. Then samples were rinsed with an aqueous solution of NaOH ($5x10^{-3}$ M) to remove uncomplexed dye. Toluidine blue was decomplexed from the surface by immersion in 50vol% acetic acid for 24h. Then absorbance of the solution was measured at 633nm and compared to a standard curve of toluidine blue. The number of sulfonate groups was corrected for nominal surface area to determine the concentration of sulfonate groups on the surface.

2.3 Protein adsorption for ultra-high vacuum analysis

When preparing adsorbed protein substrates of ultra-high vacuum surface analysis, care should be taken at all times to prevent contamination. Lab coat and gloves should be worn at all times. Metal instruments should be regularly cleaned by subsequent sonication in dichloromethane, acetone, and methanol.

When preparing for protein adsorption, buffer should be allowed to warm up to room temperature before opening to prevent condensation on the inside of the bottle, which can

introduce contamination. After the bottle is at room temperature, the buffer should be degassed for at least 30 minutes using a stir bar or sonication for agitation while using vacuum to evacuate any air present in the solution. The presence of air bubbles in the protein adsorption solution will cause the protein to denature at the bubble interface and could lead to adsorption of denatured proteins. Unless otherwise noted, the buffer used for these studies is phosphate buffered saline (137mM NaCl, 2.7mM KCl, 10mM phosphate) at pH 7.4. Buffer pH can be changed to investigate the influence of pH in adsorption. Buffer pH is adjusted using NaOH or HCl.

Before introducing the protein to the surface of interest, the substrate should be allowed to equilibrate with degassed buffer for at least an hour to allow the surface to become fully hydrated. Then the protein can be introduced to the surface. For these studies, substrates were placed into 24-well plates, to which enough degassed buffer was added to cover the substrate (400-500μl). To avoid exposure of the substrate to the air-water interface, protein is then added to the well in an equal volume to the buffer already present.

Protein adsorption can be measured at various temperatures for various amounts of time. For the experiments included in this thesis, adsorption was generally carried out for 2h at 37^{o}C. Protein adsorption is generally complete after about 30 minutes [47,41], so allowing adsorption for 2 hours should result in adsorbed protein layer that is no longer changing. Adsorption time can be increased past 2 hours to ensure maximum coverage if desired.

Following adsorption, the protein adsorption solution should be thoroughly diluted before removing the substrate. This prevents the substrate from passing through the layer of denatured protein at the air-water interface. After dilution of the protein adsorption solution, substrates were rinsed 2 times for one minute each in PBS to remove loosely bound protein. Substrates were then rinsed in water 3 times for one minute each to remove buffer salts. Samples were dried with a stream of nitrogen, then kept under inert nitrogen atmosphere until analysis.

2.4 ^{125}I-BSA preparation and adsorption

Proteins can be labeled with a radioactive tag to measure the amount of protein adsorbed to a surface. In these studies, bovine serum albumin (BSA) and fibronectin were labeled using Na^{125}I (PerkinElmer, Waltham, MA) according to the method of Horbett [64].

A 2:1 molar ratio of ICl to BSA or fibronectin was used. Albumin was suspended in borate buffer (160mM NaCl, 200mM boric acid). Fibronectin was suspended in phosphate buffer containing citric acid and azide (110mM NaCl, 10mM NaI, 10mM citric acid, 8mM phosphate, 3mM NaN_3).

To perform the labeling reaction, $Na^{125}I$ is mixed with borate buffer, which is added to a 2M NaCl solution containing unlabeled ICl and the protein solution. Unincorporated ^{125}I is separated from labeled protein by two passes through Econo Pac 10DG desalting columns (Bio-Rad Laboratories, Hercules, CA). Iodinated protein was stored at -20 C and used within 2 weeks of preparation.

To make the protein adsorption solution, a small volume (<5µl) of ^{125}I-labeled protein should be added to unlabeled protein of known solution concentration. Radioactivity is measured for the combined labeled/unlabeled solution. Specific activity is calculated based on the radioactivity and concentration of the unlabeled protein solution (counts/mass protein). Desired specific activity of the initial protein solution can vary based on the expected amount of adsorption. If the amount of adsorbed protein is expected to be low, the specific activity of the initial protein solution should be higher to allow detection of adsorbed protein above background.

Since the adsorbed amount of protein is expressed in terms of mass per surface area, it is necessary to know the available surface area for adsorption. If the surface area of the entire substrate is known, the substrate can be submerged in the protein adsorption solution. Protein adsorption then proceeds similar to the procedure described above.

Substrates are allowed to equilibrate at least an hour with degassed phosphate buffered saline (PBS) (110mM NaCl, 8mM phosphate, 10mM NaI) at pH 7.4 at room temperature. Then an equal volume of ^{125}I-labeled protein solution at twice the desired concentrations is added to the buffer. Following adsorption for 2h at 37^{o}C, protein adsorption solution should be diluted to avoid exposing the substrate to denatured proteins at the air-water interface.

If the surface are of the entire sample is not known or the substrate is not uniform on all sides, a different procedure can be used to measure adsorption on one side [176,126]. In this case, a 10µl droplet of degassed PBS (110mM NaCl, 10mM NaI, 10mM citric acid, 8mM phosphate, 3mM NaN_3) at pH 7.4 was placed on the substrate and allowed to

equilibrate for at least one hour at room temperature. Then 10µl of ^{125}I-labeled protein solutions at twice the desired concentration were added to the existing buffer on the substrates, resulting in a 20µl droplet containing the desired concentration. The nominal size of a 20ml droplet on the surface of interest can be measured to calculate the surface area. In calculating the surface area of the droplet, one assumes that no protein adsorbs outside the area of the droplet. The area of the droplet might expand if the sample is disrupted, so care should be taken that the droplet remains intact. Due to this concern, it is more desirable to use the method of submerging a sample of known surface area, but that is not always possible if all sides of the sample are not uniform. Following adsorption for 2h at 37^{o}C, the protein adsorption solution in the droplet is diluted by sequentially adding and removing 10µl aliquots of buffer to the surface.

After dilution of the protein adsorption solution, samples were washed with PBS to remove loosely bound protein following the procedure of Horbett [64]. Samples were washed for 30-90 seconds in a flow-through manner.

Retained radioactivity was measured using a gamma counter, then protein surface concentration was calculated from retained radioactivity (corrected for background), specific activity of the protein solution, and surface area of the sample. Adsorption should be repeated in triplicate at least twice on separate days. Non-radioactive iodine was included in all buffers to suppress adsorption of free ^{125}I to the surface[64].

Adsorption of multicomponent protein mixtures can also be measured using ^{125}I-labeled protein. Measurement of competitive adsorption is performed in subsequent experiments, with one experiment using one protein labeled with ^{125}I in the presence of the other protein that is unlabeled. A separate experiment then measures the adsorption of the second protein labeled using ^{125}I in the presence of the first protein, which is unlabeled. The results from the separate experiments are combined to determine the amount of each protein on the surface during competitive adsorption.

2.5 XPS analysis

XPS data were collected on a Surface Science Instruments S-Probe instrument with a monochromatized aluminum Kα x-ray source and electron flood gun for charge neutralization. Survey (1eV step size) and detail scans (0.4eV step size) were acquired using

an analyzer pass energy of 150eV and a takeoff angle of 55^{o}. The take-off angle is defined as the angle between the sample surface normal and the axis of the analyzer lens. For each sample type, generally at least two samples should be analyzed with three spectra collected on each sample.

Spectra were analyzed using the Service Physics ESCA 2000A analysis software. Atomic composition of all elements except nitrogen and sulfur were calculated using the survey scan. Atomic composition of nitrogen and sulfur were calculated using detailed scans. For protein adsorption samples, if nitrogen is unique to the protein, not present in the substrate, the nitrogen signal can be used to create an adsorption isotherm by plotting the nitrogen atomic percentage as a function of solution concentration.

Typically high resolution carbon C1s scans were collected for each protein sample. High resolution sulfur S2p and oxygen O1s scans were also collected when appropriate. The analyzer pass energy for high resolution scans was 50eV and the step size was 0.065eV.

Angle-resolved XPS measurements provide information about the variability of the surface composition with depth. As the takeoff angle of analysis is varied, different sampling depths are probed. Here, we used takeoff angles of 0°, 55°, and 75° between the detector lens axis and the sample surface normal. The sampling depths for these three takeoff angles was approximately 10, 5 and 2 nm, respectively. The sample was placed in a specially designed sample holder to allow variation of the sample position. A 12° aperture placed over the analyzer lens to reduce the acceptance angle into the detector. The number of scans taken at different angles was adjusted to optimize the signal-to-noise ratio while minimizing X-ray induced sample damage to the samples.

2.6 Calculations of coverage and thickness from XPS and ^{125}I-protein data

Combining the measurements from XPS and a mass sensitive technique, such as labeling using ^{125}I, can give information about the organization of a protein film.

The mass per area of protein adsorbed (Q) in a radiolabeled protein adsorption assay can be described as

$$Q = \gamma t \rho \qquad \text{(Eq. 2.1)}$$

where ρ is the specific weight of the protein (1.378 g/cm^3) [177], γ is the fraction of surface covered, and *t* is the thickness of protein layer.

In XPS, when a substrate is covered by an overlayer, the signal from both the substrate and overlayer is related to the fractional coverage and overlayer thickness by the following equation [61]:

Overlayer:

$$I_{k_O} = I_{o_o}\gamma\left[1 - e^{(-t/\lambda\cos\theta)}\right] \qquad \text{(Eq. 2.2)}$$

Substrate:

$$I_{k_s} = I_{o_s}\left[(1-\gamma) + \gamma e^{(-t/\lambda\cos\theta)}\right] \qquad \text{(Eq. 2.3)}$$

Where I_k is the measured intensity, I_o is the intensity of a pure sample of the substance, γ is the fraction of surface covered, and *t* is the protein overlayer thickness, λ is the inelastic mean free path of the electron, and θ is the photoelectron takeoff angle. Typically XPS atomic percentages can be used as a substitute for intensity [178], although the linearity of the relationship between intensity and atomic percentage should be confirmed.

By solving this system of two equations, the coverage and thickness can be calculated. This can give information about differences in protein adsorption behavior on different surfaces.

2.7 ToF-SIMS analysis

ToF-SIMS data were acquired on an ION-TOF 5-100 instrument (ION_TOF GmbH, Münster, Germany) using a Bi_3^+ primary ion source under static conditions (primary ion dose <10^{12} ions/cm^2) using a Bi_3^+ current between 0.15-0.35pA. The Bi_3^+ primary ion source was operated in high current bunched mode.

Spectra were obtained from 100 μm x 100 μm areas and five positive ion spectra and three negative ion spectra were collected from each sample. Two to three samples should be analyzed per condition for biological samples to obtain enough data to draw conclusions

about differences between samples. A low-energy electron beam was used for charge compensation.

Mass resolution (m/Δm) of the positive ion spectra was typically between 5500-7000 for the m/z = 27 peak. Mass scales of each positive secondary ion spectrum were typically calibrated to the CH_3^+, $C_2H_3^+$, $C_3H_5^+$, and $C_7H_7^+$ peaks before further analysis. If the $C_7H_7^+$ signal saturated the detector (on bare PS substrates), $C_8H_7^+$ was used for calibration instead of $C_7H_7^+$. The mass scales of the negative secondary ion spectra were calibrated using the CH- , O-, OH-, and C_2H- peaks.

For analysis of protein samples, peaks were identified which corresponded to unique amino acid peaks [77]. Unique amino acid peaks are listed in Table 2.1, along with the corresponding amino acid they are attributed to. Amino acid peaks that overlapped with substrate peaks were not used in analysis. Substrate peaks were eliminated using the following criteria. If the normalized intensity of a peak on the bare substrate was greater than 15-25% of the protein normalized peak intensity, that peak was assumed to originate from the substrate and not included in the amino acid peak list used for analysis.

ToF-SIMS data can be further analyzed in several ways. ToF-SIMS data can give semiquantitative information about protein surface coverage. Comparing the total protein signal for proteins adsorbed to different surfaces gives insight into how much protein is adsorbed onto the surface. To do this, one can sum the intensities from all the amino acid peaks, then normalize by the total intensity of the spectrum to account for day-to-day differences in overall ion yield. The intensity of the substrate signal can also give information about the protein coverage on the surface.

One way to look for differences between proteins adsorbed onto different surfaces is to calculate the relative exposure of the polar (hydrophilic) or nonpolar (hydrophobic) amino acids. Since nonpolar amino acids are typically buried within the protein core, exposure of these amino acids can suggest the protein is denatured on the surface [35]. This simple interpretation is complicated somewhat by the observation that hydrophobic amino acids orient toward a hydrophobic surface to minimize the entropy of the system [129]. However, comparing the hydrophilic/hydrophobic amino acid ratio of adsorbed proteins can give insight into conformational changes.

To calculate the hydrophilic/hydrophobic amino acid ratio, one simply sums the intensity of the peaks corresponding to the polar amino acids and sums the intensity of the peaks corresponding to the nonpolar amino acids, as summarized in equation 2.4.

$$\frac{hydrophilic}{hydrophobic}\,amino\ acid\ ratio = \frac{\sum polar\ amino\ acid\ peak\ intensities}{\sum nonpolar\ amino\ acid\ peak\ intensities} \qquad \text{(Eq. 2.4)}$$

If a crystal structure of the protein of interest is known, this can be a very useful tool in analyzing and interpreting ToF-SIMS data. If a protein contains only specific residues asymmetrically distributed within the protein, the intensity of peaks from those residues in the ToF-SIMS spectrum gives information about the solution exposure of those amino acids. It also gives information about the solution exposure of the area of the protein surrounding the amino acid. Baugh, et al. used this approach to identify differences in Asn, Ile, and Tyr residue exposure when the B1 domain of Protein G was immobilized in a controlled orientation via a cysteine thiol onto maleimide-oligo(ethylene glycol)-functionalized gold and bare gold substrates [69]

Using the protein crystal structure, one can also identify amino acids that are asymmetrically distributed within the protein, and use the ToF-SIMS signals from those amino acids to provide information about the orientation and conformation of the adsorbed protein. For example, if an amino acid is asymmetrically distributed within one region of the protein, measuring the peak intensity from that residue can give information about the orientation of protein on the surface [69]. When one measures amino acid peak intensity, the intensities are generally normalized to the sum of all measured amino acid peaks. This accounts for variability in the protein coverage, as well as day-to-day differences in ion yield due to instrument factors.

While the hydrophilic/hydrophobic ratio can give some overall information about conformational changes, the crystal structure can allow more directed analysis of denaturation. Using the crystal structure, one can identify amino acids that are preferentially located on the outer surface of the protein or buried within the protein. Protein viewers such as Pymol or VMD can calculate the solvent accessible surface area of the amino acids within a protein crystal structure. Also, the 'findsurfaceresidues' function in Pymol will select the surface residues within the crystal structure according to a minimum solvent exposed surface area defined by the user. Comparing the amino acid peak intensity of surface residues and

protein core residues can give insight into conformational changes upon adsorption. Again, amino acid intensities should be normalized or expressed as a ratio of surface/core amino acid intensities to account for differences in protein coverage and day-to-day instrumental variations.

Principal component analysis (PCA) is another useful tool for looking for differences between adsorbed proteins [78,83,79]. PCA uses all the peaks in the dataset to identify the greatest sources of variation between spectra. PCA can distinguish proteins based on amino acid composition [80,179], conformation [35,73], and orientation [68,180]. Prior to PCA, the dataset needs to be preprocessed. There are several options for preprocessing, and the user needs to take care to understand why each step is being taken. In the analyses included in this thesis, peaks were mean centered and normalized to the sum of the selected peaks before PCA. Peaks were normalized to the sum of the selected peaks instead of total intensity because the amino acid peaks are a small subset of the entire spectrum. Normalizing by total intensity would likely cause PCA to identify differences in protein coverage. For the analysis included here, we used a series of MATLAB (MathWorks, Inc., Natick, MA) scripts written by NESAC/BIO (see http://mvsa.nb.uw.edu).

Peaks were identified that corresponded to unique amino acid peaks. Amino acid peaks that overlapped with substrate peaks were then eliminated. Peaks used for analysis are listed in Table 2.1, along with the corresponding amino acid [77]. Intensity of amino acid peaks of interest (Trp and Cys) were normalized to the sum of all amino acid peaks to account for variations in protein surface concentration.

PCA processing of ToF-SIMS data from adsorbed proteins has been described extensively elsewhere [78,83,79].

2.8 Isolation of platelets for parallel plate flow chamber assays

Platelets were isolated from the blood of healthy donors, which had been drawn into acid citrate dextrose (ACD) tubes. Platelets were separated by differential centrifugation in the presence of Apyrase and PGE-1 and resuspended in Hepes Tyrodes buffer containing 200μg/ml BSA [181,182].

2.9 Measuring platelet binding in parallel plate flow chamber

Platelet adhesion studies were performed in a parallel plate flow chamber as previously described [183,98]. A region of interest on each substrate was drawn using a hydrophobic marking pen. The phosphate buffered saline (137mM NaCl, 2.7mM KCl, 10mM phosphate) at pH 7.4 was introduced to the surface for at least one hour. Then protein solution was introduced into the buffer at twice the desired concentration. Surfaces were incubated for 2hr at 37^{o}C. Control surfaces were incubated with BSA (500μg/ml). Surfaces were then blocked with BSA (200μg/ml) overnight at 4^{o}C.

The flow chamber (Glycotech) was prepared with the appropriate gasket to achieve the desired shears. The parallel plate flow chamber was situated on the protein coated plate and sealed using a vacuum. A 300μl bolus of washed platelets was then introduced into the flow chamber and allowed to settle for 30sec. Buffer was then pushed through the chamber at the desired shear using a syringe pump. Platelet-surface interactions were observed with a 10x objective, CCD camera, and microscope controlled by Metamorph software.

To test specificity of platelet-A1 interaction, an anti-GP1bα antibody was used [152]. Platelets were incubated with anti-GP1bα antibody AK2 (Abcam) at a concentration of 25μg/ml for 15 min at room temperature, then platelet binding was measured as described above in the presence of the antibody. Specificity of platelet binding was also measured on a control plate containing only BSA.

The number of platelets on the surface was measured using Metamorph software. Stationary platelets were defined as platelets that remained in the same position on the surface over the entire time the flow was at a particular shear. Stationary platelets were also identified using Metamorph software.

2.10 ELISA

There are many experimental factors to consider when performing an ELISA, and the times for incubation, number of rinses, etc, should be optimized for each assay.

For the ELISA experiments included in this thesis, PS (Corning), TCPS (Corning) and glass-bottom (MatTek) 96-well plates were used as substrates. Phosphate buffered saline (137mM NaCl, 2.7mM KCl, 10mM phosphate) at pH 7.4 was introduced into each well and allowed to equilibrate overnight at room temperature. VWF A1 solutions were then added to

the buffer at twice the desired concentrations, or BSA (1mg/ml) as a negative control. Substrates were incubated for 2h at 37°C.

Surfaces were blocked with BSA (200µg/ml) at room temperature for up to 18h. This relatively long incubation time was found to be necessary to minimize nonspecific interaction of the primary antibody with the surface. Primary antibodies were then incubated with the samples for 1h at 37°C. To test nonspecific secondary antibody binding, some samples were incubated with BSA (1mg/ml) for 1h at 37°C during this step and were not incubated with primary antibody. Results from this assay are included in Section 5.4.3, and show nonspecific binding was less than 20% of specific binding in all cases.

Secondary goat anti-mouse antibodies conjugated with horseradish peroxidase were incubated with the samples for 1h at 37°C. Samples were incubated with 3,3',5,5'-Tetramethylbenzidine (TMB) for 5 min, then absorbance was measured at 600nm. Absorbance values were corrected for background. Between each step, substrates were rinsed at least six times with tris buffered saline (TBS) (150mM NaCl, 10mM tris) containing 0.2 vol % tween 20.

2.11 NEXAFS

Near edge x-ray absorption fine structure (NEXAFS) measurements were performed using samples that had been prepared according to the protein adsorption procedure for ultra-high vacuum analysis, as described above.

NEXAFS spectra were taken at the National Synchrotron Light Source (NSLS) U7A beamline at Brookhaven National Laboratory using an elliptically polarized beam with ~ 85% p polarization. This beamline uses a monochromator with a 600 L/mm grating that provides a full-width half-max resolution of ~0.15 eV at the carbon K-edge (285 eV). The monochromator energy scale was calibrated using the 285.35 eV C 1s−π* transition on a graphite transmission grid placed in the x-ray path. The partial electron yield was monitored by a detector with the bias voltage maintained at −360 V for the nitrogen K-edge spectrum. The signal was divided by the beam flux during data acquisition. Samples were mounted to allow rotation about the vertical axis to alter the angle between the incident x-ray beam and the sample surface. Data was collected at different NEXAFS angles, defined as the angle between the incident X-ray beam and the sample surface.

Spectra were normalized to zero at the pre-edge and 1 at the post-edge. Difference spectra at the nitrogen k-edge were calculated to examine the angle dependence of the adsorbed protein. Calculating the difference between the spectra collected at an incident angle of 70° from the surface normal (near-glancing) and 20° from the surface normal gives information about the orientation of the amide bonds in the protein backbone.

2.12 SFG

SFG was performed to examine the adsorbed surface structure of proteins.

An equilateral CaF_2 prism was spin-coated on one side with deuterated polystyrene. Following annealing overnight at 80^{o}C in air, the polystyrene film was exposed to UV light for at least 1h to introduce oxygen groups to the surface to mimic a TCPS substrate. The prism was then brought into contact with protein in PBS (137mM NaCl, 2.7mM KCl, 10mM phosphate).

The SFG spectra were obtained by overlapping visible and tunable IR laser pulses (25 ps and 30 ps, respectively) in time and space. The visible beam with a wavelength of 532 nm was delivered by an EKSPLA Nd:YAG laser operating at 50 Hz and $AgGaS_2$ crystals to generate tunable IR laser radiation from 1000 to 4000 cm^{-1}. The bandwidth was 1 cm^{-1} for the visible pump pulses and 1-6 cm^{-1} for the IR laser radiation (1 cm^{-1} for 2750-3000 cm^{-1} and 6 cm^{-1} for higher and lower wavenumbers). Both beams were unfocused and had a diameter of approximately 3 mm at the sample. The energy for both beams was 190-240 μJ per pulse.

After allowing 2h for adsorption at room temperature, the spectra were collected with the pump beams going through the backside of the prism. The input angles of the visible and IR pump beams inside the prism were 55° and 62° versus the surface normal of the UV-treated polystyrene surface, respectively.

The SFG signal generated at the sample was then analyzed by filters and a monochromator, detected with a gated photomultiplier tube. The spectra were collected with 300-400 shots per data point in 2 cm^{-1} increments. Spectra were recorded in the ppp and ssp (sum, visible, and infrared) polarization combinations. At least 3 spectra were measured for each condition. The SFG spectra were normalized by the product of the intensities of the IR and visible spectra.

2.13 Tables for Chapter 2

Table 2.1 Positive ToF-SIMS amino acid ions

Positive Ion	Amino Acid	Mass
CH_4N	Gly	30.0346
CH_3N_2	Arg	43.0163
C_2H_6N	Ala	44.0492
CHS	Cys	44.9772
C_2H_3S	Cys	58.9941
C_2H_6NO	Ser	60.0448
C_2H_5S	Met	61.0095
C_4H_6N	Pro	68.053
C_4H_5O	Thr	69.0381
C_3H_4NO	Asn	70.0331
C_4H_8N	Pro	70.0704
$C_3H_3O_2$	Ser	71.0156
$C_4H_{10}N$	Val	72.0862
C_3H_7NO	Arg	73.0527
C_3H_8NO	Thr	74.066
C_2H_6SN	Cys	76.0292
$C_4H_5N_2$	His	81.0383
$C_4H_6N_2$	His	82.0527
C_5H_7O	Val	83.0526
C_4H_6NO	Gln/Glu	84.0474
$C_5H_{10}N$	Lys	84.0855
C_4H_8NO	Hyp	86.0672
$C_5H_{12}N$	Iso/Ile	86.0982
$C_3H_7N_2O$	Asn	87.0576
$C_3H_6NO_2$	Asp/Asn	88.0297
$C_4H_4NO_2$	Asn	98.0144
$C_4H_{10}N_3$	Arg	100.0795
$C_4H_{11}N_3$	Arg	101.0963
$C_4H_8NO_2$	Glu	102.0415
C_7H_7O	Tyr	107.0505
$C_5H_8N_3$	His	110.0759
$C_5H_{10}N_3$	Arg	112.087
$C_8H_{10}N$	Phe	120.0874
$C_6H_{11}N_2O$	Arg	127.0868
C_9H_8N	Trp	130.0685
C_9H_7O	Phe	131.0459

$C_8H_{10}NO$	Tyr	136.0831
$C_{10}H_{11}N_2$	Trp	159.0897
$C_{11}H_8NO$	Trp	170.0666

Chapter 3 Albumin Adsorption onto Polystyrene and Glass Surfaces

3.1 Abstract

Important aspects of protein adsorption are the amount, packing and conformation and orientation of the adsorbed protein. Multi-technique surface analysis was used to characterize albumin adsorption onto glass and polystyrene surfaces. Radiolabeled albumin adsorption and x-ray photoelectron spectroscopy showed that more albumin adsorbed onto polystyrene surfaces than glass surfaces. However, the protein packing on each surface was different. A model based on the x-ray photoelectron spectroscopy (XPS) data and radiolabeled albumin adsorption showed that on polystyrene surfaces, the protein film was thicker and had higher coverage than on the glass surfaces. In all cases, protein surface coverage was calculated to be less than a full monolayer. Time-of-flight secondary ion mass spectrometry (ToF-SIMS) was used to characterize the protein surface structure, a combination of conformation and orientation. Both principal component analysis and a ratio of hydrophobic to hydrophilic amino acids showed that structure of albumin adsorbed onto glass surfaces changed as the adsorption solution protein concentration was increased from 0.001 to 1mg/ml. However ToF-SIMS did not detect changes in albumin structure adsorbed onto polystyrene surfaces over the same concentration range.

3.2 Introduction

When a biomaterial is placed in contact with biological fluids, it is covered by proteins in a matter of seconds to minutes. This nonspecifically adsorbed protein layer then controls the interaction of the biomaterial with the surrounding environment [122].

Adsorption behavior is controlled by the surface properties of the material, including hydrophobicity[8], surface chemistry [9], and charge [57]. Upon adsorption, proteins undergo rearrangement and conformational changes [11]. Although protein adsorption has been studied for many years, we still have limited information about the structure of adsorbed proteins [184]. Due to the complexity of the system, it is extremely difficult to accurately predict or control how proteins will interact with surfaces, making rational design of polymers for biomaterial applications still a challenging goal.

When characterizing protein adsorption, it is important to measure the quantity of protein adsorbed onto a surface and the organization of the protein film. Previously, several techniques have been used to measure quantity of protein adsorption on surfaces, including ellipsometry [185-187] and QCM [188,189,10]. These measurements can be used to calculate film thickness, but calculation typically assumes that the adsorbed protein film has a uniform thickness. However, proteins can adsorb in islands, forming a patchy film on the surface [190,127,191].

Surface plasmon resonance (SPR) can detect the mass of protein adsorbed onto a surface [192-194]. Labeling proteins with a radioisotope is another approach to accurately measure the mass of protein adsorbed onto a surface [195,126,196,197,64,80]. X-ray photoelectron spectroscopy (XPS) can also be used to provide additional insight into the quantity of protein on a surface. XPS can also be used in conjunction with a mass measurement technique to determine if a protein layer adsorbs in a full monolayer or patchy islands [198,62].

Surface structure of an adsorbed protein, consisting of the protein conformation and orientation, has a major role in the interaction of the protein with the surrounding system. Protein conformation and orientation on surfaces has been studied with experimental techniques including FTIR [43,131], circular dichroism (CD) [8,57,128], and near-edge x-ray fine structure (NEXAFS) [36,199,200]. Although FTIR and CD can provide valuable information about the α-helical or β-sheet makeup of a protein, they are not inherently surface sensitive and present challenges for adsorbed protein studies. NEXAFS can provide information about bond orientation within a protein, but cannot give information about a disordered protein film on a surface. Time of flight secondary ion mass spectrometry (ToF-SIMS) has also been shown to be a powerful tool in examining protein structure on surfaces [35,72,201,202,73]. The sampling depth of ToF-SIMS is approximately 2nm, which is generally less than the thickness of a protein layer on a surface, thus the ions detected are sensitive to changes in conformation and orientation.

In the study presented here, we focus on the adsorption behavior of albumin, the most concentrated protein in the blood at 40mg/ml [126]. Due to its high concentration and small size, albumin is likely among the first proteins to adhere to an implanted biomaterial surface [47]. Albumin is generally considered to be nonadhesive and been extensively used as an

inert blocking agent [122,123]. It has been shown to inhibit platelet binding if it fully covers the surface [203,124]. However, upon conformational changes, platelets can adhere to adsorbed albumin [203,57,186].

The study presented here uses surface analysis techniques to characterize the adsorption of bovine serum albumin (BSA) from a wide range of solutions concentrations onto polystyrene, a hydrophobic surface, and glass, a hydrophilic surface. XPS and radiolabeling were used to measure the quantity of protein on each surface, as well as the packing density of the protein films. ToF-SIMS was used to examine the surface structure of BSA to obtain a more detailed understanding of the changes the protein undergoes when it comes in contact with a surface.

3.3 Methods

3.3.1 Substrate preparation

Glass coverslips (8mm, ProSciTech, Thuringowa, Australia) were cleaned by sequential sonication in dichloromethane, acetone, methanol. The water contact angle (measured in air) of the cleaned glass coverslips was 31^{o}+/-1 ^{o} (measured in triplicate on two samples using a goniometer). Previously reported water contact angles for glass surfaces include 15^{o} [204] and 25^{o} [145]. For polystyrene substrates, polystyrene powder (MW2500, Sigma) was dissolved in toluene (3wt%) and spin-cast onto clean glass coverslips. Polystyrene coatings were annealed overnight at 120^{o}C in air. The water contact angle (measured in air) of the polystyrene coated glass coverslips was 72^{o}+/- 2 ^{o} (measured in triplicate on two samples using a goniometer). Previously reported water contact angles for polystyrene surfaces range from 66 ^{o} to 95^{o} [205,204,206-209]

3.3.2 ^{125}I-BSA preparation and adsorption

BSA (Sigma) was labeled using $Na^{125}I$ (PerkinElmer, Waltham, MA) according to the method of Horbett [64]. A 2:1 molar ratio of ICl to BSA was used. Unincorporated ^{125}I was separated from labeled protein by two passes through Econo Pac 10DG desalting columns (Bio-Rad Laboratories, Hercules, CA). Iodinated protein was stored at -20 C and used within 2 weeks of preparation. For protein adsorption, substrates were allowed to equilibrate

overnight with degassed phosphate buffered saline (PBS) (110mM NaCl, 8mM phosphate, 10mM NaI) at pH 7.4 at room temperature. Then ^{125}I-BSA solutions at the desired concentrations were incubated with substrates for 2h at 37^{o}C. Samples were washed with PBS to remove loosely bound protein following the procedure of Horbett [64]. Retained radioactivity was measured using a gamma counter, then BSA surface concentration was calculated from retained radioactivity (corrected for background), specific activity of the protein solution, and surface area of the sample. All conditions were repeated in triplicate at least twice on separate days. Non-radioactive iodine was included in all buffers to suppress adsorption of free ^{125}I to the surface [64].

3.3.3 Protein adsorption for XPS and ToF-SIMS

Substrates were allowed to equilibrate overnight with degassed phosphate buffered saline (137mM NaCl, 2.7mM KCl, 10mM phosphate) pH 7.4 at room temperature, then BSA solutions at the desired concentrations were incubated with substrates for 2h at 37^{o}C. Following adsorption, substrates were rinsed in PBS to remove loosely bound protein, then water to remove buffer salts. Samples were dried with a stream of nitrogen, then kept under inert nitrogen atmosphere until analysis.

3.3.4 XPS analysis

XPS data were collected on a Surface Science Instruments S-Probe instrument with a monochromatized aluminum Kα x-ray source and electron flood gun for charge neutralization. Survey and detail scans were acquired at a pass energy of 150eV and a takeoff angle of 55^{o}. The take-off angle is defined as the angle between the sample surface normal and the axis of the analyzer lens. For each concentration, two samples were analyzed and three spectra were collected on each sample. Spectra were analyzed using the Service Physics ESCA 2000A analysis software. Full XPS elemental composition of all samples is listed in Table 3.1.

3.3.5 Calculations of coverage and thickness from XPS and ^{125}I-BSA data

The mass per area of protein adsorbed (Q) in a radiolabeled protein adsorption assay can be described as

$$Q = \gamma t \rho \qquad \text{(Eq. 3.1)}$$

where ρ is the specific weight of the protein (1.378g/cm^3) [177], γ is the fraction of surface covered, and *t* is the thickness of protein layer.

In XPS, when a substrate is covered by an overlayer, the signal from both the substrate and overlayer is related to the fractional coverage and overlayer thickness by the following equation [61]:

Overlayer:

$$I_k = I_o \gamma \left[1 - e^{(-t/\lambda \cos\theta)}\right] \qquad \text{(Eq. 3.2)}$$

Where I_k is the measured intensity, I_o is the intensity of a pure sample of the substance, γ is the fraction of surface covered, and *t* is the protein overlayer thickness, λ is the inelastic mean free path of the electron, and θ is the photoelectron takeoff angle. Atomic percentage nitrogen was used as a substitute for intensity [178]. To determine I_o of the protein, XPS analysis was performed on a thick film of air-dried BSA (65.7%C, 18.8%O, 15.5%N).

By solving this system of two equations, the coverage and thickness can be calculated for each sample. The values of Q and I_k for each surface at saturation were determined from Langmuir fits of the adsorption isotherms.

3.3.6 ToF-SIMS analysis

ToF-SIMS data were acquired on an IONTOF 5-100 instrument (IONTOF GmbH, Münster, Germany) using a Bi_3^+ primary ion source under static conditions (primary ion dose <10^{12} ions/cm^2) using a Bi_3^+ current between 0.15-0.35pA. Spectra were obtained from 100 μm x 100 μm areas and five positive ion spectra were collected from each sample. Three samples were analyzed per condition. A low-energy electron beam was used for charge compensation.

Mass resolution (m/Δm) of the positive ion spectra was typically between 5500-7000 for the m/z = 27 peak. Mass scales of each spectrum were calibrated to the CH_3^+, $C_2H_3^+$,

$C_3H_5^+$, and $C_7H_7^+$ peaks before further analysis. If the $C_7H_7^+$ signal saturated the detector (on bare PS substrates), $C_8H_7^+$ was used for calibration instead of $C_7H_7^+$. Peaks were identified which corresponded to unique amino acid peaks.

Amino acid peaks that overlapped with substrate peaks were then eliminated using the following criteria. If the normalized intensity of a peak on the bare substrate was greater than 15% of the protein normalized peak intensity, that peak was assumed to originate from the substrate and not included in the amino acid peak list used for analysis. Peaks used for analysis are listed in Table 3.2, along with the corresponding amino acid they are attributed to. For hydrophilic/hydrophobic peak ratio calculations, peaks labeled 'hydrophilic' were included in the hydrophilic intensity sum, and peaks labeled 'hydrophobic' were included in the hydrophobic intensity sum.

PCA processing of ToF-SIMS data from adsorbed proteins has been described extensively elsewhere [78,83,79]. Prior to PCA processing the peaks were mean centered and normalized to the sum of the selected peaks. Analysis was performed using a series of MATLAB (MathWorks, Inc., Natick, MA) scripts written by NESAC/BIO (see http://mvsa.nb.uw.edu).

3.4 Results and Discussion

3.4.1 ^{125}I BSA adsorption onto polystyrene and glass surfaces

To accurately determine the amount of protein adsorbed to each surface, radiolabeled protein adsorption was performed. This technique allows quantitative measurement of the mass of protein adsorbed onto a surface. ^{125}I-BSA measurements show an increasing surface concentration of BSA on both polystyrene and glass surfaces as the solution protein concentration increased from 0.0001mg/ml to 1mg/ml (Fig. 3.1). Adsorption onto polystyrene surfaces reaches a plateau around 400ng/cm^2 at a solution concentration of 0.001mg/ml. However on glass surfaces, the BSA surface concentration was below 100ng/cm^2. Assuming a native, globular profile for BSA with dimensions 4nm x 4nm x 14nm, monolayer coverage could range from 210-720ng/cm^2 [210,47].

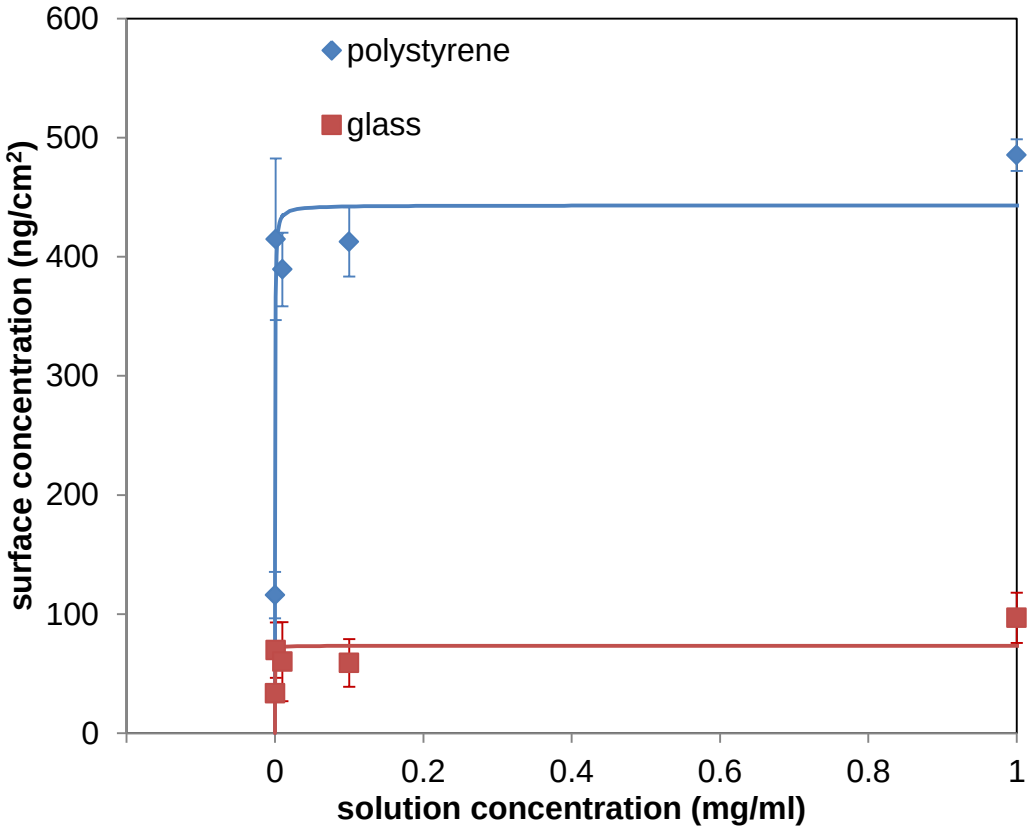

Fig. 3.1. ***^{125}I-BSA adsorption onto polystyrene and glass surfaces.*** *Polystyrene substrates show more protein adsorption than glass, with saturation reached at approximately 400ng/cm^2. Glass substrates had protein adsorption below 100ng/cm^2. Mean +/- SD, n = 6. Solid lines represent Langmuir isotherms fit to the data. X axis is offset from zero for clarity.*

3.4.2 XPS characterization of BSA adsorption onto polystyrene and glass surfaces

We used XPS to further characterize the amount of protein on each surface. Since nitrogen is not present in either substrate, protein adsorption can be tracked by following the nitrogen signal with XPS. XPS showed an increasing nitrogen signal on both polystyrene and glass surfaces as the BSA solution concentration increased from 0.0001mg/ml to 1mg/ml (Fig. 3.2). Samples with BSA adsorbed onto polystyrene showed a moderately higher nitrogen percentage than glass, indicating that more protein adsorbed to the polystyrene surface than the glass surface.

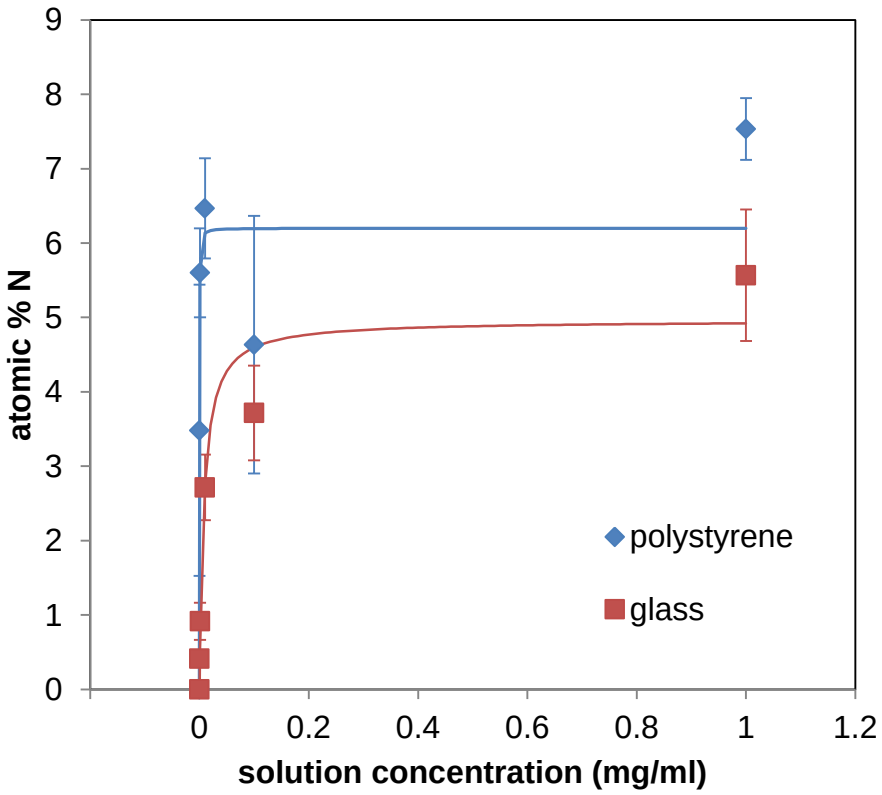

Fig. 3.2. XPS analysis of BSA adsorption onto polystyrene and glass surfaces. *BSA adsorbed onto polystyrene substrates show higher nitrogen content than glass, indicating higher protein adsorption. Mean +/- SD, n = 6: 2 samples, 3 spots/ sample. Solid lines represent Langmuir isotherms fit to the data. X axis is offset from zero for clarity.*

The observations in both ^{125}I and XPS experiments are consistent with previous literature showing that hydrophobic surfaces generally exhibit higher levels of protein adsorption than hydrophilic surfaces. Fluorescence and ^{125}I-BSA studies have shown that more BSA adsorbs onto hydrophobic polystyrene [125] or $-CH_3$ self-assembled monolayers [126,47,127] than comparative hydrophilic surfaces of silica [125], -OH SAMS[126,47], or –COOH SAMs [127]. Another study also showed more albumin adsorbed onto a hydrophobic silanized glass than untreated glass [197]. The authors also observed a strong dependence on pH, with more protein adsorbing at lower pH values.

While the reason for this difference in amount of adsorbed BSA is not fully understood, previous studies have shown that BSA diffuses [128] and spreads [47] more

quickly on hydrophilic surfaces than hydrophobic surfaces. Faster diffusion and spreading rates on the glass surface could allow the BSA to spread out more quickly, inhibiting further protein adsorption onto the surface. On the polystyrene surface, slower diffusion and spreading rates would leave more open space on the polystyrene surface for further protein adsorption. This is described by the random sequential adsorption model, which states that when a single adsorbed molecule adheres to a surface, it defines a zone that excludes molecules that arrive at later times [28].

3.4.3 Calculation of coverage and thickness of BSA

By calculating the coverage and thickness of the adsorbed BSA films, more can be learned about the protein organization on the surfaces. At saturation (solution concentration > 0.1mg/ml), the protein layer adsorbed onto polystyrene was calculated to have a thickness of 8.1nm with a coverage of 40%. On the glass surfaces, both thickness and coverage was calculated to be lower than on the polystyrene surfaces. The BSA layer adsorbed onto the glass surfaces at saturation (solution concentration > 0.1mg/ml) was calculated to have a thickness of 2.4nm with a coverage of 22%. This is comparable to a previous study of BSA adsorption onto glass, which measured BSA film thicknesses of 2.5-3.5nm [211]. Therefore, the higher protein levels on polystyrene surfaces observed by both XPS and ^{125}I results from both greater coverage and thickness of the protein layer on polystyrene surfaces than glass surfaces. The presence of a thicker BSA layer on polystyrene compared to glass could indicate that the protein is in a more upright orientation and/or less spread conformation on polystyrene surfaces compared to glass surfaces.

It is somewhat surprising that full monolayer coverage was not reached, even at the highest solution concentrations. However, previous studies have shown BSA can adsorb in a submonolayer, patchy coverage. Alternatively, proteins can follow Freundlich adsorption [212]. Ithurbide et al., showed BSA had a surface coverage of 0.5 on chromium [189]. Other XPS studies of fibronectin [198] and collagen [213] have observed submonolayer coverage upon adsorption to polymers. It is unknown if submonolayer coverage is relevant to events in vivo, but it is an important consideration for interpreting the results from techniques such as ellipsometry and QCM, where full monolayer coverage is generally assumed for thickness calculations.

3.4.4 ToF-SIMS characterization of BSA adsorption onto polystyrene and glass surfaces

To evaluate BSA surface structure on the polystyrene and glass surfaces, PCA was performed on the ToF-SIMS data. PCA of ToF-SIMS data is sensitive to changes in protein orientation and conformation [35,81,79,83,73], so PCA can be used to identify differences adsorbed protein surface structure. PCA analysis of BSA adsorption onto polystyrene and glass surfaces showed differences between the two surfaces. PC1 captured 52% of the variance in the dataset, and shows some separation between the glass and polystyrene samples (Fig. 3.3a). Glass samples tend to load negatively, while polystyrene samples tend to load positively. PC1 scores on glass increase as a function of solution concentration. PC1 does not separate the polystyrene samples, indicating the surface structure of the protein is similar, regardless of the solution concentration.

Examining the PC1 loadings (Fig. 3.3b), peaks with strong negative loadings tend to be hydrophobic (Ala, Val, Leu, Gly). These amino acids correspond to BSA on glass at a low concentration. In the positive loadings, the peaks with the highest positive loadings are hydrophilic (Glu, Lys).

The observations from these ToF-SIMS studies are consistent with previous literature. Previous ToF-SIMS studies of BSA showed that conformation was dependent on amount adsorbed when the surface was polycarbonate treated to be hydrophilic. However, on hydrophobic polycarbonate, no conformation dependence was observed [214]. Another study using sum frequency generation to measure BSA adsorption onto silica and polystyrene surfaces observed a concentration-dependent signal on silica but not polystyrene [125]. Since sum frequency generation only detects ordered species at an interface, this indicates that the ordering of BSA changed at the silica surface as concentration changed, but did not change on polystyrene [125].

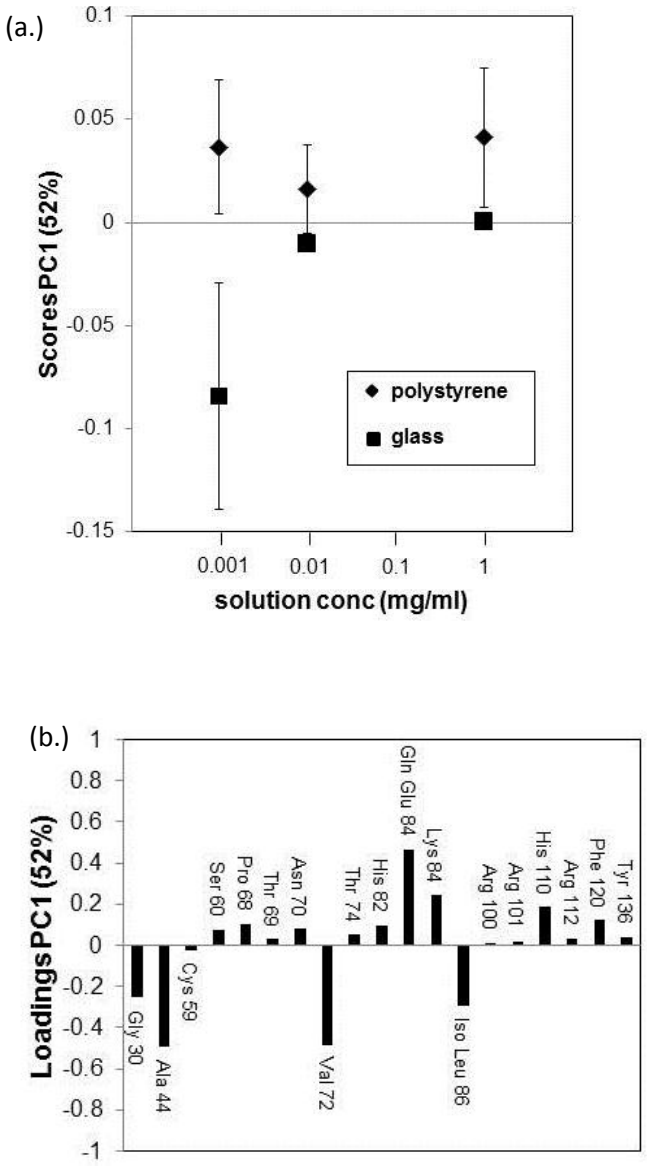

Fig. 3.3. PCA results for ToF-SIMS data from BSA adsorbed onto glass and polystyrene surfaces at a range of concentrations. *(a.) The PC1 (52% variance) scores for BSA adsorbed onto glass increase with increasing BSA surface coverage while the PC1 scores for BSA adsorbed onto polystyrene samples remain constant with increasing BSA coverage. Mean score +/- SD; n = 15 spectra (3 samples, 5 spots/sample). (b.) Loadings show hydrophobic amino acids tend to load negatively (Gly, Ala, Val, Leu), while hydrophilic amino acids tend to load positively (Glu, Lys).*

To further explore the differences between the exposure of hydrophilic and hydrophobic amino acids on the polystyrene and glass surfaces, intensity ratios of hydrophilic to hydrophobic acids were calculated. Hydrophobic/hydrophilic ratios have been

used previously to examine changes in adsorbed protein surface structure, since hydrophobic amino acids tend to be located within the core of a protein, and hydrophilic amino acids tend to be located on the solution-contacting surfaces [35]. As a protein unfolded or denatured upon adsorption onto a surface, the nonpolar amino acids in the core of the protein would be exposed. Nonpolar amino acids can be located on the outer surface of a protein, so the ratio is not an absolute measure of the extent of denaturation, but can give information about changes in protein structure. On polystyrene, the hydrophilic/hydrophobic amino acid ratio is constant over the range of solution concentrations tested (Fig. 3.4). This indicates that the relative exposure of the hydrophilic amino acids does not change. This is consistent with the PCA analysis, which showed the same scores in PC1 for BSA adsorbed onto polystyrene surfaces at all the solution concentrations tested.

In contrast, on glass surfaces the hydrophilic/hydrophobic amino acid ratio increases as the solution concentration increases. This increase indicates that more hydrophilic amino acids are exposed to the protein-solution interface at higher solution concentrations on glass than at lower concentrations. Since hydrophilic amino acids tend to be solvent-exposed, a higher hydrophilic/hydrophobic amino acid ratio could represent a more 'solution-like' conformation. This is consistent with previous studies using circular dichroism that showed albumin experienced a decreased loss of secondary structure as solution concentration increased when adsorbed to several types of SAMs [8].

At the highest surface coverages the ToF-SIMS results are similar for BSA adsorbed onto the two surfaces. At the lowest protein coverages, the adsorbed BSA films on glass surfaces have a lower hydrophilic to hydrophobic amino ratio than adsorbed BSA films on polystyrene surfaces. This suggests at low surface coverages the adsorbed BSA is more denatured on glass compared to polystyrene surfaces. The XPS and ^{125}I BSA experiments showed more protein was adsorbed onto the polystyrene surface than the glass surfaces. With less adsorbed BSA on the glass surface, the protein would have more room to spread out and unfold. Our thickness calculations also showed that the BSA layer is thicker on polystyrene compared to glass surfaces, which also supports that BSA is less denatured on the polystyrene surface compared to the glass surface.

This result contradicts with some previous studies measuring the secondary structure of BSA adsorbed onto SAMs containing different functional groups [57]. Sivarman and

Latour used CD to show that BSA α-helix and β-sheet content was closer to the native secondary structure when adsorbed onto an OH-terminated SAM compared to a CH_3-terminated SAM. In the studies here, the glass surface would be most closely represented by the OH-terminated SAM, which showed lower relatively exposure of hydrophilic amino acids from adsorbed BSA than polystyrene, which would be most closely represented by the CH_3-terminated SAM. However, results from SAM surfaces cannot necessarily be directly related to the surfaces here, as glass is not purely an -OH surface and polystyrene is not purely a -CH_3 surface. Alternatively, it is possible that the hydrophilic/hydrophobic amino acid ratio is not an appropriate measure of denaturation of BSA due to the location of polar and nonpolar amino acids within the protein. However, the thinner BSA layer observed on glass than polystyrene supports the hypothesis that BSA is more spread out, and therefore denatured, when adsorbed onto glass than polystyrene.

It could also be possible that the hydrophobic amino acid residues in adsorbed BSA orient preferentially toward the hydrophobic polystyrene surface, making the hydrophilic amino acids relatively more exposed to the protein-solution interface. This situation has been observed in a recent study of thick-film BSA adsorbed onto hydrophilic and hydrophobic surfaces [129]. Also, the difference surfaces could affect the secondary ion formation and ejection processes of the fragments from the adsorbed protein on the two surfaces (matrix effects). However, the matrix effects, if present, should have more influence on the absolute values of the hydrophilic to hydrophobic ratios than the trends of these ratios with increasing protein surface coverage.

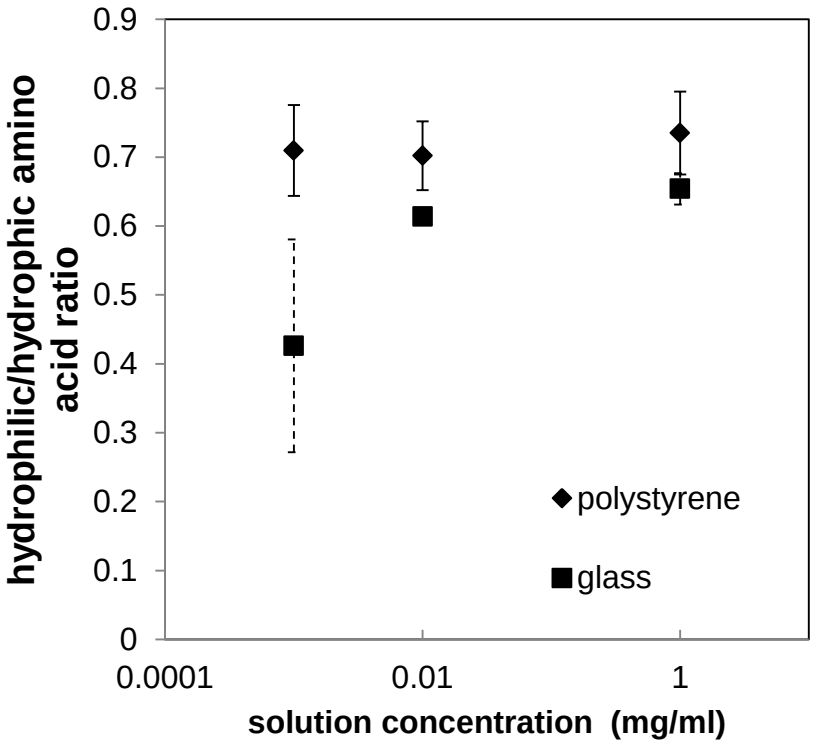

Fig. 3.4. Hydrophilic/hydrophobic amino acid intensity ratio from the ToF-SIMS data from BSA adsorbed onto polystyrene and glass surfaces. *On polystyrene, the ratio remains constant over the range of solution concentrations tested. On glass, the ratio increases as the solution concentration increases. Mean +/- SD; n = 15 spectra (3 samples, 5 spots/sample).*

3.4 Conclusions

The quantity and packing of BSA absorbed onto polystyrene and glass surfaces was examined and is summarized in Fig. 3.5. XPS and radiolabeled protein adsorption showed that more BSA adsorbed to the polystyrene surface than the glass surface for all solution protein concentrations. However, the protein packing on the two surfaces was different. On polystyrene surfaces, calculations showed that the protein film was thicker and had higher coverage than on the glass surfaces at saturation coverage (solution concentration > 0.1mg/ml). ToF-SIMS showed BSA surface structure was dependent on solution concentration when adsorbed onto glass, with PCA scores and the hydrophilic/hydrophobic amino acid ratio increasing as solution concentration increased. However, ToF-SIMS did not show a changes in PCA scores or hydrophilic/hydrophobic amino acid ration when BSA was adsorbed onto polystyrene surfaces at varying concentrations. The thinner protein layer and

lower hydrophilic/hydrophobic amino acid ratio when BSA was adsorbed onto glass than polystyrene suggests that BSA was more spread out, and potentially denatured when adsorbed onto glass than onto polystyrene.

3.4 Tables for Chapter 3

Table 3.1 XPS determined elemental compositions of BSA adsorbed onto PS and glass surfaces

Solution concentration (mg/ml)		% C	% O	% N	% Si	% Na	% F	% Zn
0								
	PS	74.5 (24.5)	17.2 (16.5)	ND	7.6 (7.8)	0.2 (0.4)	0.9 (0.6)	ND
	Glass	20.9 (6.1)	54.6 (3.8)	0.1 (0.3)	22.9 (2.0)	1.1 (0.6)	ND	0.4 (0.3)
0.0001								
	PS	87.0 (4.0)	6.9 (2.5)	3.5 (2.0)	0.8 (0.9)	ND	1.7 (0.9)	ND
	Glass	19.7 (4.2)	55.8 (1.9)	0.4 (0.4)	22.7 (1.7)	0.9 (1.0)	ND	0.4 (0.3)
0.001								
	PS	77.1 (9.0)	13.2 (5.0)	5.6 (0.6)	2.7 (3.3)	0.1 (0.2)	1.3 (0.8)	ND
	Glass	22	52.9 (3.3)	0.9 (0.2)	23.3 (1.4)	0.6 (0.7)	ND	0.4 (0.4)
0.01								
	PS	78.2 (9.0)	12.6 (6.2)	6.5 (0.7)	2.0 (3.7)	ND	0.8 (0.5)	ND
	Glass	25.9 (4.3)	49.2 (2.3)	2.7 (0.4)	20.6 (1.3)	0.3 (0.3)	1.3 (1.6)	0.1 (0.1)
0.1								
	PS	72.9 (15.8)	16.6 (11.2)	4.6 (1.7)	4.7 (4.8)	ND	1.6 (1.6)	ND
	Glass	25.6 (4.9)	49.7 (3.3)	3.7 (0.6)	20.1 (0.8)	0.4 (0.6)	0.1 (0.3)	0.3 (0.3)
1								
	PS	66.6 (10.4)	20.7 (6.8)	7.5 (0.4)	4.4 (4.3)	ND	0.8 (0.6)	ND
	Glass	29.5 (2.5)	45.4 (1.5)	5.6 (0.9)	18.7 (0.7)	0.2 (0.4)	0.6 (1.3)	0.1 (0.2)

Mean of 6 measurements on 2 samples. Standard deviation in parentheses. ND: Not detected

Table 3.2 Peaks used for the analysis of the ToF-SIMS data.

Ion	Amino acid	Mass	
CH_4N+	Gly	30.0351	Hydrophobic
C_2H_6N+	Ala	44.0492	Hydrophobic
C_2H_3S+	Cys	58.9941	Hydrophobic
C_2H_6NO+	Ser	60.0448	Hydrophilic
C_4H_6N+	Pro	68.0530	Hydrophobic
C_4H_5O+	Thr	69.0381	Hydrophilic
C_3H_4NO+	Asn	70.0331	Hydrophilic
$C_4H_{10}N+$	Val	72.0862	Hydrophobic
C_3H_8NO+	Thr	74.0660	Hydrophilic
$C_4H_6N_2+$	His	82.0527	Hydrophilic
C_4H_6NO+	Gln Glu	84.0474	Hydrophilic
$C_5H_{10}N+$	Lys	84.0855	Hydrophilic
$C_5H_{12}N+$	Iso Leu	86.0982	Hydrophobic
$C_4H_{10}N_3+$	Arg	100.0795	Hydrophilic
$C_4H_{11}N_3+$	Arg	101.0963	Hydrophilic
$C_5H_8N_3+$	His	110.0759	Hydrophilic
$C_5H_{10}N_3+$	Arg	112.0870	Hydrophilic
$C_8H_{10}N+$	Phe	120.0874	Hydrophobic
$C_8H_{10}NO+$	Tyr	136.0831	Hydrophilic

Chapter 4 Fibronectin adsorption onto titanium and sulfonated polystyrene

4.1 Abstract

Titanium is commonly used in orthopedic biomaterial implants. However, it remains a challenge to create an implant that fully integrates with the surrounding bone. Previous studies have shown osteoblast cells exhibit improved function when cultured on sulfonated surfaces compared to titanium surfaces (Helary, et al. *Acta Biomater* (2009) 5:124; Michiardi, et al. *Acta Biomat* (2010) 6:667). Since adsorbed proteins play an important role in the biological and cellular response to a material, this study characterized protein adsorption onto titanium and sulfonated surfaces. The adsorption of fibronectin (Fn), an important extracellular matrix protein, along with albumin, the most abundant protein in the blood, were examined.

Amount of protein on a surface is one characteristic that can control the biological response. Adsorption studies using ^{125}I labeling and x-ray photoelectron spectroscopy (XPS) showed a trend of higher amounts of protein adsorbed onto sulfonated polystyrene (PSS) than titanium (Ti) surfaces. Competitive adsorption of Fn and albumin did not show strong differences in the relative protein affinity of the two surfaces.

Time-of-flight secondary ion mass spectrometry (ToF-SIMS) and principal component analysis clearly showed differences between Fn adsorbed onto PSS and Ti surfaces, suggesting differences in protein structure. This could contribute to changes in exposure of cell binding sites within Fn, and result in changes in cell function.

These studies demonstrate that the adsorption of Fn and albumin are different on PSS and Ti surfaces. It is likely differences in protein amount and adsorbed Fn surface structure play a role in previously observed differences observed in osteoblast function.

4.2 Introduction

It is estimated that by 2030, close to 4 million hip and knee replacements will be performed annually in the United States [215]. Currently, titanium and its alloys are an

attractive choice for orthopedic implants due to their excellent mechanical properties [216] and corrosion resistance [217,218].

However to achieve successful integration of the implant into the bone tissue, termed osseointegration, cells must form a direct interaction with the metal surface and avoid producing an interfacial fibrous layer [219-221]. The inability of cells to integrate the implant into the existing bone can lead to implant loosening and failure. To repair or replace a failed implant, revision surgery is required, leading to greater cost and suffering for the patient [222]. The life span of a hip implant is 10-15 years [223]. As patients continue to live longer with more active lives, it is even more important to extend the life of an implant *in vivo*. To achieve this goal, the osseointegration of orthopedic implants into bones must be improved.

There have been many attempts to coat or modify titanium surfaces to address the ongoing challenge of osseointegration. As reviewed by Liu et al., [224] strategies include modifying surface roughness, UV treatment, ion implantation, manipulating the oxide layer and coating with protein. These strategies have achieved some success, but there is still additional scope for improving titanium surface properties for use in biomedical applications. Polymer grafting is another technique that has been recently shown to improve cellular response *in vitro* [225]. Titanium surfaces with sodium styrene sulfonate (NaSS) grafted onto the oxide surface layer showed greater adhesion strength of osteoblasts than untreated titanium [225].

To understand why cells interact differently with different surfaces, we need to understand how proteins adsorb onto those surfaces. *In vitro* and *in vivo*, a synthetic surface is quickly coated with a layer of adsorbed protein, which cells then contact. Among these proteins are extracellular matrix (ECM) proteins. In normal tissue, the ECM provides important signals to the surrounding cells [226]. Therefore the organization of ECM proteins on the titanium surface can provide signals to the surrounding cells [5].

The presentation of fibronectin (Fn) on implant surfaces could be an important cue to bone osteoblasts that are regenerating the bone tissue around the implant. Fn is a large glycoprotein present in the bone ECM [132,133] where it is produced by osteoblasts [227]. Fn is necessary for osteoblast adhesion [228-232] and regulates osteoblast function including

proliferation [134], differentiation [135], protein expression [233], and survival [234,235,136] through integrin signaling.

Since Fn plays an important role in ECM signaling, cell function could be influenced by the conformation of Fn adsorbed onto synthetic surfaces. Indeed, previous studies have shown that the surface to which Fn is adsorbed does affect osteoblast function. Adhesion [18,19,17,20], spreading [20], and mineralization [18] of osteoblasts and 3T3 osteoblast-like cells were different when Fn was adsorbed onto different surfaces including polystyrene [18,20], tissue culture polystyrene [18,20], collagen [18], glass [17], and SAMs [19].

Previous investigations have attempted to elucidate changes in Fn on different surfaces that could be the cause for the observed differences in cell behavior. Fn conformation has been tested on a variety of surfaces including polystyrene [41,139,236,237], tissue culture polystyrene [139,236,141,142], glass [142,147,238], SAMs [137,239,138,140,240,241], titanium [242,176,243,72], and sulfonated polystyrene [244,237]. Previous studies clearly support that the surface to which Fn is adsorbed can influence its conformation and the amount adsorbed, using measurements including ToF-SIMS [72], FTIR [41,137,239,138], antibody binding [236,140-142,241], integrin binding [240], elution ability of Fn from a surface [242,139], fluorescence [238,147,245], and radiolabeled protein adsorption [237,176].

Albumin is another protein that could influence cellular response to implants. It is the most concentrated protein in the blood at 40mg/ml [126]. Albumin is generally considered to be a non-adhesive protein, but it is present in the bone ECM [246]. It is expressed by bone marrow stem cells and osteoblast-like 3T3 cells [247]. However, its role in osteoblast adhesion is not fully defined. *In vitro*, osteoblast-like 3T3 cells showed greater adhesion [248] and proliferation [249,250] in the presence of albumin than when albumin was not present. *In vivo* during fracture healing in rats, high amounts of albumin are observed at the healing site [251]. Macrophages have also been shown to adhere to albumin-coated fluorinated substrates, which could be important for modulating the healing response [252]. Albumin is also thought to be important for lubrication [28]. These studies suggest that albumin adsorption onto titanium implants could be an important consideration in osseointegration.

Studies of single protein adsorption can give us useful information about how proteins will interact with a surface. However, the *in vivo* environment is a complex mixture of proteins, so competitive adsorption studies can give further insight into how proteins interact with each other on a surface. Previous studies of competitive adsorption show the presence of albumin has different effects on Fn affinity on different synthetic surfaces including polystyrene [204], tissue culture polystyrene [56], glass [204,252], SAMs [126,140], titanium [242], and fluorocarbon surfaces [56,252]. Competitive adsorption of Fn and albumin has also been shown to influence osteoblast adhesion *in vitro* on titanium [253,254].

In the studies presented here, Fn adsorption behavior is characterized on titanium and sulfonated polystyrene (PSS) surfaces to mimic the sulfonate modification previously performed on titanium surfaces. The influence of albumin on Fn adsorption is also examined. Radiolabeled protein adsorption and XPS were used to determine the amount of adsorbed Fn on the two surfaces. To learn about the differences in orientation and conformation of Fn on the surfaces, ToF-SIMS was used. Previous studies have shown that ToF-SIMS can distinguish between proteins in different orientations [68,69] and conformations on different surfaces [70-72,35,73,74].

4.3 Methods

4.3.1 Preparation of Ti substrates

Titanium samples (Ti) were prepared by electron beam evaporation of thin Ti layers (~50nm) onto 1cm^2 silicon wafers. Following deposition, Ti substrates were cleaned by subsequent sonication in dichloromethane, acetone, and methanol.

4.3.2 Preparation of sulfonated polystyrene (PSS) substrates

Sulfonated substrates were made by sulfonating polystyrene surfaces. Polystyrene petri dishes (Corning) were allowed to react with concentrated sulfuric acid for 1-24h at room temperature for initial experiments, and for 1h for all protein adsorption substrates. Then petri dishes were sonicated in water for 1h to remove any sulfuric acid non-covalently

associated with the surface. Petri dishes were diced into 1cm^2 pieces, then sonicated again in water, dried using a stream of nitrogen, then stored in an inert nitrogen atmosphere until use.

4.3.3 Quantification of surface sulfonate concentration

The number of sulfonate groups on the sulfonated polystyrene surface was quantified according to the method of Helary, et al. [175]. Briefly, samples were immersed in an aqueous solution of toluidine blue ($5x10^{-4}$ M) for 6h. Then samples were rinsed with an aqueous solution of NaOH ($5x10^{-3}$ M) to remove uncomplexed dye. Toluidine blue was decomplexed from the surface by immersion in 50vol% acetic acid for 24h. Then absorbance of the solution was measured at 633nm and compared to a standard curve for toluidine blue. The number of sulfonate groups was corrected for nominal surface area to determine the concentration of sulfonate groups on the surface.

4.3.4 Protein adsorption

Substrates were allowed to equilibrate overnight with degassed phosphate buffered saline (PBS) (137mM NaCl, 2.7mM KCl, 10mM phosphate) pH 7.4 at room temperature, then Fn or BSA solutions at the desired concentrations were incubated with substrates for 2h at 37^{o}C. Following adsorption, substrates were rinsed in PBS to remove loosely bound protein, then water to remove buffer salts. Samples were dried with a stream of nitrogen, then kept under inert nitrogen atmosphere until analysis.

4.3.5 ^{125}I protein adsorption

^{125}I protein adsorption was performed to determine the amount of Fn and BSA adsorbed onto Ti and PSS surfaces. Competitive adsorption effects were examined using binary protein solutions containing 1:1 and 1:10 mass ratios of Fn:BSA [56]. In plasma, BSA is approximately 1000 times more concentrated than Fn [56]. However, that ratio would not be as high in the extracellular matrix.

BSA (Sigma) and human Fn (Sigma) were labeled using Na^{125}I (PerkinElmer, Waltham, MA) according to the method of Horbett [64]. A 2:1 molar ratio of ICl to protein was used. Unincorporated ^{125}I was separated from labeled protein by two passes through

Econo Pac 10DG desalting columns (Bio-Rad Laboratories, Hercules, CA). Iodinated protein was stored at -20°C and used within 2 weeks of preparation.

Protein adsorption was carried out based on previously published protocols[176,126]. Briefly, a 10µl droplet of degassed PBS (110mM NaCl, 10mM NaI, 10mM citric acid, 8mM phosphate, 3mM NaN_3) at pH 7.4 was placed on the substrate and allowed to equilibrate for one hour at room temperature. Then 10µl of ^{125}I-labeled protein solutions at 2x concentration were added to the existing buffer droplets on the substrates, resulting in 20µl droplets containing the desired concentration. Protein solutions were incubated with substrates for 2h at 37^{o}C. Samples were washed with PBS for 30-90 seconds to remove loosely bound protein following the procedure of Horbett [64]. Retained radioactivity was measured using a gamma counter, then protein surface concentration was calculated from retained radioactivity (corrected for background), specific activity of the protein solution, and surface area of the sample. All conditions were repeated in triplicate at least twice on separate days. Non-radioactive iodine was included in all buffers to suppress adsorption of free ^{125}I to the surface [64].

Adsorption of Fn and BSA were measured individually (single component adsorption) at a range of solution concentrations. Measurement of competitive adsorption of Fn and BSA was performed in subsequent experiments, using ^{125}I BSA mixed with unlabeled Fn in one experiment, then ^{125}I Fn mixed with unlabeled BSA in a separate experiment. Fn and BSA were mixed in mass ratios of 1:1 and 1:10.

The mass per area of protein adsorbed (Q) in a radiolabeled protein adsorption assay can be described as

$$Q = \gamma t \rho \qquad \text{(Eq. 4.1)}$$

where ρ is the specific weight of the protein (1.378g/cm^3) [177], γ is the fraction of surface covered, and *t* is the thickness of protein layer.

4.3.6 XPS

XPS analysis was performed to characterize the atomic composition of the substrates. XPS was also used to create a protein adsorption isotherm. The unique nitrogen signal in the adsorbed protein was tracked as a measure of protein adsorption.

XPS data were collected on a Surface Science Instruments S-Probe instrument with a monochromatized aluminum Kα x-ray source and electron flood gun for charge neutralization. Survey and detail scans were acquired at a pass energy of 150eV and a take-off angle of 55°. The take-off angle is defined as the angle between the sample surface normal and the axis of the analyzer lens. For each concentration, two samples were analyzed and three spectra were collected on each sample.

Angle-resolved measurements were conducted at 0°, 55°, and 75° take-off angles between the detector lens axis and the sample surface normal, with a 12° aperture placed over the analyzer lens. The number of scans taken at different angles was adjusted to optimize the signal-to-noise ratio while minimizing X-ray induced sample damage to the samples.

Spectra were analyzed using the Service Physics ESCA 2000A analysis software. Full XPS elemental compositions of all samples are listed in Tables 4.3 and 4.4.

In XPS, when a substrate is covered by an overlayer, the signal from the overlayer is related to the fractional coverage and overlayer thickness by the following equation [61]:

$$I_k = I_o \gamma \left[1 - e^{(-t/\lambda \cos\theta)}\right] \qquad \text{(Eq. 4.2)}$$

Where I_k is the measured intensity, I_o is the intensity of a pure sample of the substance, γ is the fractional surface coverage, and t is the protein overlayer thickness, $\lambda$is the inelastic mean free path of the electron, and θ is the photoelectron takeoff angle. Atomic percent was used as a substitute for intensity in Eq. 4.2 [178,255] . To determine I_o for proteins, XPS analysis was performed on a thick film of air-dried BSA (65.7%C, 18.8%O, 15.5%N). This thick-film value was used for both Fn and BSA.

4.3.7 ToF-SIMS

ToF-SIMS analysis was performed to examine differences in Fn conformation on Ti and PSS.

ToF-SIMS data were acquired on an ION-TOF 5-100 instrument (ION-TOF GmbH, Münster, Germany) using a Bi_3+ primary ion source under static conditions (primary ion dose $<10^{12}$ ions/cm^2). Spectra were obtained from 100 μm x 100 μm areas and five positive ion spectra were collected from each sample. At least two replicates were analyzed per sample type. A low-energy electron beam was used for charge compensation. Mass resolution (m/Δm) of the positive ion spectra was typically between 5500-7000 for the m/z = 27 peak. Mass scales of each positive secondary ion spectrum were calibrated to the CH_3^+, $C_2H_3^+$, and $C_3H_5^+$ peaks before further analysis. The mass scales of the negative secondary ion spectra were calibrated using the CH^-, O^-, OH^-, and C_2H^- peaks. Negative secondary ions detected from the PSS surfaces are listed in Table 4.2.

Peaks were identified which corresponded to unique amino acid peaks. Amino acid peaks that overlapped with substrate peaks were then eliminated using the following criteria. If the normalized intensity of a peak on the bare substrate was greater than 25% of the protein normalized peak intensity, that peak was assumed to have a significant contribution from the substrate and was not included in the amino acid peak list used for analysis. Peaks used for analysis are listed in the appendix Table 4.5, along with the corresponding amino acid. PCA processing of ToF-SIMS data from adsorbed proteins has been described extensively elsewhere [78,83,79]. Prior to PCA processing the peaks were mean centered and normalized to the sum of the selected peaks. Analysis was performed using a series of MATLAB (MathWorks, Inc., Natick, MA) scripts written by NESAC/BIO (see http://mvsa.nb.uw.edu).

4.4 Results

4.4.1 Optimizing sulfonation time

Sulfonation of polystyrene was achieved by reacting polystyrene substrates with concentrated sulfuric acid. To determine the time dependence of sulfonation, reactions were carried out for 1, 4, and 24 hours. Using XPS to measure the atomic percentage of sulfur in the sample gives an indication of the extent of surface sulfonation. Without exposure to

sulfuric acid, sulfur content of the polystyrene substrates was 0. The atomic percentage of sulfur was similar for the 1 and 4 hr reaction time points, then decreased slightly for the 24 hr time point (Fig. 4.1a).

The oxygen/sulfur ratio also gives information about the composition of the surface. For a pure polystyrene sulfonate surface, the theoretical oxygen/sulfur ratio is 3. In these samples, the O/S ratio was over 5 for sulfonation reaction reaction times of 1 and 4 hours (Fig. 4.1b). The oxygen/sulfur ratio increases at the 24h reaction time, suggesting that other species on the surface are being oxidized or oxidized contaminants might be deposited onto the surface. For these reasons, a reaction time was limited to 1 hour for all further experiments.

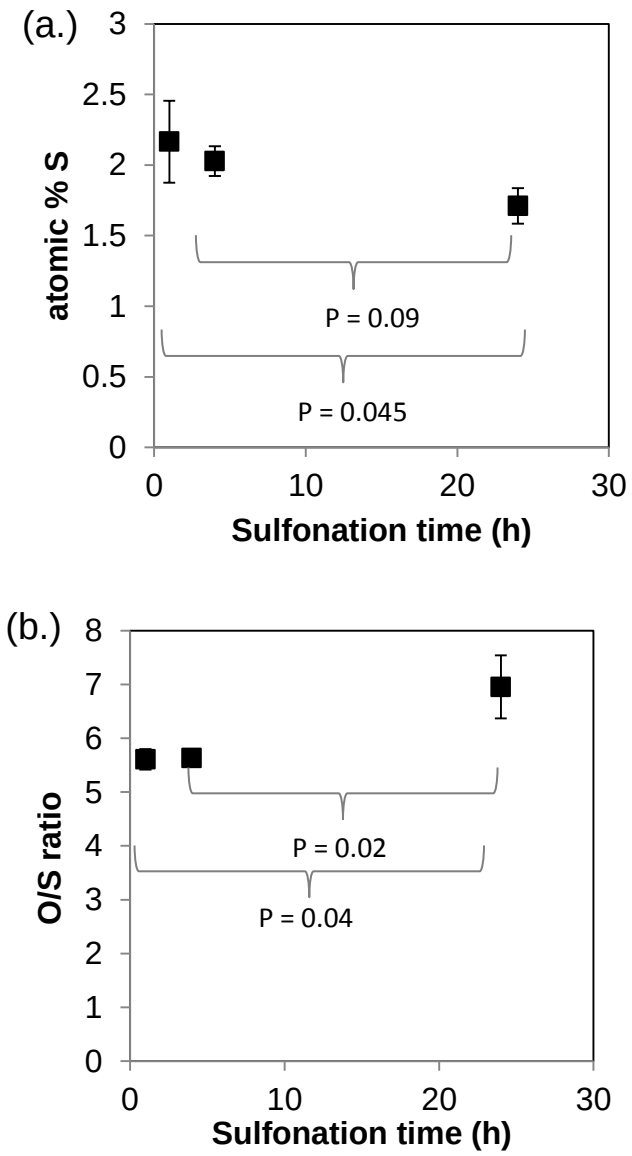

Fig. 4.1 XPS of sulfonated polystyrene. *(a.) Atomic % sulfur and (b.) Oxygen/sulfur ratio. Mean of 3 spots on one sample +/- SD.*

4.4.2 Quantifying the number of sulfonate groups on the PSS surface

We quantified the number of sulfonate groups on the PSS surfaces that had been sulfonated for 1h using the toluidine blue assay. From measurements of the toluidine blue complexation with the PSS surfaces, the number of sulfonate groups on the surface was determined to be ~$1.5 \times 10^{15}/cm^2$. The hydrodynamic radius of a sulfonate group is 0.12nm [256]. Assuming the sulfonate groups are concentrated in the outermost atomic layers at the

solution-polymer interface, the coverage of sulfonate groups on the surface was estimated to be ~65% (Table 4.1).

4.4.3 XPS characterization of sulfonated polystyrene

Comparing the high resolution C1s spectra of polystyrene to polystrene treated with sulfuric acid, some differences are observed. Following sulfonation, the full width at half max of the main peak increase from 1.3eV for untreated PS to 1.8eV for sulfonated PS (Fig. 4.2). This likely corresponds to oxidized carbon groups introduced during the sulfuric acid treatment [257]. Fitting the high resolution C 1s spectrum, after sulfonation we also detect the π^* shakeup satellite at 292eV from the aromatic rings of the styrene, demonstrating that the majority of styrene rings remain intact following sulfuric acid treatment. The fitted spectra show that in the untreated PS sample, the shakeup satellite contains 3.8% of the area of the C1s peaks. The fitted spectra show that after sulfonation, the shakeup satellite contains 2.6% of the area of the C1s peaks.

The high resolution sulfur 2p spectrum had low signal, but showed a single peak centered at 168.8eV (Fig. 4.3), consistent with previous XPS studies of sulfonated polystyrene [258-260]. The sulfur 2p peak at 169 indicates highly oxidized sulfur [257]. The high resolution oxygen 1s spectrum exhibits a single peak centered at binding energy 532.5eV (Fig. 4.4). This is consistent with previous reports of SO_3 groups in sulfonated polymers [258-260].

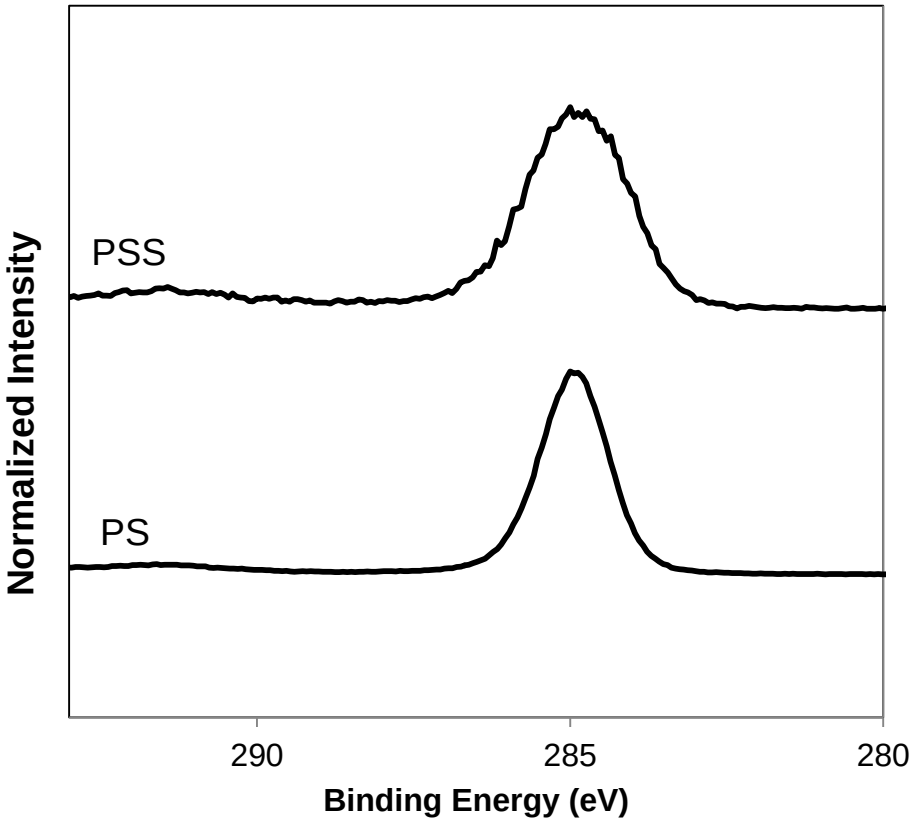

Fig. 4.2 High resolution carbon 1s XPS spectra of polystyrene and sulfonated polystyrene. *Spectra offset for clarity.*

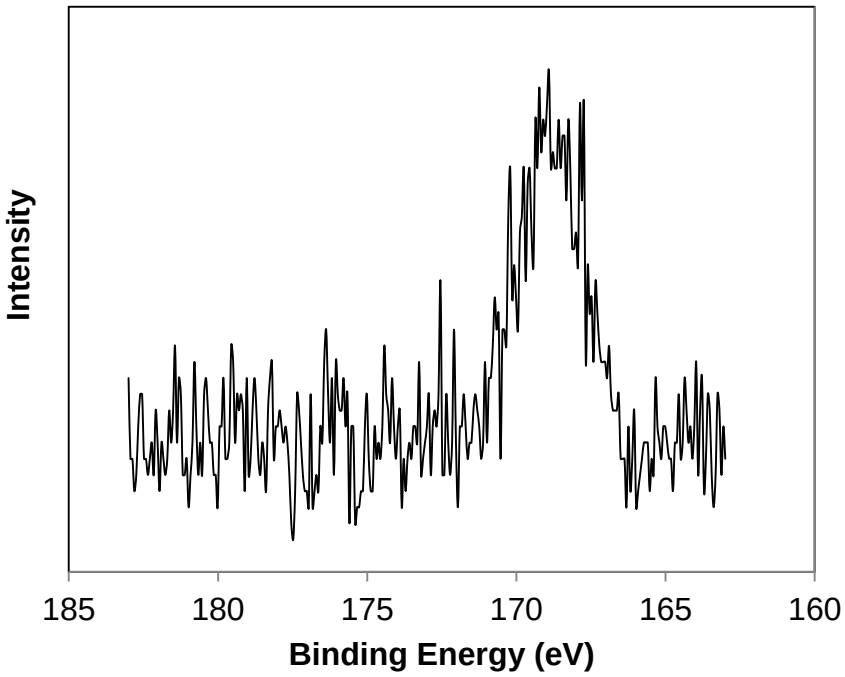

Fig. 4.3 High resolution sulfur 2p peak of sulfonated polystyrene

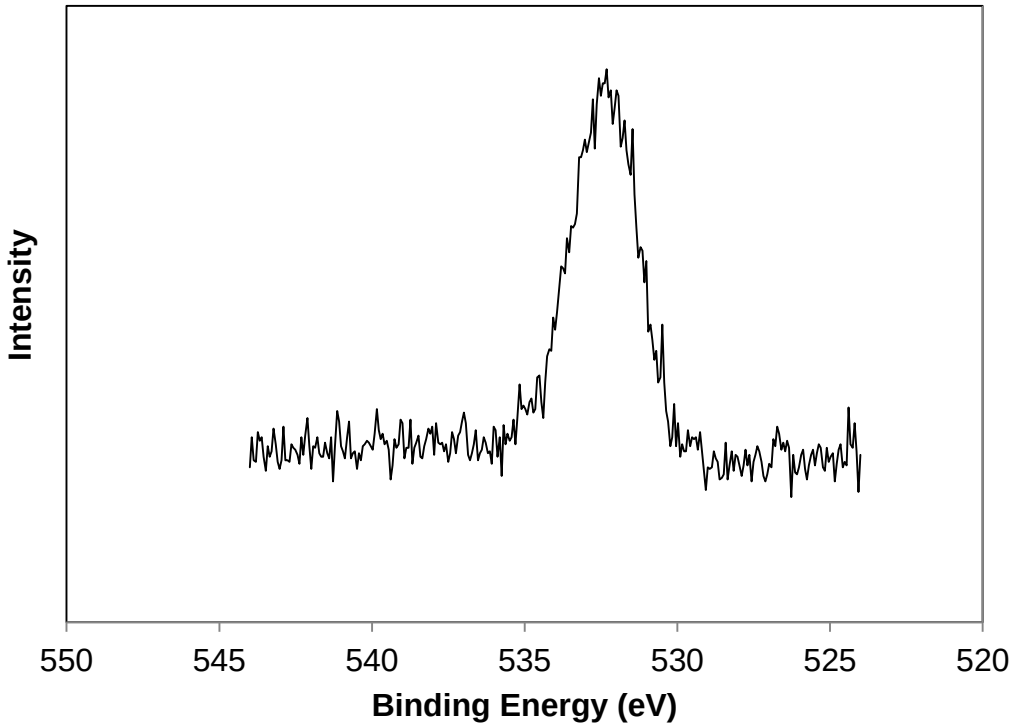

Fig. 4.4 High resolution oxygen 1s peak of sulfonated polystyrene

The XPS atomic composition of polsytrene samples sulfonated for 1 hour showed 1.8 atomic % sulfur (mean of 12 spots on 4 samples). If the full XPS sampling depth of the surface was composed entirely of sulfonated styrene groups, 8.3 atomic % sulfur would be expected (1 sulfur atom, 3 oxygen atoms, 8 carbon atoms per repeat unit).

We calculated the thickness of the styrene sulfonate later according to Eq. 4.2, using an inelastic mean free path of 0.9nm for sulfur 2p electrons [261]) and photoelectron take-off angle θ of 55^{o}. Using atomic percent sulfur as a substitute for intensity [178], a sulfur content of 1.8 atomic % corresponds to a styrene sulfonate layer 0.1nm thick if coverage was 100%. This supports submonolayer coverage, as was observed with the toluidine blue assay.

Assuming the sulfonate layer is 0.24nm thick (2x the hydrodynamic radius of 0.12nm), then 1.8 atomic % sulfur corresponds to a surface coverage of approximately 40%, similar but slightly lower than estimated from the toluidine blue asssay. The toluidine blue assay coverage estimate could be overstated by using nominal surface area in the calculation. Taking surface roughness into account would reduce the calculated coverage.

We also performed angle-resolved XPS (Fig. 4.3) to determine if the sulfonate functionalization was limited to the outermost surface, or if the sulfuric acid penetrated deeper into the polystyrene. By varying the photoelectron takeoff angle, different sampling depths can be probed. A takeoff angle of 0 degrees results in the largest sampling depth (~10nm), while a glancing takeoff angle of 75 degrees results in a shallower sampling depth (~2nm).

The PSS sample analyzed in the angle dependent study had a slightly lower atomic % sulfur than the mean of samples used for the previous calculations (1.4 versus 1.8 atomic %, respectively). This difference could be due to differences in the acceptance angle introduced by the aperture used for the angle dependent studies. The difference could also be due to a lower level of sulfonation for this sample due to experimental variability. However, even though the sulfur content is slightly lower, there is an angle dependence of the sulfur signal in the PSS (Fig. 4.5). The observed atomic % sulfur increases from 1.1 to 2.0 as the takeoff angle increases from 0 to 75°. Without exposure to sulfuric acid, sulfur content of the polystyrene substrates was 0.

This is consistent with the sulfonate groups concentrated in the outermost atomic layers of the surface and the sulfuric acid not penetrating into the polystyrene substrate. This is in agreement with previous reports using sulfuric acid to sulfonate polystyrene [262].

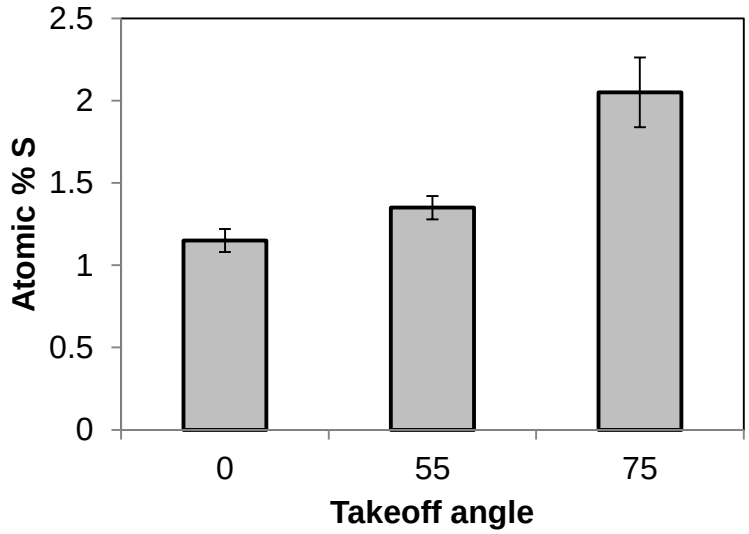

Fig. 4.5 Atomic percentage sulfur of the PSS samples as a function of photoelectron takeoff angle.

4.4.4 ^{125}I protein adsorption

Radiolabeled protein adsorption was used to determine the surface concentration of Fn and BSA adsorbed onto the Ti and PSS surfaces from single and binary protein solutions. As the concentration of the single component Fn solution was increased by three orders of magnitude, the surface coverage increased on both the Ti and PSS surfaces (Fig. 4.6). Approximately two-fold higher Fn surface coverage was observed on the PSS surface compared to the Ti surface, with a maximum Fn surface concentration of >700ng/cm^2 on PSS, and ~400ng/cm^2 on Ti.

The surface concentrations measured in this study on PSS surfaces are consistent with literature values of ^{125}I-labeled Fn adsorption onto sulfonated polystyrene surfaces. Previous publications have reported Fn surface concentrations of 200-300ng/cm^2 from solution concentrations of 10-20μg/ml [237,263]. Reports of adsorbed Fn surface concentration on other surfaces are also in the range of 300-1000ng/cm^2 (onto polystyrene [264,265,237], TCPS[264-266], glass [267], and mica [78]). The adsorbed Fn surface concentrations measured on Ti surfaces here are lower than one previously published report showing 700-

1300ng/cm^2 Fn adsorbed onto TiO_2 surfaces from a 20μg/ml Fn solution [176]. These differences could be due to surface roughness or other differences in substrate preparation between the current study and the previous report. In addition, to the authors' knowledge this is the first direct comparison of Fn surface concentration adsorbed onto Ti and PSS, so the relative amounts of Fn on the two surfaces might be more informative than the differences of absolute amounts from different previous studies. Assuming Fn forms a continuous film when adsorbed from a solution concentration of 100μg/ml, the film thickness was calculated to be 13.3nm on PSS and 7.6nm on Ti according to Eq. 4.1. These values are similar to previous values reported in atomic force microscopy studies (5-10nm on mica and poly(lactide-co-glycolide) surfaces [268]) and quartz crystal microbalance (QCM) studies (10nm on a poly(hydroxymethylsiloxane) surface [191]), so the thicknesses calculated here are similar to previously published reports.

In single component ^{125}I BSA adsorption, similar amounts of BSA adsorbed onto the sulfonated polystyrene surfaces compared to titanium surfaces (Fig. 4.7), with more BSA adsorbing to the PSS surfaces. At a solution concentration of 100μg/ml, there appears to be some aggregation of BSA on the surface, as the BSA surface concentration is higher than we would expect for a monolayer (<1000ng/cm^2) [210]. At higher BSA solution concentrations even higher BSA surface concentrations were observed, providing further indications of BSA aggregation on the Ti and PSS surfaces (data not shown).

Comparison of the ^{125}I BSA results to the XPS analysis of adsorbed BSA (Fig. 4.13) also suggests aggregation of ^{125}I BSA at 100μg/ml on the Ti and PSS surfaces. The XPS atomic % N is on the order of what we would expect for a monolayer of BSA [255], but the surface concentration measured by ^{125}I BSA adsorption is much higher than a monolayer. Assuming BSA forms a continuous film when adsorbed from a solution concentration of 100μg/ml, the film thickness was calculated to be 13.7nm on PSS and 10.8nm on Ti, according to Eq. 4.1. Previous studies using ellipsometry and QCM have reported adsorbed BSA film thickness in the range of 1-3nm on fluorinated SAM surfaces [255], TiO_2 surfaces [46], gold surfaces [269], and chromium surfaces [189], which would be representative of monolayer coverage. Therefore, samples made with BSA solution concentrations of 100μg/ml or higher are not necessarily representative of an adsorption process onto the

surface, but rather aggregation. Aggregation could have occurred during storage, during the labeling process, or during adsorption.

BSA aggregation on surfaces has been reported in the literature, including a study showing 5000ng/cm^2 ^{125}I human serum albumin adsorbed onto titanium surfaces, with surface saturation reached between 1-5mg/ml solution concentration of HSA [270]. Albumin surface concentrations approaching 6000ng/cm^2 have also been reported on surfaces of low temperature isotropic carbon [51] and silica [51] using ^{125}I labeling techniques. Other reports have shown albumin surface concentration on polymers in the range observed here, including PVC (3000ng/cm^2), silicone (2500ng/cm^2), PE (2000ng/cm^2), [257], and polyurethane (1600ng/cm^2) [271].

Another possible explanation for the high surface concentration values could be the adsorption of free ^{125}I onto the surface. However, the BSA and Fn were labeled using the same procedure and the two protein solution would likely contain the same amount of free ^{125}I. High surface concentration values were only measured using ^{125}I BSA, which suggests that free ^{125}I was not responsible. With both Fn and BSA, steps were taken to minimize the potential effect of free ^{125}I adsorption. All surfaces were preincubated with buffer containing unlabeled NaI, and NaI was present in the buffer at all times to prevent adsorption of free ^{125}I. For the ^{125}I BSA single component adsorption samples, following measurement of radioactivity, samples at higher BSA concentrations were subjected to additional rinsing to ensure that samples were well rinsed and did not contain weakly bound protein. Additional buffer and water rinses did not substantially reduce measured radioactivity present on the samples (<10%.

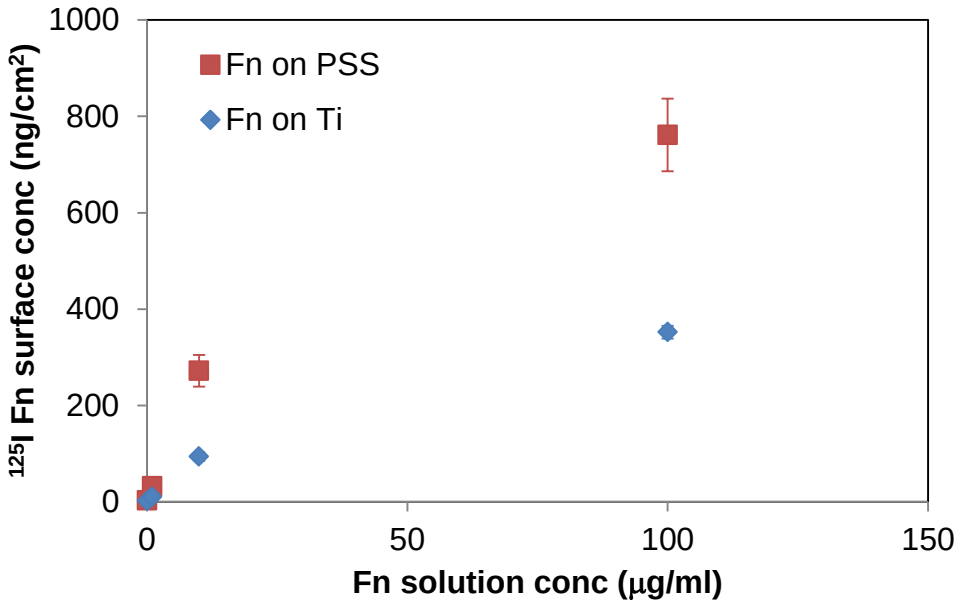

Fig. 4.6 ^{125}I Fibronectin adsorbed onto Ti and sulfonated polystyrene surfaces. *More fibronectin (approximately 2-fold) adsorbs onto the sulfonated polystyrene surfaces than titanium surfaces at all measured solution concentrations. N = 6-9. Mean +/- SEM.*

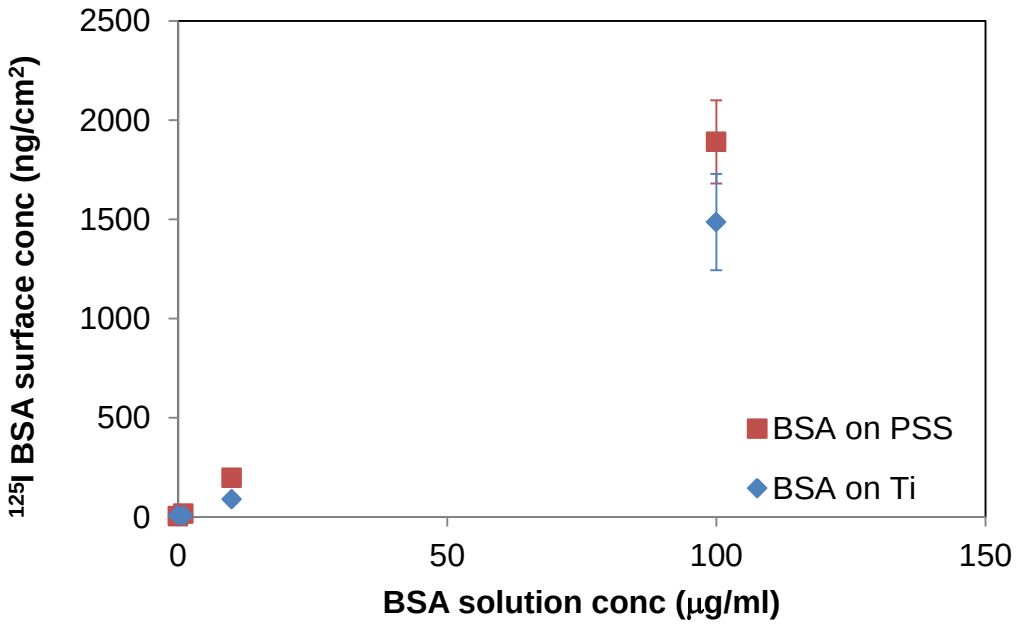

Fig. 4.7. ^{125}I BSA adsorbed onto Ti and sulfonated polystyrene surfaces. *Similar amounts of BSA adsorb onto the sulfonated polystyrene surfaces than titanium surfaces. N = 6. Mean +/- SEM.*

^{125}I protein adsorption was also used to determine the amount of Fn and BSA adsorbed from binary mixtures. In separate experiments, ^{125}I Fn mixed with unlabeled BSA

or unlabeled Fn mixed with ^{125}I BSA were coadsorbed onto Ti and PSS surfaces at mass ratios of 1:1 and 1:10. When Fn and BSA were coadsorbed in a 1:1 ratio, more protein adsorbed onto the PSS than Ti in all cases (Fig. 4.8). The total amount of protein was higher on PSS than Ti, as well as the amount of BSA or Fn individually. These results are consistent with the results from the single component films.

To examine the surface composition for potential enrichment of Fn on the surface compared to the solution composition, we took a ratio of the adsorbed masses of Fn:BSA on the surface (Fig. 4.9). Enrichment of Fn compared to the solution composition was observed in one case, in which the solution consisted of 1μg/ml Fn:1μg/ml BSA adsorbed onto PSS surfaces. In all other cases, the surface concentration of Fn was relatively lower than the solution concentration, suggested BSA adsorbed preferentially onto these surfaces. The relative amount of Fn was similar on the two surfaces, although somewhat higher on the PSS surface than the Ti surface.

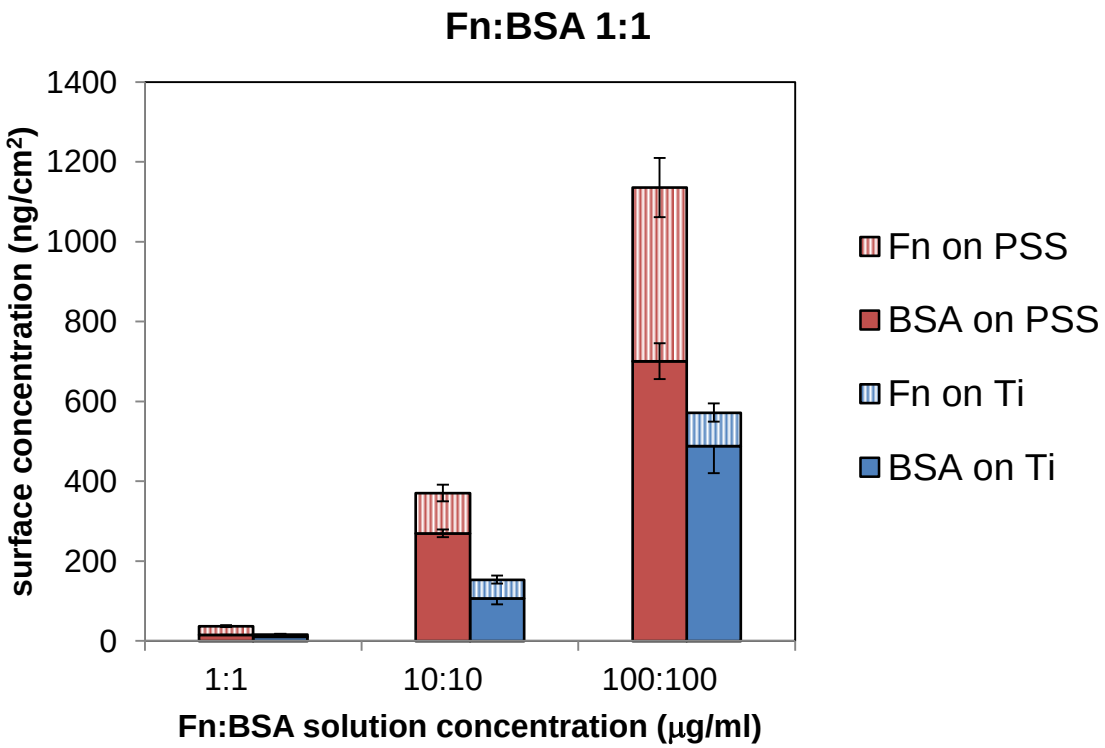

Fig. 4.8. Competitive adsorption of fibronectin and BSA at 1:1 solution concentration mass ratio onto titanium and sulfonated polystyrene surfaces. *More protein adsorbed onto the PSS than Ti in all cases. The total amount of protein was higher on PSS than Ti surfaces, as well as the amount of BSA or fibronectin individually. N = 6-9. Mean +/- SEM.*

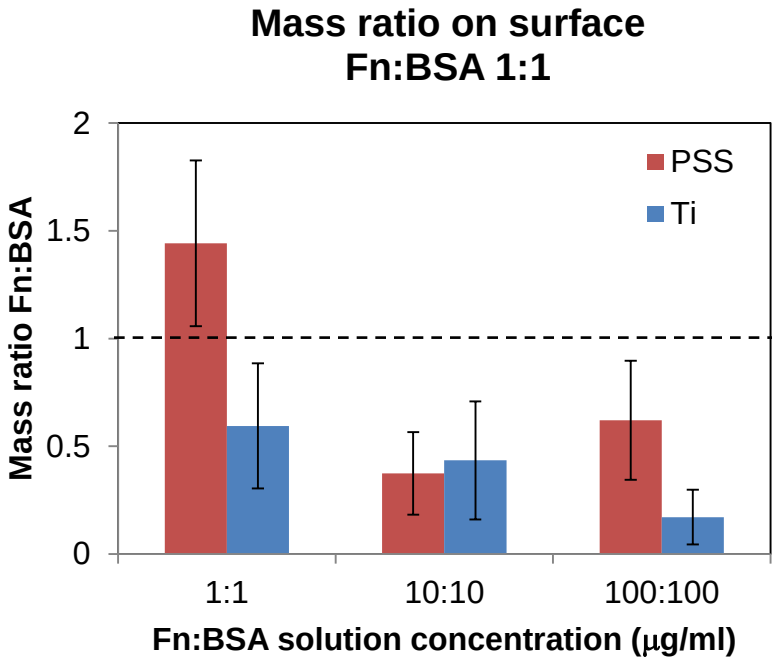

Fig. 4.9. Relative surface concentration of fibronectin and BSA adsorbed at 1:1 mass ratio solution concentration. *To examine the relative amount of adsorbed fibronectin compared to BSA on the two surfaces when adsorbed in a 1:1 mass ratio in solution, we took a ratio of the surface concentration of the two proteins. If the surface composition matched the solution composition, the ratio would be 1 in all cases (dashed line). Mean +/- SD.*

In vivo, there is more BSA than Fn present in the plasma, with BSA approximately 1000 more concentrated by mass [56]. Therefore, it is also useful to determine the amount of Fn and BSA adsorbed onto Ti and PSS when BSA is present in higher amounts. When Fn and BSA were adsorbed onto the surfaces at Fn:BSA solution mass ratios of 1:10, more total protein adsorbed onto the PSS than Ti at all solution concentrations (Fig. 4.10). The surface concentration of BSA was higher on PSS than Ti surfaces. The surface concentration of adsorbed Fn was similar on the two surfaces. Following measurement of radioactivity, samples at higher BSA concentrations were subjected to additional rinsing to ensure that samples were well rinsed. Additional buffer and water rinses did not substantially decrease the counts for the samples (<10%).

To examine the relative amount of adsorbed Fn compared to BSA on the two surfaces when adsorbed in a 1:10 mass ratio in solution, we took a ratio of the surface concentration of the two proteins (Fig. 4.11). If the surface composition matched the solution composition, the ratio would be 0.1 (dashed line). On the Ti surfaces, the surface composition approached

the solution composition. However, in all cases the surface concentration of Fn is relatively lower than the solution concentration, indicating BSA adsorbed preferentially onto these surfaces. Overall, the relative amount of Fn is similar on the two surfaces.

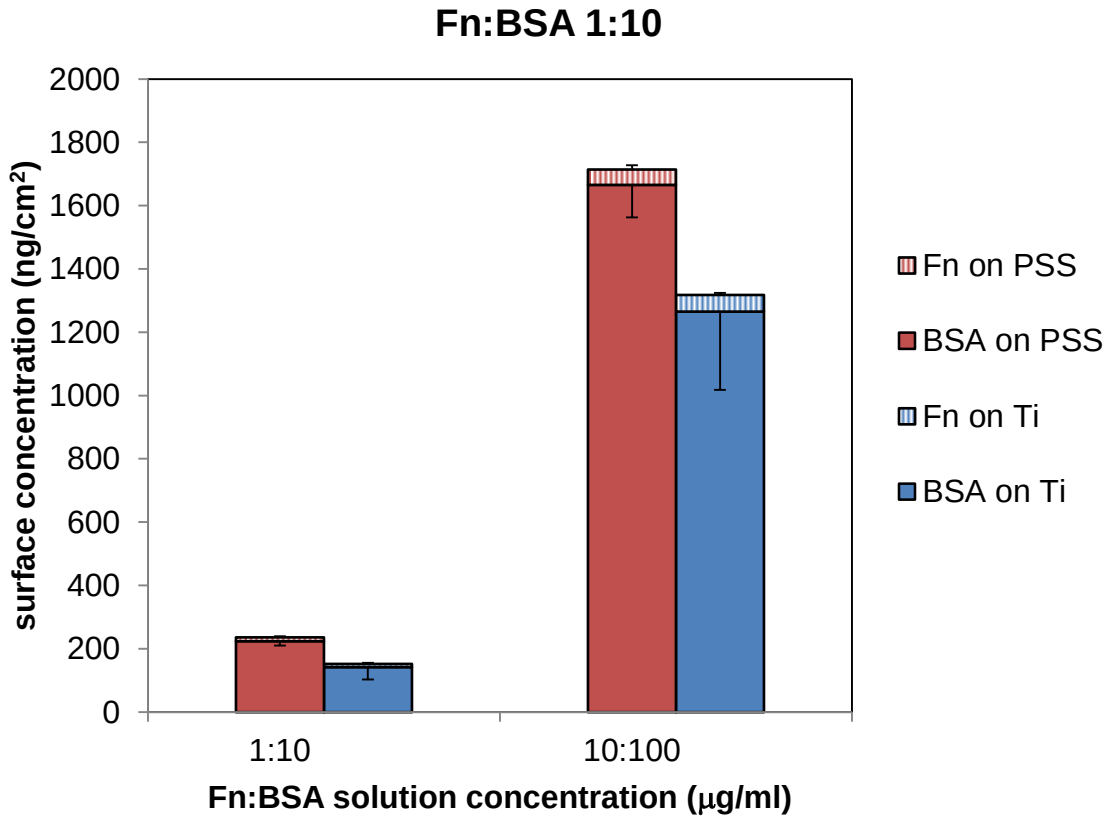

Fig. 4.10. Competitive adsorption of fibronectin and BSA at 1:10 solution concentration mass ratio onto titanium and sulfonated polystyrene surfaces. *More total protein adsorbed onto the PSS than Ti at all solution concentrations. The surface concentration of BSA was higher on PSS than Ti surfaces. The surface concentration of adsorbed fibronectin was similar on the two surfaces, except at the highest protein concentration (100μg/ml fibronectin/1000μg/ml BSA). At the highest protein concentration, more fibronectin adsorbed onto Ti than PSS. N = 6-9. Mean +/- SEM.*

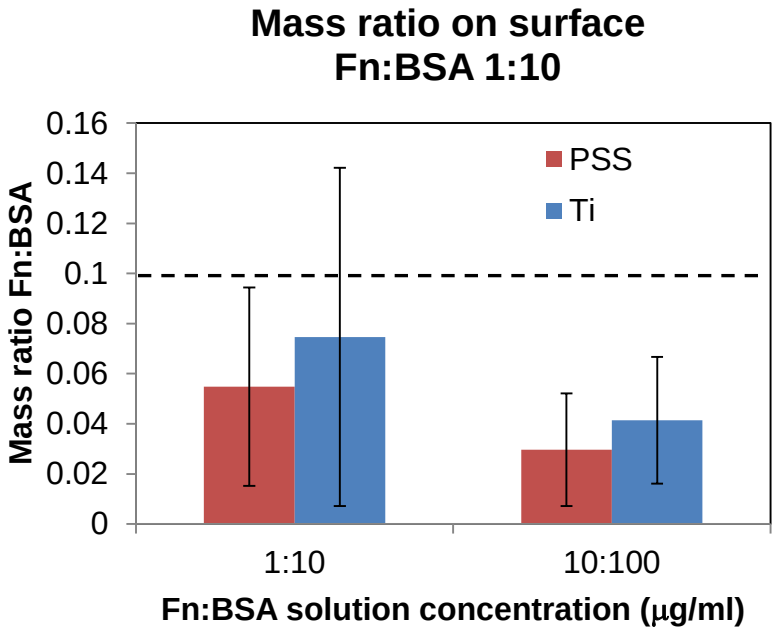

Fig. 4.11. Relative surface concentration of fibronectin and BSA adsorbed at 1:10 mass ratio solution concentration. *If the surface composition matched the solution composition, the ratio would be 0.1 (dashed line). Mean +/- SD.*

There have been previous studies of competitive adsorption of Fn and BSA onto titanium surfaces. One previous study found some differences from the current study, although some experimental details make it difficult to draw direct comparisons. Sousa, et al. [253] found that adsorbing Fn and HSA from a 1:1 mixture reduced the amount of Fn to 50% of the maximum value adsorbed from a single component solution. This is consistent with the observations in the current study. However, the previous study found that the amount of HSA adsorbed onto the surface from a 1:1 mixture with Fn decreased by approximately 80% from the maximum value adsorbed from single component solution. In our study, coadsorbing BSA with Fn in a 1:1 ratio had a varied effect depending on the concentrations examined. Here, the largest decrease in adsorbed amount of BSA was approximately 70% compared to the single component condition.

When Fn and HSA were adsorbed onto titanium surfaces in a 1:10 mass ratio in solution concentration, the previous study found that both Fn and HSA adsorption dropped to approximately 10% of the amount from a single component film [253], which is different from the result obtained here.

With higher levels of HSA in solution (HSA:Fn ratio 50 and 200) the amount of Fn on the TiO_2 surface dropped to approximately 10% of the amount from a single component film, while the amount of BSA adsorbed onto the surface remained approximately 70% of the single component solution. This result is more consistent with the results observed in the current study. The previous publication did not list the solution concentrations or the final surface concentrations; results were expressed only as percentages relative to single component adsorption. Therefore it is difficult to interpret the relative Fn:albumin surface concentration to compare to the current study.

Competitive adsorption of Fn and BSA has also been measured with PTFE surfaces [56]. For solutions with Fn:BSA mixtures of 1:1, 1:10, and 1:100 mass ratios, the amount of Fn adsorbed onto the surface decreased by approximately 50% for each 10-fold increase in the amount of BSA present. That is comparable to the results observed in the current study.

Another study measured the competitive adsorption of Fn and BSA onto $–CH_3$ and –COOH SAM surfaces [140]. Coadsorption with BSA in a 1:100 Fn:BSA ratio resulted in a decrease in the amount of Fn on the surface to approximately 25% of the value from the single component Fn solution on the –COOH SAMs and approximately 20% of the value from the single component Fn solution on the $–CH_3$ SAMs. These are comparable to the results obtained here for the 1:10 Fn:BSA ratio which resulted in a decrease in the surface concentration of Fn from 20-50% of the amount of Fn adsorbed from a single component solution onto Ti and PSS surfaces.

Competitive adsorption of Fn and BSA has also been compared on fluorocarbon and glass surfaces [252]. More BSA than Fn adsorbed onto the fluorocarbon surface, but more Fn adsorbed onto the glass surface than BSA when adsorbed from a 1:10 Fn:BSA mass ratio.

In these studies, BSA showed relatively higher surface concentration than solution concentration in almost all cases. However, there have been reports of preferential Fn adsorption onto titanium from binary solutions containing BSA. With a high relative amount of BSA in solution (Fn:BSA ratio of 1:1000) resulted in a Fn:BSA mass ratio of the surface composition to be approximately 0.02 [242]. It is possible that further increasing the relative amount of BSA in solution in these studies would have resulted in a surface enrichment of Fn compared to the solution concentration.

4.4.5 XPS protein adsorption isotherms

XPS was used to track protein adsorption onto the surfaces by measuring the nitrogen signal, as nitrogen is unique to the protein and not present in either substrate. Full XPS determined elemental composition for these samples are listed in Table 4.3. The measured XPS nitrogen signal increased on each surface as the solution concentration increased, reaching a saturation value of approximately 11 atomic % N at a solution concentration of 100μg/ml on both surfaces (Fig. 4.12). This is consistent with a previous study of Fn adsorption onto polystyrene surfaces and polystyrene treated with UV light, in which a plateau in XPS N1s atomic percentage was observed above Fn solution concentration of 50μg/ml [74]. At a Fn solution concentration of 10μg/ml, a higher XPS nitrogen signal was observed on the PSS surface compared to the Ti surface.

Assuming Fn formed a continuous film when adsorbed from a solution concentration of 100μg/ml, the film thickness was calculated from Eq. 4.2 using a mean free path of 3.5nm and a photoelectron take-off angle of 55° to be 2.7nm for both PSS and Ti surfaces. This is lower than previously published measurements of Fn film thickness discussed above (5-10nm), but still possible if Fn molecules were lying down on the surfaces.

There are some differences observed between the XPS measurements of Fn adsorption and ^{125}I Fn adsorption. XPS shows that more Fn adsorbs onto the PSS surface than Ti surface at solution concentration of 10μg/ml. However, above solution concentrations of 10μg/ml, the XPS atomic %N plateaus at the same value for Fn adsorbed onto both PSS and Ti surfaces. This is different from the ^{125}I Fn results, which showed more Fn adsorbed onto PSS surfaces than Ti surfaces at all solution concentrations measured. These results do not necessarily contradict, due to the differing sampling depths of XPS and ^{125}I Fn adsorption. It is possible that at a solution concentrations above 10μg/ml, the amount of Fn on the surface saturates the XPS %N signal, even as the total amount of protein on the surface continues to increase, which can be detected by ^{125}I Fn. Hull, et al. used AFM to show that the coverage of a Fn layer adsorbed onto mica continued to increase after a plateau in the nitrogen signal above a solution concentration of 20μg/ml [272]. The Fn film thicknesses calculated from the XPS data were thinner than those calculated from the ^{125}I Fn

data, but this could be due to the exposure of the XPS samples to ultra-high vacuum during analysis.

For the adsorption of BSA on Ti and PSS surfaces, the XPS nitrogen signal again increased as the solution concentration increased (Fig. 4.13). Higher nitrogen content was observed when BSA was adsorbed onto PSS surfaces than onto Ti surfaces, with a maximum observed nitrogen signal of 9 atomic % for adsorbed BSA on PSS compared to 6 atomic % for adsorbed BSA on Ti. Full XPS determined elemental composition for these samples are listed in Table 4.4.

Assuming BSA formed a continuous film when adsorbed from a solution concentration of 1000μg/ml, the film thickness was calculated from Eq. 4.2 using a mean free path of 3.5nm and a photoelectron take-off angle of 55° to be 1.8nm on PSS and 1nm on Ti. This agrees with the range of previously measured BSA film thicknesses mentioned above (1-3nm) and is consistent with BSA forming a monolayer on the two surfaces [255].

A lower atomic % N observed for BSA adsorbed onto the surfaces than Fn could be due to the different sizes of the two proteins. Fn is a larger protein (MW 450kDa) compared to BSA (MW 65kDa) [56]. Therefore we would expect Fn to form a thicker protein film than BSA, resulting in a higher percentage of nitrogen detected by XPS.

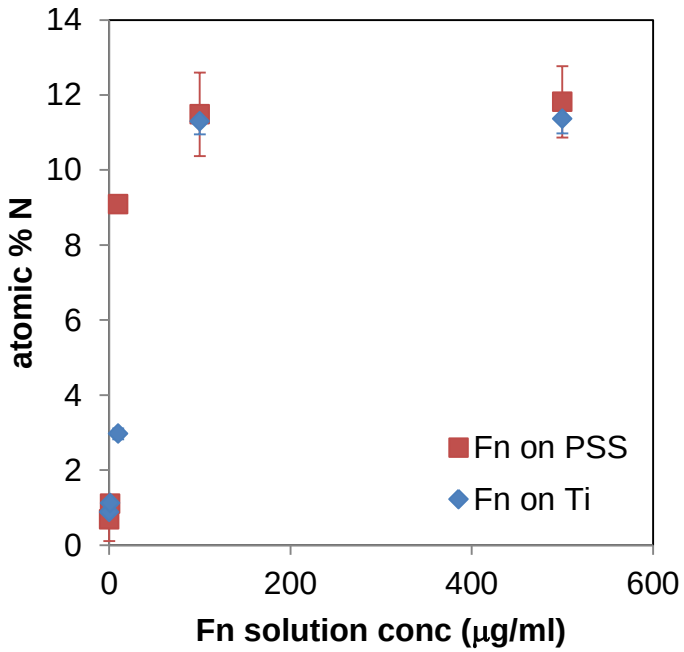

Fig. 4.12 XPS results for Fn adsorbed onto Ti and PSS surfaces. *Nitrogen adsorption isotherm shows increasing nitrogen content as the Fn solution concentration increases on both Ti and PSS. N = 6. Mean +/- SD.*

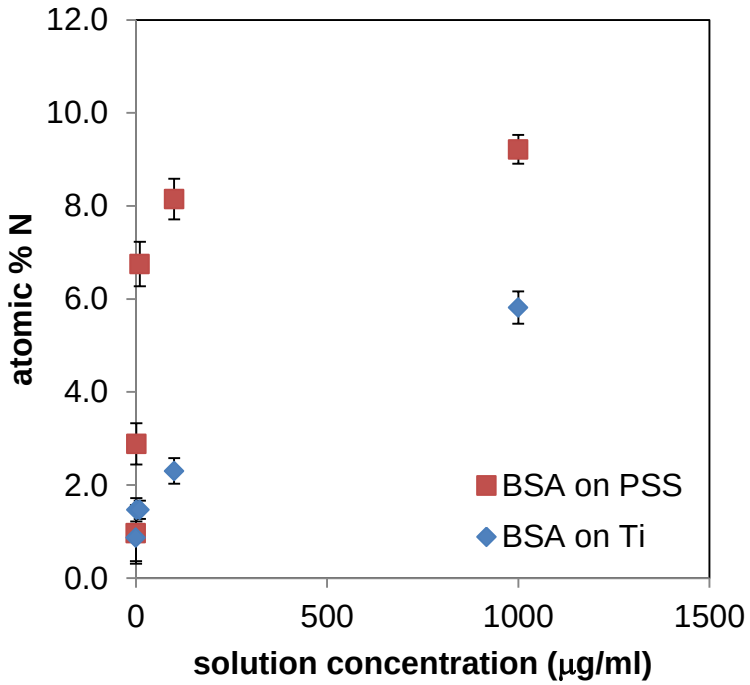

Fig. 4.13 XPS results for BSA adsorbed on Ti and PSS surfaces. *Nitrogen adsorption isotherm shows increasing nitrogen content as the BSA solution concentration increases on both Ti and PSS. N = 6. Mean +/- SD.*

4.4.6 ToF-SIMS

While it is important to understand the amount of protein adsorbed onto a surface, the structure of a protein on a surface also plays an important role in interactions with the cellular environment. Numerous studies have demonstrated Fn conformation on different surfaces affects cell adhesion and function [18,19,17,20]. We used ToF-SIMS to examine differences in surface structure, which could include conformation or orientation, of Fn adsorbed onto Ti and PSS surfaces. We used PCA to analyze the ToF-SIMS data, as it is sensitive to small changes in protein structure on surfaces [74,72,73,35,71].

PCA scores showed clear separation of Fn adsorbed from 10μg/ml and 100μg/ml solutions onto PSS and Ti surfaces (Fig. 4.14). PC1 captured 78% of the variance in the data and separated the samples adsorbed from 10μg/ml solutions onto Ti surfaces from the other samples. PC2 captured 19% of the variance in the data and clearly separated Fn adsorbed

onto Ti surfaces from Fn adsorbed onto PSS surfaces. Examining the loadings for PC2, the nonpolar amino acids (Pro, Val, Leu, Phe), tend to load negatively, corresponding to Fn adsorbed onto the Ti surfaces (Fig. 4.15). The charged amino acids (Arg, Lys, His) tend to load positively in PC2, corresponding to Fn adsorbed onto the PSS surfaces. The Arg peaks at m/z 100 and 112 load negatively. Arginine is present in two cell binding sites contained within Fn: the RGD site and the PHSRN site, so arginine exposure could be important for cell signaling.

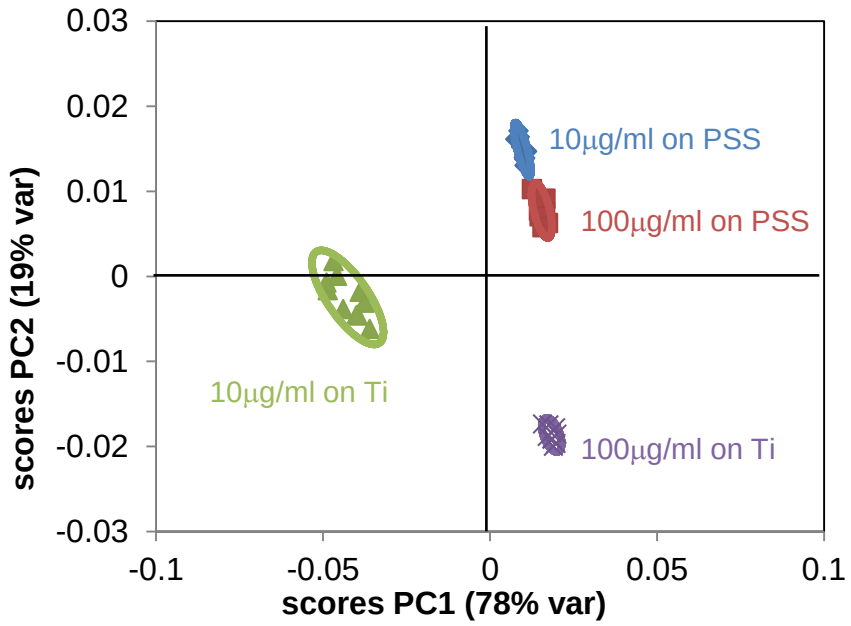

Fig. 4.14 PCA Scores of Fn adsorbed onto PSS and Ti surfaces from 10μg/ml and 100μg/ml solutions. *PC1 (78% variance) versus PC2 (19% variance) scores. PC2 clearly separates Fn adsorbed on the two surfaces. Data collected from 2 samples, 5 spots/sample.*

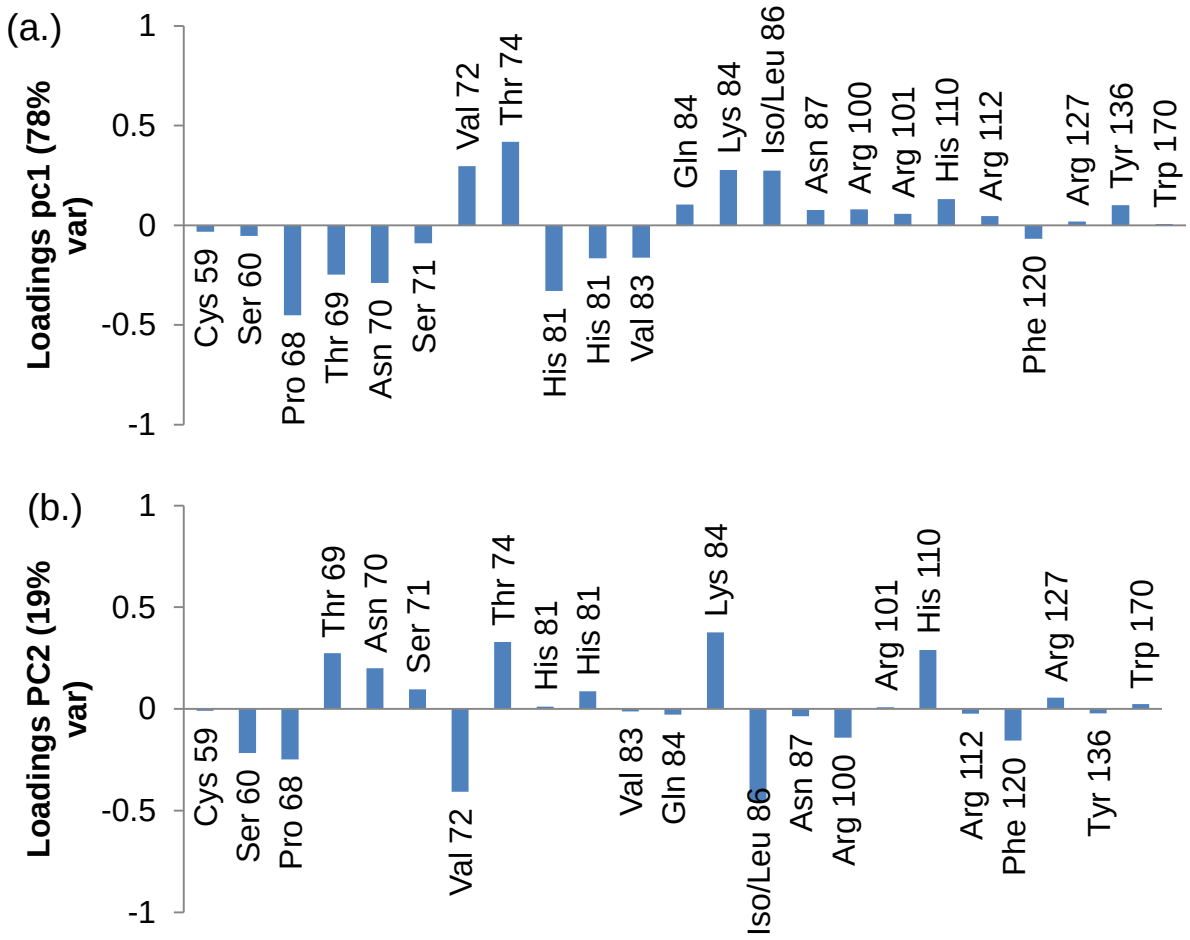

Fig. 4.15 PCA loadings of Fn adsorbed onto PSS and Ti surfaces from 10μg/ml and 100μg/ml solutions. *(a.) PC1 loadings (78% var) (b.) PC2 loadings (19% var) scores.*

4.5 Discussion

Previous studies showed improved osteoblast function using sulfonated surfaces [175,225] compared to titanium. Other studies have shown that sulfonated surfaces can increase the number of cells, strength of cell adhesion [273,274], increase cell spreading [275,276], and influence organization of F-actin distribution [277] compared to non-sulfonated surfaces. Here we examined protein adsorption to the two surfaces to understand if differences in protein adsorption could explain observed differences in cellular function.

Adsorption studies using ^{125}I show higher amount of Fn adsorbed onto PSS surfaces compared to Ti surfaces. Amount of protein on a surface is one characteristic that can control the biological response. Previous studies have shown direct correlations between the

amount of Fn adsorbed to the surface and cell adhesion strength on sulfonated polystyrene [276], silicon, and glass [240] surfaces. The higher amounts of adsorbed protein measured here on the sulfonated polystyrene surfaces compared to the titanium surfaces could contribute to the differences in osteoblast function observed in previously published reports [175,225]. Competitive Fn/BSA adsorption did not show strong differences in the surface composition between the two surfaces, so preferential Fn adsorption onto PSS from a mixture did not seem to be a strong factor in distinguishing the two surfaces under the conditions tested here.

In addition to differences in the amount of protein adsorbed onto the two surfaces, ToF-SIMS clearly showed differences between Fn adsorbed onto PSS and Ti surfaces. Surface structure is important to Fn function, so differences in Fn surface structure between the two surfaces could also contribute to differences in cell function [18,19,17,20]. The differences in protein structure on the two surfaces could contribute to differences in exposure of cell binding sites. Previous studies have shown that the RGD cell binding site is more exposed when Fn is adsorbed onto a sulfonated polystyrene surface than untreated polystyrene [263,237].

These studies clearly show that the adsorption of Fn and BSA are different on PSS and Ti surfaces. It is likely the differences in protein amount and adsorbed Fn surface structure play a role in the differences observed in cellular function in previously published reports.

4.6 Conclusions

For a material to successfully be used for orthopedic implants, osteoblasts must produce bone tissue directly in contact with the implant surface. The signals received by growing osteoblasts are influenced by the adsorbed protein layer on the implant surface. By understanding the adsorption of proteins, we can better understand the cellular response. In the studies described here, we characterized fibrinogen, an important ECM protein, adsorbed to titanium and a surface with a high concentration of sulfonate groups. By measuring the amount of protein adsorbed and its conformation, we can better understand how a novel surface presenting sulfonate groups will interact with the *in vivo* environment.

4.7 Tables for Chapter 4

Table 4.1 Quantification of Sulfonate Groups on PSS surface

	Average (n=3)	St. Dev. (n=3)
Sulfonate groups/cm^2	$1.5x10^{15}$	$0.4x10^{15}$
% surface covered by sulfonate groups[a]	65	20

[a] Sulfonate hydrodynamic radius = 0.12nm [256]

Table 4.2 Negative secondary ion fragments detected in ToF-SIMS analysis of sulfonated polystyrene surfaces.

Ion	**Mass**	**Normalized intensity**
SO_2-	63.9663	7.86E-03
SO_3-	79.9631	7.44E-02
SO_3H-	80.9696	2.86E-02
C_2HSO_3-	104.963	7.73E-04
C_5H_9SO-	117.033	9.43E-04
$C_5H_{11}SO$-	119.051	4.20E-03
$C_6H_4SO_3$-	155.995	3.93E-03
$C_6H_6O_5$-	158.015	4.72E-04
$C_7H_6SO_3$-	170.016	2.06E-03
$C_8H_6SO_3$-	182.013	8.87E-04
$C_8H_7SO_3$-	183.025	3.61E-02
$C_8H_8SO_3$-	184.027	3.66E-03
$C_8H_9SO_3$-	185.022	2.61E-03
$C_8H_{10}SO_3$-	186.026	5.06E-04
$C_7H_7SO_3Na$-	194.013	2.69E-04
$C_{12}H_3O_3$-	195.017	9.60E-04
$C_{13}H_9O_2$-	197.038	1.40E-03
$C_{13}H_{11}O_2$-	199.022	2.75E-03

$C_8H_9SO_3Na$-	208.027	1.74E-04
$C_{14}H_9O_2$-	209.036	1.14E-03
$C_8H_{10}SO_3$-$C_4H_5O_2$-	271.027	1.21E-03
$C_8H_{10}SO_3$-$C_2H_3O_2$-C_3H_4-	285.07	8.23E-04
$C_8H_{10}SO_3$-$C_2H_3O_2$-C_3H_6-	287.064	3.16E-04
$C_{15}H_{11}O_6S_2$-	350.992	1.93E-04
$C_{15}H_{12}O_6S_2$-	352.042	1.29E-04
$C_{15}H_{13}O_6S_2$-	353.038	1.03E-04
$C_8H_{10}SO_3$-C_8H_4-$C_2H_3O_2$-CH_4-	360.996	3.34E-05
$C_8H_{10}SO_3$-C_8H_4-$C_2H_3O_2$-C_2H_4	373.045	7.35E-05
$C_8H_{10}SO_3$-C_8H_4-$C_2H_3O_2$-C_3H_6-	387.027	4.16E-05

Mean of 6 measurements from 2 samples. Intensities normalized to total ion intensity. Based on [278].

Table 4.3 XPS determined elemental compositions of Fn adsorbed onto PSS and Ti surfaces

Fn Solution concentration (μg/ml)		% C	% O	% N	% S	% Ti	% Na
0							
	PSS	88.6 (1.8)	9.2 (1.1)	0.6 (0.5)	1.6 (0.3)	ND	ND
	Ti	27.3 (2.2)	51.9 (4.8)	0.4 (0.3)	ND	12.0 (5.4)	2.5 (0.6)
0.1							
	PSS	90.2 (2.6)	7.8 (1.4)	0.7 (0.6)	1.3 (0.6)	ND	0.2 (0.3)
	Ti	27.6 (1.2)	52.9 (1.1)	0.9 (0.2)	ND	16.3 (0.9)	2.2 (0.4)
1							
	PSS	83.8 (1.7)	12.2 (1.2)	1.1 (0.2)	2.2 (0.1)	ND	0.8 (0.9)
	Ti	29.2 (1.5)	51.5 (1.3)	1.1 (0.1)	ND	16.4 (0.9)	1.7 (1.0)
10							
	PSS	70.7 (1.2)	18.6 (1.0)	9.1 (0.1)	1.6 (0.1)	ND	ND
	Ti	33.2 (6.9)	48.6 (4.2)	3.0 (0.4)	ND	14.3 (2.2)	1.1 (1.3)
100							
	PSS	66.8 (1.0)	20.6 (0.7)	11.5 (1.1)	1.5 (0.1)	ND	ND
	Ti	47.6 (1.2)	35.4 (0.9)	11.3 (0.4)	ND	6.5 (0.3)	ND
500							
	PSS	68.4 (1.3)	19.1 (0.9)	11.8 (0.9)	0.6 (0.1)	ND	ND
	Ti	49.9 (1.5)	32.4 (1.2)	11.4 (0.6)	ND	6.3 (0.4)	ND

Mean of 6 measurements on 2 samples. Standard deviation in parentheses. ND: Not detected

Table 4.4 XPS determined elemental compositions of BSA adsorbed onto PSS and Ti surfaces

BSA Solution concentration (μg/ml)		% C	% O	% N	% S	% Ti	% Na
0							
	PSS	84.3 (1.0)	12.6 (0.4)	1.0 (0.6)	2.0 (0.3)	ND	ND
	Ti	28.5 (2.0)	51.1 (1.2)	0.9 (0.6)	ND	17.0 (0.7)	2.5 (1.9)
1							
	PSS	81.4 (1.7)	13.7 (1.6)	2.9 (0.4)	2.0 (0.1)	ND	0.1 (0.2)
	Ti	30.5 (1.7)	50.0 (1.4)	1.5 (0.3)	ND	18.0 (0.3)	ND
10							
	PSS	74.8 (1.8)	16.9 (1.5)	6.8 (0.5)	1.6 (0.3)	ND	ND
	Ti	30.4 (1.7)	50.4 (0.7)	1.5 (0.2)	ND	17.7 (0.9)	ND
100							
	PSS	70.3 (0.4)	20.0 (0.7)	8.2 (0.4)	1.7 (0.1)	ND	ND
	Ti	32.9 (6.3)	48.1 (4.1)	2.3 (0.3)	ND	16.7 (2.2)	ND
1000							
	PSS	69.9 (0.9)	18.9 (0.9)	9.2 (0.3)	2.0 (0.2)	ND	ND
	Ti	32.8 (0.8)	47.0 (0.3)	5.8 (0.3)	ND	14.6 (0.6)	ND

Mean of 6 measurements on 2 samples. Standard deviation in parentheses. ND: Not detected

Table 4.5 Positive amino acid secondary ion peaks used for analysis of the ToF-SIMS data

Ion	Mass	Amino acid
C_2H_3S	58.9939	Cys
C_2H_6NO	60.0454	Ser
C_4H_6N	68.053	Pro
C_4H_5O	69.038	Thr
C_3H_4NO	70.0324	Asn
$C_3H_3O_2$	71.0154	Ser
$C_4H_{10}N$	72.0867	Val
C_3H_8NO	74.0654	Thr
$C_4H_5N_2$	81.0412	His
$C_4H_6N_2$	82.0516	His
C_5H_7O	83.0525	Val
C_4H_6NO	84.0463	Gln/Glu
$C_5H_{10}N$	84.0851	Lys
$C_5H_{12}N$	86.1005	Leu/Ile
$C_3H_7N_2O$	87.0571	Asn
$C_4H_{10}N_3$	100.084	Arg
$C_4H_{11}N_3$	101.095	Arg
$C_5H_8N_3$	110.076	His
$C_5H_{10}N_3$	112.088	Arg
$C_8H_{10}N$	120.0861	Phe
$C_6H_{11}N_2O$	127.09	Arg
$C_8H_{10}NO$	136.081	Tyr
$C_{11}H_8NO$	170.065	Trp

Chapter 5 Von Willebrand Factor Structure and Function Changes on Synthetic Surfaces

5.1 Abstract

The clotting protein von Willebrand Factor (VWF) binds to platelet receptor glycoprotein 1bα (GP1bα) when VWF is activated, such as when VWF is exposed to a surface or is under high shear. However, the mechanism of surface activation is not known. This study characterizes function and adsorption behavior of the VWF A1 domain, which contains the GP1bα binding site. Surfaces tested are glass, polystyrene, and tissue culture polystyrene. At high shear rate (10 dyne/cm^2), platelets detached from A1 adsorbed onto a glass surface but rolled on A1 adsorbed onto a polystyrene surface. At low shear rate (0.2dyne/cm^2), platelets detached from A1 adsorbed onto a polystyrene surface but exhibited stationary adhesion on A1 adsorbed onto glass. X-ray photoelectron spectroscopy (XPS) showed comparable A1 amounts are present on each surface, suggesting functional differences were not explained by differences in surface coverage. A1 surface structure was investigated using ELISA, time-of-flight secondary ion mass spectrometry (ToF-SIMS) and near-edge x-ray absorption fine structure (NEXAFS). Using monoclonal antibodies binding to a nonlinear epitope within A1, ELISA showed lower antibody binding for A1 adsorbed to polystyrene than to glass or tissue culture polystyrene suggesting the 3D structure of the epitope was disrupted upon adsorption onto polystyrene. ToF-SIMS was used to identify differences in amino acid exposure, and NEXAFS showed different amide backbone ordering on the three surfaces. These studies demonstrate that the surface dependence of A1 function is likely due to differences in structure of A1 adsorbed to the surface tested here. This is an important consideration in *in vitro* models, where A1 is typically immobilized onto synthetic surfaces, and is also of likely relevance for blood-contacting biomaterials.

5.2 Introduction

von Willebrand Factor (VWF) is an adhesive blood protein responsible for platelet tethering to surfaces in high shear regions (500-800s^{-1} wall shear rates and above)[148,279,280,98,183], leading to thrombus formation. In normal circulation VWF

does not bind to platelets. However, when VWF is immobilized onto a surface it becomes competent to bind platelets through the glycoprotein 1bα (GP1bα) platelet surface receptor, which is part of the GP1bα/IX/V complex [152,279]. VWF and platelets can also aggregate in solution in high shear conditions [281,282]. Although the exact activation mode is not fully understood, it is generally believed that a conformation change within VWF exposes the GP1bα binding site located within the A1 domain of VWF [148,283-287,155,288]. This could be a change in quaternary structure, exposing the A1 domain within multi-domain VWF, or a change in tertiary structure, exposing the GP1bα binding site within the A1 domain, or both.

During vascular injury *in vivo*, VWF attaches to collagen prior to platelet binding. VWF also adsorbs to biomaterial surfaces of blood-contacting implants, along with other clotting proteins such as fibrinogen, which can lead to thrombosis and implant failure [21,23,158]. *In vitro*, different substrates are used to immobilize VWF, including glass [156,103], collagen [156,157,289], polyethylene [158], and polystyrene [159]. Since platelet binding depends on VWF structure (in solution versus on a surface), conformation or orientation changes in VWF adsorbed onto surfaces could lead to changes in function. The surface itself could also stabilize an activated conformation of VWF. Immobilized VWF is typically considered to be active, without consideration of surface effects [280], since lower shear is required for platelet-VWF binding when VWF is immobilized on a surface (<10dyne/cm^2[290]) than in solution (approx. 80dyne/cm^2 [281]). However, previous studies have not taken into account the substrate on which the experiment was performed, with some publications not even mentioning the adsorption substrate [105,106].

Previous studies clearly demonstrate that surfaces affect protein adsorption behavior. Protein coverage can vary on different surfaces [35,72,291,8,201]. Proteins can also adsorb in different orientations or conformations, [192,35,68,36,292,74,202] which can affect function[73,252,192,272,293,241,57]. However there has been little surface analysis to characterize the changes VWF undergoes following adsorption. One previous study used atomic force microscopy in aqueous conditions to examine VWF topography when adsorbed to hydrophilic and hydrophobic surfaces [160]. When full length VWF was adsorbed onto hydrophilic mica, the protein showed an extended conformation. On hydrophobic octadecyltrichlorosilane (OTS) modified glass, VWF appeared as compact structures.

Functional antibodies were also used to detect differences between VWF conformation on OTS glass and collagen VI [294]. These studies suggest that VWF adsorption can be affected by the substrate to which it is adsorbed. However, previous studies have not examined how this differential surface behavior affects VWF function in physiological flow conditions.

In the studies presented here, we focus on the isolated A1 domain of VWF since we can study the structure-function relationship of a single domain more completely than a large, multi-domain protein. The isolated A1 domain is far less complex than the full protein, and the structure is known [174]. The A1 domain contains the binding site for GP1bα, making it the critical component for platelet binding [148]. The A1 domain is also commonly used in *in vitro* studies to examine platelet adhesion [96,295-297]. We assume that some fraction of A1 domains in plasma VWF interact with the surface, and would act as predicted by studies on isolated A1. Further, there is evidence that changes in isolated A1 structure cause changes in function, as demonstrated by mutations within the A1 domain [298,287]. While studies of isolated A1 cannot be directly related to function of full-length VWF *in vivo*, they give a better understanding of activation that occurs on different surfaces, which could be an important consideration for blood contacting biomaterials. To further understand how the function of the isolated A1 domain relates to full-length VWF, we also tested the function of the full protein to different surfaces.

A1 domain function and surface structure can be evaluated using several techniques. *In vivo*, platelets adhere to VWF in high shear regions [148,279,280,98,183]. *In vitro*, this flow can be simulated using a parallel plate flow chamber. The flow chamber creates laminar flow at defined shear stresses to mimic blood flow environment [183,103,289]. The effect of surface type on adhesion in physiological flow has not been determined. Protein coverage can be measured using x-ray photoelectron spectroscopy (XPS). XPS quantitatively measures the atomic composition of the top 10nm of a sample [61]. Since nitrogen is unique to the adsorbed protein and not present in the substrates, nitrogen signal can be related to adsorbed protein amount [62,35,72,81].

Antibody studies can give insight into protein conformation [287,299,96,300,301]. Monoclonal antibodies can bind to an epitope consisting of a linear sequence of amino acids, or alternatively amino acids that are not adjacent in the peptide sequence but form a specific

3D structure [302-305]. If the structure of a nonlinear epitope is disrupted or hidden, antibody binding decreases, which is measured using ELISA [306-310]. Antibodies with nonlinear epitopes have previously been used to identify differences between wildtype A1 and A1 mutants[96,288].

ToF-SIMS is used to obtain information about the outermost amino acid side chains of an adsorbed protein. ToF-SIMS has a shallow sampling depth (~2nm [71]), smaller than most proteins. If a protein contains amino acids that are asymmetrically distributed, then differences in protein orientation and conformation can be identified in the ToF-SIMS data [69,68,74,73,180].

Near-edge x-ray absorption fine structure (NEXAFS) can give information about protein backbone ordering and orientation. The angle dependence of the nitrogen k-edge spectra provides information about the π^* orbital ordering in the protein amide backbone. This technique has previously been used to measure adsorbed protein orientation[36,69].

These methods can be applied in a multi-technique approach to gain a new understanding of A1 interaction with surfaces. In the study presented here, we use the techniques described above to perform a systematic characterization of A1 function and structure adsorbed to glass, tissue culture polystyrene (TCPS), and polystyrene (PS). Understanding A1 adsorption behavior on synthetic surfaces is critical for designing *in vitro* experiments to mimic the *in vivo* system. It could also be beneficial to material design for blood contacting biomaterials because influencing VWF adsorption could impact thrombosis on implanted devices.

5.3 Methods

5.3.1 Substrates and VWF A1 protein

Glass coverslips (8mm, ProSciTech, Thuringowa, Australia) were cleaned by sequential sonication in dichloromethane, acetone, methanol. PS and TCPS plates (Corning) were sonicated in water before use. A1 was produced in *E. coli* containing residues 1238-1472 of mature VWF with 12 residues at the N terminus from the expression vector (MRGSHHHHHHGS) [174]. The protein was generously provided by Miguel Cruz. Full-

length plasma VWF was purchased from Haematologic Technologies Inc. (Essex Junction, VT) and used without further purification.

5.3.2 Platelets

Platelets were isolated from the blood of healthy donors, which had been drawn into acid citrate dextrose (ACD) tubes. Platelets were separated by differential centrifugation in the presence of Apyrase and PGE-1 and resuspended in Hepes Tyrodes buffer containing 200μg/ml BSA [181,182].

5.3.3 Flow chamber

Platelet adhesion studies were performed in a parallel plate flow chamber as previously described [183,98]. Samples were incubated for 2h at 37^{o}C in A1 or VWF solution at the desired concentration. Control surfaces were incubated with BSA (500μg/ml). Surfaces were then blocked with BSA (200μg/ml) overnight at 4^{o}C. The flow chamber (Glycotech) was prepared with the appropriate gasket to achieve the desired shears. The parallel plate flow chamber was situated on the protein coated plate and sealed using a vacuum. A 300μl bolus of washed platelets was then introduced into the flow chamber and allowed to settle for 30sec which typically introduced >100 platelets into the field of view. Buffer was then pushed through the chamber at the desired shear and platelet-surface interactions were observed with a 10x objective, CCD camera, and microscope controlled by Metamorph software. To test specificity of platelet-A1 interaction, an anti-GP1bα antibody was used [152]. Platelets were incubated with anti-GP1bα antibody AK2 (Abcam) at a concentration of 25μg/ml for 15 min at room temperature, then platelet binding was measured as described above in the presence of the antibody.

5.3.4 Protein adsorption for XPS, ToF-SIMS, and NEXAFS

Substrates were allowed to equilibrate overnight with phosphate buffered saline (PBS) (137mM NaCl, 2.7mM KCl, 10mM phosphate) pH 7.4 at room temperature, then incubated in VWF A1 solutions at the desired concentrations for 2h at 37^{o}C. Following adsorption, substrates were rinsed twice in stirred PBS buffer to remove loosely bound

protein, then three times in stirred water to remove buffer salts [79]. Samples were dried in a nitrogen stream, then kept under an inert nitrogen atmosphere until analysis.

5.3.5 XPS analysis

XPS data were collected on a Surface Science Instruments S-Probe instrument with a monochromatized aluminum Kα x-ray source and electron flood gun for charge neutralization. Survey and detail scans were acquired at a 150 eV pass energy and a 55^{o} takeoff angle, defined as the angle between the surface normal and the analyzer. For each concentration, two samples were analyzed and three spectra were collected on each sample. Spectra were analyzed using the Service Physics ESCA 2000A analysis software.

5.3.6 ELISA

ELISA experiments were performed with antibodies 6G1, CR1, 5D2 generously provided by the Lopez lab at the Puget Sound Blood Center. The epitope for antibody 6G1 is Glu700-Asp709 at the C terminus of the A1 domain. CR1 and 5D2 bind to nonlinear epitopes within the A1 domain [96]. PS (Corning), TCPS (Corning) and glass-bottom (MatTek) 96-well plates were used for ELISA assays. Substrates were allowed to equilibrate overnight in PBS pH 7.4 at room temperature, then incubated in VWF A1 solutions at the desired concentrations, or BSA (1mg/ml) as a negative control, for 2h at 37^{o}C. Surfaces were blocked with BSA (200μg/ml) at room temperature for up to 18h. Primary antibodies were incubated with the samples for 1h at 37^{o}C. To test nonspecific secondary antibody binding, some samples were incubated with BSA (1mg/ml) for 1h at 37^{o}C and were not incubated with primary antibody. Secondary goat anti-mouse antibodies conjugated with horseradish peroxidase were incubated with the samples for 1h at 37^{o}C. Samples were incubated with TMB for 5 min, then absorbance was measured at 600nm. Between each step, substrates were rinsed with tris buffered saline (TBS) (150mM NaCl, 10mM tris) containing 0.2 vol % tween 20.

5.3.7 ToF-SIMS analysis

ToF-SIMS data were acquired on an ION-TOF 5-100 instrument (IONTOF GmgH, Munster, Germany) using a Bi_3^+ primary ion source under static conditions (primary ion dose $<10^{12}$ ions/cm^2. Spectra were obtained from 100 x 100 μm areas and five positive ion spectra were collected from each sample. Current ranged from 0.15-0.35pA. A low-energy electron beam was used for charge compensation. Mass resolution (m/Δm) of the positive ion spectra was typically between 5500-7000 for the m/z = 27 peak. Prior to analysis, spectra were mass calibrated to the CH_3^+, $C_2H_3^+$, $C_3H_5^+$, and $C_7H_7^+$ peaks. If the $C_7H_7^+$ signal saturated the detector (on bare PS substrates), $C_8H_7^+$ was used for calibration instead of $C_7H_7^+$. Peaks were identified that corresponded to unique amino acid peaks. Amino acid peaks that overlapped with substrate peaks were then eliminated. If the normalized intensity of a peak was greater than 15% of the protein normalized peak intensity, that peak was assumed to originate from the substrate and not included in the peak list. Peaks used for analysis are listed in Table 5.1, along with the corresponding amino acid [77]. Intensity of amino acid peaks of interest (Trp and Cys) were normalized to the sum of all amino acid peaks to account for variations in protein surface concentration.

5.3.8 NEXAFS

NEXAFS spectra were taken at the National Synchrotron Light Source (NSLS) U7A beamline at Brookhaven National Laboratory using an elliptically polarized beam with ~ 85% p polarization. This beamline uses a monochromator with a 600 L/mm grating that provides a full-width half-max resolution of ~0.15 eV at the carbon K-edge (285 eV). The monochromator energy scale was calibrated using the 285.35 eV C 1s−π* transition on a graphite transmission grid placed in the x-ray path. The partial electron yield was monitored by a detector with the bias voltage maintained at −360 V for the nitrogen K-edge spectrum. The signal was divided by the beam flux during data acquisition. Samples were mounted to allow rotation about the vertical axis to alter the angle between the incident x-ray beam and the sample surface. Data was collected at different NEXAFS angles, defined as the angle between the incident X-ray beam and the sample surface.

5.4 Results

5.4.1 Flow chamber studies show different A1-GP1bα binding on different surfaces

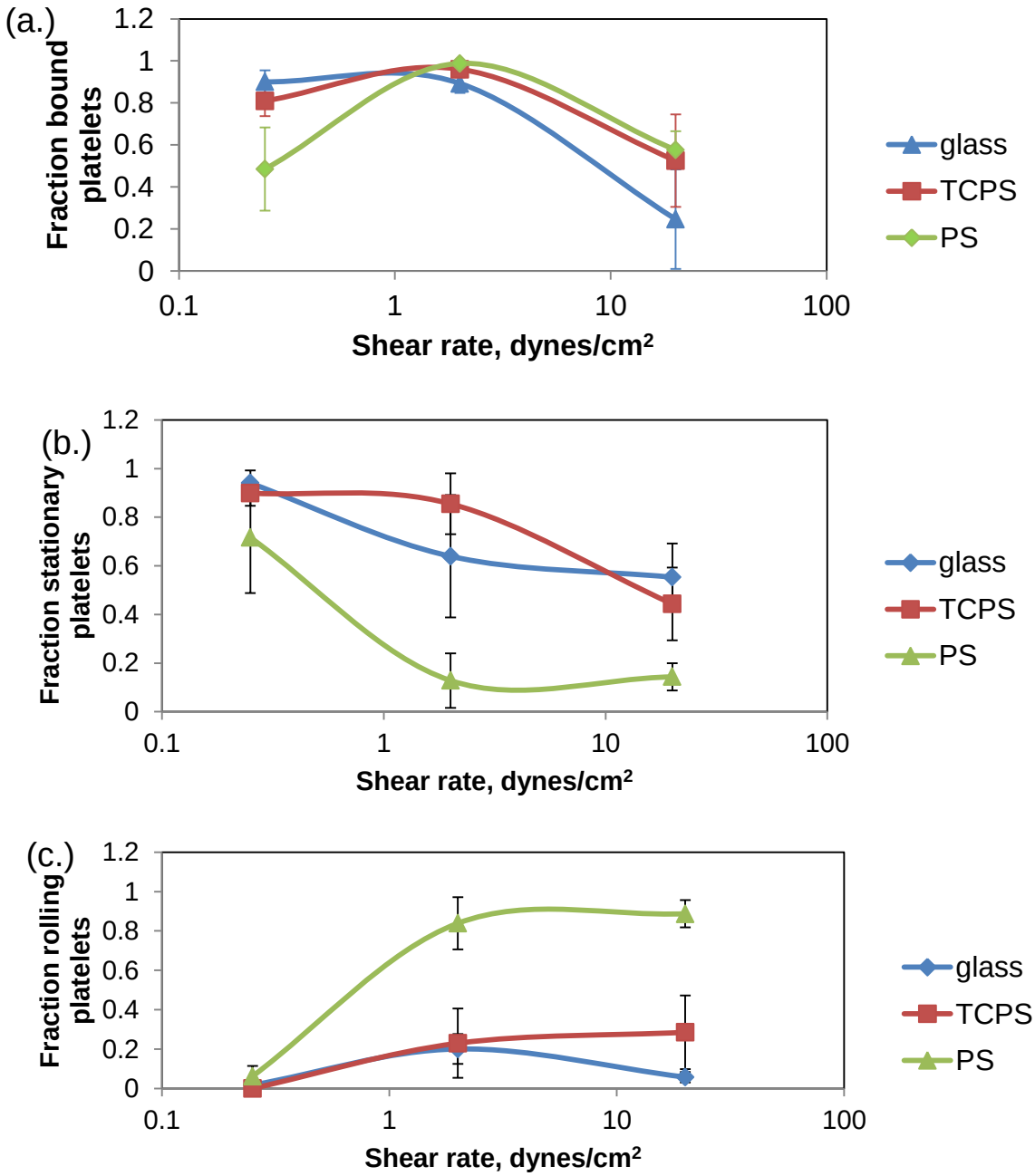

Fig. 5.1 Platelet adhesion on A1 adsorbed onto glass, TCPS, and PS. *A1 adsorbed onto each respective surface from 10 μg/ml solutions. Platelets were introduced at 2dyne/cm^2 for 30sec, then shear rate was increased or decreased. (a.) Fraction bound platelets is the number of platelets in the field of view relative to the initial number of platelets at 2 dyne/cm^2. (b.) Fraction stationary platelets is calculated relative to the number of platelets in the field of view at the specified shear rate. (c.) Fraction stationary platelets is calculated relative to the number of platelets in the field of view at the specified shear rate. A1 is adsorbed onto*

each surface at a solution concentration of 10μg/ml. Lines are included to guide the eye. Each graph represents at least 2 replicate studies performed on different days.

Under normal conditions in the blood, platelets do not bind VWF. However, under high shear, when exposed to small molecule activators such as the antibiotic ristocetin, or attached to a surface [102,96,152], VWF becomes competent to bind the GP1bα platelet receptor [148]. Activation is generally believed to involve a conformational change. This could be a change in quaternary structure, exposing the A1 domain within multi-domain VWF, or a change in tertiary structure, exposing the GP1bα binding site within the A1 domain, or both. Therefore, A1 surface conformation could influence platelet binding.

Under flow *in vitro* and *in vivo*, the platelet binding to active VWF on a surface is characterized by rolling behavior [102,98,103-106]. Platelet adhesion and rolling is influenced by the amount of GP1bα–A1 binding, controlled by adsorbed A1 amount [104,103] or GP1bα receptor density [103,104]. GP1bα–A1 binding can also be influenced by A1 conformation, as observed in A1 mutants [311,312], so binding might be influenced by A1 surface structure. Previous studies used x-ray crystallography to show differences in conformation between wildtype A1 and a I546V mutant. In flow chamber studies, the I546V mutant exhibited enhanced platelet binding, with platelet adhesion at a shear rate of 0.1dyne/cm^2, while the wildtype A1 only exhibited platelet binding above 1dyne/cm^2 [312].

In vitro, platelet adhesion can be studied in a physiologically relevant flow assay in a parallel plate flow chamber in which A1 is adsorbed to a surface of interest and platelets are flowed across the surface [183,98,289]. In this assay, platelets in contact with the surface are clearly differentiated from free floating. At the same distance from the surface, platelets rolling via GP1bα interactions have velocities typically less than 2% of the free flow velocity of non-interacting platelets [279].

Previous studies have demonstrated that the A1-GP1ba bond is shear-enhanced, meaning there is an increase in binding when force on the bond is increased up to a threshold [102,105,98]. To examine the shear-dependent binding behavior on the three surfaces, platelet adhesion under flow was measured at a range of shears. On each surface, platelets were introduced at an intermediate shear rate (2dyne/cm^2). This shear rate was maintained for 30sec, then the shear rate was increased or decreased. The fraction of bound platelets was

calculated relative to the initial number of platelets on the surface at 2 dyne/cm^2. The number of platelets in the field of view was approximately 100-200 platelets for each surface.

As the shear rate increased from 2dyne/cm^2 to 20dyne/cm^2, the fraction of bound platelets decreased on all three surfaces (Fig. 5.1a). Of the three surfaces, the largest fraction of platelets detached from the glass surface, suggesting that A1 adsorbed to glass surfaces is least able to support GP1bα binding at high shear rates. The fraction of platelets remaining is similar on the polystyrene and TCPS surfaces.

However at high shear, the fraction of platelets rolling on the polystyrene surface was significantly higher than on the glass or TCPS surfaces (Fig. 5.1c). This demonstrates that even though the number of platelets on the surface is similar on the polystyrene and TCPS surfaces, A1 is able to better mediate rolling adhesion when it is adsorbed to polystyrene. It is important for in vitro systems to be able to produce rolling behavior since platelet adhesion to VWF in vivo typically exhibits rolling behavior [279,313].

As the shear rate decreased from 2dyne/cm^2 to 0.2dyne/cm^2, the fraction of platelets bound to the surface decreased on both the polystyrene and TCPS surfaces (Fig. 5.1a). This demonstrates shear-enhanced platelet binding, since platelet binding to A1 on the surface was greater at an intermediate shear than a low shear. More platelets detached from A1 adsorbed onto the polystyrene surface than the other surfaces, suggesting the greatest shear-enhanced adhesion occurs when A1 is adsorbed onto polystyrene. Previous studies have also demonstrated shear-enhanced adhesion when A1 was adsorbed onto a polystyrene surface using AFM to measure increases in A1-GP1bα bond lifetime with increased bond force [102].

When A1 was adsorbed to the glass surface, platelet detachment was not observed as the shear rate decreased (Fig. 5.1a). It might be necessary to reduce the shear even further to observed shear-enhanced adhesion, or it is possible that shear-enhanced adhesion was eliminated when A1 was adsorbed onto the glass surfaces. Previous studies have shown elimination of platelet binding to A1 adsorbed onto glass surfaces below 1dyne/cm^2, which is different from the result observed here. However those studies used an A1 surface created using 10 times higher solution concentration of A1 than the surfaces used here [312,314]. It is possible that the differences in solution concentration lead to differences in protein packing on the surface, resulting in changes in function. A previous study used circular dichroism to

demonstrate that adsorbed albumin showed decreased loss of secondary structure as adsorption concentration increased [8]. Therefore, A1 adsorbed onto a glass surface at a lower solution concentration than the previous studies could be more likely to undergo a change in surface structure that could result in the elimination of shear-enhanced adhesion.

In addition to the number of platelets, there are also differences in platelet behavior when interacting with A1 adsorbed onto the three surfaces at low shear rates. Of the platelets remaining on the surface as the shear decreases, almost all platelets bound to A1 adsorbed onto the glass and TCPS surfaces remain stationary (Fig. 5.1b). A1 adsorbed onto the polystyrene surface, in contrast, allows platelets detachment at low shear, suggesting weaker A1-GP1bα interaction. No morphological changes were observed in platelets, suggesting that platelets were not activated on any of the surfaces, as expected due to the presence of activation inhibitors during the experiment as described in the methods.

Specificity of platelet-A1 interactions was tested by measuring platelet binding over BSA surfaces, and measuring platelet binding over A1 surfaces in the presence of an anti-GP1bα antibody AK2 [152]. For both negative control conditions, the number of platelets binding at a given shear was less than 10% of the number of platelets bound to the experimental A1 surfaces (data not shown). This demonstrates that the platelet adhesion shown in Fig. 5.1 are mediated by the specific A1-GP1bα interaction.

5.4.2 XPS shows comparable surface concentration of A1 on different surfaces

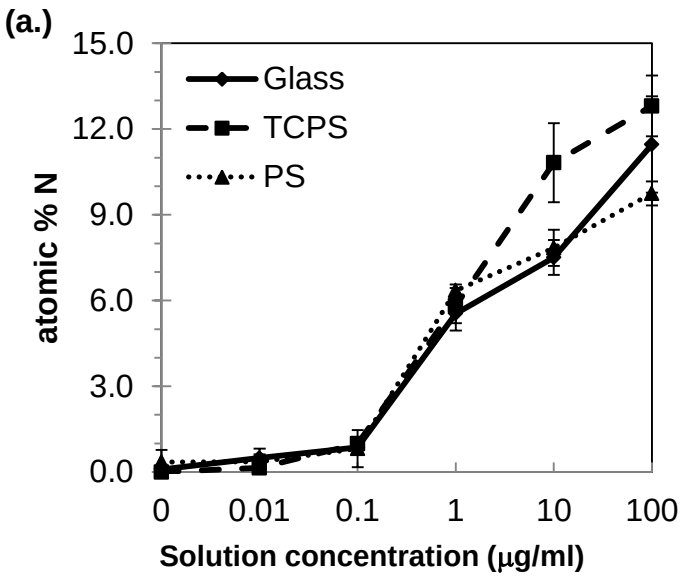

Fig. 5.2 XPS results for A1 adsorbed onto glass, TCPS, and PS from a range of solution concentrations. *Nitrogen atomic percentage is used as a marker of protein adsorption since nitrogen is not present in the substrates. (a.) XPS shows comparable amounts of protein on each surface over the measured concentration range. At a solution concentration of 10 μg/ml there is a slightly higher nitrogen percentage on TCPS than the other two surfaces. The amount of protein on the surfaces approaches a monolayer at a solution concentration of 100 μg/ml. Mean +/- SD, n=6.*

One possible explanation of the differences in GP1bα binding could be differences in A1 surface concentration [104]. XPS was used to test this hypothesis. Since nitrogen is unique to the protein, XPS nitrogen signal was used to track the amount of protein on each surface [35,72,81,292,80,315]. Full elemental composition is listed in Table 5.2. On each surface the nitrogen percentage increased as the solution concentration increased. The nitrogen signal increased to 10-13 atomic% nitrogen for surfaces exposed to A1 solutions of 100 μg/ml (Fig. 5.2). The nitrogen percentage in A1 is 17%, as calculated from the amino acid structure. The approach of the measured XPS atomic % nitrogen to the A1 value is consistent with the formation of approximately a monolayer of A1 on the surfaces since the dimensions of A1 (approx. 3.5 x 5 x 5 nm[174]) are similar to the 5nm sampling depth of XPS.

XPS results do not support the hypothesis that differences in platelet adhesion are due to differences in A1 surface concentration. For adsorption from 10 μg/ml solutions, the

amount of adsorbed A1 was comparable on the glass and PS surfaces, but these surfaces showed significantly different behavior in the flow chamber assay.

Although previous studies show that proteins can adsorb in different amounts on different surfaces [8,57,53,316,317], it is not unexpected that all three surfaces show similar adsorption profiles. The adsorption on all three surfaces approaches a monolayer, so the final protein surface concentration is comparable [80,33,318].

5.4.3 ELISA using antibodies binding to nonlinear epitopes within A1

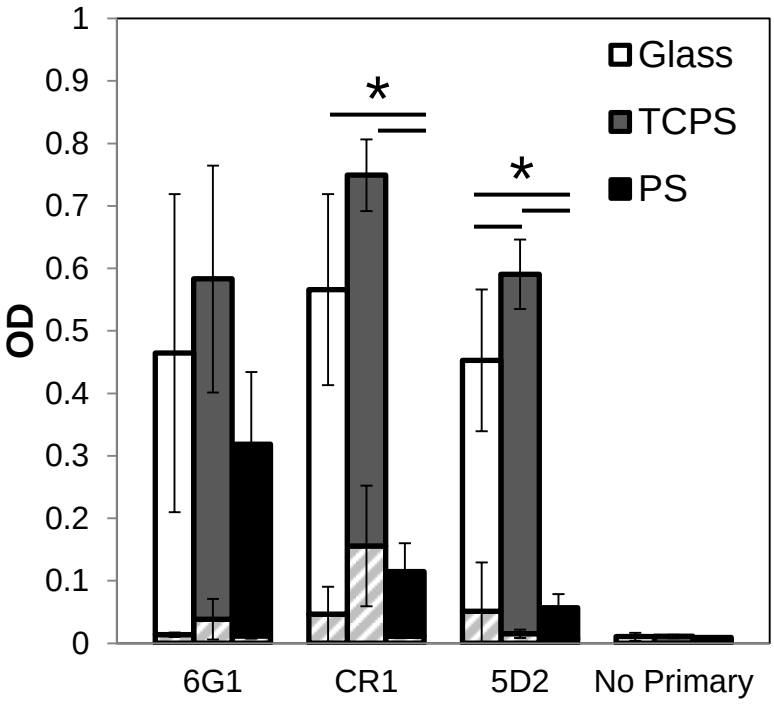

Fig. 5.3 ELISA results from A1 adsorbed onto glass, TCPS, and PS using 6G1, CR1, and 5D2 monoclonal antibodies. *The linear antibody 6G1 shows approximately the same level of binding when A1 is adsorbed to each surface. Antibodies CR1 and 5D2, which bind to nonlinear epitopes within A1, show lower binding when A1 is bound to PS than the other two surfaces. A1 adsorbed at 10 μg/ml. Negative controls of antibody binding to BSA surfaces (striped bars) and binding of the secondary antibody without primary antibody showed minimal activity. Mean +/- SD, n=6-9. * $p < 0.05$.*

To understand A1 function on a surface, it is important to understand protein surface concentration and surface structure. Since A1 function is sensitive to changes in conformation [312,311], differences in A1 surface conformation could affect A1- GP1bα binding. Orientation of A1 on the surface could also affect function [180].

One method to test adsorbed protein surface organization is to measure antibody binding activity. Previous studies identified VWF monoclonal antibodies that bind to different regions of A1, termed 6G1, CR1, and 5D2 [96]. The epitope for antibody 6G1 is Glu700-Asp709 at the C terminus of the A1 domain. The 6G1 epitope should not be sensitive to conformation changes in A1 since the epitope is short and within a flexible protein tail that does not have secondary structure. The exact amino acids comprising the epitopes for antibodies CR1 and 5D2 are not known. Antibodies CR1 and 5D2 do not bind to short linear fragments of A1, meaning the respective epitopes are nonlinear in the amino acid sequence. This means the epitopes exist in 3D space within the intact protein and are therefore sensitive to conformation [96,299,307]. We can determine the epitope availability based on the level of antibody binding.

When A1 was adsorbed onto glass, TCPS, and PS, antibody 6G1 showed no statistically significant difference in binding ($p < 0.05$) between the three surfaces (Fig. 3). This suggests a comparable A1 concentration on each surface, consistent with the XPS results.

Antibodies CR1 and 5D2 showed different results from antibody 6G1. Both CR1 and 5D2 showed lower binding to A1 adsorbed onto PS compared to the other two surfaces ($p<0.05$) (Fig. 5.3). Previous characterization shows that CR1 and 5D2 binding is dependent on the presence of an intact disulfide bond between the two cysteine residues within A1 [96]. Loss of the disulfide bond would disrupt A1 conformation, suggesting CR1 and 5D2 recognize native A1. This suggests A1 conformation is disrupted to a greater extent when A1 is adsorbed to PS than TCPS and glass. The packing of A1 on the surface could affect conformation, therefore affecting antibody binding. Previous studies using circular dichroism have demonstrated that adsorbed albumin experienced a decreased loss of secondary structure as solution concentration increased [8]. However, in the experiments here the amount of A1 is approximately the same on all three surfaces, so differences in A1 on the surface should not influence the results.

Since the epitopes for CR1 and 5D2 antibodies are not known, we cannot identify exact structural changes from this assay. We can conclude that the antibodies CR1 and 5D2 are less able to bind their nonlinear epitopes when A1 is adsorbed to PS than when A1 is

adsorbed to TCPS and glass, suggesting a different surface structure (either conformation or orientation) when A1 is adsorbed onto PS.

5.4.4 ToF-SIMS shows differential exposure of amino acid side chains

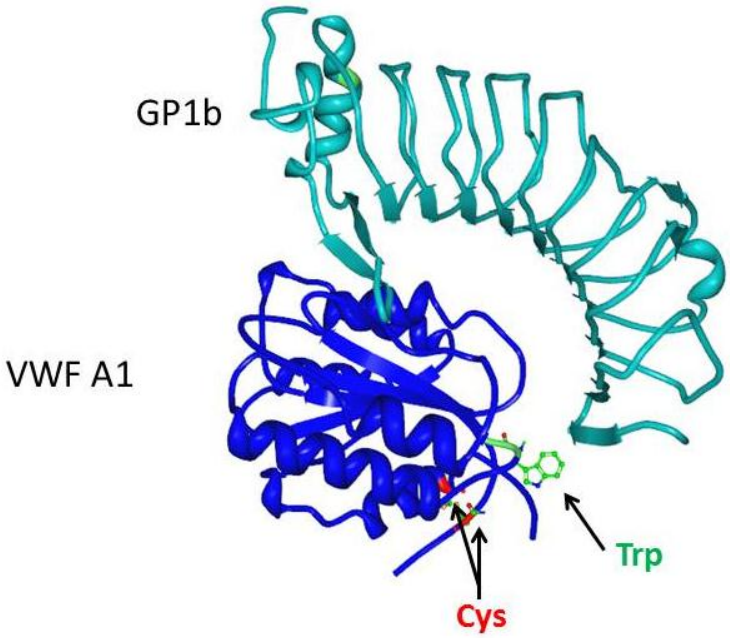

Fig. 5.4 The crystal structure of A1 bound to the extracellular portion of GP1bα (PDB 1sq0). *Trp and Cys residues highlighted.*

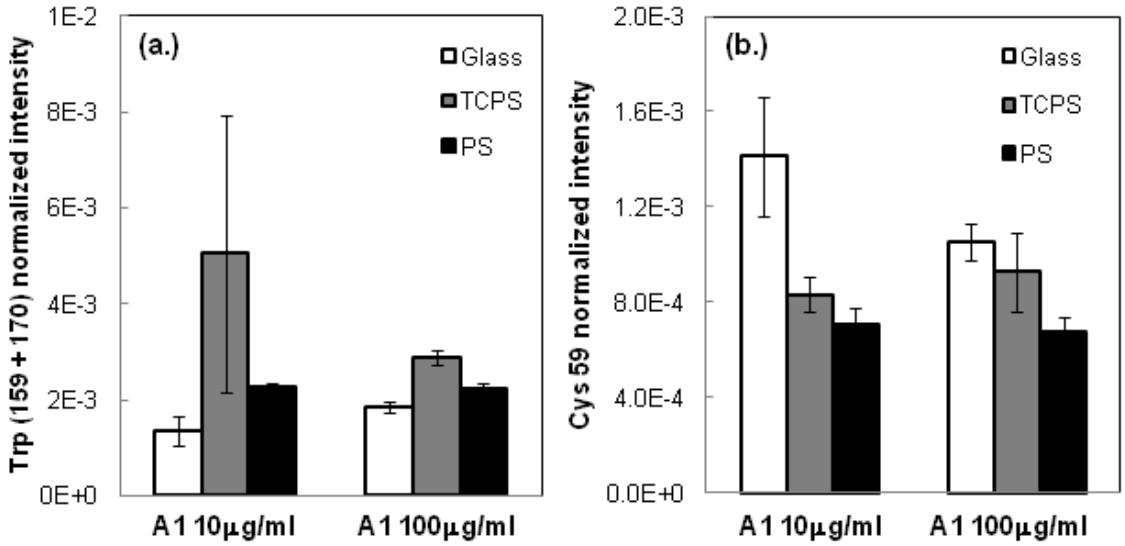

Fig. 5.5 ToF-SIMS peak intensity of (a.) Trp peaks (m/z 159+170) and (b.) Cys peak (m/z 59) normalized to the sum of the amino acid peaks. *A1 adsorbed onto glass, TCPS, and PS from 10 µg/ml and 100 µg/ml solutions. (a.) Trp exposure was lowest when A1 was adsorbed onto glass. (b.) Cys exposure was lowest when A1 was adsorbed onto PS and highest when A1 was adsorbed onto glass. Mean +/- SD, n=10 All differences in intensity between surfaces were statistically significant ($p < 0.05$) with the exception of Cys intensity between the glass and TCPS surfaces.*

We used ToF-SIMS to further explore the differences in orientation and conformation when A1 was adsorbed onto the three surfaces. Previous studies show that ToF-SIMS can identify differences in protein orientation and conformation [72,68,69] due to the technique's shallow sampling depth of ~2nm. We determined the relative solution exposure of specific amino acids by comparing the normalized intensities of amino acid peaks.

In these studies, we focus on the exposure of cysteine and tryptophan due to their asymmetric distribution within A1 and importance in protein function. A1 contains two Cys residues, disulfide bonded to each other. In the A1 amino acid sequence, the two Cys residues are far apart near the N- and C-terminal at positions 509 and 695, respectively. However, in 3D space, the residues are in close proximity, allowing disulfide bonding (Fig. 5.4). Several studies have shown the presence of the S-S bond is important for A1 function, with the loss of the S-S bond resulting in activation [319,295]. Trp is also of interest for

ToF-SIMS analysis because A1 contains only one Trp at residue 550 (Fig. 5.4). Trp550 electrostatically interacts with GP1bα during binding [298], so Trp exposure gives information about accessibility of a region of the GP1bα binding site.

Trp solution exposure was examined by calculating the sum of Trp m/z 159 + 170 peaks normalized by the sum of the intensity of all amino acid peaks. The observed differences in Trp exposure on the glass and PS surfaces (Fig. 5.5) were consistent with functional measurements. Within each adsorption concentration the Trp exposure was lowest on the glass surface. Since the Trp550 residue in A1 electrostatically interacts with GP1bα, this is consistent with the flow chamber results at high shear which showed the least adhesion of platelets on A1 adsorbed onto glass surfaces. Trp intensity was higher when A1 was adsorbed onto the polystyrene surface than glass surface, and this surface also showed higher platelet number at high shear. However, at low shear, platelets behaved differently with low binding on polystyrene surfaces and higher binding on glass surfaces. In contrast, for A1 adsorbed onto TCPS the Trp peak intensity did not directly relate to platelet function at high shear. In the flow chamber assay, platelets showed similar behavior on A1 adsorbed onto TCPS and glass. However, Trp showed higher exposure when A1 was adsorbed to TCPS than to PS and glass.

The inability to form a direct relationship between Trp exposure and A1 function for all surfaces at both high and low shear suggests that the functional differences observed in this study are likely not due solely to orientation differences on different surfaces. If the accessibility of the GP1bα binding site on the three surfaces was solely due to orientation, the Trp exposure as measured by ToF-SIMS would be expected to directly relate to binding site exposure. Since we do not observe this relationship, the functional differences are likely due to both conformation and orientation effects, especially for the TCPS surface. The interpretation is complicated somewhat by the fact that Trp550 is at one end of the GP1bα binding site. Since the A1- GP1bα interaction involves multiple residues, the exposure of the Trp residue might not be an appropriate marker of binding site exposure even if it gives information about the solution exposure of that portion of the protein.

When A1 was adsorbed onto glass, TCPS, and PS, there were differences in the normalized Cys peak intensity. Of the three surfaces, the Cys exposure was highest when A1 was adsorbed onto glass, which showed most platelet detachment at high shear (Fig. 5). Cys

intensity was lowest when A1 was adsorbed onto PS, which showed platelet detachment at low shear. A1 on TCPS showed intermediate Cys intensity. Cys intensity in the ToF-SIMS spectrum should be affected by the solution exposure of the amino acid. The intensity could also be influenced by the presence or absence of a disulfide bond between the two Cys amino acids. Okamato, et al. showed that the intensity of fragments originating from the Cys residues was higher when the disulfide bond was broken compared to when it was intact [320]. Therefore, the high Cys signal when A1 is adsorbed onto a glass surface could also be due to the loss of disulfide bonding during or after adsorption.

In the A1 crystal structure, Cys and Trp are close in 3D space, separated by <1nm. Therefore, it may seem surprising that Cys and Trp amino acid ratios show different trends: Cys least exposed on PS and Trp least exposed on glass. These observations again point to conformation differences between the surfaces, since orientation differences alone would likely not be sufficient to cause the observed changes in Cys and Trp exposure.

When A1 is adsorbed to glass, Trp is less solvent-exposed than on PS and TCPS and Cys residues are more exposed. This could correspond with an A1 surface structure on glass in which the GP1bα binding site is near the surface, blocking binding and leading to detachment observed at high shear in the flow chamber experiments. When A1 is adsorbed to PS, the Trp is more exposed than when A1 is adsorbed to glass and the Cys is less exposed than A1 on glass and TCPS. This suggests that the GP1bα binding site is more exposed when A1 is adsorbed to PS than glass, leading to more platelet adhesion and rolling at high shear.

Platelet behavior is different on the three surfaces at low shear, with platelets detaching from A1 adsorbed onto the polystyrene surface and remaining stationary on A1 adsorbed onto glass surfaces. This suggests that access to the region of A1 containing Trp550 is not essential for GP1ba binding at low shear. Instead, the region of A1 containing the Cys residues appear to be more important.

Comparing respective Cys and Trp exposure on different surfaces, we observed less difference when A1 is adsorbed at higher concentration versus lower concentration. This further suggests that conformation is a more important effect than orientation to explain the observed differences. At adsorption from higher solution concentrations, a higher surface density could prevent conformational changes, resulting in similar behavior on different

surfaces. Previous studies using circular dichroism of adsorbed albumin showed decreased loss of secondary structure as adsorption concentration increased [8], supporting the hypothesis that higher surface packing inhibits protein unfolding.

5.4.5 NEXAFS shows differences in amide backbone ordering

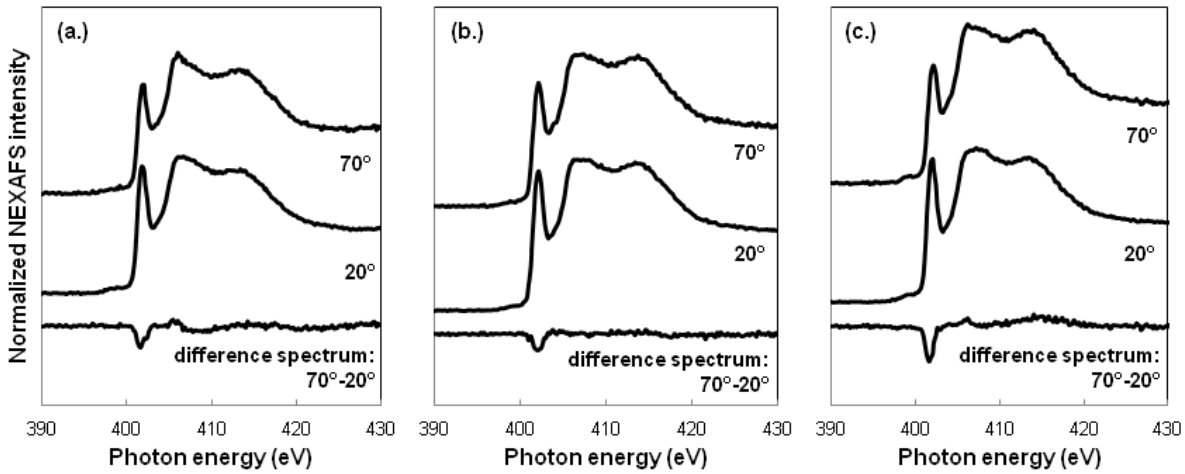

Fig. 5.6 NEXAFS nitrogen k-edge spectra of A1 adsorbed onto (a.) Glass, (b.) TCPS, (c.) PS. *Spectra collected at incident angles 70°, 20°. Strongest dichroism of the π* feature was observed when A1 was adsorbed onto PS, as shown in the difference spectrum of 70°-20°. A1 adsorbed at 10 μg/ml. Spectra offset for clarity.*

In addition to examining the side chain exposure, we were also interested in the protein backbone secondary structure. The NEXAFS nitrogen k-edge spectra of A1 adsorbed onto glass, TCPS, and PS exhibit strong π* absorption resonances around 400eV (Fig. 5.6) corresponding to the protein amide backbone [321-326].

In protein films containing ordered structures, the intensity of the π* feature varies with changing NEXAFS angle [200]. Because the π* orbitals within α-helices are oriented in many directions, they typically only contribute slightly to the angle-dependent NEXAFS signal [36,327]. In contrast, ordered β-sheet structures typically contribute the majority of the angle-dependent NEXAFS signal for surface bound peptides and proteins, as shown in previous studies examining the orientation peptides and proteins on surfaces [69,36,328].

To examine the NEXAFS angle dependence, we calculated the difference spectrum between spectra collected at 70° and 20° incident angle (Fig. 5.6). The difference spectra

showed different dichroisms when A1 was adsorbed onto glass, TCPS, and PS. A1 adsorbed onto PS shows a slightly stronger dichroism, suggesting that the amide π* orbitals are most organized on this surface. This could be due to A1 adopting a wider range of orientations on glass and TCPS. The dichroism is somewhat weak on all the surfaces, likely because the beta sheets within A1 are not completely parallel, and the NEXAFS signal is averaged over all the π* orbitals in the beta sheets.

The negative polarity of the dichroisms shows the x-rays are more strongly coupled with the amide π* orbitals when the x-rays are at a glancing incident angle compared to a near-normal incident angle. This suggests that the amide bonds are oriented more parallel to the surface than perpendicular on all three surfaces [36,69].

5.4.5 Measuring platelet adhesion to adsorbed full-length VWF using a parallel plate flow chamber

It can be useful to work with model proteins or isolated binding domains to attain a detailed understanding of surface structure and function. It is also useful to understand how the behavior of an isolated domain relates to the full-length structure.

To explore the influence of surface type on full-length VWF, VWF was adsorbed onto glass, TCPS, and polystyrene as performed with the A1 domain. Measuring platelet adhesion using a parallel plate flow chamber showed some differences from the behavior of the isolated A1 domain.

The number of platelets on each surface remained relatively constant over the range of shears tested (Fig. 5.7a). There was no decrease in the number of platelets on the surface at high shear, in contrast with the detachment behavior observed when platelets were in contact with adsorbed A1. This could be due to a higher concentration of A1 domains present on the surfaces created using full-length VWF (A1 solution concentration 0.4μM versus VWF solution concentration 114μM). The fraction of bound platelets is not significantly different on the different surfaces at a shear rate of 2 or 20 dyne/cm^2. There is a small decrease in the fraction bound when the shear decreases to 0.5 dyne/cm^2.

Approximately 30% of the platelets detach from the surface compared to the number bound at 2 dyne/cm^2 for VWF adsorbed onto the glass and polystyrene surfaces. Slightly more platelets remain attached to VWF adsorbed onto the TCPS surface. Platelet detachment

at low shear rates demonstrates shear-enhanced adhesion, as there was an increase in binding when force on the bond was increased [102,105,98].

Of the platelets on the surface at each respective shear rate, some fraction of the platelets were stationary. At the high shear rate (20 dyne/cm^2), only about 10% of the platelets were stationary on VWF adsorbed onto glass and polystyrene surfaces (Fig. 5.7b). Somewhat more platelets were stationary on VWF adsorbed onto TCPS, indicating stronger platelet binding. At lower shear rates, there was high variability in the fraction of stationary platelets. However, there was a trend of more stationary platelets on VWF adsorbed onto TCPS than the other two surfaces at 2 dyne/cm^2. At the lowest shear measured here (0.5 dyne/cm^2), the fraction of stationary platelets was not significantly different on the three surfaces, with means ranging from 53% to 70% stationary.

Overall, these results suggest that the ability of full-length VWF to bind platelets is very similar when adsorbed onto glass and polystyrene. There is slightly more platelet-VWF interaction when VWF is adsorbed onto TCPS as indicated by the higher fraction bound and fraction stationary, but it is not a strong difference. These results do not necessarily mean that VWF function is the same on all materials, but minimal differences were observed under the conditions tested here.

In these experiments, VWF was adsorbed at a relatively high solution concentration (114μM). It is possible that at a lower surface coverage of VWF, platelet behavior would be different on the different surfaces. Previous studies have demonstrated that high protein packing on a surface inhibits protein unfolding [8], which could be different on different surfaces. Extent of unfolding of VWF could influence its function, as previous studies have demonstrated that removal of neighboring domains to A1 increase interaction with GP1bα [151].

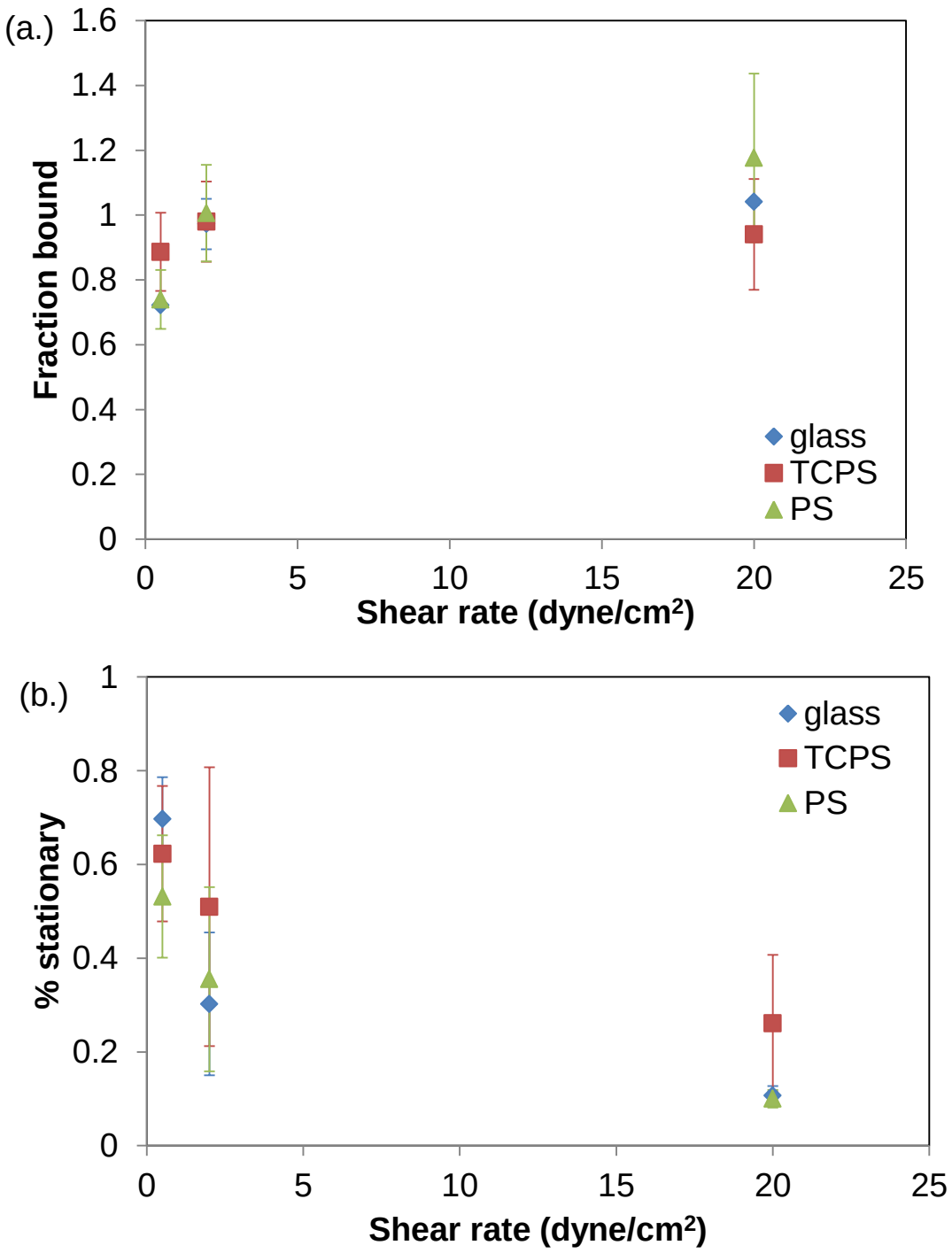

Fig. 5.7 Platelet adhesion on VWF adsorbed onto glass, TCPS, and PS. *Platelets were introduced at 2 dyne/cm^2 for 30sec, then shear rate was increased or decreased. (a.) Fraction bound platelets is the number of platelets in the field of view relative to the initial number of platelets at 2 dyne/cm^2. (b.) Fraction stationary platelets is calculated relative to the number of platelets in the field of view at the specified shear rate. VWF adsorbed onto each respective surface from 114µM solutions. Values represent mean +/- SD of at least two separate measurements on different days.*

5.4.6 XPS analysis of full-length VWF

We used XPS to further characterize the amount of protein on each surface at the solution concentration used for the flow chamber experiments. Since nitrogen is not present in either substrate, protein adsorption can be tracked by following the nitrogen signal with XPS. Full atomic composition is listed in Table 5.3.

XPS shows that a very similar amount of protein adsorbs onto each surface, resulting in a nitrogen signal of approximately 9% (Fig. 5.8). Therefore, any observed differences in VWF function cannot be explained by differences in surface coverage.

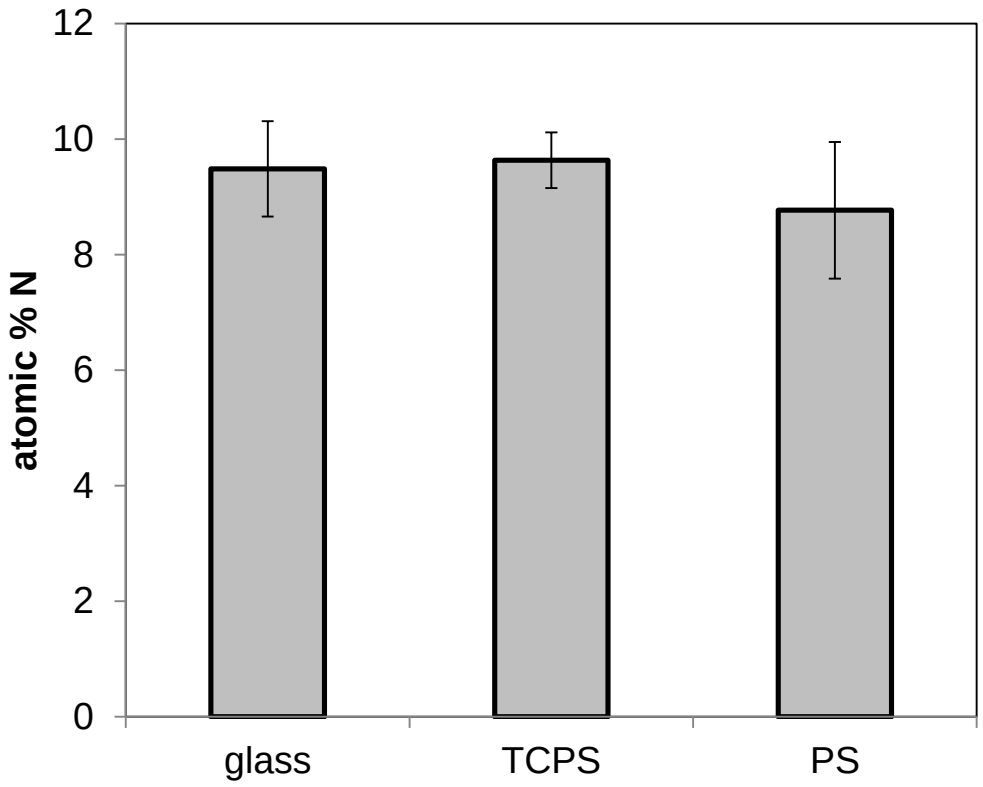

Fig. 5.8 XPS results for VWF adsorbed onto glass, TCPS, and PS at a solution concentration 114μM. *Nitrogen atomic percentage is used as a marker of protein adsorption since nitrogen is not present in the substrates. XPS shows a comparable amount of VWF on each surface. Mean +/- SD, n=6.*

5.4.7 ToF-SIMS analysis of full-length VWF

VWF is a large protein and the crystal structure of the full molecule is not known. Since we cannot identify specific peaks to give information about surface structure, is it useful to use principal component analysis since it calculates the greatest sources of variance in the data using all the peaks in the dataset [78,83,79].

PCA of ToF-SIMS data from VWF adsorbed onto glass, TCPS, and polystyrene shows overlapping of the 95% confidence interval ellipses for the three sample types (Fig. 5.9). VWF adsorbed onto TCPS does show some difference from the other two surfaces, but still partially overlaps. This is consistent with the results from the functional studies, which showed that VWF behaved very similarly when adsorbed to glass and polystyrene, with some small differences when adsorbed to TCPS.

The overlapping 95% confidence intervals suggest that ToF-SIMS does not detect strong differences in the amino acid exposure of VWF adsorbed to the three surfaces. The lack of difference could be attributed to the large size of the protein. A previous study demonstrated that differences in adsorbed protein conformation were more readily detected using a small protein (myoglobin) than a large protein (fibrinogen) [35].

The sampling depth of ToF-SIMS is on the order of 1-2nm [75]. A large protein such as VWF (270kDa [329]) could adsorb in a layer significantly thicker than the ToF-SIMS sampling depth. If the protein layer is thick, there could be differences in the interaction between VWF and the respective surfaces that would not be detected by ToF-SIMS. In addition, the solution-exposed amino acids could be different when VWF is adsorbed onto the three surfaces. However, the large amino acid signal from the rest of the protein could prevent subtle differences in amino acid exposure from being detected.

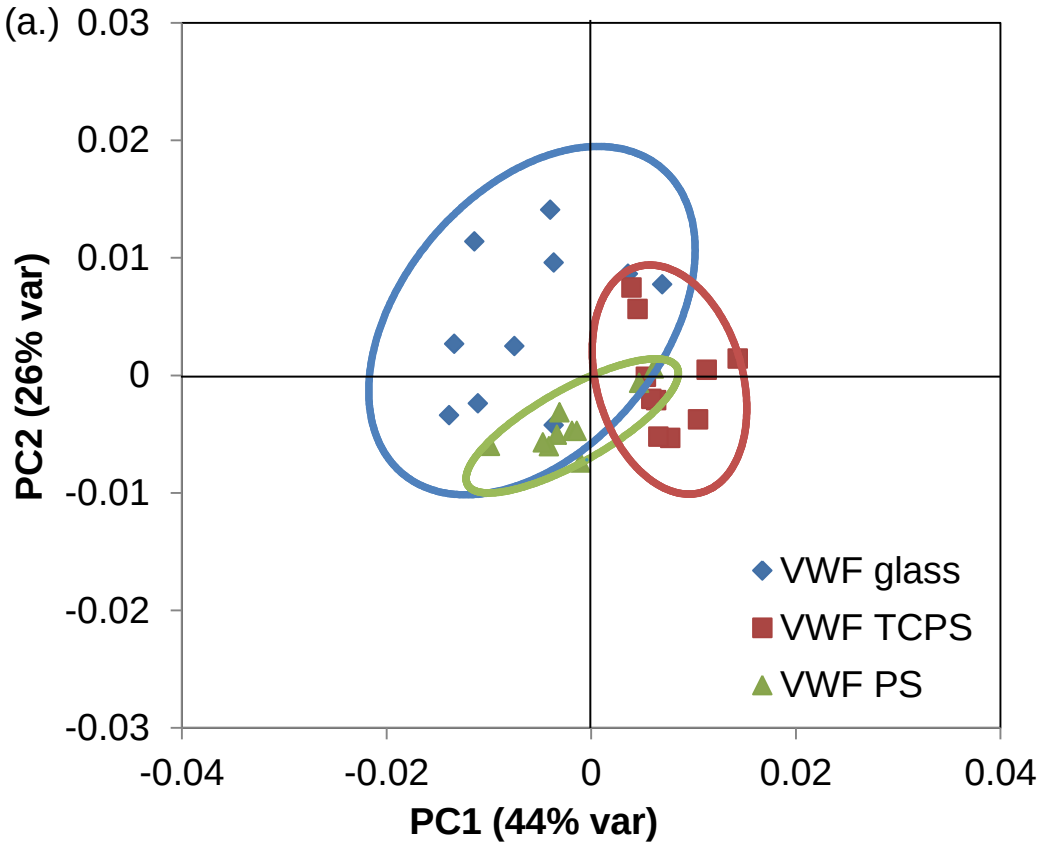

Fig. 5.9 PCA scores of VWF adsorbed onto glass, TCPS, and polystyrene. *Scores of PC1 (44% var) versus PC2 (26%). Ellipses represent score 95% confidence intervals. VWF adsorbed onto each respective surface from 114μM solutions. Spectra collected on 2 samples, 5 spots/sample, for each sample type.*

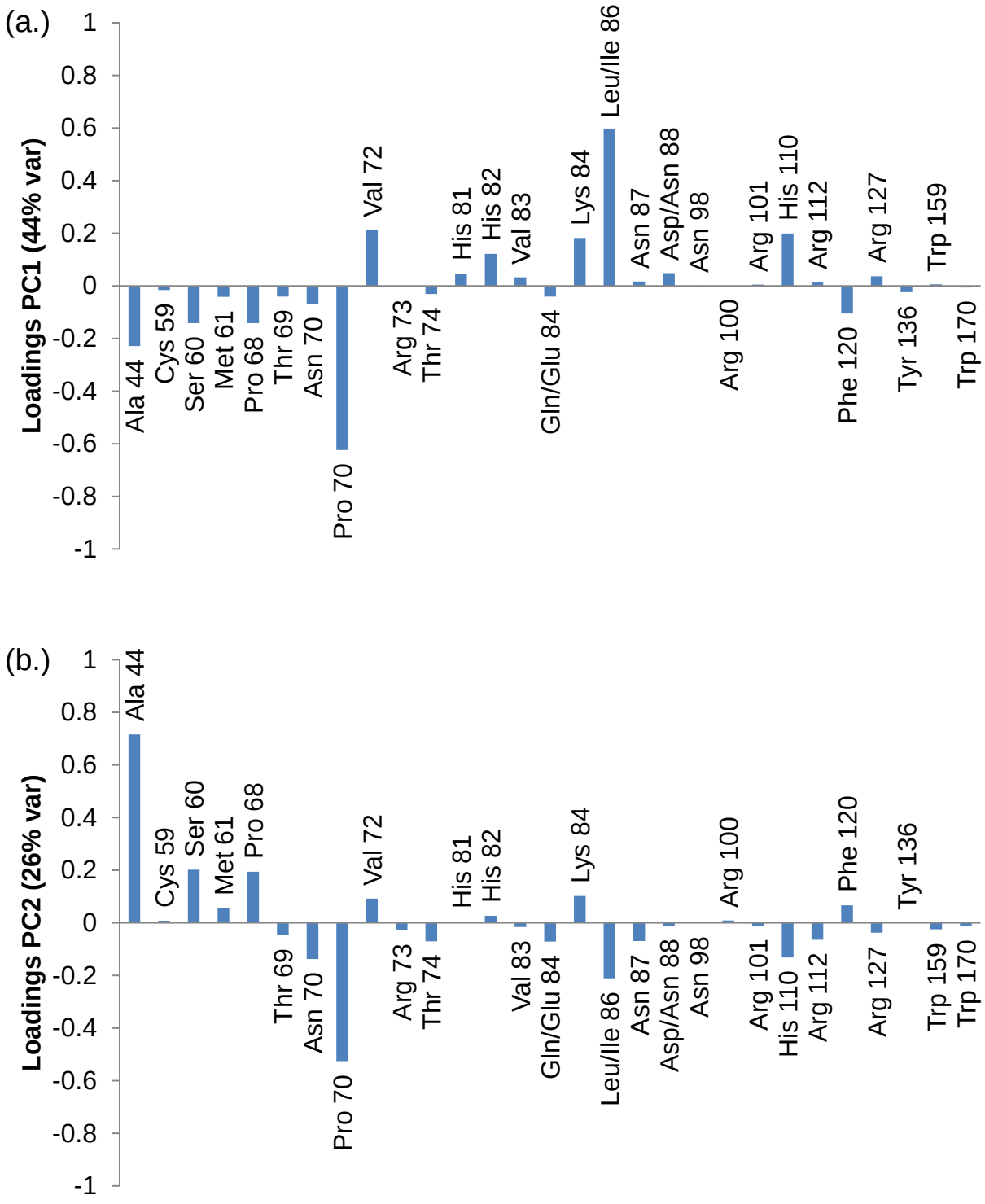

Fig. 5.10 PCA loadings of VWF adsorbed onto glass, TCPS, and polystyrene. *(a.) Loadings of PC1 (44% var) (b.) Loadings of PC2 (26%).*

5.5 Discussion

A1 function is different when adsorbed onto glass, TCPS, and PS. At high shear, platelets showed detachment from A1 adsorbed onto all surfaces, with the greatest detachment observed on glass. At low shear, platelets exhibited stationary adhesion to A1 adsorbed onto glass, while they detached off A1 adsorbed onto the polystyrene surfaces. A potential hypothesis to explain these differences in behavior is a difference in surface concentration. However, XPS studies showed that a comparable amount of A1 is adsorbed onto all three surfaces, with the same nitrogen composition on glass and polystyrene surfaces. Therefore, the differences in rolling velocity cannot be accounted for by protein surface concentration.

Another potential explanation for the lack of observed platelet binding on glass is the removal of A1 by the flow or platelets. A1 could potentially be more easily removed from glass than the other two surfaces if it is more weakly immobilized. Alternatively, A1 could be totally misfolded and denatured when adsorbed onto glass. However, we know that the A1 is still present and active on the glass surface throughout the experiment because some platelets do bind at higher shears. The ability of antibodies CR1 and 5D2 to maintain recognition when A1 is adsorbed onto glass also suggest that A1 is not totally denatured or misfolded.

Instead, these studies suggest that differences in protein surface structure are responsible for the different behavior observed. There could be differences in A1 surface conformation, orientation, or both. While it is difficult to distinguish between conformation and orientation differences, we can compare hypotheses based on the results presented here.

There are several results that point to conformational differences of A1 on the three surfaces that resulted in the functional differences observed in the flow chamber assays. ELISA showed different binding of antibodies with nonlinear epitopes. Previous studies showed that the antibodies are sensitive to the presence of the S-S bond in A1, suggesting antibody binding is dependent on A1 conformation [96]. The ToF-SIMS data is also consistent with conformation differences on the surfaces, with a conformation on glass in which the Trp is buried at the protein-surface interface and the Cys is more exposed to the solution. This could make the GP1bα binding site inaccessible at high shear. However, the

region of A1 near the Trp residue does not appear to be essential for GP1ba binding at low shear, where platelets exhibit stationary adhesion on glass surfaces. The NEXAFS data showed A1 adsorbed onto PS had a stronger angle dependence than the other two surfaces. This difference could be due to conformation differences. NEXAFS signal depends on ordering [36,69], so the conformation of A1 on PS could be more ordered than the other two surfaces.

Some results are also consistent with A1 adopting different orientations on different surfaces. The ToF-SIMS amino acid peak intensities showed A1 on glass had lower Trp exposure and higher Cys exposure. This data is consistent with an orientation of A1 on glass in which the GP1b binding site is toward the surface, and less accessible for platelet binding at high shear than A1 on the other surfaces. However, the Trp and Cys residues are close together, so it is unlikely the two amino acids would show opposite trends (Trp low and Cys high). In addition, if A1 was only in a different orientations, not conformations, we would expect the trends in platelet binding to be consistent between high and low shears due solely to the relative accessibility of the GP1bα binding site. In fact, platelet adhesion is markedly different at high and low shears. At high shear, platelets detach from A1 adsorbed onto glass surfaces but A1 adsorbed onto polystyrene surfaces mediates platelet rolling. At low shear, platelets show stationary adhesion on A1 adsorbed onto glass, but detach from A1 adsorbed onto polystyrene surfaces. The differences observed in the ELISA assays could potentially be explained by differences in A1 orientation. However, the binding sites for antibodies CR1 and 5D2 are not known, so we cannot conclude if low binding of antibodies CR1 and 5D2, as observed in A1 adsorbed onto PS, is consistent with an orientation in which the GP1b binding site is accessible. The differences in NEXAFS polarization dependence could be consistent with different orientations [69,36]. The amide bonds of A1 could be oriented more parallel to the surface when A1 is adsorbed onto PS than glass or TCPS, leading to stronger angle dependence when A1 is adsorbed onto glass. However, the NEXAFS signal is also dependent on ordering [36,69], so there could be a contribution from protein conformation.

Overall, the data support conformation differences in A1 on the three surfaces, but we cannot rule out that there are also orientation differences.

The differences in surface structure of A1 adsorbed on to the three surfaces tested here resulted in differences in the shear-enhanced adhesion observed when platelets interacted with A1 on the surfaces. The A1-GP1bα bond has been demonstrated to undergo shear-enhanced adhesion [105,295,102,314,106]. This has been proposed to be due to changes in dissociation rate and bond lifetime with varying shear. One previous study demonstrated that the A1-GP1bα dissociation rate constant k_{off} varied exponentially (4.2 +/- 0.8 s^{-1} to 7.3+/- 0.4 s^{-1}) as a function of the force applied to the bond (from 36 to 217 pN) [105]. Dissociation rate constants were determined by pause time analysis of transient capture/release events.

Bond lifetimes as a function of force have also been measured using AFM. A1-GP1bα bond lifetime increased as force on the bond increased to a maximum of approximately 20pN [107,102]. Type 2B mutation I1309V showed a maximum life time at decreased force (approx. 10pN) and type 2B mutations R1306Q and R1450E showed elimination of force-enhanced bond lifetime [102].

Previous studies suggest that the conformation of A1 and its stability is important in controlling GP1bα binding and regulating shear adhesion. Auton et al. have used urea denaturation to demonstrate that A1 undergoes a transition in conformation to an intermediate state in which it has a high affinity for GP1bα [107,330].

Disruption of the disulfide bond within A1 is one way previous studies have probed the effects of conformational changes within A1. One previous showed less GP1bα binding when the disulfide bond was present within A1 than when it was reduced and alkylated [331]. Another study demonstrated that reduction and alkylation of the disulfide bond within the A1 domain influenced shear enhanced adhesion. When binding to reduced and alkylated A1, platelets showed stable adhesion at low shear ($50s^{-1}$), but eliminated binding at high shear ($1500s^{-1}$). A1 containing the intact disulfide bond showed shear enhanced adhesion, with low binding at low shear ($50s^{-1}$), and higher binding as shear increased up to $1000s^{-1}$ [295]. Auton, et al. used circular dichroism to determine that disruption of the disulfide bond within A1 by reduction and carboxyamidation resulted in ~10% loss of α-helical structure compared to the native conformation. This loss of secondary structure resulted in an increase of the GPIbα binding affinity of the A1 domain ~20-fold relative to the native conformation,

again suggesting that disrupting the native A1 conformation leads to increased A1-GP1bα interaction [330].

The structure of the A1 domain has also been disrupted using pH. A previous study exposed the A1 domain to low pH between 2.5 and 3.5 to disrupt the protein secondary structure, then increased the pH to induce refolding. When the pH was increased quickly, A1-GP1bα binding was higher than when the A1 pH was increased slowly, which would presumably allow better refolding into the native state [331]. This suggests that denaturing A1 using low pH, then quickly increasing the pH causes a transition into a high-affinity conformation.

Mutations within A1 also point to the importance of A1 conformation in controlling GP1bα–A1 binding. A class of mutations within the A1 domain, termed type 2B mutations, result in the reduction or elimination of a shear threshold for A1- GP1bα binding [106]. Type 2B mutations are not located within the A1- GPIbα binding site, but are clustered near the disulfide linkage within A1 [332,285]. These mutations can introduce conformational changes within the A1 domain. Previous studies used x-ray crystallography to show differences in conformation between wildtype A1 and a I546V (type 2B) mutant [311,312]. In flow chamber studies, the I546V mutant exhibited enhanced platelet binding, with platelet adhesion at a shear rate of 0.1dyne/cm^2, while the wildtype A1 only exhibited platelet binding above 1dyne/cm^2 [312]. Auton, et al. also showed that type 2B mutations R1306Q and I1309V were stabilized in an intermediate state between native and denatured compared to wildtype A1 by urea denaturation [330,107]. Type 2B mutation I1309V showed a maximum life time at decreased force (approx. 10pN) and type 2B mutations R1306Q and R1450E showed elimination of force-enhanced bond lifetime [102].

In the studies presented here, platelets exhibited strong shear-enhanced behavior when binding to A1 adsorbed onto PS. A previous study using AFM has also demonstrated increased bond lifetime with increasing force when A1 was adsorbed onto PS [102]. Although there could be differences in orientation between A1 on the different surfaces, here we will focus on hypotheses for differences in A1 conformation, due to its likely importance in A1 function. When A1 was adsorbed onto PS, it is likely not in a conformation similar to the conformation induced by type 2B mutations, since type 2B mutations weaken or eliminate the shear-enhanced response as described above. Previous studies have

demonstrated binding of antibodies of CR1 and 5D2 binding is dependent on the presence of an intact disulfide bond within A1 [96]. Since the antibodies showed low binding to A1 adsorbed onto PS, this suggests that the disulfide bond may be disrupted within A1. However, previous studies have shown that reduction and alkylation of the disulfide bond results in stable adhesion at low shear, but eliminated binding at high shear [295], which is not consistent with the function of A1 adsorbed onto PS. A1 adsorbed onto PS also showed relatively lower ToF-SIMS Cys intensity than A1 adsorbed onto the other two surfaces, which is consistent with a higher degree of disulfide bonding [320], although the Cys intensity will also be influenced by the solution exposure of the amino acid.

Therefore the low binding of antibodies CR1 and 5D2 suggests a conformational change within A1 when adsorbed onto PS that is distinct from disruption of the disulfide bond. The functional studies are consistent with A1 on the PS surface stabilized in a native conformation compared to the conformation on the glass and TCPS surface. Platelet rolling on A1 adsorbed onto PS is also consistent with A1 stabilized in the native conformation, as compared to type 2B mutations which exhibit stationary adhesion at low shear [102].

When A1 was adsorbed onto the glass surface, shear-enhanced adhesion was not observed in the studies performed here. Platelets showed stationary adhesion at low shear rates on A1 adsorbed onto glass, and detached at high shear. One hypothesis is that platelets detach from A1 adsorbed onto a glass surface because A1 is totally denatured and not functional. However, platelet binding at low and intermediate shear demonstrate that the protein is still functional. Therefore, it is likely that A1 conformation on glass is stabilized in a high affinity conformation. This could be similar to the conformation induced by type 2B mutations, which results in elimination of shear-enhanced adhesion and reduced binding at high shear as described above. Type 2B mutations also result in near-stationary adhesion at low shear with little rolling [102,105,106], as also observed when A1 was adsorbed onto glass surfaces. A1 function on glass was also consistent with an A1 conformation in which the disulfide bond is disrupted. The high Cys signal in ToF-SIMS when A1 is adsorbed onto the glass surface is also consistent with loss of disulfide bonding [320], although the ToF-SIMS signal is also influenced by the solution exposure of the amino acid. However, relatively high binding of antibodies CR1 and 5D2 to A1 adsorbed onto glass suggest that the disulfide bond is intact when A1 is adsorbed onto glass. It is also possible that A1 adopts a

conformation when adsorbed onto glass that is different from the conformation induced by type 2B mutations, but is still high affinity, potentially analogous to the high affinity A1 intermediate structures described by Auton, et al. [107].

When A1 was adsorbed onto TCPS, it exhibited intermediate behavior compared to the other two surfaces. Shear-enhanced adhesion was observed when A1 was adsorbed onto TCPS, but platelet adhesion was higher than PS at low shear and higher than glass at high shear. The high binding of antibodies CR1 and 5D2 suggest that the disulfide bond in still intact within A1. ToF-SIMS Cys intensity was intermediate between the other two surfaces, which could suggest that A1 adsorbed onto TCPS has a higher degree of intact disulfide bonds than A1 adsorbed onto glass. The presence of shear-enhanced adhesion is consistent with a conformation of A1 adsorbed onto TCPS in which the A1 is not fully stabilized in a high affinity state, as observed on glass, but it stabilized in an intermediate state that is able to bind GP1bα at lower shears than when adsorbed onto PS.

The differences in A1 function on the different surfaces are likely influenced by surface chemistry, as well as the surface charge. PS is neutral, while glass and TCPS are negatively charged. Charge is asymmetrically distributed across the A1 domain, with an area of positive electrostatic potential on the face interacting with GP1bα and an area of negative electrostatic potential on the face opposite the binding site [285]. The A1-surface interaction could be influenced by the presence of charge, resulting conformational differences in the adsorbed proteins leading to the functional differences observed in these studies. Few rolling platelets were observed on A1 adsorbed onto both negatively charged surfaces. So it is possible that the presence of a negatively charged surface induces a high affinity conformation that mediates stationary binding, not a rolling interaction. This could be similar to the conformation induced by type 2B mutation R1450E, which exhibited nearly stationary adhesion at low shear and showed elimination of the force-enhanced lifetime of the A1-GP1bα bond [102].

5.6 Conclusions

These studies demonstrate that the surface to which A1 is adsorbed has an impact on protein adsorption and platelet binding and should be an important consideration when

designing *in vitro* experiments. Since A1 function is surface-dependent, this could also be a design consideration for biomaterials used in blood contacting implants in high shear regions.

Studies of full-length VWF did not demonstrate strong differences in function when adsorbed to the three surfaces tested here. ToF-SIMS studies also supported that adsorbed VWF did not have significantly different surface structure on the different surfaces. That does not necessarily mean that VWF function is always the same on all surfaces. It is possible that differences would be observed at lower surface coverage, where the proteins would not be as tightly packed together on the surface. Due to differences in adsorption conditions between A1 and full-length VWF (lower A1 solution concentration than VWF) it is difficult to directly compare the function of the two proteins. Therefore, these studies do not necessarily indicate that the behavior of the isolated A1 is different from the behavior of full-length VWF.

5.7 Tables for Chapter 5

Table 5.1 Peaks used for ToF-SIMS analysis

Positive ion	Amino Acid	Mass
C_2H_6N	Ala	44.0492
C_2H_3S	Cys	58.9941
C_2H_6NO	Ser	60.0448
C_2H_6NO	Met	61.0095
C_4H_6N	Pro	68.0530
C_4H_5O	Thr	69.0381
C_3H_4NO	Asn	70.0331
$C_4H_{10}N$	Pro	70.0704
$C_4H_{10}N$	Val	72.0862
C_3H_7NO	Arg	73.0527
C_3H_8NO	Thr	74.0660
$C_4H_5N_2$	His	81.0383
$C_4H_6N_2$	His	82.0527
C_5H_7O	Val	83.0526
C_4H_6NO	Gln, Glu	84.0474
$C_5H_{10}N$	Lys	84.0855
$C_5H_{12}N$	Iso, Leu	86.0982
$C_3H_7N_2O$	Asn	87.0576
$C_3H_6NO_2$	Asp, Asn	88.0297
$C_4H_4NO_2$	Asn	98.0144
$C_4H_{10}N_3$	Arg	100.0795
$C_4H_{11}N_3$	Arg	101.0963
$C_5H_8N_3$	His	110.0759
$C_5H_{10}N_3$	Arg	112.0870
$C_8H_{10}N$	Phe	120.0874
$C_6H_{11}N_2O$	Arg	127.0868
$C_8H_{10}NO$	Tyr	136.0831
$C_{10}H_{11}N_2$	Trp	159.0897
$C_{11}H_8NO$	Trp	170.0666

Table 5.2 XPS determined elemental compositions of adsorbed A1

A1 Solution concentration (mg/ml)		% C	% O	% N	% Si
0	Glass	25.4 (4.4)	53.2 (3.6)	0.1 (0.2)	21.7 (1.1)
	TCPS	86.3 (1.1)	13.7 (1.1)	ND	ND
	PS	97.0 (0.2)	3.0 (0.2)	ND	ND
0.01	Glass	24.9 (3.6)	52.7 (3.6)	0.5 (0.1)	21.9 (0.6)
	TCPS	87.3 (2.6)	12.9 (2.9)	0.1 (0.2)	ND
	PS	97.3 (1.0)	2.4 (0.6)	0.4 (0.5)	ND
0.1	Glass	25.8 (3.9)	52.1 (2.8)	0.9 (0.2)	21.2 (1.4)
	TCPS	85.6 (0.4)	13.5 (0.5)	1.0 (0.2)	ND
	PS	95.6 (1.5)	3.6 (1.0)	0.8 (0.6)	ND
1	Glass	35.1 (1.5)	43.1 (2.2)	5.5 (0.6)	16.3 (1.8)
	TCPS	80.2 (1.9)	13.9 (1.8)	5.8 (0.6)	ND
	PS	83.4 (1.6)	10.3 (1.8)	6.4 (0.2)	ND
10	Glass	40.2 (2.4)	38.0 (1.9)	7.5 (0.6)	14.3 (1.2)
	TCPS	72.1 (1.3)	17.1 (0.6)	10.8 (1.4)	ND
	PS	79.2 (1.3)	12.9 (1.5)	7.8 (0.6)	ND
100	Glass	50.5 (6.0)	29.2 (4.9)	11.5 (1.7)	8.8 (2.8)
	TCPS	69.6 (0.9)	17.6 (0.8)	12.8 (1.1)	ND
	PS	74.6 (1.6)	15.3 (1.8)	9.7 (0.4)	ND

Mean of 6 measurements on 2 samples. Standard deviation in parentheses. ND: Not detected

Table 5.3 XPS determined elemental compositions of adsorbed VWF

VWF Solution concentration (µM)		% C	% O	% N	% Si
0	Glass	25.4 (4.4)	53.2 (3.6)	0.1 (0.2)	21.7 (1.1)
	TCPS	86.3 (1.1)	13.7 (1.1)	ND	ND
	PS	97.0 (0.2)	3.0 (0.2)	ND	ND
114	Glass	51.7 (7.1)	30.2 (4.2)	9.5 (0.8)	8.7 (2.7)
	TCPS	70.7 (0.9)	19.7 (0.7)	9.6 (0.5)	ND
	PS	72.9 (2.2)	18.3 (1.5)	8.8 (1.2)	ND

Mean of 6 measurements on 2 samples. Standard deviation in parentheses. ND: Not detected

Chapter 6 Creating defined collagen substrates

6.1 Abstract

Collagen is commonly used as an in vitro substrate due to its important role in many biological functions. However, as with any biological material, it can be challenging create a collagen substrate that has well-defined characteristics.

Here, we examined collagen substrates created using protein from two different manufacturers. X-ray photoelectron spectroscopy and time-of-flight secondary ion mass spectrometry (ToF-SIMS) to measure the amount of collagen adsorbed. More collagen adsorbed onto a tissue culture polystyrene (TCPS) surface from one source than the other source. ToF-SIMS was used to identify differences in the behavior of the A1 domain of von Willebrand Factor interacting with the different collagen substrates adsorbed onto TCPS. Using collagen from one source, the collagen + A1 substrates were more similar to A1-only substrates, as measured by PCA scores. Using collagen from the other source, collagen + A1 substrates were more similar to the collagen-only substrates. This could be due to adsorption of A1 onto the underlying TCPS substrate.

Sum frequency generation vibrational spectroscopy was used to characterize the surface structure of collagen adsorbed at two different pH values. Collagen adsorbed from even a modestly acidic pH (6.5) solution showed markedly less ordering of the protein amide backbone than collagen adsorbed from solution at pH 8.0. This ordering difference could affect collagen function, since its helical structure is important for the recognition of collagen-binding proteins.

These results demonstrate that experimental conditions can greatly affect creation of collagen substrates, and thorough characterization is necessary to create a defined collagen substrate.

6.2 Introduction

Collagen is an important extracellular matrix (ECM) protein in the body, making up 25-35% of the body's total protein [161]. There are over 20 types of collagen that have been

identified to date, with type I being the most prevalent [333]. The collagen types are encoded by different genes and vary in their amino acid structure and location within the body.

In vivo, several collagen types (including types I, II, and III) form a hierarchical fibril structure. Collagen can also form a hexagonal network (including type X) or a fibril associated structure with interruptions in triple helix (including type IX and XII) [163]. To form fibrils, the smallest unit is the peptide chain, containing a high concentration of glycine, proline, and hydroxyproline amino acids. Three peptide chains come together to form a left-handed helix approximately 300nm long and 1.5nm wide, making it more elongated than an α-helix. The presence of the rigid proline residues in the helix prevent the formation of α-helices [161]. Then three of these helices join together in a right-handed helix to form a microfibril. These microfibrils can then form larger fibrillar bundles.

In addition to its structural and mechanical properties, collagen interacts with other ECM molecules, clotting proteins, cell adhesion proteins, and growth factors [162]. Different types of collagen can interact with different cell integrins, affecting cell function [333]. Collagen is also important for tissue engineering applications, where it can provide structural stability, support cell attachment and signaling, and promote angiogenesis [168-170].

Since collagen plays such an important biological role, it is commonly used as a substrate for *in vitro* assays [171]. However, previous studies have shown that differences in preparation of the collagen substrate can affect cell function [172,173,169]. Several groups have attempted to produce defined collagen substrates [334,171,172], but it is challenging due to the heterogeneity of the extent of fibril formation in the protein. Further characterization is needed to understand how variations in the experimental conditions and sample preparation methods affect the final structure and composition of the collagen substrates. This information is needed so well-defined collagen substrates can be designed and fabricated for specific biological applications.

This study analyzes collagen substrates created using protein from two different manufacturers, quantifying the amount of protein contained within the substrate. We also examine the interaction of von Willebrand Factor (VWF) A1 domain with substrates produced from these two collagen sources. VWF is a collagen-binding clotting protein

[148]. We characterize collagen adsorbed at different pH values to determine the effect of acidity on collagen structure. These studies allow us to gain a deeper understanding of collagen substrates which will lead to better defined *in vitro* systems that are more easily related to *in vivo* function.

6.3 Methods

6.3.1 Materials

Human placenta type III collagen was purchased from Sigma (Source 1) and Abcam (Source 2) and used without further purification. The A1 domain of von Willebrand Factor (VWF) was produced in *E. coli* containing residues 1238-1472 of mature VWF with 12 residues at the N terminus from the expression vector (MRGSHHHHHHGS) [174]. The protein was generously provided by Miguel Cruz. Unless otherwise noted, substrates were tissue culture treated polystyrene dishes (Corning).

6.3.2 Protein adsorption for XPS and ToF-SIMS analysis

TCPS substrates were allowed to equilibrate overnight at room temperature with degassed phosphate buffered saline (PBS) (137mM NaCl, 2.7mM KCl, 10mM phosphate) at pH 6.5 or 8.0, depending on the experiment. Experiments comparing collagen from Source 1 to Source 2 were performed at pH 6.5. All experiments comparing pH conditions used collagen obtained from Source 2. Then collagen solutions at the desired pH were incubated with substrates for 2h at 37^{o}C. Following adsorption, substrates were rinsed in PBS to remove loosely bound protein, then water to remove buffer salts. Samples were dried with a stream of nitrogen, then stored under inert nitrogen atmosphere until analysis. Samples were analyzed within two weeks.

6.3.3 XPS

XPS data were collected on a Surface Science Instruments S-Probe instrument with a monochromatized aluminum Kα x-ray source and electron flood gun for charge neutralization. Survey and detail scans were acquired at a pass energy of 150eV and a

takeoff angle of 55°. The take-off angle is defined as the angle between the sample surface normal and the axis of the analyzer lens. For each concentration, two samples were analyzed and three spectra were collected on each sample. Spectra were analyzed using the Service Physics ESCA 2000A analysis software.

6.3.4 ToF-SIMS

ToF-SIMS data were acquired on an ION-TOF 5-100 instrument (ION_TOF GmbH, Münster, Germany) using a Bi_3^+ primary ion source under static conditions (primary ion dose $<10^{12}$ ions/cm^2). Spectra were obtained from 100 μm x 100 μm areas and five positive ion spectra were collected from each sample. One to two samples were analyzed per condition. A low-energy electron beam was used for charge compensation. Mass resolution (m/Δm) of the positive ion spectra was typically between 5500-7000 for the m/z = 27 peak. Mass scales of each spectrum were calibrated to the CH_3^+, $C_2H_3^+$, and $C_3H_5^+$ peaks before further analysis.

Peaks were identified which corresponded to unique amino acid peaks. Amino acid peaks that overlapped with substrate peaks were eliminated using the following criteria. If the normalized intensity of a peak on the bare substrate was greater than 25% of the protein normalized peak intensity, that peak was assumed to have a significant contribution from the substrate and was not included in the amino acid peak list used for analysis. Peaks used for analysis are listed in the appendix in Table 6.2, along with the corresponding amino acid associated with each peak.

PCA processing of ToF-SIMS data from adsorbed proteins has been described extensively elsewhere [78,83,79]. Prior to PCA processing, peaks were mean centered and normalized to the sum of the selected peaks. Analysis was performed using a series of MATLAB (MathWorks, Inc., Natick, MA) scripts written by NESAC/BIO (see http://mvsa.nb.uw.edu).

6.3.5 SFG

The SFG vibrational spectra were obtained with an EKSPLA SFG system by overlapping visible and tunable IR laser pulses (25 ps and 30ps, respectively) in time and

space. The visible beam with a wavelength of 532 nm was delivered by an EKSPLA Nd:YAG laser operating at 50 Hz with 3 outputs, one at 1064 nm and 2 at 532 nm generated with second-harmonic crystals. One of the 532 nm beams is used for SFG, the other one together with the 1064 nm are pumping an EKSPLA optical parametric generation/amplification and difference frequency unit to obtain tunable IR laser radiation from 1000 to 4000 cm^{-1}. The bandwidth was 1 cm^{-1} for the visible pump pulses and 1-6 cm^{-1} for the IR laser radiation (1 cm^{-1} for 2750-3000 cm^{-1} and 6 cm^{-1} for higher and lower wavenumbers). Both beams were unfocused and had a diameter of approximately 3 mm at the sample. The energy for both beams was 190-240 μJ per pulse.

An equilateral CaF_2 prism was spin-coated on one side with deuterated polystyrene. Following annealing overnight at 80°C in air, the polystyrene film was exposed to UV light for at least 1h to introduce oxygen groups to the surface to mimic the TCPS substrate. The prism was then brought into contact with PBS at the desired pH as described above, then collagen was introduced to the solution. After allowing 2h for adsorption at room temperature, the spectra were collected with the pump beams going through the backside of the prism. The input angles of the visible and IR pump beams inside the prism were 55° and 62°, respectively, versus the surface normal of the UV-treated polystyrene surface.

The SFG signal generated at the sample and emitted from the backside of the prism was analyzed by filters and a monochromator, then detected with a gated photomultiplier tube. The spectra were collected with 300-400 shots per data point in 2 cm^{-1} increments. Spectra were recorded in the ppp and ssp (sum, visible, and infrared) polarization combinations. The SFG spectra were normalized by the product of the intensities of the IR and visible spectra.

6.4 Results and discussion

6.4.1 Characterizing collagen from different sources

There are several considerations when trying to create a defined protein substrate. One consideration is the source of protein used for preparing the substrate.

Some proteins can be produced through recombinant expression in bacteria or eukaryotic cells. For some larger proteins, such as collagen, it is possible to isolate the intact

protein from an animal or human source. In the first part of this study we used intact isolated protein and examined the difference in adsorption behavior between protein obtained from two different commercial sources.

6.4.1.1 Amount adsorbed - XPS

When trying to create a defined biological substrate, such as a collagen substrate, it is important to know how much protein is on the surface. XPS was used to characterize the amount of collagen adsorbed onto the surface (Fig. 6.1). Table 6.1 lists the full XPS determined elemental compositions for all the samples.

Although both collagen samples were adsorbed using the same experimental (100μg/ml solution concentration, pH 6.5, TCPS substrate), a higher nitrogen signal was detected when collagen from source 2 was used. Adsorption from source 2 resulted in a nitrogen signal of approximately 11%, while adsorption from source 1 resulted in a nitrogen signal of approximately 7%. This indicates that more collagen adsorbed to the surface from the source 2 sample than source 1. The difference in adsorption amount could be due to differing levels of solubility of the collagen at pH 6.5

An XPS nitrogen content of 11% approaches what would be expected from a monolayer of protein adsorbed onto a surface [335]. An XPS nitrogen content of 7 atomic % suggests submonolayer coverage or a very thin layer of collagen on the surface. XPS by itself cannot distinguish between a thin layer that fully covers a surface and a thicker layer with partial surface coverage.

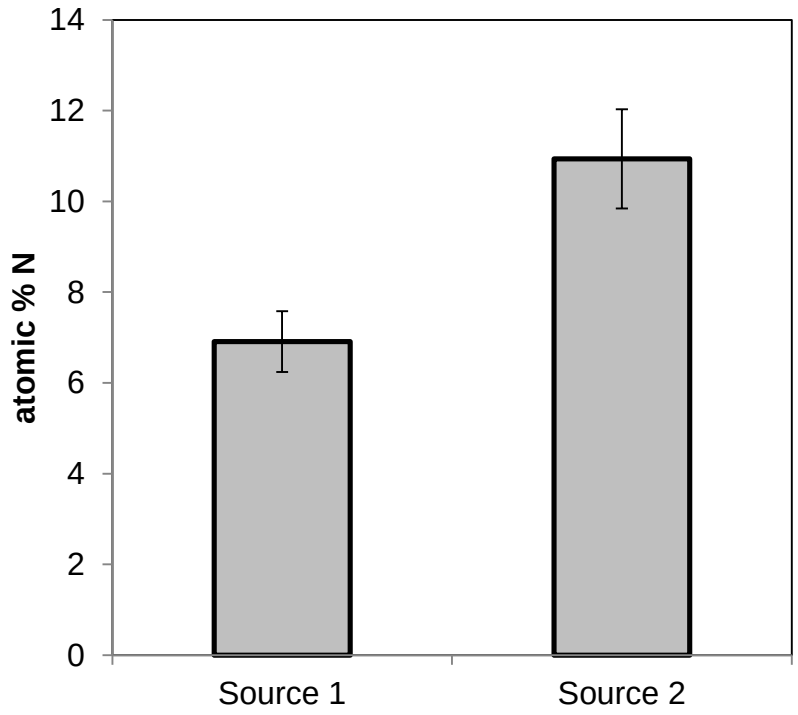

Fig. 6.1 XPS atomic percent nitrogen for collagen adsorbed at 100 μg/ml (pH 6.5) onto TCPS surfaces. *Mean +/- SD. Source 1 represents mean of 9 spots on 3 samples. Source 2 represents mean of 6 spots on 2 samples. The atomic percent nitrogen are significantly different ($p < 0.01$) on the two surfaces.*

6.4.1.2 Amount adsorbed - ToF-SIMS

ToF-SIMS can also provide semiquantitative insight into the amount of protein on a surface, by comparing the total amino acid signal on each surface. Examining the sum of intensities from all amino acid peaks normalized to the total secondary ion intensity (amino acid plus substrate peaks), we again see that the amount of protein on the surface is higher when Source 2 collagen is used (Fig. 6.2). Consistent with the amino acid peak intensities, the intensities of peaks associated with the TCPS substrate are attenuated more by adsorption of Source 2 collagen than the Source 1 substrates (Fig. 6.3a) when adsorbed collagen is present. The higher nitrogen signal observed with XPS for the Source 2 samples compared to the Source 1 samples, could be due to either an increased thickness or surface coverage of the collagen layer. Figure 6.2 shows that subsequent adsorption of A1 onto the Source 1 collagen surfaces further attenuates the TCPS substrate signal (see Table 6.3 for a list of characteristic polystyrene peaks characteristic used to track the attenuation of the TCPS

signals). In contrast, adsorption of collagen from Source 2 almost completely attenuates the substrate signal, and subsequent A1 adsorption does not significantly reduce the signal further (Fig. 6.3b).

Attenuation of substrate signal is affected by both overlayer coverage and thickness. However, ToF-SIMS has a shallower sampling depth than XPS (~2nm vs 5nm for the experimental conditions used in these studies), so adsorption of even a thin protein layer would be expected to greatly attenuate the ToF-SIMS substrate signal. Therefore the presence of a relatively high ToF-SIMS substrate signal intensity following adsorption of collagen from Source 1 is consistent with formation of a patchy or sub-monolayer collagen layer containing exposed regions of the TCPS substrate. The further reduction of the TCPS signals following adsorption of A1 onto the Source 1 collagen surface suggests A1 is adsorbing onto exposed TCPS regions. Thus, the XPS and ToF-SIMS results suggest the difference between the two collagen surfaces is primarily due to a difference in surface coverage and not thickness of the fibrils.

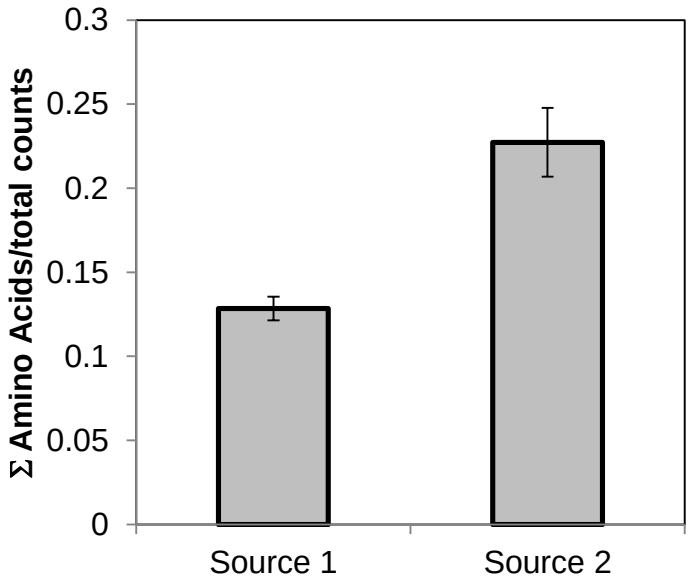

Fig. 6.2 ToF-SIMS amino acid intensity of adsorbed collagen. *The sum of intensities from all amino acid positive secondary ion peaks normalized by the total positive secondary ion intensity. Mean +/- SD. Source 1 represents the mean of 5 spots on 1 sample. Source 2 represents the mean of 15 spots on 3 samples.*

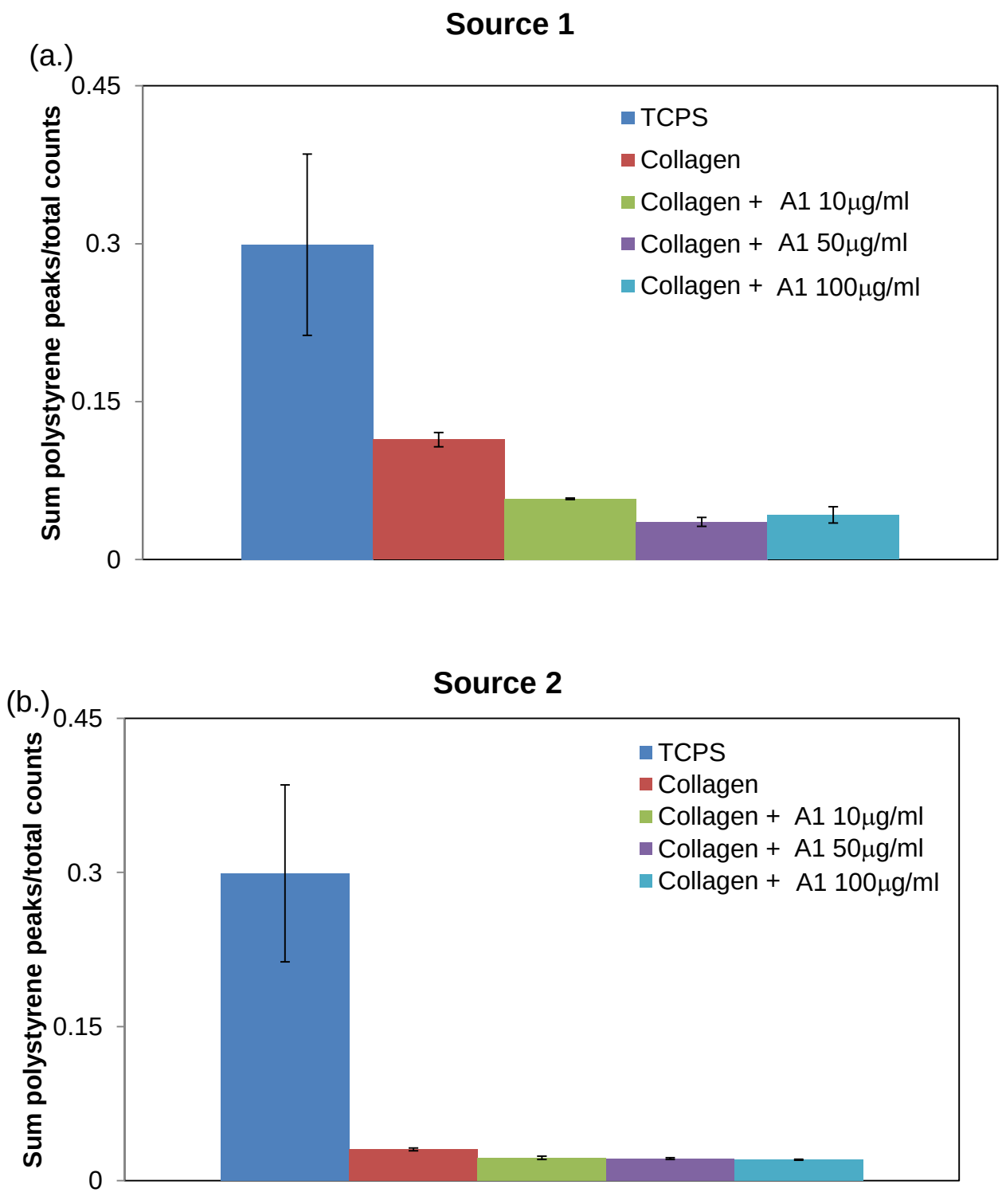

Fig. 6.3 ToF-SIMS peak intensity of TCPS substrate. *Sum of polystyrene peaks normalized to the total counts for each respective spectrum. (a.) For Source 1 collagen, values represent mean +/- SD of 5 spots on 1 sample. (b.) For bare TCPS and Source 2 collagen, values represent mean +/- SD of 10 spots on 2 samples.*

Hydroxyproline, proline, and glycine are amino acids prevalent in the amino acid structure of collagen. We can calculate the proportion of the amino acid signal that can be assigned to each amino acid, which provides information about the amino acid content of the collagen samples from the different suppliers.

Collagen from both sources showed similar amino acid content of the three major amino acids in collagen (Fig. 6.4). Normalized hydroxyproline intensity (m/z 86.0672) was higher in Source 1 collagen ($p < 0.05$); normalized proline intensity (m/z 68.0530 + 70.0704) was higher for Source 2 collagen ($p < 0.05$); normalized glycine intensity (m/z 30.0346) was higher in Source I collagen ($p < 0.05$). The CH_4N (m/z 30.0346) peak could originate from any of the amino acids, but it is the fragment generated from glycine amino acids. The amino acid intensities calculated here as a percentage of the total amino acid signal are similar to the ratios of amino acids in the primary sequence of type III collagen [336,337]. Although we cannot assume that all amino acids have the same secondary ionization probability, as a first approximation this demonstrates that the collagens have similar composition to what would be expected based on the primary amino acid sequence.

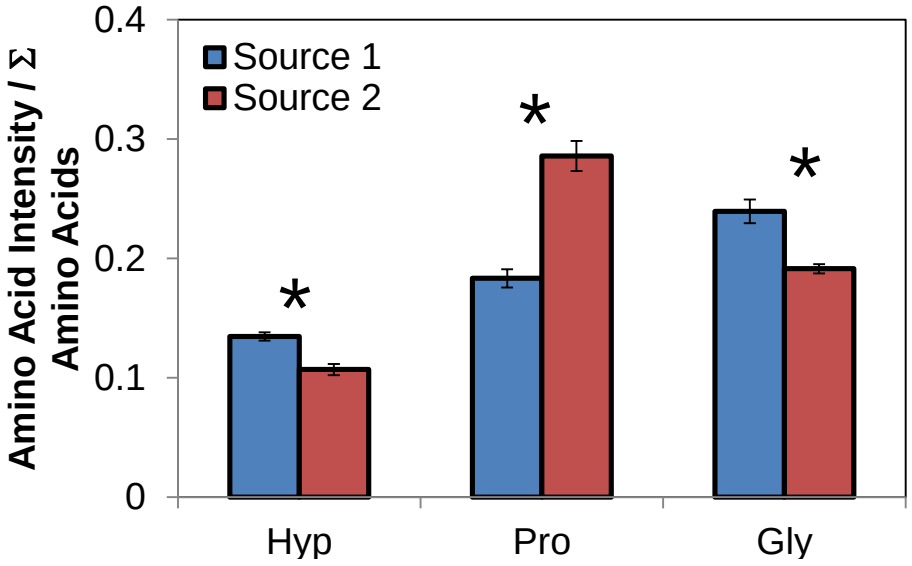

Fig. 6.4 Amino acid content of collagen adsorbed onto TCPS. *Hydroxyproline intensity (m/z 86.0672), proline intensity (m/z 68.0530 + 70.0704), and glycine (m/z 30.0346) normalized to the sum of intensity of all amino acid peaks. Mean +/- SD. Source 1 represents the mean of 5 spots on 1 sample. Source 2 represents the mean of 15 spots on 3 samples. *$p < 0.05$.*

6.4.1.3 Differences in A1 interaction with collagen and TCPS

Many proteins interact with collagen to play roles in ECM assembly, cell adhesion, and blood clotting [162,338], including the clotting protein VWF [164,165]. During the normal thrombosis process that occurs in vivo, VWF interacts with collagen to facilitate initial platelet tethering and the beginning of clot formation [279]. Previous studies have demonstrated that the platelet-binding domain of VWF, the A1 domain, interacts with collagen [288,339].

To better understand the interaction of collagen with A1, it is useful to create a well-defined, integrated collagen-A1 protein system. ToF-SIMS is a tool that can be used to characterize this binary-protein system. Although each protein contains the same amino acids, ToF-SIMS/PCA can clearly distinguish between single protein films based on differences in amino acid composition [78,79,340]. ToF-SIMS has also been used to distinguish between proteins adsorbed in mixtures: binary and ternary mixtures [78,341,342,81,179] and more complex protein systems including 5 protein mixtures [343] and whole plasma [80,179].

ToF-SIMS and PCA have also been used to track the changes in a protein film when one protein is layered on top of another [344]. Martin, et al. showed that PCA could distinguish collagen samples from a layered system of collagen + osteopontin. PCA loadings showed that the collagen-only samples loaded strongly with glycine and proline peaks, as expected due to the high glycine and proline content of collagen.

Using ToF-SIMS/ PCA to compare A1 adsorbed onto collagen surfaces from Source 1 and A1, PC1, which captures 72% of the variance in the dataset, clearly distinguishes the collagen and A1 single component films. The collagen surface has a negative PC1 score while the A1 surface has a positive PC1 score (Fig. 6.5a). The PC1 loadings (Fig. 6.5b) show the amino acid fragments from glycine and hydroxyproline have strong negative loadings, corresponding to the collagen samples as expected. The Val, Lys, and Leu/Ile peaks have strong positive loadings, corresponding to the A1 samples.

For samples that have been sequentially exposed to Source 1 collagen and then A1, the scores are intermediate between the single component collagen and A1. When A1 is

immobilized at the lowest concentration (10μg/ml), the scores for PC1 are the lowest, and closest to the collagen scores. As the A1 concentration increases, the scores for PC1 increase and approach the scores of the single component A1 sample. This suggests that as the A1 concentration increases, the surface becomes more similar to the A1-only surface and the collagen is less concentrated within the ToF-SIMS sampling depth. Even at the lowest A1 concentration, the scores are slightly closer to the A1-only surface than the collagen-only surface, suggesting the surface is more similar to A1 than collagen.

These results suggest that one could control the amount of A1 on the surface by varying the solution concentration of A1. This could be due to different amounts of A1 binding to collagen. Alternatively, the changes observed could be due to A1 adsorbing to the surface underlying the collagen that is exposed due to low collagen coverage. XPS and ToF-SIMS indicate the TCPS surface is not completely covered by the Source 1 collagen, so at least part of the A1 adsorption is likely from binding to the exposed regions of the TCPS.

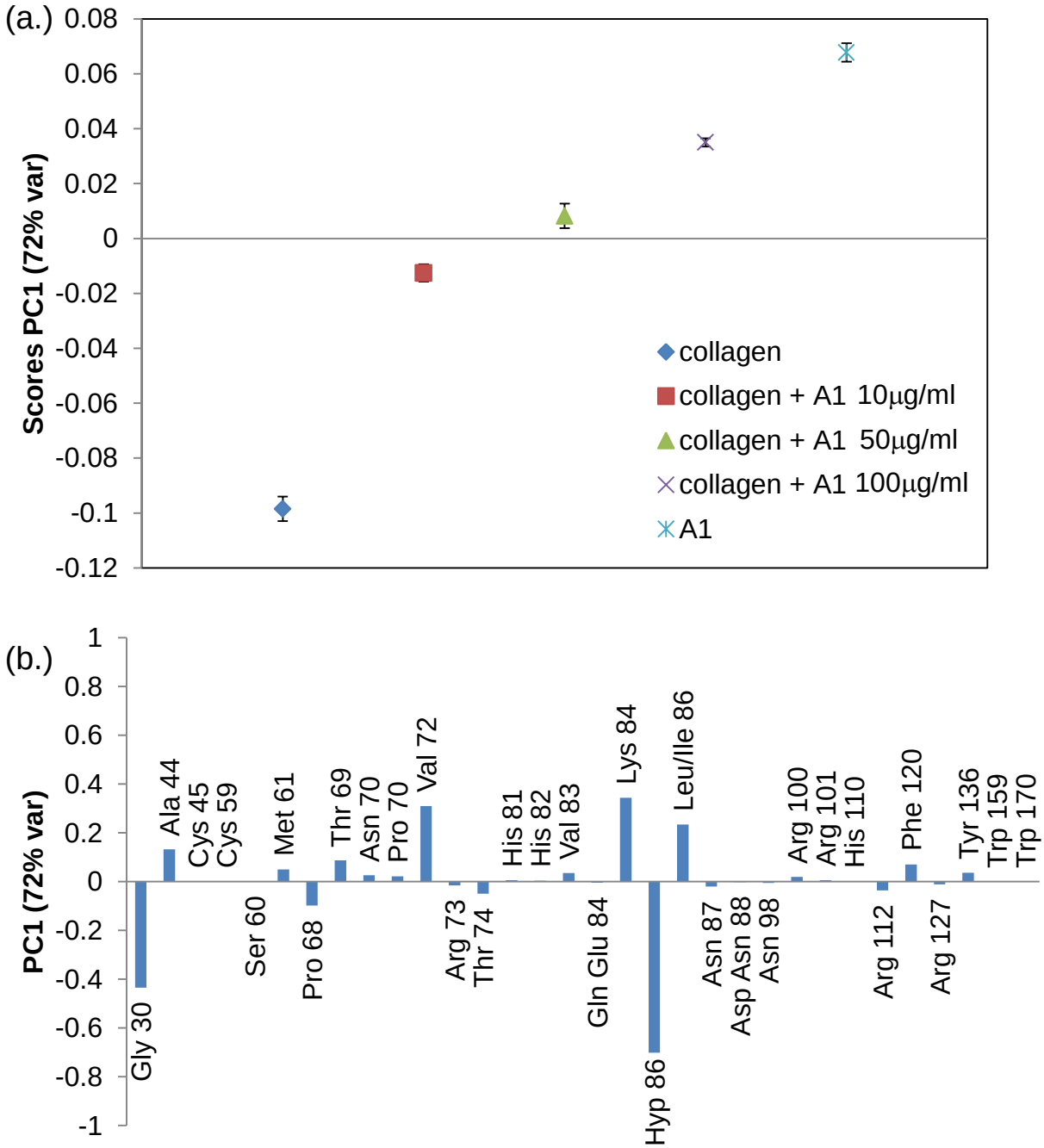

Fig. 6.5 ToF-SIMS/PCA results for adsorbed collagen, A1 and collagen + A1 samples prepared from varying A1 solution concentrations. *The collagen was from Source 1. PC1 scores (72% variance) clearly separate collagen from A1. The collagen + A1 samples have intermediate scores on PC1. Amino acids that are prevalent in collagen (Gly, Hyp) load negatively, corresponding to the collagen samples. Scores represent mean +/- SD of 5 spots on 1 sample. Error bars are present on all samples, but in some cases are smaller than the size of the marker.*

Different results are observed, however, from ToF-SIMS/PCA processing of samples prepared using Source 2 collagen (Fig. 6.6). PC1 (89% variance) again clearly separates the single component collagen from A1. As with Source 1 collagen, the negative loadings corresponding to the Source 2 collagen samples are dominated by peaks from Gly, Pro, and Hyp (Fig. 6.6b). Val, Lys, Leu/Iso, and Ala load strongly positively, corresponding to the A1 samples.

However, when A1 is introduced to the Source 2 collagen substrate, the trends in the scores are different from the Source 1 collagen samples. Varying A1 solution concentration results in samples with similar PC1 scores. The PC1 scores from theses mixed A1-collagen samples are also closer to the collagen-only sample than the A1-only sample, in contrast with the samples made with collagen from Source 1.

The similarity of the A1-collagen samples to the Source 2 collagen samples could be due to several factors. The Source 2 collagen could have a lower A1 binding capacity compared to Source 1 collagen, with a saturation point for A1 binding onto Source 2 collagen already reached at an A1 solution concentration of 10μg/ml.

Alternatively, A1 could be preferentially adsorbing to the underlying TCPS substrate. Even though A1 has been demonstrated to interact with collagen, it also adsorbs onto the TCPS substrate as shown by the A1 results in Figs. 6.5 and 6.6. Since the XPS and ToF-SIMS results indicate Source 1 collagen covers a lower fraction of the TCPS surface, significantly more of the underlying TCPS on Source 1 collagen samples would be available for A1 adsorption. This could result in increasing amounts of A1 adsorption onto the exposed TCPS regions as the A1 solution concentration is increased. Since the Source 2 collagen covered more of the TCPS surface, this sample has significantly lower amounts of exposed TCPS available for A1 adsorption, even at the highest A1 solution concentration of 100μg/ml.

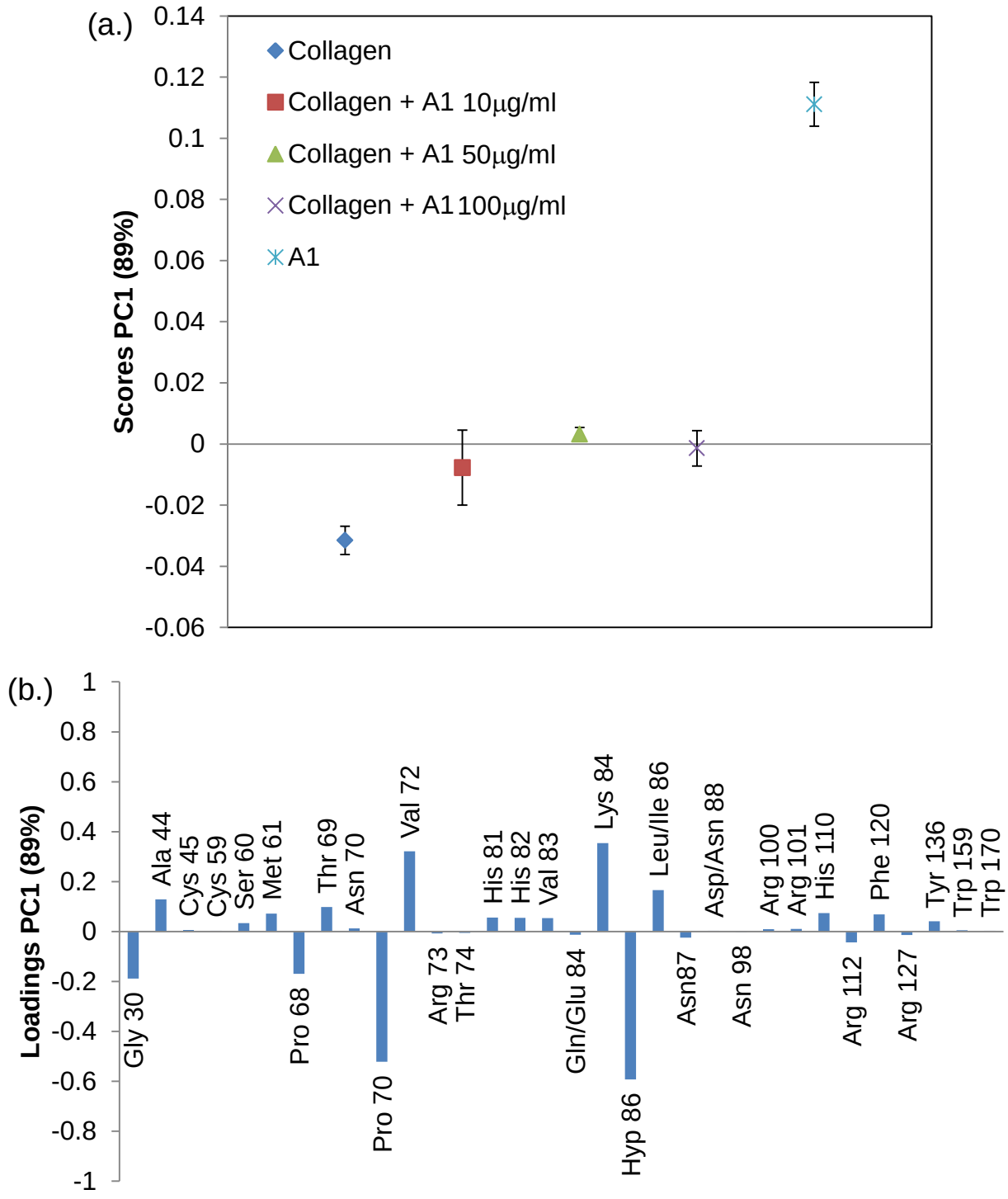

Fig. 6.6 ToF-SIMS/PCA results for adsorbed collagen, A1 and collagen + A1 prepared from varying A1 solution concentrations. *Collagen was from Source 2. PC1 scores (89% variance) clearly separate collagen from A1. All collagen + A1 samples have similar PC1 scores that are intermediate between the collagen and A1 samples. Amino acids that are prevalent in collagen (Gly, Pro, Hyp) load negatively, corresponding to the collagen samples. Scores represent mean +/- SD of 10 spots on 2 samples.*

These results demonstrate that proteins from different suppliers that are identified as the same material can exhibit differences in their adsorption behavior and interactions with other proteins. This could be due to differing levels of solubility of the collagen from different sources. This highlights that the source of materials is an important consideration, especially in biological systems, and should be a consideration in experimental design. If it is necessary to switch commercial suppliers during an experiment, it is important to characterize the material from the new source to ensure that the new material behaves in a comparable manner to the previous material.

6.4.2 Characterizing collagen substrates formed at different pH

In vivo, collagen forms a fibrillar structure that is extremely well controlled [345]. *In vitro*, the fibrillar structure can be strongly influenced by the experimental conditions. While the process of self-assembly is not entirely understood, previous studies have demonstrated that reducing the pH of collagen disrupts the fibrillar structure and denatures the collagen molecules [346-349]. Raising the pH allows self-assembly of the fibrils [350-352] and varying the pH can affect fibril size [353,354] and mechanical properties [354].

When collagen is denatured, its biological activity can be markedly different from when it is in a fibrillar form. Previous studies have shown that fewer platelets adhere to heat-denatured than collagen fibrils [355,356]. Studies of numerous cell types have demonstrated that cells cultured on fibrillar collagen exhibit different behavior from cells cultured on denatured collagen, including adhesion [357-364], morphology [173,365-367], proliferation [368-371], differentiation [372,373], migration [371,374], protein expression [375].

The fibrillar state of collagen can also influence its ability to interact with other proteins. For example, more fibronectin binds to denatured collagen than fibrillar collagen [376,359].

When collagen is denatured, it is hypothesized that binding sites are exposed that are cryptic in the native molecule [377]. Previous studies suggest that different integrin binding sites are exposed when collagen is denatured than when it is in a helical conformation. Both cell studies [378,379,367] and studies using soluble integrins [380] have shown that different integrins bind to denatured collagen compared to fibrils.

Also supporting the hypothesis that different integrins are involved in binding denatured collagen and fibrils, several studies have shown that RGD was not involved in cell adhesion to fibrillar collagen, but binding to denatured collagen is RGD-dependent [379,381-384,358,357]. Since integrin signaling controls so many aspects of cell behavior, including adhesion, migration, and survival [385], changes in integrin binding induced by denatured collagen can have major impacts on cell behavior.

While collagen fibrils form in solution, it is possible that the fibril formation could be influence by the presence of a surface. Elliott, et al. demonstrated that collagen fibrils formed on SAMs terminated with CH_3 groups than SAMs terminated with COOH, NH_2, and OH groups using AFM [386]. Zhu, et al. used AFM to demonstrate that fibrils of immunoglobulin light chain formed at lower surface concentrations and faster on mica surfaces than in solution [387].

The studies described above show the importance of the helical structure of collagen in controlling the biological response. However, there are numerous studies in the literature which use collagen in low pH solutions to create collagen substrates for *in vitro* testing [388-390,339,288,391,392]. These low pH collagen substrates likely do not represent the fibrillar collagen present *in vivo*. Several groups have attempted to produce defined collagen substrates [334,171,172], but further characterization is needed to create a well-controlled system.

The presence of fibrils is typically evaluated by microscopy, including TEM [347,354,352], AFM [353,393], and SEM [394,395]. Several techniques have been used to study the triple-helical structure of collagen, including x-ray diffraction [351,350,396,397], NMR [398,167] and synchrotron radiation scattering studies [399]. Crystal structures of some collagen molecules have also been elucidated [397,400,401].

In addition to these techniques, sum frequency generation has also been used to examine the secondary structure of collagen fibrils [402]. Rocha-Mendoza, et al. [402] found that the methylene groups within the pyrrolidine rings of proline and hydroxyproline are tilted relative to the axis perpendicular to the main axis of the collagen fiber. They also found a strong amide signal arising from the helical peptide backbone.

Here we use SFG to identify differences in the surface structure of collagen adsorbed from solution at differing levels of acidity.

6.4.2.1 Protein ordering - SFG

SFG clearly shows differences in the surface structure of collagen adsorbed from pH 6.5 versus pH 8.0 solutions. All collagen used for pH comparison experiments was obtained from Source 2. In the CH region, differences are clearly observed between the spectra from the two samples, suggesting different ordering of side chains. Collagen adsorbed at pH 8.0 shows a strong peak around 2940cm^{-1} (Fig. 6.7), corresponding to the CH_3 Fermi resonance [36]. The peak at 2910 cm^{-1} corresponds to the asymmetric methylene stretch, with a shoulder corresponding to the methylene Fermi resonance [36]. Collagen adsorbed at pH 6.5 also shows peaks at 2910 cm^{-1} and 2940 cm^{-1}, but at much lower intensity.

Collagen adsorbed at pH 6.5 shows peaks at 2880 cm^{-1} and 2850 cm^{-1} that are not observed when collagen is adsorbed at pH 8.0. These peaks correspond to the symmetric stretches of the methylene side chains [402,403].

The amide I region of the SFG spectrum provides information about the peptide backbone ordering. In this region, collagen adsorbed at pH 8.0 shows significantly higher SFG signal than collagen adsorbed at pH 6.5 (Fig. 6.8). The peaks in the amide region arise from the ordered helical structure of the amide bonds of the peptide backbone [402,115].

This demonstrates that collagen adsorbed from a solution of pH 6.5 contains little helical content and is mostly disordered on the surface. In contrast, collagen adsorbed from a solution of pH 8.0 has an ordered peptide backbone and retains helical structure on the surface.

Reported SFG peaks for helical structures include 1650 cm^{-1} for an α-helix [115,116] and 1635 cm^{-1} for a 3-10 helix [117]. The signal from a collagen helix would be expected to be different from these two helices due to the differences in structure [115].

The presence of multiple amide peaks suggests that there are different secondary structures within the adsorbed collagen. The peak at 1630 cm^{-1} could arise from β-sheet structures that form during the process of adsorption [118].

From these measurements, we can begin to understand the collagen secondary structure on at the surface when exposed to each pH value. The SFG amide signals suggests that at pH 6.5, the peptide backbone of the collagen molecules are almost totally disordered on the surface. Even though the backbone is not ordered, there is some ordering of

methylene groups in the amino acid side chains, likely from hydrophobic interactions with the surface [36]. When collagen is adsorbed from a solution at pH 8.0, the amide backbone of the collagen molecules exhibit significant ordering. Some of this ordering could arise from β-sheet structures formed during the adsorption process, as suggested by a peak at 1630 cm^{-1}. adsorption [118]. The collagen is not likely forming α-helical structures due to the absence of a peak 1650cm^{-1} [115,116]. The collagen helix is distinct in structure from the α-helix, so it is not surprising that it would exhibit different SFG peaks. A recent paper also identified three subbands within the amide spectrum (~1629–1635 cm^{-1}, ~1639–1645 cm^{-1}, and ~1657–1675 cm^{-1}), which correspond to the peaks observed in Fig. 6.8. The authors proposed that the three peaks represent the carbonyl groups in each peptide of the Gly-X-Y tripeptide [404]. So the conformation of collagen on the surface could be such that the carbonyl groups of the peptide are ordered. It can be challenging to make peak assignments within the CH region to determine precise differences in side chain ordering. However, we do observe that collagen adsorbed from solution of pH 8.0 shows different peaks from collagen adsorbed at pH 6.5, indicating that the side chain molecules exhibit different ordering. This could be due to constraints on the side chain introduced by the ordered peptide backbone at pH 8.0 which are not present in the disordered peptide backbone at pH 6.5.

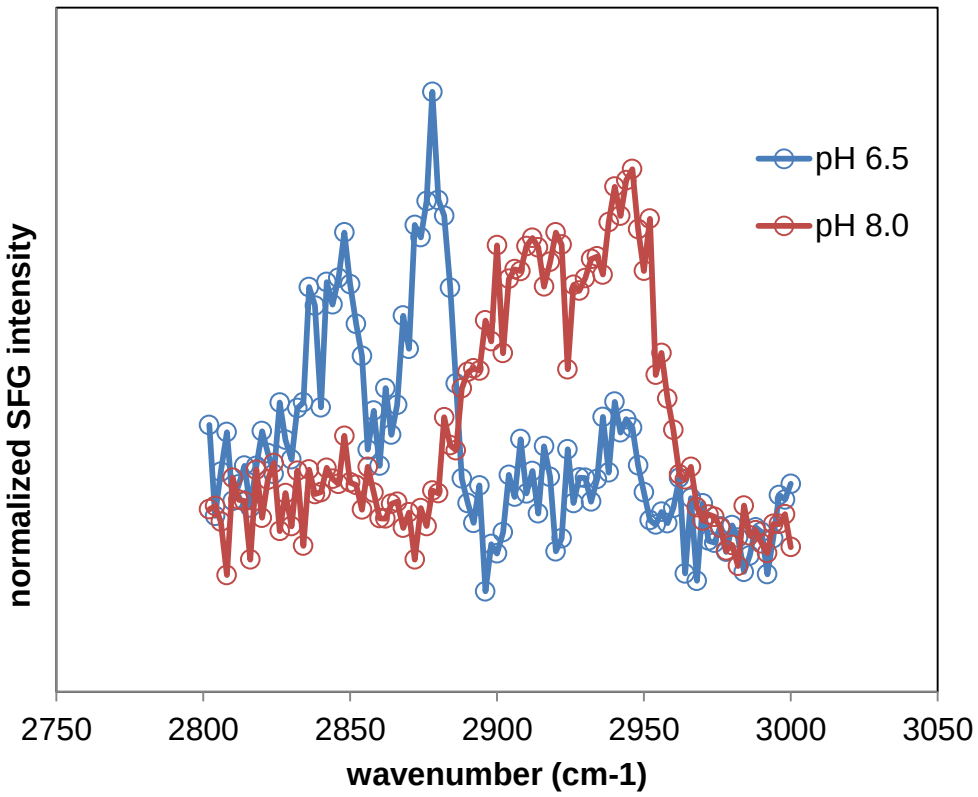

Fig. 6.7 SFG spectra in the CH region. *Source 2 collagen was adsorbed at pH 6.5 and pH 8.0 onto UV-PS. The spectra were collected in the SSP polarization combination. Data at each pH are an average of 3 spectra.*

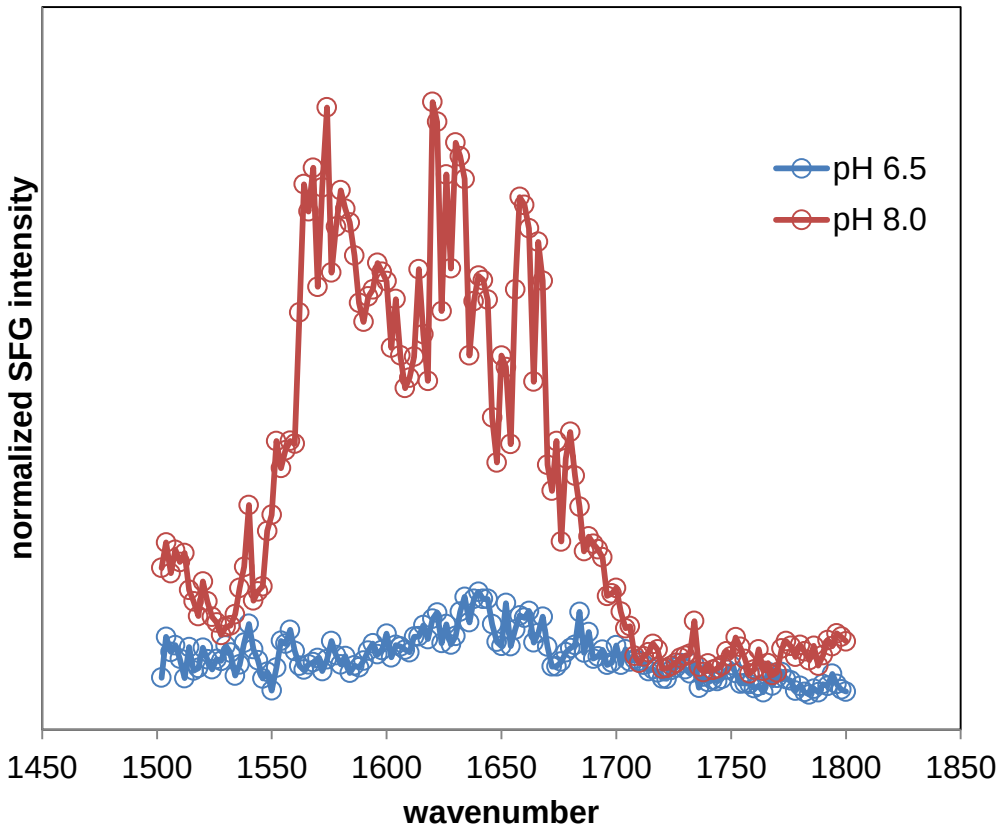

Fig. 6.8 SFG spectra in the Amide I region. *Source 2 collagen was adsorbed at pH 6.5 and pH 8.0 onto UV-PS. Spectra were collected in the PPP polarization combination. Data at each pH are an average of 3 spectra.*

6.4.2.2 Amount adsorbed - XPS

An SFG signal is only generated from ordered structures at interface where the inversion symmetry is broken. The signal intensity also depends on the amount of ordered species present. We used XPS to measure the amount of Source 2 collagen on the surface when adsorbed from solutions of pH 6.5 and 8.0. Full atomic composition is listed in Table 6.1.

A higher XPS nitrogen signal (11 vs. 2 atomic %) was detected when collagen was adsorbed from a pH 6.5 solution compared to a 8.0 solution (see Table 1). This indicates that more collagen adsorbed to the surface from a solution of pH 6.5 compared pH 8.0. Thus, the higher SFG signals observed from adsorption at pH 8.0 solution were not due to higher

amounts of protein on the surface. Instead, the higher SFG signal observed when collagen was adsorbed at pH 8.0 was due to increased ordering of the collagen on the surface.

The lower surface concentration of collagen at pH 8.0 than 6.5 can be explained by the theory of random sequential adsorption of proteins. This model states that a single molecule adsorbs to the surface and defines a zone to which no other particles arriving at later times can adsorb [28]. For spheres, protein saturation would occur at 55% coverage according to the model. For a particles with higher aspect ratios, saturation coverage would be lower (eg. 40% for aspect ratio of 7.5). Although experimental evidence shows that proteins can achieve higher coverage than predicted by the model [28], the model demonstrates why a helical collagen molecule with a high aspect ratio (1.5nm height, 300nm length [163]) would exhibit lower surface coverage than a denatured collagen molecule with a much lower aspect ratio.

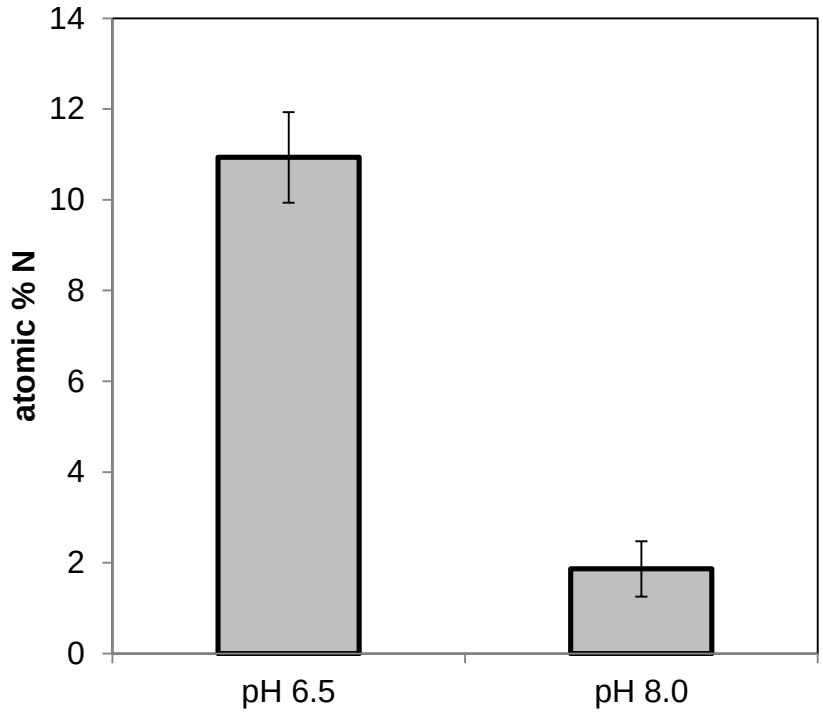

Fig. 6.9 XPS atomic percent nitrogen measured from collagen adsorbed onto TCPS surfaces at pH 6.5 and 8.0 (100μg/ml). *Mean +/- SD. Mean of 6 spots on 2 samples. Atomic percentage nitrogen is significantly different ($p < 0.01$) between the two pH conditions.*

6.5 Conclusions

When creating a biological substrate, it is important to control the experimental conditions under which the substrate is created. It is also important to fully characterize the substrate to be able to interpret the behavior of the system.

Here, we examined collagen substrates created using protein from two different manufacturers. We identified differences in their adsorption behavior and differences in the way a collagen-binding protein interacted with the collagen substrate. More collagen adsorbed onto a tissue culture polystyrene (TCPS) surface from one source than the other source. ToF-SIMS was used to identify differences in the behavior of the A1 domain of von Willebrand Factor interacting with the different collagen substrates adsorbed onto TCPS. Using collagen from one source, the collagen + A1 substrates were more similar to A1-only substrates, as measured by PCA scores. Using collagen from the other source, collagen + A1 substrates were more similar to the collagen-only substrates. This could be due to adsorption of A1 onto the underlying TCPS substrate.

We also characterized collagen adsorbed at two different pH values. Collagen adsorbed from even a modestly acidic pH (6.5) solution showed markedly less ordering of the protein amide backbone than collagen adsorbed from a pH 8.0 solution. Since collagen's helical structure is important for the recognition of collagen-binding proteins, this suggests that solubilizing collagen in acidic solutions should be used cautiously when creating in vitro substrates to mimic in vivo protein-protein interactions.

6.6 Tables for Chapter 6

Table 6.1 XPS determined elemental compositions of collagen adsorbed onto TCPS at 100μg/ml

	% C	% O	% N	% Na
TCPS	87.2 (1.1)	12.8 (1.1)	ND	ND
Collagen Source 1 pH 6.5	76.3 (0.5)	16.2 (0.4)	7.3 (0.5)	ND
Collagen Source 2 pH 6.5	69.6 (0.9)	19.2 (0.9)	11.2 (1.0)	ND
Collagen Source 2 pH 8.0	88.6 (0.5)	8.9 (0.5)	2.0 (0.7)	0.5 (0.7)

Mean of 6 measurements on 2 samples. Standard deviation in parentheses. ND: Not detected

Table 6.2 Positive ToF-SIMS amino acid ions used for PCA

Positive Ion	Amino Acid	Mass
CH_4N	Gly	30.0346
C_2H_6N	Ala	44.0492
CHS	Cys	44.9772
C_2H_3S	Cys	58.9941
C_2H_6NO	Ser	60.0448
C_2H_5S	Met	61.0095
C_4H_6N	Pro	68.053
C_4H_5O	Thr	69.0381
C_3H_4NO	Asn	70.0331
C_4H_8N	Pro	70.0704
$C_4H_{10}N$	Val	72.0862
C_3H_7NO	Arg	73.0527
C_3H_8NO	Thr	74.066
$C_4H_5N_2$	His	81.0383
$C_4H_6N_2$	His	82.0527
C_5H_7O	Val	83.0526
C_4H_6NO	Gln/Glu	84.0474
$C_5H_{10}N$	Lys	84.0855
C_4H_8NO	Hyp	86.0672
$C_5H_{12}N$	Iso/Ile	86.0982
$C_3H_7N_2O$	Asn	87.0576
$C_3H_6NO_2$	Asp/Asn	88.0297
$C_4H_4NO_2$	Asn	98.0144
$C_4H_{10}N_3$	Arg	100.0795
$C_4H_{11}N_3$	Arg	101.0963
$C_5H_8N_3$	His	110.0759
$C_5H_{10}N_3$	Arg	112.087
$C_8H_{10}N$	Phe	120.0874
$C_6H_{11}N_2O$	Arg	127.0868
$C_8H_{10}NO$	Tyr	136.0831
$C_{10}H_{11}N_2$	Trp	159.0897
$C_{11}H_8NO$	Trp	170.0666

Table 6.3 Polystyrene peaks used for ToF-SIMS analysis

Positive Ion	Mass
C_5H_5	65.0403
C_6H_5	77.0399
C_6H_6	78.044
C_6H_7	79.0539
C_7H_7	91.0557
C_7H_8	92.057
C_8H_7	103.0564
C_8H_8	104.0625
C_8H_9	105.0744
C_9H_7	115.058
C_9H_8	116.0613
C_9H_9	117.0725
$C10H_7$	127.0547
$C10H_8$	128.0588
$C10H_9$	129.0723

Chapter 7 Overall Conclusions

7.1 Conclusions

Adsorption of proteins onto surfaces has been studied since at least the early 1960s [405] and has remained an active area of research since that time [32,64,212]. This field has continued to develop due to the importance of adsorbed proteins in controlling the biological response to implanted materials. The composition and structure of the adsorbed protein layer has been demonstrated to affect a variety of cell functions and other biological responses [1,5,6].

In addition to implanted biomaterials, protein adsorption also has impacts in other areas, including tissue engineering [406,244], sensors [2,3], and marine biofouling [4]. Another area where adsorbed proteins are important that perhaps does not receive as much attention is the creation of model *in vitro* systems. Many types of scientific experiments are conducted *in vitro* due to the relative ease of performing the experiment, cost, and the ability to control variables in a manner that is not possible *in vivo* [407-410]. Adsorbed proteins are used to create cell culture substrates [17,58], models of vascular injury [313,334], and diagnostics [411-415].

A thorough characterization of the adsorbed protein layer is necessary to understanding the biological response to an implanted material or creating a controlled, reproducible *in vitro* system. Combining multiple analysis techniques is essential for understanding how proteins interact with a surface.

In this thesis, a variety of techniques were used to characterize different aspects of protein systems. The amount of protein adsorbed to surfaces was measured using XPS and radiolabeled proteins. Protein conformation and orientation were probed using ToF-SIMS, NEXAFS, SFG, and ELISA. Each of these techniques measures different aspects of the adsorbed protein layer, and together they give a more complete understanding of the system.

BSA showed higher adsorption onto polystyrene than glass surfaces with calculations showing submonolayer coverage on both surfaces. ToF-SIMS showed that there were differences in protein structure on the two surfaces, but the surface structure of BSA did not change on polystyrene surfaces across the solution concentrations measured.

The A1 domain of von Willebrand Factor adsorbed in similar amounts onto glass, TCPS, and polystyrene surfaces. However, ToF-SIMS showed differences in solution exposure of amino acids on the three surfaces and NEXAFS showed differences in ordering. ELISA also measured differences in binding of an antibody recognizing a nonlinear epitope within A1. Functional studies using a parallel plate flow chamber demonstrated different platelet binding when A1 was adsorbed onto the three surfaces. Further studies using full-length VWF did not show strong differences in platelet binding or surface structure measured by ToF-SIMS. However, it is possible that under different experimental conditions, differences would be observed.

Protein adsorption was also different onto titanium oxide versus sulfonated polystyrene surfaces. More protein adsorbed onto the sulfonated polystyrene surfaces than titanium oxide surfaces, and ToF-SIMS demonstrated that fibronectin adopted a different surface structure on the two surfaces.

Surface analysis was also useful for characterizing collagen substrates created under different experimental conditions. Collagen obtained from different sources exhibited different adsorption behavior, both in amount adsorbed and interaction with another protein. SFG was also used to identify differences in ordering of collagen adsorbed from solutions at different pH values.

These studies demonstrated that the surface type can have a large impact on adsorbed proteins, both in amount adsorbed and surface structure. For adsorption of the A1 domain of von Willebrand Factor, these studies demonstrated that the surface type has an effect on protein function. These studies also showed that surface analysis is very useful in creating defined *in vitro* protein substrates. In all cases, it was crucial to use multiple analysis techniques to understand these systems.

7.2 Future Directions

There are many opportunities for additional studies to build on the work in this thesis. In the study of A1 on synthetic surfaces, we observed differences in protein function and surface structure on surfaces commonly used as *in vitro* substrates. However, it is not entirely clear which properties of the respective surfaces resulted in the differences in behavior of adsorbed protein.

To better understand the role of specific functional groups, adsorption could be performed on surfaces consisting of more well-defined chemistry, such as alkanethiol self-assembled monolayers (SAMs). SAMs are a widely used model system to determine influence of various surface chemistries by varying the functional group to change characteristics such as charge or hydrophobicity of the surface [126,416,417]. SAMS are also able to be fabricated in a reproducible manner [418], again allowing for better control of the system and clearer interpretation of differences in protein structure and function.

In addition to NEXAFS, circular dichroism (CD) could be a useful tool for identifying and understanding conformational changes of A1 upon adsorption to different surfaces [8,293]. CD gives information about the secondary structure content of proteins, both in solution and on a surface [419,420]. Sum frequency generation can also give information about protein secondary structure on a surface [36,69], so that could be an additional useful tool to examine protein conformational changes.

In chapter 4, ToF-SIMS clearly demonstrated that adsorbed fibronectin was different on titanium oxide and sulfonated polystyrene surfaces. However, since fibronectin is such a large molecule, it is difficult to interpret the amino acid peak loadings to identify what the differences in surface structure are between the protein adsorbed onto the two surfaces.

Measuring binding of an antibody that recognizes cell-binding sites, either RGD or the PHSRN synergy site [421], could be useful in providing additional information about the differences in fibronectin surface structure between the two surfaces [17,58,142]. If cell binding sites within fibronectin are differentially exposed on the two surfaces, that would give further evidence that the adsorbed protein layer is responsible for the differences in cell function observed in previous studies. This would also suggest that the sulfonated polystyrene surface does not just increase cell function by allowing more protein to adsorb, but causes proteins to adsorb in a different conformation.

Cell studies would also be useful in further understanding the differences in the reaction to the adsorbed protein layer between the titanium oxide and sulfonated polystyrene surfaces. Osteoblasts or another cell type could be cultured on adsorbed fibronectin surfaces. Integrin-blocking antibodies could be applied to the cell culture system to prevent specific integrin interaction with the protein substrate [17,58,18]. If the presence of an anti-integrin antibody eliminated the differences in cell function on surfaces of fibronectin adsorbed onto

titanium oxide and PSS, this would suggest that differential exposure of the integrin-binding sites within fibronectin adsorbed onto the two surfaces did cause differences in cell function. This experiment could be challenging if blocking the integrins prevented cell adhesion.

It is generally accepted that acidic conditions denature the collagen fibrils, but the role of pH in the formation and denaturation of collagen fibrils is not well defined [346-349]. Studies in the literature routinely work at lower pH values [388,390,339,288]. In the studies reported in this thesis, the presence of even a moderately acidic solution was sufficient to eliminate most of the amide signal in the SFG measurements, suggesting that the peptide backbone was disordered. It would be interesting to look at a series of pH values to determine the point at which the collagen starts to denature and if the structure changes further as the solution continues to become more acidic.

Creating a defined collagen substrate is challenging because, like many biological substances, there can be high variability between material from different subjects and it is sensitive to variations in experimental conditions [334,171,172]. If a defined, reproducible collagen substrate were created, it would be a useful tool for studying many biological systems. Since so many proteins bind to collagen [162], creating a defined collagen substrate would allow easier *in vitro* testing of the protein-protein interactions that occur *in vivo*. Cultured cells can also be impacted by differences in the underlying collagen layer [357-364], so having a defined collagen substrate would allow better comparisons of cell behavior during *in vitro* testing.

One potential tool to measure protein interactions with collagen is ToF-SIMS. ToF-SIMS has been used previously to identify differences in multicomponent films [79-82]. It can also identify differences in adsorbed protein structure based on orientation and conformation [70-72,35,73,74]. It is possible that ToF-SIMS could identify differences in the structure of different proteins interacting with collagen based on protein orientation and/or conformation.

Some studies that were not included in this thesis attempted to identify differences between the structure of wildtype A1 and A1 mutant when interacting with collagen. Previously published ELISA studies had shown differential antibody binding to the wildtype A1 versus A1 mutant when immobilized onto collagen [288]. The ELISA results were

reproduced in our lab, but ToF-SIMS did not identify differences between the wildtype A1 and A1 mutant when immobilized onto collagen.

These results demonstrate the difficulty of using ToF-SIMS to look for differences in amino acid exposure against an amino acid background, in this case collagen. ToF-SIMS has been used to identify differences in some very complicated systems, including full extracellular matrix [422-424]. However, in this case we are trying to identify differences in one protein layered on top of another. While the sampling depth of ToF-SIMS is small, it is possible that in this case, it was not small enough to distinguish between small differences in A1 structure. In these studies, it also appeared that only a small amount of A1 was immobilized onto the collagen substrate, effectively decreasing the signal to noise ratio in the measurements.

Increasing the amount of A1 in the system and decreasing the contribution of the collagen signal would both be ways to improve the signal to noise ratio. For the ToF-SIMS studies in this thesis, Bi_3^+ was used as the primary ion source. However, recently primary ion sources have become commercially available that have even smaller sampling depths. Of particular interest is using a large cluster of argon atoms as a primary ion source [425-427]. At a constant energy, as the cluster size of the primary ion increases, the amount of energy per atom decreases. So using a large cluster, the energy is deposited closer to the surface [428,429]. This results in material being sputtered from closer to the surface, and a shallower sampling depth [76].

The use of a cluster argon primary ion beam in a system like a protein of interest layered over collagen could give more information than a Bi primary ion beam about changes in the structure of the overlayer protein.

More broadly in the field of protein adsorption research, tools continue should continue to be developed and improved for the study of proteins on surfaces. ToF-SIMS has proven to be a very useful tool in identifying differences between adsorbed proteins. Developing a better understanding of the fragmentation and ionization process will allow more accurate interpretation of ToF-SIMS analysis of proteins. Currently, it is not well understood how the presence of different neighboring molecules influence protein fragmentation and ionization [430]. Work has been performed to understand the collision process [429,431,76], but more work to understand the high energy fragmentation and

ionization process would allow further quantitation of ToF-SIMS data [432]. While it will likely be difficult to fully quantify ToF-SIMS data due to the matrix effect [75], interpretation could be enhanced.

Introduction of new primary ion sources with variable sampling depths as mentioned above could also improve the utility of ToF-SIMS to study protein systems.

In addition to experimental techniques, computational modeling has the ability to help us better understand the interactions between proteins and surfaces on a molecular level [433,186,434,241]. Computational models can test many more parameters than would be reasonable or possible to do in experiments and point toward experiments that will likely yield the most useful results. In conjunction with experimental evidence to validate the model, computational modeling can give detailed information that would be difficult to obtain otherwise [433,435,436].

While the field of protein adsorption research has been active for several decades, there are still many questions to be answered. Combining multiple analysis techniques will allow the best understanding of protein behavior, allowing the design of new, more effective biomaterials and better control of *in vitro* systems.

Bibliography

1. Brash JL (2000) Exploiting the current paradigm of blood-material interactions for the rational design of blood-compatible materials. Journal of Biomaterials Science, Polymer Edition 11:1135-1146

2. Reimhult K, Petersson K, Krozer A (2008) QCM-D Analysis of the Performance of Blocking Agents on Gold and Polystyrene Surfaces. Langmuir 24 (16):8695-8700

3. Geelhood SJ, Horbett TA, Ward WK, Wood MD, Quinn MJ (2007) Passivating protein coatings for implantable glucose sensors: Evaluation of protein retention. Journal of Biomedical Materials Research Part B: Applied Biomaterials 81B (1):251-260

4. Fant C, Sott K, Elwing H, Hook F (2000) Adsorption behavior and enzymatically or chemically induced cross-linking of a mussel adhesive protein. Biofouling: The Journal of Bioadhesion and Biofilm Research 16 (2):119 - 132

5. Horbett TA (1994) The role of adsorbed proteins in animal cell adhesion. Colloids and Surfaces B: Biointerfaces 2 (1-3):225-240

6. García AJ (2005) Get a grip: integrins in cell-biomaterial interactions. Biomaterials 26 (36):7525-7529

7. Andrade JD, Hlady V, Wei AP, Ho CH, Lea AS, Jeon SI, Lin YS, Stroup E (1992) Proteins at interfaces: Principles, multivariate aspects, protein resistant surfaces, and direct imaging and manipulation of adsorbed proteins. Clinical Materials 11 (1-4):67-84

8. Sivaraman B, Fears KP, Latour RA (2009) Investigation of the Effects of Surface Chemistry and Solution Concentration on the Conformation of Adsorbed Proteins Using an Improved Circular Dichroism Method. Langmuir 25 (5):3050-3056. doi:10.1021/la8036814

9. Collier TO, Thomas CH, Anderson JM, Healy KE (2000) Surface chemistry control of monocyte and macrophage adhesion, morphology, and fusion. Journal of Biomedical Materials Research 49 (1):141-145

10. Roach P, Farrar D, Perry CC (2005) Interpretation of Protein Adsorption: Surface-Induced Conformational Changes. Journal of the American Chemical Society 127 (22):8168-8173. doi:10.1021/ja042898o

11. Buijs J, Norde W, Lichtenbelt JWT (1996) Changes in the Secondary Structure of Adsorbed IgG and F(ab')2 Studied by FTIR Spectroscopy. Langmuir 12 (6):1605-1613. doi:10.1021/la950665s

12. Jung S-Y, Lim S-M, Albertorio F, Kim G, Gurau MC, Yang RD, Holden MA, Cremer PS (2003) The Vroman Effect: A Molecular Level Description of Fibrinogen Displacement. Journal of the American Chemical Society 125 (42):12782-12786. doi:10.1021/ja037263o

13. Nakanishi K, Sakiyama T, Imamura K (2001) On the adsorption of proteins on solid surfaces, a common but very complicated phenomenon. Journal of Bioscience and Bioengineering 91 (3):233-244

14. Wahlgren M, Arnebrant T (1991) Protein adsorption to solid surfaces. Trends in Biotechnology 9 (1):201-208

15. Hlady V, Buijs J (1996) Protein adsorption on solid surfaces. Current Opinion in Biotechnology 7 (1):72-77

16. Gray JJ (2004) The interaction of proteins with solid surfaces. Current Opinion in Structural Biology 14 (1):110-115

17. García AJ, Ducheyne P, Boettiger D (1998) Effect of surface reaction stage on fibronectin-mediated adhesion of osteoblast-like cells to bioactive glass. Journal of Biomedical Materials Research 40 (1):48-56. doi:10.1002/(sici)1097-4636(199804)40:1<48::aid-jbm6>3.0.co;2-r

18. Stephansson SN, Byers BA, García AJ (2002) Enhanced expression of the osteoblastic phenotype on substrates that modulate fibronectin conformation and integrin receptor binding. Biomaterials 23 (12):2527-2534

19. Keselowsky BG, Collard DM, García AJ (2003) Surface chemistry modulates fibronectin conformation and directs integrin binding and specificity to control cell adhesion. Journal of Biomedical Materials Research Part A 66A (2):247-259. doi:10.1002/jbm.a.10537

20. Velzenberger E, Pezron I, Legeay G, Nagel M-D, Kirat KE (2008) Probing Fibronectin-Surface Interactions: A Multitechnique Approach. Langmuir 24 (20):11734-11742. doi:10.1021/la801727p

21. Wu Y, Zhang M, Hauch KD, Horbett TA (2008) Effect of adsorbed von Willebrand factor and fibrinogen on platelet interactions with synthetic materials under flow conditions. Journal of Biomedical Materials Research 85A:829-839

22. Wu Y, Simonovsky FI, Ratner BD, Horbett TA (2005) The role of adsorbed fibrinogen in platelet adhesion to polyurethane surfaces: A comparison of surface hydrophobicity, protein adsorption, monoclonal antibody binding, and platelet adhesion. Journal of Biomedical Materials Research Part A 74A (4):722-738

23. Tsai W-B, Grunkemeier JM, McFarland CD, Horbett TA (2002) Platelet adhesion to polystyrene-based surfaces preadsorbed with plasmas selectively depleted in fibrinogen, fibronectin, vitronectin, or von Willebrand's factor. Journal of Biomedical Materials Research 60 (3):348-359

24. Onuchic JN, Wolynes PG (2004) Theory of protein folding. Current Opinion in Structural Biology 14 (1):70-75

25. Privalov PL, Makhatadze GI (1993) Contribution of Hydration to Protein Folding Thermodynamics : II. The Entropy and Gibbs Energy of Hydration. Journal of Molecular Biology 232 (2):660-679

26. Nicholls A, Sharp KA, Honig B (1991) Protein folding and association: Insights from the interfacial and thermodynamic properties of hydrocarbons. Proteins: Structure, Function, and Bioinformatics 11 (4):281-296. doi:10.1002/prot.340110407

27. Makhatadze GI, Privalov PL (1993) Contribution of Hydration to Protein Folding Thermodynamics : I. The Enthalpy of Hydration. Journal of Molecular Biology 232 (2):639-659

28. Norde W, Horbett TA, Brash JL (2012) Proteins at Interfaces III: Introductory Overview. In: Proteins at Interfaces III. pp 1-32

29. Norde W, Lyklema J (1979) Thermodynamics of protein adsorption. Theory with special reference to the adsorption of human plasma albumin and bovine pancreas ribonuclease at polystyrene surfaces. Journal of Colloid and Interface Science 71 (2):350-366

30. Hoffman AS (1999) Non-Fouling Surface Technologies. Journal of Biomaterials Science, Polymer Edition 10:1011-1014

31. Norde W (1994) Protein adsorption at solid surfaces: A thermodynamic approach. Pure & Appl Chem 66 (3):491-496

32. Norde W (2008) My voyage of discovery to proteins in flatland ...and beyond. Colloids and Surfaces B: Biointerfaces 61 (1):1-9

33. Brash JL, Ten Hove P (1993) Protein adsorption studies on 'standard' polymeric materials. Journal of Biomaterials Science, Polymer Edition 4:591-599

34. Price ME, Cornelius RM, Brash JL (2001) Protein adsorption to polyethylene glycol modified liposomes from fibrinogen solution and from plasma. Biochimica et Biophysica Acta (BBA) - Biomembranes 1512 (2):191-205

35. Michel R, Pasche S, Textor M, Castner DG (2005) Influence of PEG Architecture on Protein Adsorption and Conformation. Langmuir 21 (26):12327-12332

36. Weidner T, Apte JS, Gamble LJ, Castner DG (2009) Probing the Orientation and Conformation of a-Helix and b-Strand Model Peptides on Self-Assembled Monolayers Using Sum Frequency Generation and NEXAFS Spectroscopy. Langmuir 26 (5):3433-3440. doi:10.1021/la903267x

37. Prime KL, Whitesides GM (1993) Adsorption of proteins onto surfaces containing end-attached oligo(ethylene oxide): a model system using self-assembled monolayers. J Am Chem Soc 115 (23):10714-10721

38. Ostuni E, Chapman RG, Holmlin RE, Takayama S, Whitesides GM (2001) A Survey of Structure-Property Relationships of Surfaces that Resist the Adsorption of Protein. Langmuir 17 (18):5605-5620. doi:10.1021/la010384m

39. Garcia AJ, Reyes CD (2005) Bio-adhesive Surfaces to Promote Osteoblast Differentiation and Bone Formation. Journal of Dental Research 84 (5):407-413. doi:10.1177/154405910508400502

40. Noh H, Vogler EA (2006) Volumetric interpretation of protein adsorption: Mass and energy balance for albumin adsorption to particulate adsorbents with incrementally increasing hydrophilicity. Biomaterials 27 (34):5801-5812

41. Baujard-Lamotte L, Noinville S, Goubard F, Marque P, Pauthe E (2008) Kinetics of conformational changes of fibronectin adsorbed onto model surfaces. Colloids and Surfaces B: Biointerfaces 63 (1):129-137

42. Castillo EJ, Koenig JL, Andersen JM, Lo J (1984) Characterization of protein adsorption on soft contact lenses: I. Conformational changes of adsorbed human serum albumin. Biomaterials 5 (6):319-325

43. Ishiguro R, Yokoyama Y, Maeda H, Shimamura A, Kameyama K, Hiramatsu K (2005) Modes of conformational changes of proteins adsorbed on a planar hydrophobic polymer

surface reflecting their adsorption behaviors. Journal of Colloid and Interface Science 290 (1):91-101

44. Sethuraman A, Vedantham G, Imoto T, Przybycien T, Belfort G (2004) Protein unfolding at interfaces: Slow dynamics of alpha-helix to beta-sheet transition. Proteins: Structure, Function, and Bioinformatics 56 (4):669-678

45. van der Scheer A, Feijen J, Elhorst JK, Krugers Dagneaux PGLC, Smolders CA (1978) The feasibility of radiolabeling for human serum albumin (HSA) adsorption studies. Journal of Colloid and Interface Science 66 (1):136-145. doi:10.1016/0021-9797(78)90194-7

46. Giacomelli CE, Esplandiú MJ, Ortiz PI, Avena MJ, De Pauli CP (1999) Ellipsometric Study of Bovine Serum Albumin Adsorbed onto Ti/TiO2 Electrodes. Journal of Colloid and Interface Science 218 (2):404-411

47. Wertz CF, Santore MM (2001) Effect of Surface Hydrophobicity on Adsorption and Relaxation Kinetics of Albumin and Fibrinogen: Single-Species and Competitive Behavior. Langmuir 17 (10):3006-3016. doi:10.1021/la0017781

48. Xu L-C, Siedlecki CA (2007) Effects of surface wettability and contact time on protein adhesion to biomaterial surfaces. Biomaterials 28 (22):3273-3283

49. Felsovalyi F, Patel T, Mangiagalli P, Kumar SK, Banta S (2012) Effect of thermal stability on protein adsorption to silica using homologous aldo-keto reductases. Protein Science 21 (8):1113-1125. doi:10.1002/pro.2099

50. Vroman L, Adams AL (1969) Findings with the recording ellipsometer suggesting rapid exchange of specific plasma proteins at liquid/solid interfaces. Surface Science 16:438-446

51. Feng L, Andrade JD (1994) Protein adsorption on low temperature isotropic carbon: III. Isotherms, competitivity, desorption and exchange of human albumin and fibrinogen. Biomaterials 15 (5):324-333

52. Norde W, Giacomelli CE (2000) BSA structural changes during homomolecular exchange between the adsorbed and the dissolved states. Journal of Biotechnology 79 (3):259-268

53. Brash JL, Uniyal S, Pusineri C, Schmitt A (1983) Interaction of fibrinogen with solid surfaces of varying charge and hydrophobic--hydrophilic balance : II. Dynamic exchange between surface and solution molecules. Journal of Colloid and Interface Science 95 (1):28-36

54. Ball V, Huetz P, Elaissari A, Cazenave JP, Voegel JC, Schaaf P (1994) Kinetics of exchange processes in the adsorption of proteins on solid surfaces. Proceedings of the National Academy of Sciences of the United States of America 91 (15):7330-7334
55. Lewandowska K, Balachander N, Sukenik CN, Culp LA (1989) Modulation of fibronectin adhesive functions for fibroblasts and neural cells by chemically derivatized substrata. Journal of Cellular Physiology 141 (2):334-345
56. Grainger DW, Pavon-Djavid G, Migonney V, Josefowicz M (2003) Assessment of fibronectin conformation adsorbed to polytetrafluoroethylene surfaces from serum protein mixtures and correlation to support of cell attachment in culture. Journal of Biomaterials Science, Polymer Edition 14:973-988
57. Sivaraman B, Latour RA (2010) The Adherence of platelets to adsorbed albumin by receptor-mediated recognition of binding sites exposed by adsorption-induced unfolding. Biomaterials 31 (6):1036-1044
58. Garcia AJ, Vega MD, Boettiger D (1999) Modulation of Cell Proliferation and Differentiation through Substrate-dependent Changes in Fibronectin Conformation. Mol Biol Cell 10 (3):785-798
59. van der Zijpp YJT, Poot AA, Feijen J (2003) ICAM-1 and VCAM-1 expression by endothelial cells grown on fibronectin-coated TCPS and PS. Journal of Biomedical Materials Research Part A 65A (1):51-59. doi:10.1002/jbm.a.10327
60. Lan MA, Gersbach CA, Michael KE, Keselowsky BG, García AJ (2005) Myoblast proliferation and differentiation on fibronectin-coated self assembled monolayers presenting different surface chemistries. Biomaterials 26 (22):4523-4531
61. Ratner BD, Castner DG (2008) Electron Spectroscopy for Chemical Analysis. In: Vickerman JC, Gilmore IS (eds) Surface Analysis - The Principal Techniques. 2 edn. Wiley Publishers, UK,
62. Ratner BD, Horbett TA (1981) Analysis of the Organization of Protein Films on Solid Surfaces by ESCA. J Colloid Interface Sci 83 (2):630-642
63. Scofield JH (1976) Hartree-Slater subshell photoionization cross-sections at 1254 and 1487 eV. Journal of Electron Spectroscopy and Related Phenomena 8 (2):129-137. doi:10.1016/0368-2048(76)80015-1

64. Horbett TA (1986) Techniques for Protein Adsorption Studies. In: Williams DF (ed) Techniques of Biocompatibility Testing, vol II. CRC Series in Biocompatibility. CRC Press, Inc., Boca Raton, Florida, pp 183-214

65. Pressman D, Eisen HN (1950) The Zone of Localization of Antibodies. The Journal of Immunology 64 (4):273-279

66. Eisen HN, Sherman B, Pressman D (1950) The Zone of Localization of Antibodies IX. The Journal of Immunology 65 (5):543-558

67. Bailey GS (1994) Labeling of Peptides and Proteins by Radioiodination Basic Protein and Peptide Protocols. In: Walker JM (ed), vol 32. Methods in Molecular Biology. Humana Press, pp 441-448. doi:10.1385/0-89603-268-X:441

68. Wang H, Castner DG, Ratner BD, Jiang S (2004) Probing the Orientation of Surface-Immobilized Immunoglobulin G by Time-of-Flight Secondary Ion Mass Spectrometry. Langmuir 20 (5):1877-1887. doi:10.1021/la035376f

69. Baugh L, Weidner T, Baio JE, Nguyen P-CT, Gamble LJ, Stayton PS, Castner DG (2010) Probing the Orientation of Surface-Immobilized Protein G B1 Using ToF-SIMS, Sum Frequency Generation, and NEXAFS Spectroscopy. Langmuir 26 (21):16434-16441. doi:10.1021/la1007389

70. Xia N, Castner DG (2003) Preserving the structure of adsorbed protein films for time-of-flight secondary ion mass spectrometry analysis. Journal of Biomedical Materials Research Part A 67A (1):179-190

71. Michel R, Castner DG (2006) Advances in time-of-flight secondary ion mass spectrometry analysis of protein films. Surface and Interface Analysis 38 (11):1386-1392

72. Tidwell CD, Castner DG, Golledge SL, Ratner BD, Meyer K, Hagenhoff B, Benninghoven A (2001) Static time-of-flight secondary ion mass spectrometry and x-ray photoelectron spectroscopy characterization of adsorbed albumin and fibronectin films. Surface and Interface Analysis 31 (8):724-733

73. Xia N, May CJ, McArthur SL, Castner DG (2002) Time-of-Flight Secondary Ion Mass Spectrometry Analysis of Conformational Changes in Adsorbed Protein Films. Langmuir 18 (10):4090-4097. doi:doi:10.1021/la020022u

74. Lhoest J-B, Detrait E, Aguilar PvdBd, Bertrand P (1998) Fibronectin adsorption, conformation, and orientation on polystyrene substrates studied by radiolabeling, XPS, and ToF SIMS. Journal of Biomedical Materials Research 41 (1):95-103

75. Vickerman JC, Swift A (1997) Secondary Ion Mass Spectrometry - the Surface Mass Spectrometry. In: Vickerman JC (ed) Surface Analysis: The Principal Techniques. John Wiley & Sons, New York, NY,

76. Paruch R, Rzeznik L, Russo MF, Garrison BJ, Postawa Z (2009) Molecular Dynamics Study of the Effect of Surface Topography on Sputtering Induced by 20 keV Au3 and C60 Clusters. The Journal of Physical Chemistry C 114 (12):5532-5539. doi:10.1021/jp906139d

77. Samuel NT, Wagner MS, Dornfeld KD, Castner DG (2001) Analysis of Poly(amino acids) by Static Time-of-Flight Secondary Ion Mass Spectrometry (TOF-SIMS). Surface Science Spectra 8 (3):163-184

78. Lhoest J-B, Wagner MS, Tidwell CD, Castner DG (2001) Characterization of adsorbed protein films by time of flight secondary ion mass spectrometry. Journal of Biomedical Materials Research 57 (3):432-440

79. Wagner MS, Castner DG (2001) Characterization of Adsorbed Protein Films by Time-of-Flight Secondary Ion Mass Spectrometry with Principal Component Analysis. Langmuir 17 (15):4649-4660

80. Wagner MS, Horbett TA, Castner DG (2003) Characterizing multicomponent adsorbed protein films using electron spectroscopy for chemical analysis, time-of-flight secondary ion mass spectrometry, and radiolabeling: capabilities and limitations. Biomaterials 24 (11):1897-1908

81. Wagner MS, Horbett TA, Castner DG (2003) Characterization of the Structure of Binary and Ternary Adsorbed Protein Films Using Electron Spectroscopy for Chemical Analysis, Time-of-Flight Secondary Ion Mass Spectrometry, and Radiolabeling. Langmuir 19 (5):1708-1715. doi:doi:10.1021/la0260382

82. Brüning C, Hellweg S, Dambach S, Lipinsky D, Arlinghaus HF (2006) Improving the interpretation of ToF-SIMS measurements on adsorbed proteins using PCA. Surface and Interface Analysis 38 (4):191-193. doi:10.1002/sia.2233

83. Wagner MS, Castner DG (2004) Analysis of adsorbed proteins by static time-of-flight secondary ion mass spectrometry. Applied Surface Science 231-232:366-376

84. Wold S, Esbensen K, Geladi P (1987) Principal component analysis. Chemometrics and Intelligent Laboratory Systems 2 (1-3):37-52

85. Graham D, Castner D (2012) Multivariate Analysis of ToF-SIMS Data from Multicomponent Systems: The Why, When, and How. Biointerphases 7 (1-4):1-12. doi:10.1007/s13758-012-0049-3

86. Chinn JA, Phillips JRE, Lew KR, Horbett TA (1996) Tenacious Binding of Fibrinogen and Albumin to Pyrolite Carbon and Biomer. Journal of Colloid and Interface Science 184 (1):11-19

87. Engvall E, Perlmann P (1971) Enzyme-linked immunosorbent assay (ELISA) quantitative assay of immunoglobulin G. Immunochemistry 8 (9):871-874. doi:10.1016/0019-2791(71)90454-x

88. Berglund L, Andrade J, Odeberg J, Uhlén M (2008) The epitope space of the human proteome. Protein Science 17 (4):606-613. doi:10.1110/ps.073347208

89. Kiener T, Jia Q, Lim X, He F, Meng T, Kwong Chow V, Kwang J (2012) Characterization and specificity of the linear epitope of the enterovirus 71 VP2 protein. Virology Journal 9 (1):55

90. Haste Andersen P, Nielsen M, Lund O (2006) Prediction of residues in discontinuous B-cell epitopes using protein 3D structures. Protein Science 15 (11):2558-2567. doi:10.1110/ps.062405906

91. Van Regenmortel MHV (1996) Mapping Epitope Structure and Activity: From One-Dimensional Prediction to Four-Dimensional Description of Antigenic Specificity. Methods 9 (3):465-472. doi:10.1006/meth.1996.0054

92. Barlow DJ, Edwards MS, Thornton JM (1986) Continuous and discontinuous protein antigenic determinants. Nature 322 (6081):747-748

93. Frank R (1992) Spot-synthesis: an easy technique for the positionally addressable, parallel chemical synthesis on a membrane support. Tetrahedron 48 (42):9217-9232. doi:10.1016/S0040-4020(01)85612-X

94. Cunningham BC, Wells JA (1989) High-resolution epitope mapping of hGH-receptor interactions by alanine-scanning mutagenesis. Science (New York, NY) 244 (4908):1081-1085

95. Soga S, Kuroda D, Shirai H, Kobori M, Hirayama N (2010) Use of amino acid composition to predict epitope residues of individual antibodies. Protein Engineering Design and Selection 23 (6):441-448. doi:10.1093/protein/gzq014

96. De Luca M, Facey DA, Favaloro EJ, Hertzberg MS, Whisstock JC, McNally T, Andrews RK, Berndt MC (2000) Structure and function of the von Willebrand factor A1 domain: analysis with monoclonal antibodies reveals distinct binding sites involved in recognition of the platelet membrane glycoprotein Ib-IX-V complex and ristocetin-dependent activation. Blood 95 (1):164-172

97. Hochmuth RM, Mohandas N, Blackshear Jr PL (1973) Measurement of the Elastic Modulus for Red Cell Membrane Using a Fluid Mechanical Technique. Biophysical Journal 13 (8):747-762. doi:10.1016/s0006-3495(73)86021-7

98. Savage B, Saldívar E, Ruggeri ZM (1996) Initiation of Platelet Adhesion by Arrest onto Fibrinogen or Translocation on von Willebrand Factor. Cell 84 (2):289-297

99. Hubbell JA, McIntire LV (1986) Technique for visualization and analysis of mural thrombogenesis. Review of Scientific Instruments 57 (5):892-897

100. Kroll MH, Hellums JD, McIntire LV, Schafer AI, Moake JL (1996) Platelets and shear stress. Blood 88 (5):1525-1541

101. Tangelder GJ, Slaaf DW, Arts T, Reneman RS (1988) Wall shear rate in arterioles in vivo: least estimates from platelet velocity profiles. Am J Physiol Heart Circ Physiol 254 (6):H1059-1064

102. Yago T, Lou J, Wu T, Yang J, Miner JJ, Coburn L, Lopez J, Cruz MA, Dong J-F, McIntire LV, McEver RP, Zhu C (2008) Platelet glycoprotein Ib forms catch bonds with human WT vWF but not with type 2B von Willebrand disease vWF. The Journal of Clinical Investigation 118 (9):3195-3207

103. Cranmer SL, Ulsemer P, Cooke BM, Salem HH, de la Salle C, Lanza F, Jackson SP (1999) Glycoprotein (GP) Ib-IX-transfected Cells Roll on a von Willebrand Factor Matrix under Flow. J Biol Chem 274 (10):6097-6106. doi:10.1074/jbc.274.10.6097

104. Fredrickson BJ, Dong J-F, McIntire LV, Lopez JA (1998) Shear-Dependent Rolling on von Willebrand Factor of Mammalian Cells Expressing the Platelet Glycoprotein Ib-IX-V Complex. Blood 92 (10):3684-3693

105. Doggett TA, Girdhar G, Lawshe A, Schmidtke DW, Laurenzi IJ, Diamond SL, Diacovo TG (2002) Selectin-Like Kinetics and Biomechanics Promote Rapid Platelet Adhesion in Flow: The GPIbalpha -vWF Tether Bond. Biophys J 83 (1):194-205

106. Doggett TA, Girdhar G, Lawshe A, Miller JL, Laurenzi IJ, Diamond SL, Diacovo TG (2003) Alterations in the intrinsic properties of the GPIb{alpha}-VWF tether bond define the kinetics of the platelet-type von Willebrand disease mutation, Gly233Val. Blood 102 (1):152-160. doi:10.1182/blood-2003-01-0072

107. Auton M, Sedlak E, Marek J, Wu T, Zhu C, Cruz MA (2009) Changes in Thermodynamic Stability of von Willebrand Factor Differentially Affect the Force-Dependent Binding to Platelet GPIb(alpha). Biophysical Journal 97 (2):618-627

108. Chang K-C, Tees DFJ, Hammer DA (2000) The state diagram for cell adhesion under flow: Leukocyte rolling and firm adhesion. Proceedings of the National Academy of Sciences 97 (21):11262-11267. doi:10.1073/pnas.200240897

109. Caputo KE, Hammer DA (2005) Effect of Microvillus Deformability on Leukocyte Adhesion Explored Using Adhesive Dynamics Simulations. Biophysical Journal 89 (1):187-200. doi:http://dx.doi.org/10.1529/biophysj.104.054171

110. Dong C, Lei XX (2000) Biomechanics of cell rolling: shear flow, cell-surface adhesion, and cell deformability. Journal of Biomechanics 33 (1):35-43. doi:http://dx.doi.org/10.1016/S0021-9290(99)00174-8

111. Jadhav S, Eggleton CD, Konstantopoulos K (2005) A 3-D Computational Model Predicts that Cell Deformation Affects Selectin-Mediated Leukocyte Rolling. Biophysical Journal 88 (1):96-104. doi:http://dx.doi.org/10.1529/biophysj.104.051029

112. Park EYH, Smith MJ, Stropp ES, Snapp KR, DiVietro JA, Walker WF, Schmidtke DW, Diamond SL, Lawrence MB (2002) Comparison of PSGL-1 Microbead and Neutrophil Rolling: Microvillus Elongation Stabilizes P-Selectin Bond Clusters. Biophysical Journal 82 (4):1835-1847. doi:http://dx.doi.org/10.1016/S0006-3495(02)75534-3

113. Shen YR (1989) Surface properties probed by second-harmonic and sum-frequency generation. Nature 337 (6207):519-525

114. Weidner T, Samuel NT, McCrea K, Gamble LJ, Ward RS, Castner DG (2010) Assembly and structure of alpha-helical peptide films on hydrophobic fluorocarbon surfaces. Biointerphases 5 (1):9-16

115. Nguyen KT, Le Clair SpV, Ye S, Chen Z (2009) Orientation Determination of Protein Helical Secondary Structures Using Linear and Nonlinear Vibrational Spectroscopy. The Journal of Physical Chemistry B 113 (36):12169-12180. doi:10.1021/jp904153z

116. Chen X, Wang J, Sniadecki JJ, Even MA, Chen Z (2005) Probing α-Helical and β-Sheet Structures of Peptides at Solid/Liquid Interfaces with SFG. Langmuir 21 (7):2662-2664. doi:10.1021/la050048w

117. Ye S, Nguyen KT, Chen Z (2010) Interactions of Alamethicin with Model Cell Membranes Investigated Using Sum Frequency Generation Vibrational Spectroscopy in Real Time in Situ. The Journal of Physical Chemistry B 114 (9):3334-3340. doi:10.1021/jp911174d

118. Nguyen KT, King JT, Chen Z (2010) Orientation Determination of Interfacial β-Sheet Structures in Situ. The Journal of Physical Chemistry B 114 (25):8291-8300. doi:10.1021/jp102343h

119. Weidner T, Breen NF, Li K, Drobny GP, Castner DG (2010) Sum frequency generation and solid-state NMR study of the structure, orientation, and dynamics of polystyrene-adsorbed peptides. Proceedings of the National Academy of Sciences 107 (30):13288-13293. doi:10.1073/pnas.1003832107

120. Bianconi A (1980) Surface X-ray absorption spectroscopy: Surface EXAFS and surface XANES. Applications of Surface Science 6 (3–4):392-418. doi:10.1016/0378-5963(80)90024-0

121. Gelamo EL, Silva CHTP, Imasato H, Tabak M (2002) Interaction of bovine (BSA) and human (HSA) serum albumins with ionic surfactants: spectroscopy and modelling. Biochimica et Biophysica Acta (BBA) - Protein Structure and Molecular Enzymology 1594 (1):84-99

122. Kottke-Marchant K, Anderson JM, Umemura Y, Marchant RE (1989) Effect of albumin coating on the in vitro blood compatibility of Dacron® arterial prostheses. Biomaterials 10 (3):147-155

123. Marois Y, Chakfé N, Guidoin R, Duhamel RC, Roy R, Marois M, King MW, Douville Y (1996) An albumin-coated polyester arterial graft: in vivo assessment of biocompatibility and healing characteristics. Biomaterials 17 (1):3-14

124. Skarja GA, Kinlough-Rathbone RL, Perry DW, Rubens FD, Brash JL (1997) A cone-and-plate device for the investigation of platelet biomaterial interactions. Journal of Biomedical Materials Research 34 (4):427-438

125. Kim J, Somorjai GA (2003) Molecular Packing of Lysozyme, Fibrinogen, and Bovine Serum Albumin on Hydrophilic and Hydrophobic Surfaces Studied by Infrared-Visible Sum Frequency Generation and Fluorescence Microscopy. Journal of the American Chemical Society 125 (10):3150-3158

126. Gonçalves IC, Martins MCL, Barbosa MA, Ratner BD (2005) Protein adsorption on 18-alkyl chains immobilized on hydroxyl-terminated self-assembled monolayers. Biomaterials 26 (18):3891-3899

127. Dupont-Gillain CC, Fauroux CMJ, Gardner DCJ, Leggett GJ (2003) Use of AFM to probe the adsorption strength and time-dependent changes of albumin on self-assembled monolayers. Journal of Biomedical Materials Research Part A 67A (2):548-558

128. Vieira EP, Rocha S, Carmo Pereira M, Mohwald H, Coelho MAN (2009) Adsorption and Diffusion of Plasma Proteins on Hydrophilic and Hydrophobic Surfaces: Effect of Trifluoroethanol on Protein Structure. Langmuir 25 (17):9879-9886. doi:10.1021/la9009948

129. Mouhib T, Delcorte A, Poleunis C, Henry M, Bertrand P (2010) C60 SIMS depth profiling of bovine serum albumin protein-coating films: a conformational study. Surface and Interface Analysis 42 (6-7):641-644. doi:10.1002/sia.3349

130. Tanaka M, Mochizuki A, Shiroya T, Motomura T, Shimura K, Onishi M, Okahata Y (2002) Study on kinetics of early stage protein adsorption on poly(2-methoxyethylacrylate) (PMEA) surface. Colloids and Surfaces A: Physicochemical and Engineering Aspects 203 (1-3):195-204

131. Jeyachandran YL, Mielczarski E, Rai B, Mielczarski JA (2009) Quantitative and Qualitative Evaluation of Adsorption/Desorption of Bovine Serum Albumin on Hydrophilic and Hydrophobic Surfaces. Langmuir

132. Weiss R, Reddi A (1980) Synthesis and localization of fibronectin during collagenous matrix-mesenchymal cell interaction and differentiation of cartilage and bone in vivo. Proceedings of the National Academy of Sciences 77 (4):2074-2078

133. Weiss R, Reddi A (1981) Appearance of fibronectin during the differentiation of cartilage, bone and bone marrow. J Cell Biol 88 (3):630-636

134. Ku Y, Chung C-P, Jang J-H (2005) The effect of the surface modification of titanium using a recombinant fragment of fibronectin and vitronectin on cell behavior. Biomaterials 26 (25):5153-5157

135. Datta N, Holtorf HL, Sikavitsas VI, Jansen JA, Mikos AG (2005) Effect of bone extracellular matrix synthesized in vitro on the osteoblastic differentiation of marrow stromal cells. Biomaterials 26 (9):971-977

136. Frisch SM, Ruoslahti E (1997) Integrins and anoikis. Current Opinion in Cell Biology 9 (5):701-706

137. Cheng S-S, Chittur KK, Sukenik CN, Culp LA, Lewandowska K (1994) The Conformation of Fibronectin on Self-Assembled Monolayers with Different Surface Composition: An FTIR/ATR Study. Journal of Colloid and Interface Science 162 (1):135-143

138. Culp LA, Sukenik CN (1998) Cell type-specific modulation of fibronectin adhesion functions on chemically-derivatized self-assembled monolayers. Journal of Biomaterials Science, Polymer Edition 9:1161-1176

139. Grinnell F, Feld M (1981) Adsorption characteristics of plasma fibronectin in relationship to biological activity. Journal of Biomedical Materials Research 15 (3):363-381

140. McClary KB, Ugarova T, Grainger DW (2000) Modulating fibroblast adhesion, spreading, and proliferation using self-assembled monolayer films of alkylthiolates on gold. Journal of Biomedical Materials Research 50 (3):428-439. doi:10.1002/(sici)1097-4636(20000605)50:3<428::aid-jbm18>3.0.co;2-h

141. Underwood PA, Steele JG, Dalton BA (1993) Effects of polystyrene surface chemistry on the biological activity of solid phase fibronectin and vitronectin, analysed with monoclonal antibodies. J Cell Sci 104 (3):793-803

142. Pettit D, Hoffman A, Horbett T (1994) Correlation between corneal epithelial cell outgrowth and monoclonal antibody binding to the cell binding domain of adsorbed fibronectin. Journal of Biomedical Materials Research 28 (6):685-691

143. Liu Y, Kao WJ (2002) Human macrophage adhesion on fibronectin: The role of substratum and intracellular signalling kinases. Cellular Signalling 14 (2):145-152

144. Faucheux N, Tzoneva R, Nagel M-D, Groth T (2006) The dependence of fibrillar adhesions in human fibroblasts on substratum chemistry. Biomaterials 27 (2):234-245

145. Altankov G, Grinnell F, Groth T (1996) Studies on the biocompatibility of materials: Fibroblast reorganization of substratum-bound fibronectin on surfaces varying in wettability. Journal of Biomedical Materials Research 30 (3):385-391. doi:10.1002/(sici)1097-4636(199603)30:3<385::aid-jbm13>3.0.co;2-j

146. Koenig AL, Gambillara V, Grainger DW (2003) Correlating fibronectin adsorption with endothelial cell adhesion and signaling on polymer substrates. Journal of Biomedical Materials Research Part A 64A (1):20-37. doi:10.1002/jbm.a.10316

147. Iuliano DJ, Saavedra SS, Truskey GA (1993) Effect of the conformation and orientation of adsorbed fibronectin on endothelial cell spreading and the strength of adhesion. Journal of Biomedical Materials Research 27 (8):1103-1113. doi:10.1002/jbm.820270816

148. Lenting PJ, Pegon JN, Groot E, Groot PGd (2010) Regulation of von Willebrand factor-platelet interactions. Thromb Haemos 104 (3):449-455. doi: 10.1160/TH09-11-0777

149. Lenting PJ, Denis CV (2007) von Willebrand factor A1 domain: stuck in the middle. Journal of Thrombosis and Haemostasis 5 (7):1361-1362

150. Cruz MA, Diacovo TG, Emsley J, Liddington R, Handin RI (2000) Mapping the Glycoprotein Ib-binding Site in the von Willebrand Factor A1 Domain. J Biol Chem 275 (25):19098-19105. doi:10.1074/jbc.M002292200

151. Ulrichts H, Udvardy M, Lenting PJ, Pareyn I, Vandeputte N, Vanhoorelbeke K, Deckmyn H (2006) Shielding of the A1 Domain by the D'D3 Domains of von Willebrand Factor Modulates Its Interaction with Platelet Glycoprotein Ib-IX-V. J Biol Chem 281 (8):4699-4707. doi:10.1074/jbc.M513314200

152. Dong J-F, Berndt MC, Schade A, McIntire LV, Andrews RK, Lopez JA (2001) Ristocetin-dependent, but not botrocetin-dependent, binding of von Willebrand factor to the platelet glycoprotein Ib-IX-V complex correlates with shear-dependent interactions. Blood 97 (1):162-168. doi:10.1182/blood.V97.1.162

153. Mccarty OJT, Calaminus SDJ, Berndt MC, Machesky LM, Watson SP (2006) von Willebrand factor mediates platelet spreading through glycoprotein Ib and aIIb B3 in the presence of botrocetin and ristocetin, respectively. Journal of Thrombosis and Haemostasis 4 (6):1367-1378

154. Vanhoorelbeke K, Cauwenberghs N, Vauterin S, Schlammadinger A, Mazurier C, Deckmyn H (2000) A Reliable and Reproducible ELISA Method to Measure Ristocetin Cofactor Activity of von Willebrand Factor. Thromb Haemos 83 (1):107-113

155. Martin C, Morales LD, Cruz MA (2007) Purified A2 domain of von Willebrand factor binds to the active conformation of von Willebrand factor and blocks the interaction with platelet glycoprotein Ib. Journal of Thrombosis and Haemostasis 5 (7):1363-1370

156. Novak L, Deckmyn H, Damjanovich S, Harsfalvi J (2002) Shear-dependent morphology of von Willebrand factor bound to immobilized collagen. Blood 99 (6):2070-2076. doi:10.1182/blood.V99.6.2070

157. Bendetowicz AV, Wise RJ, Gilbert GE (1999) Collagen-bound von Willebrand Factor Has Reduced Affinity for Factor VIII. J Biol Chem 274 (18):12300-12307. doi:10.1074/jbc.274.18.12300

158. Kwak D, Wu Y, Horbett TA (2005) Fibrinogen and von Willebrand's factor adsorption are both required for platelet adhesion from sheared suspensions to polyethylene preadsorbed with blood plasma. Journal of Biomedical Materials Research Part A 74A (1):69-83

159. Ulrichts H, Vanhoorelbeke K, Girma JP, Lenting PJ, Vauterin S, Deckmyn H (2005) The von Willebrand factor self-association is modulated by a multiple domain interaction. Journal of Thrombosis and Haemostasis 3 (3):552-561

160. Raghavachari M, Tsai H-M, Kottke-Marchant K, Marchant RE (2000) Surface dependent structures of von Willebrand factor observed by AFM under aqueous conditions. Colloids and Surfaces B: Biointerfaces 19 (4):315-324

161. Horton HR, Moran LA, Ochs RS, Rawn JD, Scrimgeour KG (1996) Principles of Biochemistry. 2 edn. Prentice-Hall, Inc.,

162. Di Lullo GA, Sweeney SM, Körkkö J, Ala-Kokko L, San Antonio JD (2002) Mapping the Ligand-binding Sites and Disease-associated Mutations on the Most Abundant Protein in the Human, Type I Collagen. Journal of Biological Chemistry 277 (6):4223-4231. doi:10.1074/jbc.M110709200

163. Buehler MJ (2006) Nature designs tough collagen: Explaining the nanostructure of collagen fibrils. Proceedings of the National Academy of Sciences 103 (33):12285-12290. doi:10.1073/pnas.0603216103

164. Pareti FI, Fujimura Y, Dent JA, Holland LZ, Zimmerman TS, Ruggeri ZM (1986) Isolation and characterization of a collagen binding domain in human von Willebrand factor. Journal of Biological Chemistry 261 (32):15310-15315

165. Pareti FI, Niiya K, McPherson JM, Ruggeri ZM (1987) Isolation and characterization of two domains of human von Willebrand factor that interact with fibrillar collagen types I and III. Journal of Biological Chemistry 262 (28):13835-13841

166. Dzamba BJ, Wu H, Jaenisch R, Peters DM (1993) Fibronectin binding site in type I collagen regulates fibronectin fibril formation. The Journal of Cell Biology 121 (5):1165-1172. doi:10.1083/jcb.121.5.1165

167. Nishida N, Sumikawa H, Sakakura M, Shimba N, Takahashi H, Terasawa H, Suzuki E-i, Shimada I (2003) Collagen-binding mode of vWF-A3 domain determined by a transferred cross-saturation experiment. Nat Struct Mol Biol 10 (1):53-58

168. Steffens GCM, Yao C, Prevel P, Markowicz M, Schenck P, Noah EM, Pallua N (2004) Modulation of Angiogenic Potential of Collagen Matrices by Covalent Incorporation of Heparin and Loading with Vascular Endothelial Growth Factor. Tissue Engineering 10 (9-10):1502-1509. doi:doi:10.1089/ten.2004.10.1502

169. Chevallay B, Herbage D (2000) Collagen-based biomaterials as 3D scaffold for cell cultures: applications for tissue engineering and gene therapy. Medical and Biological Engineering and Computing 38 (2):211-218. doi:10.1007/BF02344779

170. Pachence JM (1996) Collagen-based devices for soft tissue repair. Journal of Biomedical Materials Research 33 (1):35-40. doi:10.1002/(SICI)1097-4636(199621)33:1<35::AID-JBM6>3.0.CO;2-N

171. Elliott J, Halter M, Plant A, Woodward J, Langenbach K, Tona A (2008) Evaluating the performance of fibrillar collagen films formed at polystyrene surfaces as cell culture substrates. Biointerphases 3 (2):19-28. doi:10.1116/1.2912936

172. Elliott JT, Tona A, Woodward JT, Jones PL, Plant AL (2002) Thin Films of Collagen Affect Smooth Muscle Cell Morphology. Langmuir 19 (5):1506-1514. doi:10.1021/la026216r

173. Elliott JT, Woodward JT, Langenbach KJ, Tona A, Jones PL, Plant AL (2005) Vascular smooth muscle cell response on thin films of collagen. Matrix Biology 24 (7):489-502. doi:10.1016/j.matbio.2005.07.005

174. Emsley J, Cruz M, Handin R, Liddington R (1998) Crystal Structure of the von Willebrand Factor A1 Domain and Implications for the Binding of Platelet Glycoprotein Ib. J Biol Chem 273 (17):10396-10401. doi:10.1074/jbc.273.17.10396

175. Helary G, Noirclere F, Mayingi J, Migonney V (2009) A new approach to graft bioactive polymer on titanium implants: Improvement of MG 63 cell differentiation onto this coating. Acta Biomaterialia 5 (1):124-133

176. Sousa SR, Bras MM, Moradas-Ferreira P, Barbosa MA (2007) Dynamics of Fibronectin Adsorption on TiO2 Surfaces. Langmuir 23 (13):7046-7054. doi:10.1021/la062956e

177. Chick H, Martin CJ (1913) The Density and Solution Volume of some Proteins. Biochem J 7 (1):92-96

178. Castle JE, Baker MA (1999) The feasibility of an XPS expert system demonstrated by a rule set for carbon contamination. Journal of Electron Spectroscopy and Related Phenomena 105 (2–3):245-256. doi:10.1016/S0368-2048(99)00065-1

179. Wagner MS, Shen M, Horbett TA, Castner DG (2003) Quantitative time-of-flight secondary ion mass spectrometry for the characterization of multicomponent adsorbed protein films. Applied Surface Science 203-204 (0):704-709

180. Liu F, Dubey M, Takahashi H, Castner DG, Grainger DW (2010) Immobilized Antibody Orientation Analysis Using Secondary Ion Mass Spectrometry and Fluorescence Imaging of Affinity-Generated Patterns. Analytical Chemistry 82 (7):2947-2958. doi:10.1021/ac902964q

181. Goto S, Salomon DR, Ikeda Y, Ruggeri ZM (1995) Characterization of the Unique Mechanism Mediating the Shear-dependent Binding of Soluble von Willebrand Factor to Platelets. J Biol Chem 270 (40):23352-23361. doi:10.1074/jbc.270.40.23352

182. Penkala RA (2010) Understanding the regulation of the shear-enhanced binding of the platelet protein GPIb[alpha] and the A1 domain of von Willebrand Factor. University of Washington, Seattle, Washington

183. Goto S, Ikeda Y, Saldivar E, Ruggeri Z (1998) Distinct mechanisms of platelet aggregation as a consequence of different shearing flow conditions. J Clin Invest 101 (2):479-486

184. Castner DG, Ratner BD (2002) Biomedical surface science: Foundations to frontiers. Surface Science 500 (1-3):28-60

185. Cuypers P, Hermens W, Hemker H (1978) Ellipsometry as a tool to study protein films at liquid-solid interfaces. Analytical Biochemistry 84:56-67

186. Hylton DM, Shalaby SW, Robert A. Latour J (2005) Direct correlation between adsorption-induced changes in protein structure and platelet adhesion. Journal of Biomedical Materials Research Part A 73A (3):349-358

187. Sierakowski MR, Freitas RA, Fujimoto J, Petri DFS (2002) Adsorption behavior of oxidized galactomannans onto amino-terminated surfaces and their interaction with bovine serum albumin. Carbohydrate Polymers 49 (2):167-175

188. Glomm WR, Halskau O, Hanneseth A-MD, Volden S (2007) Adsorption Behavior of Acidic and Basic Proteins onto Citrate-Coated Au Surfaces Correlated to Their Native Fold, Stability, and pI. The Journal of Physical Chemistry B 111 (51):14329-14345. doi:doi:10.1021/jp074839d

189. Ithurbide A, Frateur I, Galtayries A, Marcus P (2007) XPS and flow-cell EQCM study of albumin adsorption on passivated chromium surfaces: Influence of potential and pH. Electrochimica Acta 53 (3):1336-1345

190. Green RJ, Davies J, Davies MC, Roberts CJ, Tendler SJB (1997) Surface plasmon resonance for real time in situ analysis of protein adsorption to polymer surfaces. Biomaterials 18 (5):405-413

191. Giamblanco N, Yaseen M, Zhavnerko G, Lu JR, Marletta G (2011) Fibronectin Conformation Switch Induced by Coadsorption with Human Serum Albumin. Langmuir 27 (1):312-319. doi:10.1021/la104127q

192. Cheng F, Gamble LJ, Castner DG (2008) XPS, TOF-SIMS, NEXAFS, and SPR Characterization of Nitrilotriacetic Acid-Terminated Self-Assembled Monolayers for Controllable Immobilization of Proteins. Analytical Chemistry 80 (7):2564-2573. doi:10.1021/ac702380w

193. Jung LS, Campbell CT, Chinowsky TM, Mar MN, Yee SS (1998) Quantitative Interpretation of the Response of Surface Plasmon Resonance Sensors to Adsorbed Films. Langmuir 14 (19):5636-5648. doi:10.1021/la971228b

194. Jung LS, Shumaker-Parry JS, Campbell CT, Yee SS, Gelb MH (2000) Quantification of Tight Binding to Surface-Immobilized Phospholipid Vesicles Using Surface Plasmon

Resonance: Binding Constant of Phospholipase A2. Journal of the American Chemical Society 122 (17):4177-4184. doi:10.1021/ja993879v

195. Archambault JG, Brash JL (2004) Protein resistant polyurethane surfaces by chemical grafting of PEO: amino-terminated PEO as grafting reagent. Colloids and Surfaces B: Biointerfaces 39 (1-2):9-16

196. Leibner ES, Barnthip N, Chen W, Baumrucker CR, Badding JV, Pishko M, Vogler EA (2009) Superhydrophobic effect on the adsorption of human serum albumin. Acta Biomaterialia 5 (5):1389-1398

197. Van Dulm P, Norde W (1983) The adsorption of human plasma albumin on solid surfaces, with special attention to the kinetic aspects. Journal of Colloid and Interface Science 91 (1):248-255

198. Paynter R, Ratner B, Horbett T, Thomas H (1984) XPS Studies on the Organization of Adsorbed Protein Films on Fluoropolymers. J Colloid Interface Sci 101 (1):233-245

199. Baugh L, Weidner T, Baio JE, Nguyen P-CT, Gamble LJ, Stayton PS, Castner DG Probing the Orientation of Surface-Immobilized Protein G B1 Using ToF-SIMS, Sum Frequency Generation, and NEXAFS Spectroscopy. Langmuir:null-null. doi:10.1021/la1007389

200. Liu X, Jang C-H, Zheng F, Jurgensen A, Denlinger JD, Dickson KA, Raines RT, Abbott NL, Himpsel FJ (2006) Characterization of Protein Immobilization at Silver Surfaces by Near Edge X-ray Absorption Fine Structure Spectroscopy. Langmuir 22 (18):7719-7725. doi:10.1021/la060988w

201. Henry M, Bertrand P (2004) Influence of polymer surface hydrophilicity on albumin adsorption. Surface and Interface Analysis 36 (8):729-732

202. Henry M, Dupont-Gillain C, Bertrand P (2003) Conformation Change of Albumin Adsorbed on Polycarbonate Membranes as Revealed by ToF-SIMS. Langmuir 19 (15):6271-6276. doi:doi:10.1021/la034081z

203. Amiji M, Park H, Park K (1992) Study on the prevention of surface-induced platelet activation by albumin coating. Journal of Biomaterials Science, Polymer Edition 3:375-388

204. Nonckreman CJ, Rouxhet PG, Dupont-Gillain CC (2007) Dual radiolabeling to study protein adsorption competition in relation with hemocompatibility. Journal of Biomedical Materials Research Part A 81A (4):791-802. doi:10.1002/jbm.a.31111

205. Asthana H, Erickson BL, Drzal LT (1997) Sulfonation of polymer surfaces - II. Chemical changes on polypropylene and polystyrene surfaces after gas phase sulfonation. Journal of Adhesion Science and Technology 11 (10):1269-1288

206. Tsuji H, Satoh H, Ikeda S, Gotoh Y, Ishikawa J (1998) Contact angle lowering of polystyrene surface by silver-negative-ion implantation for improving biocompatibility and introduced atomic bond evaluation by XPS. Nuclear Instruments and Methods in Physics Research Section B: Beam Interactions with Materials and Atoms 141 (1–4):197-201. doi:http://dx.doi.org/10.1016/S0168-583X(98)00090-1

207. Davies J, Nunnerley CS, Brisley AC, Sunderland RF, Edwards JC, Krüger P, Knes R, Paul AJ, Hibbert S (2000) Argon plasma treatment of polystyrene microtiter wells. Chemical and physical characterisation by contact angle, ToF-SIMS, XPS and STM. Colloids and Surfaces A: Physicochemical and Engineering Aspects 174 (3):287-295. doi:http://dx.doi.org/10.1016/S0927-7757(00)00497-0

208. Guruvenket S, Rao GM, Komath M, Raichur AM (2004) Plasma surface modification of polystyrene and polyethylene. Applied Surface Science 236 (1–4):278-284. doi:http://dx.doi.org/10.1016/j.apsusc.2004.04.033

209. Ellison AH, Zisman WA (1954) Wettability Studies on Nylon, Polyethylene Terephthalate and Polystyrene. The Journal of Physical Chemistry 58 (6):503-506. doi:10.1021/j150516a013

210. Sigal GB, Mrksich M, Whitesides GM (1998) Effect of Surface Wettability on the Adsorption of Proteins and Detergents. Journal of the American Chemical Society 120 (14):3464-3473. doi:10.1021/ja970819l

211. Bull HB (1956) Adsorption of bovine serum albumin on glass. Biochimica et Biophysica Acta 19 (0):464-471. doi:http://dx.doi.org/10.1016/0006-3002(56)90469-3

212. Horbett TA, Brash JL (1987) Proteins at Interfaces: Current Issues and Future Prospects. In: Proteins at Interfaces, vol 343. ACS Symposium Series, vol 343. American Chemical Society, pp 1-33. doi:doi:10.1021/bk-1987-0343.ch001 10.1021/bk-1987-0343.ch001

213. Dewez J-L, Berger V, Schneider Y-J, Rouxhet PG (1997) Influence of Substrate Hydrophobicity on the Adsorption of Collagen in the Presence of Pluronic F68, Albumin, or Calf Serum. Journal of Colloid and Interface Science 191 (1):1-10

214. Henry M, Dupont-Gillain C, Bertrand P (2008) Characterization of Insulin Adsorption in the Presence of Albumin by Time-of-Flight Secondary Ion Mass Spectrometry and X-ray Photoelectron Spectroscopy. Langmuir 24 (2):458-464. doi:doi:10.1021/la701850p

215. Kurtz S, Ong K, Lau E, Mowat F, Halpern M (2007) Projections of Primary and Revision Hip and Knee Arthroplasty in the United States from 2005 to 2030. J Bone Joint Surg Am 89 (4):780-785. doi:10.2106/jbjs.f.00222

216. Niinomi M (2008) Mechanical biocompatibilities of titanium alloys for biomedical applications. Journal of the Mechanical Behavior of Biomedical Materials 1 (1):30-42

217. Geetha M, Singh AK, Asokamani R, Gogia AK (2009) Ti based biomaterials, the ultimate choice for orthopaedic implants - A review. Progress in Materials Science 54 (3):397-425

218. Van Noort R (1987) Titanium: The implant material of today. Journal of Materials Science 22 (11):3801-3811. doi:10.1007/bf01133326

219. Albrektsson T, Jacobsson M (1987) Bone-metal interface in osseointegration. The Journal of Prosthetic Dentistry 57 (5):597-607

220. Legeros RZ, Craig RG (1993) Strategies to affect bone remodeling: Osteointegration. Journal of Bone and Mineral Research 8 (S2):S583-S596. doi:10.1002/jbmr.5650081328

221. Puleo DA, Nanci A (1999) Understanding and controlling the bone-implant interface. Biomaterials 20 (23-24):2311-2321

222. Kurtz S, Mowat F, Ong K, Chan N, Lau E, Halpern M (2005) Prevalence of Primary and Revision Total Hip and Knee Arthroplasty in the United States From 1990 Through 2002. J Bone Joint Surg Am 87 (7):1487-1497. doi:10.2106/jbjs.d.02441

223. Dorr LD, Kane Iii TJ, Conaty JP (1994) Long-term results of cemented total hip arthroplasty in patients 45 years old or younger: A 16-year follow-up study. The Journal of Arthroplasty 9 (5):453-456

224. Liu X, Chu PK, Ding C (2004) Surface modification of titanium, titanium alloys, and related materials for biomedical applications. Materials Science and Engineering: R: Reports 47 (3-4):49-121

225. Michiardi A, Hélary G, Nguyen PCT, Gamble LJ, Anagnostou F, Castner DG, Migonney V (2010) Bioactive polymer grafting onto titanium alloy surfaces. Acta Biomaterialia 6 (2):667-675

226. Damsky CH (1999) Extracellular matrix-integrin interactions in osteoblast function and tissue remodeling. Bone 25 (1):95-96

227. Winnard RG, Gerstenfeld LC, Toma CD, Franceschi RT (1995) Fibronectin gene expression, synthesis, and accumulation during in vitro differentiation of chicken osteoblasts. Journal of Bone and Mineral Research 10 (12):1969-1977. doi:10.1002/jbmr.5650101217

228. Howlett CR, Evans MDM, Walsh WR, Johnson G, Steele JG (1994) Mechanism of initial attachment of cells derived from human bone to commonly used prosthetic materials during cell culture. Biomaterials 15 (3):213-222

229. Gronthos S, Stewart K, Graves SE, Hay S, Simmons PJ (1997) Integrin Expression and Function on Human Osteoblast-like Cells. Journal of Bone and Mineral Research 12 (8):1189-1197. doi:10.1359/jbmr.1997.12.8.1189

230. Pierschbacher MD, Ruoslahti E (1984) Cell attachment activity of fibronectin can be duplicated by small synthetic fragments of the molecule. Nature 309 (5963):30-33

231. Saito T, Albelda SM, Brighton CT (1994) Identification of integrin receptors on cultured human bone cells. Journal of Orthopaedic Research 12 (3):384-394. doi:10.1002/jor.1100120311

232. Puleo DA, Bizios R (1992) Mechanisms of fibronectin-mediated attachment of osteoblasts to substrates in vitro. Bone and Mineral 18 (3):215-226

233. Carvalho RS, Schaffer JL, Gerstenfeld LC (1998) Osteoblasts induce osteopontin expression in response to attachment on fibronectin: Demonstration of a common role for integrin receptors in the signal transduction processes of cell attachment and mechanical stimulation. Journal of Cellular Biochemistry 70 (3):376-390. doi:10.1002/(sici)1097-4644(19980901)70:3<376::aid-jcb11>3.0.co;2-j

234. Hock JM, Krishnan V, Onyia JE, Bidwell JP, Milas J, Stanislaus D (2001) Osteoblast Apoptosis and Bone Turnover. Journal of Bone and Mineral Research 16 (6):975-984. doi:10.1359/jbmr.2001.16.6.975

235. Globus RK, Doty SB, Lull JC, Holmuhamedov E, Humphries MJ, Damsky CH (1998) Fibronectin is a survival factor for differentiated osteoblasts. J Cell Sci 111 (10):1385-1393

236. Grinnell F, Feld MK (1982) Fibronectin adsorption on hydrophilic and hydrophobic surfaces detected by antibody binding and analyzed during cell adhesion in serum-containing medium. Journal of Biological Chemistry 257 (9):4888-4893

237. Kowalczyńska HM, Nowak-Wyrzykowska M, Kołos R, Dobkowski J, Kamiński J (2008) Semiquantitative evaluation of fibronectin adsorption on unmodified and sulfonated polystyrene, as related to cell adhesion. Journal of Biomedical Materials Research Part A 87A (4):944-956. doi:10.1002/jbm.a.31868

238. Baugh L, Vogel V (2004) Structural changes of fibronectin adsorbed to model surfaces probed by fluorescence resonance energy transfer. Journal of Biomedical Materials Research Part A 69A (3):525-534. doi:10.1002/jbm.a.30026

239. Giroux TA, Cooper SL (1990) FTIR/ATR studies of human fibronectin adsorption onto plasma derivatized polystyrene. Journal of Colloid and Interface Science 139 (2):351-362

240. Lee MH, Ducheyne P, Lynch L, Boettiger D, Composto RJ (2006) Effect of biomaterial surface properties on fibronectin-[alpha]5[beta]1 integrin interaction and cellular attachment. Biomaterials 27 (9):1907-1916

241. Michael KE, Vernekar VN, Keselowsky BG, Meredith JC, Latour RA, Garcia AJ (2003) Adsorption-Induced Conformational Changes in Fibronectin Due to Interactions with Well-Defined Surface Chemistries. Langmuir 19 (19):8033-8040. doi:10.1021/la034810a

242. Michiardi A, Aparicio C, Ratner BD, Planell JA, Gil J (2007) The influence of surface energy on competitive protein adsorption on oxidized NiTi surfaces. Biomaterials 28 (4):586-594

243. MacDonald DE, Deo N, Markovic B, Stranick M, Somasundaran P (2002) Adsorption and dissolution behavior of human plasma fibronectin on thermally and chemically modified titanium dioxide particles. Biomaterials 23 (4):1269-1279

244. Pernodet N, Rafailovich M, Sokolov J, Xu D, Yang N-L, McLeod K (2003) Fibronectin fibrillogenesis on sulfonated polystyrene surfaces. Journal of Biomedical Materials Research Part A 64A (4):684-692. doi:10.1002/jbm.a.10394

245. Antia M, Islas LD, Boness DA, Baneyx G, Vogel V (2006) Single molecule fluorescence studies of surface-adsorbed fibronectin. Biomaterials 27 (5):679-690. doi:10.1016/j.biomaterials.2005.06.014

246. Anselme K (2000) Osteoblast adhesion on biomaterials. Biomaterials 21 (7):667-681

247. Ishida K, Sawada N, Yamaguchi M (2004) Expression of albumin in bone tissues and osteoblastic cells: involvement of hormonal regulation. Int J Mol Med 14 (5):891-895

248. Alves CM, Yang Y, Carnes DL, Ong JL, Sylvia VL, Dean DD, Agrawal CM, Reis RL (2007) Modulating bone cells response onto starch-based biomaterials by surface plasma treatment and protein adsorption. Biomaterials 28 (2):307-315

249. Ishida K, Yamaguchi M (2004) Role of albumin in osteoblastic cells: enhancement of cell proliferation and suppression of alkaline phosphatase activity. International journal of molecular medicine 14 (6):1077-1081

250. Bernards MT, Qin C, Jiang S (2008) MC3T3-E1 cell adhesion to hydroxyapatite with adsorbed bone sialoprotein, bone osteopontin, and bovine serum albumin. Colloids and Surfaces B: Biointerfaces 64 (2):236-247

251. Yamaguchi M, Igarashi A, Misawa H, Tsurusaki Y (2003) Enhancement of albumin expression in bone tissues with healing rat fractures. Journal of Cellular Biochemistry 89 (2):356-363. doi:10.1002/jcb.10510

252. Godek ML, Michel R, Chamberlain LM, Castner DG, Grainger DW (2009) Adsorbed serum albumin is permissive to macrophage attachment to perfluorocarbon polymer surfaces in culture. Journal of Biomedical Materials Research Part A 88A (2):503-519

253. Sousa SR, Lamghari M, Sampaio P, Moradas-Ferreira P, Barbosa MA (2008) Osteoblast adhesion and morphology on TiO2 depends on the competitive preadsorption of albumin and fibronectin. Journal of Biomedical Materials Research Part A 84A (2):281-290. doi:10.1002/jbm.a.31201

254. Yang Y, Cavin R, Ong JL (2003) Protein adsorption on titanium surfaces and their effect on osteoblast attachment. Journal of Biomedical Materials Research Part A 67A (1):344-349. doi:10.1002/jbm.a.10578

255. Ray S, Shard AG (2011) Quantitative analysis of adsorbed proteins by X-ray photoelectron spectroscopy. Analytical Chemistry 83 (22):8659-8666. doi:10.1021/ac202110x

256. Böhme U, Scheler U (2007) Hydrodynamic Size and Electrophoretic Mobility of Poly(styrene sulfonate) versus Molecular Weight. Macromolecular Chemistry and Physics 208 (19-20):2254-2257. doi:10.1002/macp.200700386

257. Young BR, Pitt WG, Cooper SL (1988) Protein adsorption on polymeric biomaterials I. Adsorption isotherms. Journal of Colloid and Interface Science 124 (1):28-43. doi:10.1016/0021-9797(88)90321-9

258. Kowalczynska HM, Mrozek P, Kaminski J (1993) Surface Sulfonation of Styrene/Methyl Methacrylate Copolymers Studied by X-Ray Photoelectron Spectroscopy. Journal of Colloid and Interface Science 160 (2):317-323. doi:10.1006/jcis.1993.1402

259. Nasef MM, Saidi H, Nor HM, Yarmo MA (2000) XPS studies of radiation grafted PTFE-g-polystyrene sulfonic acid membranes. Journal of Applied Polymer Science 76 (3):336-349. doi:10.1002/(sici)1097-4628(20000418)76:3<336::aid-app9>3.0.co;2-e

260. Nasef MM, Saidi H, Yarmo MA (2000) Surface investigations of radiation grafted FEP-g-polystyrene sulfonic acid membranes using XPS. Journal of New Materials for Electrochemical Systems 3:311-319

261. Powell CJ, Jablonski A (2010) NIST Electron Inelastic-Mean-Free-Path Database, vol Version 1.2. National Institute of Standards and Technology,

262. Curtis AS, Forrester JV, McInnes C, Lawrie F (1983) Adhesion of cells to polystyrene surfaces. The Journal of Cell Biology 97 (5):1500-1506. doi:10.1083/jcb.97.5.1500

263. Kowalczyńska HM, Nowak-Wyrzykowska M, Kołos R, Dobkowski J, Kamiński J (2005) Fibronectin adsorption and arrangement on copolymer surfaces and their significance in cell adhesion. Journal of Biomedical Materials Research Part A 72A (2):228-236. doi:10.1002/jbm.a.30238

264. Grinnell F, Feld MK (1981) Adsorption characteristics of plasma fibronectin in relationship to biological activity. Journal of Biomedical Materials Research 15 (3):363-381. doi:10.1002/jbm.820150308

265. Underwood PA, Steele JG, Dalton BA (1993) Effects of polystyrene surface chemistry on the biological activity of solid phase fibronectin and vitronectin, analysed with monoclonal antibodies. Journal of Cell Science 104 (3):793-803

266. Hughes RC, Pena SDJ, Clark J, Dourmashkin RR (1979) Molecular requirements for the adhesion and spreading of hamster fibroblasts. Experimental Cell Research 121 (2):307-314. doi:10.1016/0014-4827(79)90009-0

267. Jönsson U, Malmqvist M, Ronnberg I (1985) Adsorption of immunoglobulin G, protein A, and fibronectin in the submonolayer region evaluated by a combined study of ellipsometry and radiotracer techniques. Journal of Colloid and Interface Science 103 (2):360-372

268. Cheung JWC, Walker GC (2008) Immuno-Atomic Force Microscopy Characterization of Adsorbed Fibronectin. Langmuir 24 (24):13842-13849. doi:10.1021/la802452v

269. Ying P, Viana AS, Abrantes LM, Jin G (2004) Adsorption of human serum albumin onto gold: a combined electrochemical and ellipsometric study. Journal of Colloid and Interface Science 279 (1):95-99

270. Sousa SR, Moradas-Ferreira P, Saramago B, Viseu Melo L, Barbosa MA (2004) Human Serum Albumin Adsorption on TiO2 from Single Protein Solutions and from Plasma. Langmuir 20 (22):9745-9754. doi:10.1021/la049158d

271. Lee RG, Adamson C, Kim SW (1974) Competitive adsorption of plasma proteins onto polymer surfaces. Thrombosis Research 4 (3):485-490. doi:10.1016/0049-3848(74)90083-8

272. Hull JR, Tamura GS, Castner DG (2007) Structure and Reactivity of Adsorbed Fibronectin Films on Mica. Biophysical Journal 93 (8):2852-2860

273. Kowalczyńska HM, Kamiński Jw (1994) Substratum sulfonation and cell adhesion. Colloids and Surfaces B: Biointerfaces 2 (1–3):291-298. doi:10.1016/0927-7765(94)80043-X

274. Kowalczynska HM, Kaminski J (1991) Adhesion of L1210 cells to modified styrene copolymer surfaces in the presence of serum. Journal of Cell Science 99 (3):587-593

275. Kowalczynska HM, Nowak-Wyrzykowska M (2003) Modulation of adhesion, spreading and cytoskeleton organization of 3T3 fibroblasts by sulfonic groups present on polymer surfaces. Cell Biol Int (27):101-114

276. Miller T, Boettiger D (2002) Control of Intracellular Signaling by Modulation of Fibronectin Conformation at the Cell−Materials Interface†. Langmuir 19 (5):1723-1729. doi:10.1021/la0261500

277. Kowalczynska HM, Nowak-Wyrzykowska M (1999) Adhesion of L1210 cells to sulfonated styrene copolymer surfaces: imaging of F-actin AND alpha-actinin. Cell Biol Int 23 (5):359-372

278. Zorn G, Baio JE, Weidner T, Migonney V, Castner DG (2011) Characterization of Poly(sodium styrene sulfonate) Thin Films Grafted from Functionalized Titanium Surfaces. Langmuir 27 (21):13104-13112. doi:10.1021/la201918y

279. Ruggeri ZM (2007) Von Willebrand factor: Looking back and looking forward. Thromb Haemos 98 (1):55-62. doi: http://dx.doi.org/10.1160/TH07-04-0279

280. Savage B, Almus-Jacobs F, Ruggeri ZM (1998) Specific Synergy of Multiple Substrate-Receptor Interactions in Platelet Thrombus Formation under Flow. Cell 94 (5):657-666

281. Shankaran H, Alexandridis P, Neelamegham S (2003) Aspects of hydrodynamic shear regulating shear-induced platelet activation and self-association of von Willebrand factor in suspension. Blood 101 (7):2637-2645. doi:10.1182/blood-2002-05-1550

282. Ajzenberg N, Ribba A-S, Rastegar-Lari G, Meyer D, Baruch D (2000) Effect of recombinant von Willebrand factor reproducing type 2B or type 2M mutations on shear-induced platelet aggregation. Blood 95 (12):3796-3803

283. Andrews RK, Berndt MC (2004) Platelet physiology and thrombosis. Thrombosis Research 114 (5-6):447-453

284. Groot E, de Groot PG, Fijnheer R, Lenting PJ (2007) The presence of active von Willebrand factor under various pathological conditions. Current Opinion in Hematology 14 (3):284-289. doi:10.1097/MOH.0b013e3280dce531

285. Huizinga EG, Tsuji S, Romijn RAP, Schiphorst ME, de Groot PG, Sixma JJ, Gros P (2002) Structures of Glycoprotein Ibalpha and Its Complex with von Willebrand Factor A1 Domain. Science 297 (5584):1176-1179. doi:10.1126/science.107355

286. Siediecki CA, Lestini BJ, Kottke-Marchant KK, Eppell SJ, Wilson DL, Marchant RE (1996) Shear-dependent changes in the three-dimensional structure of human von Willebrand factor. Blood 88 (8):2939-2950

287. Hulstein JJJ, de Groot PG, Silence K, Veyradier A, Fijnheer R, Lenting PJ (2005) A novel nanobody that detects the gain-of-function phenotype of von Willebrand factor in ADAMTS13 deficiency and von Willebrand disease type 2B. Blood 106 (9):3035-3042. doi:10.1182/blood-2005-03-1153

288. Morales LD, Martin C, Cruz MA (2006) The interaction of von Willebrand factor-A1 domain with collagen: mutation G1324S (type 2M von Willebrand disease) impairs the conformational change in A1 domain induced by collagen. Journal of Thrombosis and Haemostasis 4 (2):417-425. doi:10.1111/j.1538-7836.2006.01742.x

289. Alevriadou BR, Moake JL, Turner NA, Ruggeri ZM, Folie BJ, Phillips MD, Schreiber AB, Hrinda ME, McIntire LV (1993) Real-time analysis of shear-dependent thrombus formation and its blockade by inhibitors of von Willebrand factor binding to platelets. Blood 81 (5):1263-1276

290. Wu Y-P, van Breugel HHFI, Lankhof H, Wise RJ, Handin RI, de Groot PG, Sixma JJ (1996) Platelet Adhesion to Multimeric and Dimeric von Willebrand Factor and to Collagen

Type III Preincubated With von Willebrand Factor. Arterioscler Thromb Vasc Biol 16 (5):611-620

291. Cao L, Chang M, Lee C-Y, Castner DG, Sukavaneshvar S, Ratner BD, Horbett TA (2007) Plasma-deposited tetraglyme surfaces greatly reduce total blood protein adsorption, contact activation, platelet adhesion, platelet procoagulant activity, and in vitro thrombus deposition. Journal of Biomedical Materials Research Part A 81A (4):827-837

292. Baio JE, Weidner T, Interlandi G, Mendoza-Barrera C, Canavan HE, Michel R, Castner DG (2011) Probing albumin adsorption onto calcium phosphates by x-ray photoelectron spectroscopy and time-of-flight secondary ion mass spectrometry. journal article 29:04D113. doi:http://dx.doi.org/10.1116/1.3613919

293. Sivaraman B, Latour RA (2010) The relationship between platelet adhesion on surfaces and the structure versus the amount of adsorbed fibrinogen. Biomaterials 31 (5):832-839

294. Kang I, Raghavachari M, Hofmann CM, Marchant RE (2007) Surface-dependent expression in the platelet GPIb binding domain within human von Willebrand factor studied by atomic force microscopy. Thrombosis Research 119 (6):731-740

295. Miyata S, Ruggeri ZM (1999) Distinct Structural Attributes Regulating von Willebrand Factor A1 Domain Interaction with Platelet Glycoprotein Ibalpha under Flow. J Biol Chem 274 (10):6586-6593. doi:10.1074/jbc.274.10.6586

296. Kumar RA, Dong J-f, Thaggard JA, Cruz MA, Lopez JA, McIntire LV (2003) Kinetics of GPIb{alpha}-vWF-A1 Tether Bond under Flow: Effect of GPIb{alpha} Mutations on the Association and Dissociation Rates. Biophys J 85 (6):4099-4109

297. Miura S, Li CQ, Cao Z, Wang H, Wardell MR, Sadler JE (2000) Interaction of von Willebrand Factor Domain A1 with Platelet Glycoprotein Ibalpha -(1-289). Slow intrinsic binding kinetics mediate rapid platelet adhesion J Biol Chem 275 (11):7539-7546. doi:10.1074/jbc.275.11.7539

298. Dumas JJ, Kumar R, McDonagh T, Sullivan F, Stahl ML, Somers WS, Mosyak L (2004) Crystal Structure of the Wild-type von Willebrand Factor A1-Glycoprotein Ib{alpha} Complex Reveals Conformation Differences with a Complex Bearing von Willebrand Disease Mutations. J Biol Chem 279 (22):23327-23334. doi:10.1074/jbc.M401659200

299. Davies DR, Cohen GH (1996) Interactions of protein antigens with antibodies. Proceedings of the National Academy of Sciences 93 (1):7-12

300. Stites WE (1997) Protein-Protein Interactions: Interface Structure, Binding Thermodynamics, and Mutational Analysis. Chemical Reviews 97 (5):1233-1250. doi:10.1021/cr960387h

301. Kuwabara I, Maruyama H, Kamisue S, Shima M, Yoshioka A, Maruyama IN (1999) Mapping of the minimal domain encoding a conformational epitope by lambda-phage surface display: factor VIII inhibitor antibodies from haemophilia A patients. Journal of Immunological Methods 224 (1-2):89-99

302. Jones S, Thornton JM (1996) Principles of protein-protein interactions. Proceedings of the National Academy of Sciences 93 (1):13-20

303. Davies DR, Padlan EA, Sheriff S (1990) Antibody-Antigen Complexes. Annual Review of Biochemistry 59 (1):439-473. doi:doi:10.1146/annurev.bi.59.070190.002255

304. Reineke U, Sabat R, Volk H-D, Schneider-Mergener J (1998) Mapping of the interleukin-10/interleukin-10 receptor combining site. Protein Science 7 (4):951-960. doi:10.1002/pro.5560070412

305. Chakrabarti P, Janin J (2002) Dissecting protein–protein recognition sites. Proteins: Structure, Function, and Bioinformatics 47 (3):334-343. doi:10.1002/prot.10085

306. Stanker LH, Serban AV, Cleveland E, Hnasko R, Lemus A, Safar J, DeArmond SJ, Prusiner SB (2010) Conformation-Dependent High-Affinity Monoclonal Antibodies to Prion Proteins. The Journal of Immunology 185 (1):729-737. doi:10.4049/jimmunol.0902930

307. Korth C, Stierli B, Streit P, Moser M, Schaller O, Fischer R, Schulz-Schaeffer W, Kretzschmar H, Raeber A, Braun U, Ehrensperger F, Hornemann S, Glockshuber R, Riek R, Billeter M, Wuthrich K, Oesch B (1997) Prion (PrPSc)-specific epitope defined by a monoclonal antibody. Nature 390 (6655):74-77

308. Paramithiotis E, Pinard M, Lawton T, LaBoissiere S, Leathers VL, Zou W-Q, Estey LA, Lamontagne J, Lehto MT, Kondejewski LH, Francoeur GP, Papadopoulos M, Haghighat A, Spatz SJ, Head M, Will R, Ironside J, O'Rourke K, Tonelli Q, Ledebur HC, Chakrabartty A, Cashman NR (2003) A prion protein epitope selective for the pathologically misfolded conformation. Nat Med 9 (7):893-899

309. Mendiaz EA, Chang DG, Boone TC, Grant JR, Wypych J, Aguero B, Egrie JC, Langley KE (1996) Epitope Mapping and Immunoneutralization of Recombinant Human Stem-Cell

Factor. European Journal of Biochemistry 239 (3):842-849. doi:10.1111/j.1432-1033.1996.0842u.x

310. Song CY, Chen WL, Yang MC, Huang JP, Mao SJT (2005) Epitope Mapping of a Monoclonal Antibody Specific to Bovine Dry Milk. Journal of Biological Chemistry 280 (5):3574-3582. doi:10.1074/jbc.M407031200

311. Celikel R, Ruggeri ZM, Varughese KI (2000) von Willebrand factor conformation and adhesive function is modulated by an internalized water molecule. Nat Struct Mol Biol 7 (10):881-884

312. Fukuda K, Doggett TA, Bankston LA, Cruz MA, Diacovo TG, Liddington RC (2002) Structural Basis of von Willebrand Factor Activation by the Snake Toxin Botrocetin. Structure 10 (7):943-950

313. Ruggeri ZM, Mendolicchio GL (2007) Adhesion Mechanisms in Platelet Function. Circ Res 100 (12):1673-1685. doi:10.1161/01.RES.0000267878.97021.ab

314. Fukuda K, Doggett T, Laurenzi IJ, Liddington RC, Diacovo TG (2005) The snake venom protein botrocetin acts as a biological brace to promote dysfunctional platelet aggregation. Nat Struct Mol Biol 12 (2):152-159

315. Wagner MS, McArthur SL, Shen M, Horbett TA, Castner DG (2002) Limits of detection for time of flight secondary ion mass spectrometry (ToF-SIMS) and X-ray photoelectron spectroscopy (XPS): detection of low amounts of adsorbed protein. Journal of Biomaterials Science, Polymer Edition 13:407-428

316. Williams RL, Williams DF (1988) Albumin adsorption on metal surfaces. Biomaterials 9 (3):206-212

317. Unsworth LD, Sheardown H, Brash JL (2005) Polyethylene oxide surfaces of variable chain density by chemisorption of PEO-thiol on gold: Adsorption of proteins from plasma studied by radiolabelling and immunoblotting. Biomaterials 26 (30):5927-5933

318. Norde W, Anusiem ACI (1992) Adsorption, desorption and re-adsorption of proteins on solid surfaces. Colloids and Surfaces 66 (1):73-80

319. Auton M, Sowa KE, Smith SM, Sedlak E, Vijayan KV, Cruz MA (2010) Destabilization of the A1 Domain in von Willebrand Factor Dissociates the A1A2A3 Tri-domain and Provokes Spontaneous Binding to Glycoprotein Ib-alpha and Platelet Activation under Shear

Stress. Journal of Biological Chemistry 285 (30):22831-22839. doi:10.1074/jbc.M110.103358

320. Okamoto M, Ishikawa K, Tanji N, Aoyagi S (2012) Investigation of the damage on the outermost hair surface using ToF-SIMS and XPS. Surface and Interface Analysis 44 (6):736-739. doi:10.1002/sia.3878

321. Gordon ML, Cooper G, Morin C, Araki T, Turci CsC, Kaznatcheev K, Hitchcock AP (2003) Inner-Shell Excitation Spectroscopy of the Peptide Bond: Comparison of the C 1s, N 1s, and O 1s Spectra of Glycine, Glycyl-Glycine, and Glycyl-Glycyl-Glycine. The Journal of Physical Chemistry A 107 (32):6144-6159. doi:10.1021/jp0344390

322. Zubavichus Y, Zharnikov M, Schaporenko A, Grunze M (2004) NEXAFS study of glycine and glycine-based oligopeptides. Journal of Electron Spectroscopy and Related Phenomena 134 (1):25-33

323. Zubavichus Y, Shaporenko A, Grunze M, Zharnikov M (2007) NEXAFS Spectroscopy of Homopolypeptides at All Relevant Absorption Edges: Polyisoleucine, Polytyrosine, and Polyhistidine. The Journal of Physical Chemistry B 111 (33):9803-9807. doi:10.1021/jp073922y

324. Cooper G, Gordon M, Tulumello D, Turci C, Kaznatcheev K, Hitchcock AP (2004) Inner shell excitation of glycine, glycyl-glycine, alanine and phenylalanine. Journal of Electron Spectroscopy and Related Phenomena 137-140 (0):795-799

325. Wilks RG, MacNaughton JB, Kraatz HB, Regier T, Moewes A (2006) Combined X-ray Absorption Spectroscopy and Density Functional Theory Examination of Ferrocene-Labeled Peptides. The Journal of Physical Chemistry B 110 (12):5955-5965. doi:10.1021/jp056573l

326. Hitchcock AP, Morin C, Heng YM, Cornelius RM, Brash JL (2002) Towards practical soft X-ray spectromicroscopy of biomaterials. Journal of Biomaterials Science -- Polymer Edition 13 (8):919-937

327. Baio JE, Weidner T, Samuel NT, McCrea K, Baugh L, Stayton PS, Castner DG (2010) Multitechnique characterization of adsorbed peptide and protein orientation: LK3-10 and Protein G B1. journal article 28:C5D1-C5D8. doi:http://dx.doi.org/10.1116/1.3456176

328. Polzonetti G, Battocchio C, Iucci G, Dettin M, Gambaretto R, Di Bello C, Carravetta V (2006) Thin films of a self-assembling peptide on TiO2 and Au studied by NEXAFS, XPS and IR spectroscopies. Materials Science and Engineering: C 26 (5-7):929-934

329. Furlan M (1996) Von Willebrand factor: molecular size and functional activity. Annals of Hematology 72 (6):341-348. doi:10.1007/s002770050184

330. Auton M, Zhu C, Cruz MA (2010) The Mechanism of VWF-Mediated Platelet GPIb[alpha] Binding. Biophysical Journal 99 (4):1192-1201

331. Miyata S, Goto S, Federici AB, Ware J, Ruggeri ZM (1996) Conformational Changes in the A1 Domain of von Willebrand Factor Modulating the Interaction with Platelet Glycoprotein Ib. Journal of Biological Chemistry 271 (15):9046-9053. doi:10.1074/jbc.271.15.9046

332. Sadler JE, Budde U, Eikenboom JCJ, Favaloro EJ, Hill FGH, Holmberg L, Ingerslev J, Lee CA, Lillicrap D, Mannucci PM, Mazurier C, Meyer D, Nichols WL, Nishino M, Peake IR, Rodeghiero F, Schneppenheim R, Ruggeri ZM, Srivastava A, Montgomery RR, Federici AB, The Working Party On Von Willebrand Disease C (2006) Update on the pathophysiology and classification of von Willebrand disease: a report of the Subcommittee on von Willebrand Factor. Journal of Thrombosis and Haemostasis 4 (10):2103-2114. doi:10.1111/j.1538-7836.2006.02146.x

333. Heino J (2007) The collagen family members as cell adhesion proteins. BioEssays 29 (10):1001-1010. doi:10.1002/bies.20636

334. Hansen RR, Tipnis AA, White-Adams TC, Di Paola JA, Neeves KB (2011) Characterization of Collagen Thin Films for von Willebrand Factor Binding and Platelet Adhesion. Langmuir 27 (22):13648-13658. doi:10.1021/la2023727

335. Dufrêne YF, Marchal TG, Rouxhet PG (1999) Probing the organization of adsorbed protein layers: complementarity of atomic force microscopy, X-ray photoelectron spectroscopy and radiolabeling. Applied Surface Science 144-145:638-643

336. Dalgleish R (1997) The Human Type I Collagen Mutation Database. Nucleic Acids Res 25 (1):181-187

337. Dalgleish R (1998) The Human Collagen Mutation Database 1998. Nucleic Acids Res 26 (1):253-255

338. Lisman T, Raynal N, Groeneveld D, Maddox B, Peachey AR, Huizinga EG, de Groot PG, Farndale RW (2006) A single high-affinity binding site for von Willebrand factor in collagen III, identified using synthetic triple-helical peptides. Blood 108 (12):3753-3756. doi:10.1182/blood-2006-03-011965

339. Bonnefoy A, Romijn RA, Vandervoort PAH, Rompaey IV, Vermylen J, Hoylaerts MF (2006) von Willebrand factor A1 domain can adequately substitute for A3 domain in recruitment of flowing platelets to collagen. Journal of Thrombosis and Haemostasis 4 (10):2151-2161

340. Sanni OD, Wagner MS, Briggs D, Castner DG, Vickerman JC (2002) Classification of adsorbed protein static ToF-SIMS spectra by principal component analysis and neural networks. Surface and Interface Analysis 33 (9):715-728. doi:10.1002/sia.1438

341. Malyarenko DI, Chen H, Wilkerson AL, Tracy ER, Cooke WE, Manos DM, Sasinowski M, Semmes OJ (2004) Ga+ TOF-SIMS lineshape analysis for resolution enhancement of MALDI MS spectra of a peptide mixture. Applied Surface Science 231-232 (0):357-361

342. Bernsmann F, Lawrence N, Hannig M, Ziegler C, Gnaser H (2008) Protein films adsorbed on experimental dental materials: ToF-SIMS with multivariate data analysis. Analytical and Bioanalytical Chemistry 391 (2):545-554

343. Berman ESF, Wu L, Fortson SL, Kulp KS, Nelson DO, Wu KJ (2009) Chemometric and statistical analyses of ToF-SIMS spectra of increasingly complex biological samples. Surface and Interface Analysis 41 (2):97-104. doi:10.1002/sia.2953

344. Martin SM, Ganapathy R, Kim TK, Leach-Scampavia D, Giachelli CM, Ratner BD (2003) Characterization and analysis of osteopontin-immobilized poly(2-hydroxyethyl methacrylate) surfaces. Journal of Biomedical Materials Research Part A 67A (1):334-343. doi:10.1002/jbm.a.10060

345. Gelse K, Pöschl E, Aigner T (2003) Collagens—structure, function, and biosynthesis. Advanced Drug Delivery Reviews 55 (12):1531-1546. doi:10.1016/j.addr.2003.08.002

346. Yuan L, Veis A (1973) The self-assembly of collagen molecules. Biopolymers 12 (6):1437-1444. doi:10.1002/bip.1973.360120618

347. Silver FH, Trelstad RL (1980) Type I collagen in solution. Structure and properties of fibril fragments. Journal of Biological Chemistry 255 (19):9427-9433

348. Schmitt FO, Hall CE, Jakus MA (1942) Electron microscope investigations of the structure of collagen. Journal of Cellular and Comparative Physiology 20 (1):11-33. doi:10.1002/jcp.1030200103

349. Russell AE (1974) Effect of pH on thermal stability of collagen in the dispersed and aggregated states Biochem J 139 (1):277-280

350. Köster S, Leach JB, Struth B, Pfohl T, Wong JY (2006) Visualization of Flow-Aligned Type I Collagen Self-Assembly in Tunable pH Gradients. Langmuir 23 (2):357-359. doi:10.1021/la062473a

351. Köster S, Evans HM, Wong JY, Pfohl T (2007) An In Situ Study of Collagen Self-Assembly Processes. Biomacromolecules 9 (1):199-207. doi:10.1021/bm700973t

352. Harris JR, Reiber A (2007) Influence of saline and pH on collagen type I fibrillogenesis in vitro: Fibril polymorphism and colloidal gold labelling. Micron 38 (5):513-521. doi:10.1016/j.micron.2006.07.026

353. Jiang F, Hörber H, Howard J, Müller DJ (2004) Assembly of collagen into microribbons: effects of pH and electrolytes. Journal of Structural Biology 148 (3):268-278. doi:10.1016/j.jsb.2004.07.001

354. Christiansen DL, Huang EK, Silver FH (2000) Assembly of type I collagen: fusion of fibril subunits and the influence of fibril diameter on mechanical properties. Matrix Biology 19 (5):409-420. doi:10.1016/S0945-053X(00)00089-5

355. Santoro SA (1986) Identification of a 160,000 dalton platelet membrane protein that mediates the initial divalent cation-dependent adhesion of platelets to collagen. Cell 46 (6):913-920. doi:10.1016/0092-8674(86)90073-5

356. Morton LF, Peachey AR, Zijenah LS, Goodall AH, Humphries MJ, Barnes MJ (1994) Conformation-dependent platelet adhesion to collagen involving integrin alpha 2 beta 1-mediated and other mechanisms: multiple alpha 2 beta 1-recognition sites in collagen type I. Biochem J 299 (3):791-797

357. Yamamoto M, Yamato M, Aoyagi M, Yamamoto K (1995) Identification of Integrins Involved in Cell Adhesion to Native and Denatured Type I Collagens and the Phenotypic Transition of Rabbit Arterial Smooth Muscle Cells. Experimental Cell Research 219 (1):249-256. doi:10.1006/excr.1995.1225

358. Taubenberger AV, Woodruff MA, Bai H, Muller DJ, Hutmacher DW (2010) The effect of unlocking RGD-motifs in collagen I on pre-osteoblast adhesion and differentiation. Biomaterials 31 (10):2827-2835. doi:10.1016/j.biomaterials.2009.12.051

359. Aumailley M, Timpl R (1986) Attachment of cells to basement membrane collagen type IV. The Journal of Cell Biology 103 (4):1569-1575. doi:10.1083/jcb.103.4.1569

360. Khew ST, Tong YW (2007) The Specific Recognition of a Cell Binding Sequence Derived from Type I Collagen by Hep3B and L929 Cells. Biomacromolecules 8 (10):3153-3161. doi:10.1021/bm700587j

361. Grab B, Miles AJ, Furcht LT, Fields GB (1996) Promotion of Fibroblast Adhesion by Triple-helical Peptide Models of Type I Collagen-derived Sequences. Journal of Biological Chemistry 271 (21):12234-12240. doi:10.1074/jbc.271.21.12234

362. Rubin K, Höök M, öbrink B, Timpl R (1981) Substrate adhesion of rat hepatocytes: Mechanism of attachment to collagen substrates. Cell 24 (2):463-470. doi:10.1016/0092-8674(81)90337-8

363. Schor SL, Court J (1979) Different mechanisms in the attachment of cells to native and denatured collagen. Journal of Cell Science 38 (1):267-281

364. Gowen BB, Borg TK, Ghaffar A, Mayer EP (2000) Selective adhesion of macrophages to denatured forms of type I collagen is mediated by scavenger receptors. Matrix Biology 19 (1):61-71. doi:10.1016/s0945-053x(99)00052-9

365. Jones PL, Jones FS, Zhou B, Rabinovitch M (1999) Induction of vascular smooth muscle cell tenascin-C gene expression by denatured type I collagen is dependent upon a beta3 integrin-mediated mitogen-activated protein kinase pathway and a 122-base pair promoter element. Journal of Cell Science 112 (4):435-445

366. Huang C-J, Chien Y-L, Ling T-Y, Cho H-C, Yu J, Chang Y-C (2010) The influence of collagen film nanostructure on pulmonary stem cells and collagen–stromal cell interactions. Biomaterials 31 (32):8271-8280. doi:10.1016/j.biomaterials.2010.07.038

367. Jokinen J, Dadu E, Nykvist P, Käpylä J, White DJ, Ivaska J, Vehviläinen P, Reunanen H, Larjava H, Häkkinen L, Heino J (2004) Integrin-mediated Cell Adhesion to Type I Collagen Fibrils. Journal of Biological Chemistry 279 (30):31956-31963. doi:10.1074/jbc.M401409200

368. Schuliga M, Ong SC, Soon L, Zal F, Harris T, Stewart AG (2010) Airway smooth muscle remodels pericellular collagen fibrils: implications for proliferation. American Journal of Physiology - Lung Cellular and Molecular Physiology 298 (4):L584-L592. doi:10.1152/ajplung.00312.2009

369. Jones PL, Crack J, Rabinovitch M (1997) Regulation of Tenascin-C, a Vascular Smooth Muscle Cell Survival Factor That Interacts with the α vβ 3 Integrin to Promote Epidermal

Growth Factor Receptor Phosphorylation and Growth. The Journal of Cell Biology 139 (1):279-293

370. Koyama H, Raines EW, Bornfeldt KE, Roberts JM, Ross R (1996) Fibrillar Collagen Inhibits Arterial Smooth Muscle Proliferation through Regulation of Cdk2 Inhibitors. Cell 87 (6):1069-1078. doi:10.1016/s0092-8674(00)81801-2

371. Egles C, Shamis Y, Mauney JR, Volloch V, Kaplan DL, Garlick JA (2008) Denatured Collagen Modulates the Phenotype of Normal and Wounded Human Skin Equivalents. J Invest Dermatol 128 (7):1830-1837

372. Mauney J, Volloch V (2009) Collagen I matrix contributes to determination of adult human stem cell lineage via differential, structural conformation-specific elicitation of cellular stress response. Matrix Biology 28 (5):251-262. doi:10.1016/j.matbio.2009.04.002

373. Mauney J, Volloch V (2009) Progression of human bone marrow stromal cells into both osteogenic and adipogenic lineages is differentially regulated by structural conformation of collagen I matrix via distinct signaling pathways. Matrix Biology 28 (5):239-250. doi:10.1016/j.matbio.2009.04.003

374. Scharffetter-Kochanek K, Eberhard Klein C, Heinen G, Mauch C, Schaefer T, Adelmann-Grill BC, Goerz G, Fusenig NE, Krieg TM, Plewig G (1992) Migration of a Human Keratinocyte Cell Line (HACAT) to Interstitial Collagen Type I Is Mediated by the [agr]2[beta]1-Integrin Receptor. J Investig Dermatol 98 (1):3-11

375. Abraham LC, Vorrasi J, Kaplan DL (2004) Impact of collagen structure on matrix trafficking by human fibroblasts. Journal of Biomedical Materials Research Part A 70A (1):39-48. doi:10.1002/jbm.a.30057

376. Johansson S, Höök M (1980) Heparin enhances the rate of binding of fibronectin to collagen. . Biochem J 187 (2):521-524

377. Davis GE, Bayless KJ, Davis MJ, Meininger GA (2000) Regulation of Tissue Injury Responses by the Exposure of Matricryptic Sites within Extracellular Matrix Molecules. The American Journal of Pathology 156 (5):1489-1498. doi:10.1016/s0002-9440(10)65020-1

378. Tuckwell DS, Ayad S, Grant ME, Takigawa M, Humphries MJ (1994) Conformation dependence of integrin-type II collagen binding. Inability of collagen peptides to support alpha 2 beta 1 binding, and mediation of adhesion to denatured collagen by a novel alpha 5 beta 1-fibronectin bridge. Journal of Cell Science 107 (4):993-1005

379. Davis GE (1992) Affinity of integrins for damaged extracellular matrix: αvβ3 binds to denatured collagen type I through RGD sites. Biochemical and Biophysical Research Communications 182 (3):1025-1031. doi:10.1016/0006-291x(92)91834-d

380. Kern A, Eble J, Golbik R, KÜhn K (1993) Interaction of type IV collagen with the isolated integrins α1β1 and α2β1. European Journal of Biochemistry 215 (1):151-159. doi:10.1111/j.1432-1033.1993.tb18017.x

381. Pfaff M, Aumailley M, Specks U, Knolle J, Zerwes HG, Timpl R (1993) Integrin and Arg-Gly-Asp Dependence of Cell Adhesion to the Native and Unfolded Triple Helix of Collagen Type VI. Experimental Cell Research 206 (1):167-176

382. Ruggiero F, Champliaud M-F, Garrone R, Aumailley M (1994) Interactions between Cells and Collagen V Molecules or Single Chains Involve Distinct Mechanisms. Experimental Cell Research 210 (2):215-223. doi:10.1006/excr.1994.1032

383. Gullberg D, Gehlsen KR, Turner DC, Ahlén K, Zijenah LS, Barnes MJ, Rubin K (1992) Analysis of alpha 1 beta 1, alpha 2 beta 1 and alpha 3 beta 1 integrins in cell--collagen interactions: identification of conformation dependent alpha 1 beta 1 binding sites in collagen type I. EMBO Journal 11 (11):3865-3873

384. Berman A, Morozevich G, Karmansky I, Gleiberman A, Bychkova V (1993) Adhesion of Mouse Hepatocytes to Type I Collagen: Role of Supramolecular Forms and Effect of Proteolytic Degradation. Biochemical and Biophysical Research Communications 194 (1):351-357. doi:10.1006/bbrc.1993.1827

385. Hynes RO (2002) Integrins: Bidirectional, Allosteric Signaling Machines. Cell 110 (6):673-687. doi:10.1016/s0092-8674(02)00971-6

386. Elliott JT, Woodward JT, Umarji A, Mei Y, Tona A (2007) The effect of surface chemistry on the formation of thin films of native fibrillar collagen. Biomaterials 28 (4):576-585. doi:http://dx.doi.org/10.1016/j.biomaterials.2006.09.023

387. Zhu M, Souillac PO, Ionescu-Zanetti C, Carter SA, Fink AL (2002) Surface-catalyzed Amyloid Fibril Formation. Journal of Biological Chemistry 277 (52):50914-50922. doi:10.1074/jbc.M207225200

388. Cruz MA, Yuan H, Lee JR, Wise RJ, Handin RI (1995) Interaction of the von Willebrand Factor (vWF) with Collagen. Journal of Biological Chemistry 270 (18):10822-10827. doi:10.1074/jbc.270.18.10822

389. Roth GJ, Titani K, Hoyer LW, Hickey MJ (1986) Localization of binding sites within human von Willebrand factor for monomeric type III collagen. Biochemistry 25 (26):8357-8361. doi:10.1021/bi00374a004

390. Cruz MA, Handin RI, Wise RJ (1993) The interaction of the von Willebrand factor-A1 domain with platelet glycoprotein Ib/IX. The role of glycosylation and disulfide bonding in a monomeric recombinant A1 domain protein. Journal of Biological Chemistry 268 (28):21238-21245

391. Hoylaerts MF, Yamamoto H, Nuyts K, Vreys I, Deckmyn H, Vermylen J (1997) von Willebrand factor binds to native collagen VI primarily via its A1 domain. Biochem J 324 (1):185-191

392. Saelman EU, Nieuwenhuis HK, Hese KM, de Groot PG, Heijnen HF, Sage EH, Williams S, McKeown L, Gralnick HR, Sixma JJ (1994) Platelet adhesion to collagen types I through VIII under conditions of stasis and flow is mediated by GPIa/IIa (alpha 2 beta 1-integrin). Blood 83 (5):1244-1250

393. Woodcock SE, Johnson WC, Chen Z (2005) Collagen adsorption and structure on polymer surfaces observed by atomic force microscopy. Journal of Colloid and Interface Science 292 (1):99-107. doi:10.1016/j.jcis.2005.05.059

394. Williams BR, Gelman RA, Poppke DC, Piez KA (1978) Collagen fibril formation. Optimal in vitro conditions and preliminary kinetic results. Journal of Biological Chemistry 253 (18):6578-6585

395. Bruns RR, Gross J (1974) High-resolution analysis of the modified quarter-stagger model of the collagen fibril. Biopolymers 13 (5):931-941. doi:10.1002/bip.1974.360130509

396. Hulmes DJ, Wess TJ, Prockop DJ, Fratzl P (1995) Radial packing, order, and disorder in collagen fibrils. Biophysical Journal 68 (5):1661-1670. doi:10.1016/s0006-3495(95)80391-7

397. Orgel JPRO, Irving TC, Miller A, Wess TJ (2006) Microfibrillar structure of type I collagen in situ. Proceedings of the National Academy of Sciences 103 (24):9001-9005. doi:10.1073/pnas.0502718103

398. Wittebort RJ, Clark AM (1992) Structural Studies of Collagen by Solid State NMR. Bulletin of Magnetic Resonance 14:303-306

399. Puxkandl R, Zizak I, Paris O, Keckes J, Tesch W, Bernstorff S, Purslow P, Fratzl P (2002) Viscoelastic properties of collagen: synchrotron radiation investigations and structural model. Philosophical Transactions of the Royal Society of London Series B: Biological Sciences 357 (1418):191-197. doi:10.1098/rstb.2001.1033

400. Boudko SP, Engel J, Okuyama K, Mizuno K, Bächinger HP, Schumacher MA (2008) Crystal Structure of Human Type III Collagen Gly991–Gly1032 Cystine Knot-containing Peptide Shows Both 7/2 and 10/3 Triple Helical Symmetries. Journal of Biological Chemistry 283 (47):32580-32589. doi:10.1074/jbc.M805394200

401. Herr AB, Farndale RW Structural insights into the interactions between platelet receptors and fibrillar collagen. Journal of Biological Chemistry. doi:10.1074/jbc.R109.013219

402. Rocha-Mendoza I, Yankelevich DR, Wang M, Reiser KM, Frank CW, Knoesen A (2007) Sum Frequency Vibrational Spectroscopy: The Molecular Origins of the Optical Second-Order Nonlinearity of Collagen. Biophysical Journal 93 (12):4433-4444. doi:10.1529/biophysj.107.111047

403. Wang J, Buck SM, Chen Z (2002) Sum Frequency Generation Vibrational Spectroscopy Studies on Protein Adsorption. The Journal of Physical Chemistry B 106 (44):11666-11672. doi:10.1021/jp021363j

404. Reiser Karen M, McCourt Alexander B, Yankelevich Diego R, Knoesen A (2012) Structural Origins of Chiral Second-Order Optical Nonlinearity in Collagen: Amide I Band. Biophysical journal 103 (10):2177-2186

405. Vroman L (1962) Effect of Adsorbed Proteins on the Wettability of Hydrophilic and Hydrophobic Solids. Nature 196 (4853):476-477

406. Calonder C, Matthew HWT, Van Tassel PR (2005) Adsorbed layers of oriented fibronectin: A strategy to control cell–surface interactions. Journal of Biomedical Materials Research Part A 75A (2):316-323. doi:10.1002/jbm.a.30417

407. Silliman CC, Wang M (2006) The merits of in vitro versus in vivo modeling in investigation of the immune system. Environmental Toxicology and Pharmacology 21 (2):123-134. doi:10.1016/j.etap.2005.07.002

408. Ziats NP, Miller KM, Anderson JM (1988) In vitro and in vivo interactions of cells with biomaterials. Biomaterials 9 (1):5-13. doi:10.1016/0142-9612(88)90063-4

409. Hanks CT, Wataha JC, Sun Z (1996) In vitro models of biocompatibility: a review. Dental materials : official publication of the Academy of Dental Materials 12 (3):186-193
410. Horbett TA, Cheng CM, Ratner BD, Hoffman AS, Hanson SR (1986) The kinetics of baboon fibrinogen adsorption to polymers: In vitro and in vivo studies. Journal of Biomedical Materials Research 20 (6):739-772. doi:10.1002/jbm.820200608
411. Vashist SK, Dixit CK, MacCraith BD, O'Kennedy R (2011) Effect of antibody immobilization strategies on the analytical performance of a surface plasmon resonance-based immunoassay. Analyst 136 (21):4431-4436
412. Storri S, Santoni T, Minunni M, Mascini M (1998) Surface modifications for the development of piezoimmunosensors. Biosensors and Bioelectronics 13 (3–4):347-357. doi:10.1016/s0956-5663(97)00119-x
413. Vikholm I (2005) Self-assembly of antibody fragments and polymers onto gold for immunosensing. Sensors and Actuators B: Chemical 106 (1):311-316. doi:10.1016/j.snb.2004.07.034
414. Vikholm-Lundin I, Albers WM (2006) Site-directed immobilisation of antibody fragments for detection of C-reactive protein. Biosensors and Bioelectronics 21 (7):1141-1148. doi:10.1016/j.bios.2005.04.011
415. Caruso F, Rodda E, Furlong DN (1996) Orientational Aspects of Antibody Immobilization and Immunological Activity on Quartz Crystal Microbalance Electrodes. Journal of Colloid and Interface Science 178 (1):104-115. doi:10.1006/jcis.1996.0098
416. Tidwell CD, Ertel SI, Ratner BD, Tarasevich BJ, Atre S, Allara DL (1997) Endothelial Cell Growth and Protein Adsorption on Terminally Functionalized, Self-Assembled Monolayers of Alkanethiolates on Gold. Langmuir 13 (13):3404-3413. doi:10.1021/la9604341
417. Rodrigues SN, Gonçalves IC, Martins MCL, Barbosa MA, Ratner BD (2006) Fibrinogen adsorption, platelet adhesion and activation on mixed hydroxyl-/methyl-terminated self-assembled monolayers. Biomaterials 27 (31):5357-5367
418. Ulman A (1996) Formation and structure of self-assembled monolayers. Chemical Reviews 96 (4):1533
419. Sreerama N, Woody RW (1993) A self-consistent method for the analysis of protein secondary structure from circular dichroism. Analytical Biochemistry 209 (1):32-44

420. Sreerama N, Woody RW (2000) Estimation of Protein Secondary Structure from Circular Dichroism Spectra: Comparison of CONTIN, SELCON, and CDSSTR Methods with an Expanded Reference Set. Analytical Biochemistry 287 (2):252-260. doi:10.1006/abio.2000.4880

421. Aota S, Nomizu M, Yamada KM (1994) The short amino acid sequence Pro-His-Ser-Arg-Asn in human fibronectin enhances cell-adhesive function. Journal of Biological Chemistry 269 (40):24756-24761

422. Brown BN, Barnes CA, Kasick RT, Michel R, Gilbert TW, Beer-Stolz D, Castner DG, Ratner BD, Badylak SF (2010) Surface characterization of extracellular matrix scaffolds. Biomaterials 31 (3):428-437

423. Canavan HE, Cheng X, Graham DJ, Ratner BD, Castner DG (2004) Surface Characterization of the Extracellular Matrix Remaining after Cell Detachment from a Thermoresponsive Polymer. Langmuir 21 (5):1949-1955. doi:10.1021/la048546c

424. Canavan HE, Graham DJ, Cheng X, Ratner BD, Castner DG (2006) Comparison of Native Extracellular Matrix with Adsorbed Protein Films Using Secondary Ion Mass Spectrometry. Langmuir 23 (1):50-56. doi:10.1021/la062330o

425. Rabbani S, Barber AM, Fletcher JS, Lockyer NP, Vickerman JC (2011) TOF-SIMS with Argon Gas Cluster Ion Beams: A Comparison with C60+. Analytical Chemistry 83 (10):3793-3800. doi:10.1021/ac200288v

426. Wehbe N, Tabarrant T, Brison J, Mouhib T, Delcorte A, Bertrand P, Moellers R, Niehuis E, Houssiau L (2012) TOF-SIMS depth profiling of multilayer amino-acid films using large Argon cluster Arn+, C60+ and Cs+ sputtering ions: A comparative study. Surface and Interface Analysis:n/a-n/a. doi:10.1002/sia.5121

427. Aoyagi S, Moritani K, Mochiji K (2011) Evaluation of immobilized polypeptides with different C-terminal residues using argon gas-cluster SIMS. Surface and Interface Analysis 43 (1-2):344-349. doi:10.1002/sia.3554

428. Rzeznik L, Czerwinski B, Garrison BJ, Winograd N, Postawa Z (2007) Microscopic Insight into the Sputtering of Thin Polystyrene Films on Ag{111} Induced by Large and Slow Ar Clusters. The Journal of Physical Chemistry C 112 (2):521-531. doi:10.1021/jp076667q

429. Garrison BJ, Postawa Z (2008) Computational view of surface based organic mass spectrometry. Mass Spectrometry Reviews 27 (4):289-315. doi:10.1002/mas.20165

430. Brison J, Guillot J, Douhard B, Vitchev RG, Migeon HN, Houssiau L (2009) On the understanding of positive and negative ionization processes during ToF-SIMS depth profiling by co-sputtering with cesium and xenon. Nuclear Instruments and Methods in Physics Research Section B: Beam Interactions with Materials and Atoms 267 (3):519-524. doi:10.1016/j.nimb.2008.11.026

431. Garrison BJ, Postawa Z, Ryan KE, Vickerman JC, Webb RP, Winograd N (2009) Internal Energy of Molecules Ejected Due to Energetic C60 Bombardment. Analytical Chemistry 81 (6):2260-2267. doi:10.1021/ac802399m

432. Muramoto S, Graham DJ, Wagner MS, Lee TG, Moon DW, Castner DG (2011) ToF-SIMS Analysis of Adsorbed Proteins: Principal Component Analysis of the Primary Ion Species Effect on the Protein Fragmentation Patterns. The Journal of Physical Chemistry C 115 (49):24247-24255. doi:10.1021/jp208035x

433. Agashe M, Raut V, Stuart SJ, Latour RA (2004) Molecular Simulation To Characterize the Adsorption Behavior of a Fibrinogen γ-Chain Fragment. Langmuir 21 (3):1103-1117. doi:10.1021/la0478346

434. Latour R (2008) Molecular simulation of protein-surface interactions: Benefits, problems, solutions, and future directions (Review). Biointerphases 3 (3):FC2-FC12. doi:10.1116/1.2965132

435. Raut VP, Agashe MA, Stuart SJ, Latour RA (2005) Molecular Dynamics Simulations of Peptide−Surface Interactions. Langmuir 21 (4):1629-1639. doi:10.1021/la047807f

436. Yancey J, Vellore N, Collier G, Stuart S, Latour R (2010) Development of molecular simulation methods to accurately represent protein-surface interactions: The effect of pressure and its determination for a system with constrained atoms. Biointerphases 5 (3):85-95. doi:10.1116/1.3493470

VITA

Elaine Hillenmeyer Tronic was born in Indianapolis, Indiana. In 2006 she graduated with highest honors from Case Western Reserve University, earning a Bachelor's of Science in Engineering in Biomedical Engineering. She spent a year performing tissue engineering research at the University of Liverpool before moving to Seattle to pursue further studies. In 2012 she earned a Doctor of Philosophy at the University of Washington in Bioengineering under the guidance of Dr. David Castner.